

**Appropriately Complex Modelling of Healthy Human
Walking**

Michael Paul **MCGRATH**

2014

**Submitted in Partial Fulfilment of the Requirements of the Degree
of Doctor of Philosophy**

CONTENTS

LIST OF FIGURES	VI
LIST OF TABLES	IX
ACKNOWLEDGEMENTS	XI
NOMENCLATURE	XII
LIST OF ABBREVIATIONS	XV
ABSTRACT	XVI
1 GENERAL INTRODUCTION	1
1.1 DEFINITIONS	2
1.2 CHAPTER SUMMARY	3
2 LITERATURE REVIEW	6
2.1 SIMPLE MODELS	6
2.2 COMPLEX MODELS	11
2.2.1 <i>Muscle modelling</i>	11
2.2.2 <i>Common assumptions</i>	13
2.2.3 <i>Solution methods</i>	14
2.2.4 <i>Static Optimisation</i>	15
2.2.5 <i>Dynamic optimisation</i>	16
2.3 VALIDATION	18
2.4 CASE STUDY	19
2.5 DISCUSSION	23
2.6 RESEARCH QUESTIONS AND PROJECT AIMS	25
3 SIMPLE MODELS	28
3.1 INTRODUCTION	28
3.2 LITERATURE	29
3.3 THE MODELS	30
3.4 THE MODELLING FRAMEWORK	31
3.4.1 <i>Lagrangian Dynamics</i>	31
3.4.2 <i>Numerical integration</i>	37
3.4.3 <i>Ground reaction force calculations</i>	38
3.5 SIMULATION METHODS	40
3.6 RESULTS	41
3.7 DISCUSSION	46

3.8	CONCLUSIONS	49
4	SINGLE SUPPORT MODELS	50
4.1	INTRODUCTION	50
4.2	LITERATURE	50
4.3	THE MODELLING FRAMEWORK	52
4.3.1	<i>Introduction</i>	52
4.3.2	<i>Generalised formula for n-link chain equations of motion</i>	52
4.3.3	<i>Numerical integration</i>	60
4.3.4	<i>Ground reaction force calculations</i>	60
4.4	SEQUENTIAL MODEL DEVELOPMENT	61
4.4.1	<i>Three degrees-of-freedom (Model 3)</i>	61
4.4.2	<i>Four degrees-of-freedom (Model 4)</i>	63
4.4.3	<i>Seven degrees-of-freedom (Model 5)</i>	65
4.5	SIMULATION METHODS	67
4.5.1	<i>Joint moments</i>	67
4.5.2	<i>Optimisation parameters</i>	68
4.5.3	<i>Cost function</i>	69
4.5.4	<i>Algorithms</i>	70
4.6	RESULTS	74
4.6.1	<i>Model 3 – Three degrees-of-freedom</i>	74
4.6.2	<i>Model 4 - Four degrees-of-freedom</i>	82
4.6.3	<i>Model 5 - Seven degrees-of-freedom</i>	86
4.7	DISCUSSION	90
4.8	CONCLUSIONS	95
5	DOUBLE SUPPORT AND FULL GAIT CYCLE MODELS	97
5.1	INTRODUCTION	97
5.2	THE MODELLING FRAMEWORK	98
5.2.1	<i>Lagrangian multipliers and constraints</i>	98
5.2.2	<i>Four-chain example</i>	100
5.2.3	<i>Numerical integration</i>	103
5.2.4	<i>Ground reaction force calculations</i>	104
5.3	DOUBLE SUPPORT MODEL	105
5.3.1	<i>Phase 1: Lead heel contact to lead foot flat</i>	105
5.3.2	<i>Phase 2: Lead foot flat to trail foot toe-rise</i>	106
5.3.3	<i>Phase 3: Trail foot toe-rise to trail foot toe-off</i>	107
5.4	SIMULATION METHODS	108
5.4.1	<i>Joint moments</i>	108

5.4.2	<i>Optimisation parameters</i>	109
5.4.3	<i>Cost function</i>	109
5.4.4	<i>Algorithms</i>	109
5.5	RESULTS	109
5.6	FULL GAIT CYCLE SIMULATION	113
5.6.1	<i>Sum model</i>	114
5.7	DISCUSSION	118
5.8	CONCLUSIONS	121
6	DATA COLLECTION AND ANALYSIS	123
6.1	INTRODUCTION	123
6.2	LITERATURE	124
6.3	METHOD	125
6.3.1	<i>Participant recruitment</i>	125
6.3.2	<i>The research environment</i>	126
6.3.3	<i>Calibration</i>	127
6.3.4	<i>Marker positioning</i>	128
6.3.5	<i>Anthropometric measurements</i>	129
6.3.6	<i>Experimental method</i>	130
6.3.7	<i>Post-processing</i>	131
6.3.8	<i>Simulation setup</i>	134
6.3.9	<i>Statistical Analysis</i>	135
6.4	RESULTS	136
6.4.1	<i>RMS errors</i>	136
6.4.2	<i>Discontinuities</i>	139
6.4.3	<i>The best results</i>	141
6.4.4	<i>The worst results</i>	146
6.4.5	<i>Inter-subject comparisons</i>	152
6.5	DISCUSSION	155
6.6	CONCLUSIONS	158
7	GENERAL DISCUSSION	159
7.1	INTRODUCTION	159
7.2	RESEARCH QUESTION 1	160
7.3	RESEARCH QUESTION 2	161
7.4	RESEARCH QUESTION 3	162
7.5	RESEARCH QUESTION 4	163
7.6	GENERAL LIMITATIONS	164
7.7	FUTURE WORK	166

7.8	GENERAL CONCLUSIONS	168
APPENDICES		169
A.1	FORMULAE FOR GENERALISED BODY PARAMETERS	169
A.2	MATLAB CODE FOR THE GENERATION OF THE EQUATIONS OF MOTION FOR AN N-LINK, OPEN CHAIN	170
A.3	LETTER CONFIRMING ETHICAL APPROVAL	174
A.4	RECRUITMENT POSTER	175
A.5	PARTICIPANT INFORMATION SHEET	176
A.6	RESEARCH PARTICIPANT CONSENT FORM	179
A.7	ALL PRACTICAL DATA	180
A.7.1	<i>Subject 1</i>	181
A.7.2	<i>Subject 2</i>	183
A.7.3	<i>Subject 3</i>	185
A.7.4	<i>Subject 4</i>	187
A.7.5	<i>Subject 5</i>	189
A.7.6	<i>Subject 6</i>	191
A.7.7	<i>Subject 7</i>	193
A.7.8	<i>Subject 8</i>	195
A.7.9	<i>Subject 9</i>	197
A.7.10	<i>Subject 10</i>	199
A.8	PRELIMINARY INVESTIGATION OF FUTURE WORK	201
A.9	RATIONALE BEHIND SEQUENTIAL COMPLEXITY INCREASES	209
REFERENCES		211

LIST OF FIGURES

FIGURE 1.1: A SUMMARY OF THE PROPOSED OUTLINE OF THE THESIS.....	5
FIGURE 2.1: INVERTED PENDULUM MODEL (BUCZEK ET AL., 2006)	6
FIGURE 2.2: EXAMPLES OF MULTI-SEGMENT MODELS, INCORPORATING SPRINGS AND DAMPERS (PANDY & BERME, 1988B)	8
FIGURE 2.3: A HILL-TYPE MUSCLE MODEL (ARNOLD ET AL., 2010)	12
FIGURE 2.4: EXAMPLE OF MASS-SPRING-DAMPER MECHANISM TO MODEL FOOT CONTACT (YAMAGUCHI & ZAJAC, 1990)	13
FIGURE 2.5: AN EXAMPLE OF A COMPLEX MODEL INCORPORATING A LARGE NUMBER OF INDIVIDUAL MUSCLES (ARNOLD ET AL., 2010)	15
FIGURE 2.6: PANDY AND ANDERSON’S COMPLEX GAIT MODEL (FRANK C. ANDERSON & PANDY, 2001B)	20
FIGURE 2.7: A SUMMARY OF THE OUTLINE OF THE THESIS AND WHERE EACH RESEARCH QUESTION WILL BE ADDRESSED	27
FIGURE 3.1: FREE BODY DIAGRAMS FOR A) MODEL 1 (INCLUDING THE CALCULATION APPROXIMATIONS IN BOLD) AND B) MODEL 2.	31
FIGURE 3.2: THE LINEAR VELOCITY COMPONENTS FOR MODELS 1 AND 2 AT DIFFERENT WALKING VELOCITIES. THE SHADED AREAS INDICATE EXPERIMENTAL DATA AND DOUBLE SUPPORT PERIODS. THE LINE THICKNESSES OF MODEL 2’S VELOCITY COMPONENT CURVES HAVE BEEN INCREASED SO AS TO HELP DISTINGUISH BETWEEN THE TWO MODELS’ RESULTS. THIS IS DIFFICULT, PARTICULARLY FOR THE VERTICAL COMPONENT OF VELOCITY, WHERE THE RESULTS WERE ALMOST IDENTICAL. .	43
FIGURE 3.3: THE GRF COMPONENTS FOR MODELS 1 (TOP SIX) AND 2 (BOTTOM SIX) MODELS AT DIFFERENT WALKING VELOCITIES	44
FIGURE 3.4: THE HIP JOINT MOMENTS (FLEXION POSITIVE) FOR MODELS 1 (RED) AND 2 (BLUE) MODELS AT DIFFERENT WALKING VELOCITIES.....	46
FIGURE 4.1: THE GEOMETRY OF ANY GIVEN SEGMENT	53
FIGURE 4.2: MODEL 3: A THREE DEGREES-OF-FREEDOM MODEL OF HUMAN WALKING	62
FIGURE 4.3: CENTRE OF PRESSURE MOTION DURING STANCE (WHITTLE, 2007)	63
FIGURE 4.4: THE REAL-LIFE POSITION OF THE GRF (LEFT) AND HOW IT IS APPROXIMATED BY THE MODEL (RIGHT).....	64
FIGURE 4.5: MODEL 4: A FOUR DEGREES-OF-FREEDOM MODEL OF HUMAN WALKING	65
FIGURE 4.6: MODEL 5: A SEVEN DEGREES-OF-FREEDOM MODEL OF HUMAN WALKING	66
FIGURE 4.7: MOMENT NODES AND INTERPOLATION.....	68
FIGURE 4.8: ILLUSTRATION OF LOCAL OPTIMISATION BEHAVIOUR. THE DOTS INDICATE THE INITIAL ESTIMATE AND THE STARS SHOW THE SOLUTIONS THE SOLVER FOUND.....	71
FIGURE 4.9: 3D PLOT OF A COST FUNCTION.....	72
FIGURE 4.10: FROM MULTIPLE RANDOM START POINTS, THE CHOSEN FIRST START POINT FINDS A LOCAL MINIMUM (THE STAR) CREATING THE FIRST BASIN (THE RING)	73
FIGURE 4.11: BASIN EXPANSION (BOTTOM) AND A NEW START POINT WITHIN AN EXISTING BASIN (TOP)	73
FIGURE 4.12: THE KINEMATIC PREDICTIONS FOR MODEL 3.....	75
FIGURE 4.13: THE KINEMATIC PREDICTIONS (SOLID) VS THE EMPIRICAL MEANS (DOTTED) FOR MODEL 3	76
FIGURE 4.14: THE JOINT MOMENT PREDICTIONS FOR MODEL 3	76
FIGURE 4.15: THE GRF PREDICTIONS FOR THE MODEL 3	77

FIGURE 4.16: MODEL 3.1: A THREE DEGREES-OF-FREEDOM MODEL OF HUMAN WALKING WITH A STATIC FOOT	78
FIGURE 4.17: THE KINEMATIC PREDICTIONS FOR MODEL 3.1.....	79
FIGURE 4.18: THE KINEMATIC PREDICTIONS (SOLID) VS THE EMPIRICAL MEANS (DOTTED) FOR MODEL 3.1	79
FIGURE 4.19: THE JOINT MOMENT PREDICTIONS FOR MODEL 3.1	80
FIGURE 4.20: THE GRF PREDICTIONS FOR MODEL 3.1.....	80
FIGURE 4.21: THE KINEMATIC PREDICTIONS FOR MODEL 4.....	83
FIGURE 4.22: THE KINEMATIC PREDICTIONS (SOLID) VS THE EMPIRICAL MEANS (DOTTED) FOR MODEL 4	84
FIGURE 4.23: THE JOINT MOMENT PREDICTIONS FOR MODEL 4	85
FIGURE 4.24: THE GRF PREDICTIONS FOR MODEL 4.....	85
FIGURE 4.25: THE SEGMENT ANGLE PREDICTIONS FOR MODEL 5. BLUE IS STANCE LEG; RED IS SWING LEG.	88
FIGURE 4.26: THE KINEMATIC PREDICTIONS (SOLID) VS THE EMPIRICAL MEANS (DOTTED) FOR MODEL 5	89
FIGURE 4.27: THE JOINT MOMENT PREDICTIONS FOR MODEL 5. BLUE IS STANCE LEG; RED IS SWING LEG.....	89
FIGURE 4.28: THE GRF PREDICTIONS FOR MODEL 5.....	90
FIGURE 4.29: THE MEAN GRF RMS ERROR WITH INCREASING MODEL COMPLEXITY FROM LEFT TO RIGHT	95
FIGURE 5.1: A FOUR SEGMENT CLOSED CHAIN	100
FIGURE 5.2: DS MODEL, PHASE 1: A FREE BODY DIAGRAM	106
FIGURE 5.3: DS MODEL, PHASE 2: A FREE BODY DIAGRAM	107
FIGURE 5.4: DS MODEL, PHASE 3: A FREE BODY DIAGRAM	108
FIGURE 5.5: THE SEGMENT ANGLE PREDICTIONS FOR THE DS MODEL. BLUE IS LEAD LEG; RED IS TRAIL LEG.	111
FIGURE 5.6: THE KINEMATIC PREDICTIONS (SOLID) VS THE EMPIRICAL MEANS (DOTTED) FOR THE DS MODEL.....	111
FIGURE 5.7: THE JOINT MOMENT PREDICTIONS FOR THE DS MODEL. BLUE IS LEAD LEG; RED IS TRAIL LEG.....	112
FIGURE 5.8: THE GRF MOMENT PREDICTIONS FOR THE DS MODEL.....	112
FIGURE 5.9: THE KINEMATIC PREDICTIONS (SOLID) VS THE EMPIRICAL MEANS (DOTTED) FOR THE SUM MODEL.....	114
FIGURE 5.10: THE SEGMENT ANGLE PREDICTIONS FOR THE SUM MODEL	115
FIGURE 5.11: THE JOINT MOMENT PREDICTIONS FOR THE SUM MODEL.....	116
FIGURE 5.12: THE GRF MOMENT PREDICTIONS FOR THE SUM MODEL.....	116
FIGURE 6.1: THE UNIVERSITY OF SALFORD’S BRIAN BLATCHFORD LAB.....	126
FIGURE 6.2: CAMERA CALIBRATION AND SETTING THE ORIGIN	127
FIGURE 6.3: THE MARKER PLACEMENT	129
FIGURE 6.4: THE JOINT CENTRE PREDICTIONS FOR SUBJECT #2	142
FIGURE 6.5: THE SEGMENT ANGLE PREDICTIONS FOR SUBJECT #2.....	143
FIGURE 6.6: THE KINEMATIC PREDICTIONS (SOLID) VS THE EXPERIMENTAL TRIAL DATA (DOTTED) FOR SUBJECT #2.....	144
FIGURE 6.7: THE GRF PREDICTIONS FOR SUBJECT #5.....	145
FIGURE 6.8: THE JOINT MOMENT PREDICTIONS FOR SUBJECT #6	146
FIGURE 6.9: THE KINEMATIC PREDICTIONS (SOLID) VS THE EXPERIMENTAL TRIAL DATA (DOTTED) FOR SUBJECT #9.....	147
FIGURE 6.10: THE JOINT CENTRE PREDICTIONS FOR SUBJECT #9	148
FIGURE 6.11: THE KINEMATIC PREDICTIONS (SOLID) VS THE EXPERIMENTAL TRIAL DATA (DOTTED) FOR SUBJECT #6.....	149
FIGURE 6.12: THE SEGMENT ANGLES PREDICTIONS FOR SUBJECT #6	150

FIGURE 6.13: THE GRF PREDICTIONS FOR SUBJECT #6.....	151
FIGURE 6.14: THE JOINT MOMENT PREDICTIONS FOR SUBJECT #10	152
FIGURE 6.15: COMPARISON OF RMS ERRORS AGAINST HEIGHT FOR ALL SUBJECTS	154
FIGURE 6.16: COMPARISON OF RMS ERRORS AGAINST MASS FOR ALL SUBJECTS	154
FIGURE 6.17: COMPARISON OF RMS ERRORS AGAINST GAIT CYCLE TIME FOR ALL SUBJECTS	155
FIGURE A.1: BODY PROPORTIONS BASED ON HEIGHT (WINTER, 1979, 1991)	169
FIGURE A.2: THE KINEMATIC PREDICTIONS (SOLID) VS THE EMPIRICAL MEANS (DOTTED) FOR THE CONTINUOUS MODEL.....	201
FIGURE A.3: THE SEGMENT ANGLE PREDICTIONS FOR THE CONTINUOUS MODEL	202
FIGURE A.4: THE JOINT CENTRE POSITION PREDICTIONS FOR THE CONTINUOUS MODEL	203
FIGURE A.5: THE JOINT MOMENT PREDICTIONS FOR THE CONTINUOUS MODEL.....	204
FIGURE A.6: THE GRF MOMENT PREDICTIONS FOR THE CONTINUOUS MODEL.....	204

LIST OF TABLES

TABLE 3.1: VALUES FOR MODEL PARAMETERS.....	40
TABLE 3.2: AVERAGE TEMPORAL SPATIAL PARAMETERS FOR WINTER’S DATA	41
TABLE 3.3: THE RMS OF THE DIFFERENCE BETWEEN MODELS 1 AND 2 PREDICTIONS.....	45
TABLE 3.4: THE RMS OF THE DIFFERENCES BETWEEN THE MODELS’ PREDICTIONS AND THE EXPERIMENTAL DATA	45
TABLE 4.1: VALUES FOR MODEL PARAMETERS OF MODEL 3.....	62
TABLE 4.2: VALUES FOR MODEL PARAMETERS OF MODEL 4.....	65
TABLE 4.3: VALUES FOR MODEL PARAMETERS OF MODEL 5.....	66
TABLE 4.4: VALUES FOR MODEL PARAMETERS OF MODEL 3.1.....	78
TABLE 4.5: THE PREDICTION RMS ERRORS WITH THE EXPERIMENTAL DATA FOR MODELS 3 AND 3.1	82
TABLE 4.6: THE RMS ERRORS FROM THE EXPERIMENTAL MEANS FOR MODEL 4	86
TABLE 4.7: THE RMS ERRORS FROM THE EXPERIMENTAL MEANS FOR MODEL 5	87
TABLE 4.8: THE RMS ERRORS FROM THE EXPERIMENTAL MEANS FOR ALL MODELS.....	94
TABLE 5.1: THE RMS ERROR VALUES FOR THE DS MODEL.....	113
TABLE 5.2: THE RMS ERROR VALUES FOR THE SUM MODEL.....	117
TABLE 5.3: DISCONTINUITIES AT BOTH TOE-OFF AND FOOT CONTACT EVENTS, DURING THE FULL GAIT CYCLE, FOR THE SUM MODEL	118
TABLE 6.1: THE MEAN RMS ERROR VALUES FOR EACH SUBJECT, FOR THE DIFFERENT KINEMATIC AND KINETIC VALUES.....	137
TABLE 6.2: THE MEAN RMS ERROR VALUES FOR EACH COMPARISON PARAMETER, ACROSS ALL SUBJECTS	138
TABLE 6.3: THE MEAN DISCONTINUITY VALUES FOR EACH SUBJECT, FOR THE DIFFERENT KINEMATIC AND KINETIC VALUES	139
TABLE 6.4: THE MEAN DISCONTINUITY VALUES FOR EACH COMPARISON PARAMETER, ACROSS ALL SUBJECTS	140
TABLE 6.5: THE PEARSON’S CORRELATION COEFFICIENTS (p) WITH THEIR RESPECTIVE P-VALUES, AND SPEARMAN’S RANK CORRELATION COEFFICIENT (p_s) WITH THEIR RESPECTIVE P-VALUES, FOR COMPARISONS OF RMS ERRORS AND CERTAIN SUBJECT CHARACTERISTICS	153
TABLE A.1: THE FORMULAE FOR CALCULATING GENERALISED BODY PARAMETERS AS FUNCTIONS OF A PERSON’S HEIGHT AND WEIGHT (WINTER, 1979, 1991).....	169
TABLE A.2: CHARACTERISTICS OF EACH OF THE SUBJECTS	180
TABLE A.3: THE RMS ERROR VALUES FOR SUBJECT 1.....	181
TABLE A.4: THE DISCONTINUITY VALUES FOR SUBJECT 1	182
TABLE A.5: THE RMS ERROR VALUES FOR SUBJECT 2.....	183
TABLE A.6: THE DISCONTINUITY VALUES FOR SUBJECT 2	184
TABLE A.7: THE RMS ERROR VALUES FOR SUBJECT 3.....	185
TABLE A.8: THE DISCONTINUITY VALUES FOR SUBJECT 3	186
TABLE A.9: THE RMS ERROR VALUES FOR SUBJECT 4.....	187
TABLE A.10: THE DISCONTINUITY VALUES FOR SUBJECT 4	188
TABLE A.11: THE RMS ERROR VALUES FOR SUBJECT 5.....	189
TABLE A.12: THE DISCONTINUITY VALUES FOR SUBJECT 5	190

TABLE A.13: THE RMS ERROR VALUES FOR SUBJECT 6	191
TABLE A.14: THE DISCONTINUITY VALUES FOR SUBJECT 6	192
TABLE A.15: THE RMS ERROR VALUES FOR SUBJECT 7	193
TABLE A.16: THE DISCONTINUITY VALUES FOR SUBJECT 7	194
TABLE A.17: THE RMS ERROR VALUES FOR SUBJECT 8	195
TABLE A.18: THE DISCONTINUITY VALUES FOR SUBJECT 8	196
TABLE A.19: THE RMS ERROR VALUES FOR SUBJECT 9	197
TABLE A.20: THE DISCONTINUITY VALUES FOR SUBJECT 9	198
TABLE A.21: THE RMS ERROR VALUES FOR SUBJECT 10	199
TABLE A.22: THE DISCONTINUITY VALUES FOR SUBJECT 10	200
TABLE A.23: THE RMS ERROR VALUES FOR THE CONTINUOUS MODEL.....	205
TABLE A.24: DISCONTINUITIES FOR THE CONTINUOUS MODEL	207
TABLE A.25: COMPARISON OF THE ANGULAR VELOCITIES, IN °/s, AT THE TRANSITION FROM DOUBLE TO SINGLE SUPPORT FOR THE SUM AND CONTINUOUS MODELS. IN BOLD ARE THE LARGEST DIFFERENCES.	208

ACKNOWLEDGEMENTS

I would like to extend my gratitude to my supervisors, Prof Richard Baker and Prof David Howard, for giving me the opportunity to work on this project and for all the support and help they have provided along the way. I would also like to acknowledge the contribution of the University of Salford, which provided the funding to support the project. My thanks also go to my parents, family and friends for everything they have done for me. Finally, I'd like to thank Katy and Meg for all their support.

NOMENCLATURE

Roman characters

<i>a</i>	Linear acceleration OR a term in a quadratic equation
<i>B</i>	A matrix in the equations of motion formulation
<i>b</i>	An element of the matrix B OR a term in a quadratic equation
<i>C</i>	A matrix in the equations of motion formulation
<i>c</i>	An element of the matrix C OR a term in a quadratic equation
<i>d</i>	Position of segment centre of mass along long axis of segment OR a set of values formed by the differences in the rankings of two data sets
DCM	Direction cosine matrix
<i>dt</i>	A change in time
<i>e</i>	Position of segment centre of mass perpendicular to long axis of segment
<i>f</i>	A function $f(\dots)$ OR the f^{th} term
<i>F</i>	Force
<i>g</i>	Acceleration due to gravity OR a function $g(\dots)$
GRF	Ground reaction force
<i>h</i>	A function $h(\dots)$ OR the h^{th} term
<i>H</i>	Vector of the hip joint centre
<i>I</i>	Moment of inertia of segment
<i>i</i>	The i^{th} term
<i>j</i>	The j^{th} term
<i>k</i>	Spring constant
<i>K</i>	A group of terms
<i>l</i>	Length of segment
<i>L</i>	Lagrange function
<i>m</i>	Mass of segment

M	Moment
m	Total number of ...
n	Total number of ...
O	Axis origin
Q	Generalised force term
$q/\dot{q}/\ddot{q}$	Generalised positional/velocity/acceleration term
S	Step length
\mathbf{S}	Vector of the sacrum
T	Kinetic energy
t	Time
V	Potential energy
v	Resultant linear velocity
w	Work done
$x/\dot{x}/\ddot{x}$	x linear position/velocity/acceleration
$\hat{x},/\hat{y}/\hat{z}$	Vector of an axis
$y/\dot{y}/\ddot{y}$	y linear position/velocity/acceleration

Greek characters

α	Rotational acceleration
Δ	Change in a variable
$\theta/\dot{\theta}/\ddot{\theta}$	Angular position/velocity/acceleration
λ	Lagrangian multiplier
ρ	Correlation coefficient
σ	Standard deviation
φ	Joint angle
ω	Rotational velocity

Superscript/Subscript

$1/2/3$	Related to mass/segment 1/2/3...
A	Of the ankle joint
C	Centripetal component
G	Gravitational Component
GRF	Of the ground reaction force
H	Of the hip joint
K	Of the knee joint
L	Of the leading leg
M	Muscle component OR of the metatarsal joint
P	Of the pelvis/in the pelvic axis
p, q	Related to matrix element in row p , column q
S	Spearman's rank
St	Of the stance leg
Sw	Of the swing leg
T	Of the trailing leg
t	Time OR total/resultant

LIST OF ABBREVIATIONS

2D	Two Dimensional
3D	Three Dimensional
BW	Bodyweight
CM	Centre of Mass
COP	Centre of Pressure
DOF	Degree(s)-of-freedom
FC	Foot Contact event
GRF	Ground Reaction Force
HAT	Head, Arms and Trunk
IP	Inverted Pendulum
<i>L</i>ASIS	Left Anterior Superior Iliac Spine
LED	Light emitting diode
<i>L</i>PSIS	Left Posterior Superior Iliac Spine
PD	Pelvic Depth
PW	Pelvic Width
<i>r</i>ASIS	Right Anterior Superior Iliac Spine
RMS	Root mean squared
<i>r</i>PSIS	Right Posterior Superior Iliac Spine
TO	Toe-off event

ABSTRACT

Modelling human gait has become an invaluable tool in a wide range of fields such as robotics and rehabilitation. With progress in computing, model complexity has advanced quickly but nevertheless, the contributions of incremental increases in model complexity are poorly understood. This thesis addresses this through a series of modelling studies.

The first investigation examined the advantages and disadvantages of inverted pendulum (IP) models of walking, using a forward dynamics approach, by comparing to a normal set of experimental gait data. It was shown that the biggest failing of these models is their inability to adequately simulate double stance.

The second investigation sought to highlight the effects of additional model complexities on the kinematics and kinetics, using optimisation. The additions, added one-by-one, were a knee joint, an ankle and static foot, a moving foot and a swing leg. The presence of a knee joint and an ankle moment were shown to be largely responsible for the initial peak in the vertical ground force reaction (GRF) curve. The second peak in this curve was achieved through a combination of heel rise and the presence of a swing leg. This gave mathematical evidence for the true determinants of human gait.

A double support model was produced next, using a novel method to constrain both feet to the ground and calculate the GRF distribution. This was run in conjunction with the best single support model to simulate a whole gait cycle. Despite the problem of discontinuities at the transitions between double and single support, the whole gait cycle simulation had mean kinematic and mean GRF errors of less than a single standard deviation from the normal experimental data set.

The final study collected gait and anthropometric data from ten subjects, which was then applied to the full gait cycle model. The model was shown to be adaptable to different people; a property that would be important for any computational model to be used in clinical assessment and diagnostics.

1 GENERAL INTRODUCTION

The modelling of human movement is a concept that has applications in a wide range of fields such as prosthetics (Pedersen et al., 1997; Srinivasan et al., 2009), robotics (Ephanov & Hurmuzlu, 2002; Rostami & Bessonnet, 2001) and rehabilitation (Yamaguchi & Zajac, 1990). It provides an understanding of the underlying processes that determine why humans walk the way they do. It can help identify specific impairments affecting people with pathologies that inhibit their ability to walk in a natural manner and hence the appropriate treatment or orthotic can be prescribed. In industry, where the health and safety of workers is paramount, it can be used to investigate actions that may cause potential injury.

For a process that most people take for granted and perform every day without thinking about it, comprehending the way in which we walk, and why it is so, is not only intriguing from a scientific perspective but also practically beneficial. In spite of this, our understanding of walking is still quite limited. For years, conceptual modelling was the standard in the gait analysis field (Saunders et al., 1953) i.e. models based on observation and theories rather than measurable evidence. Using simplified approximations of the geometries relevant to walking and broadly based on observation, gait was defined as having six different mechanisms, or '*gait determinants*'. These were pelvic rotation and obliquity, stance phase knee flexion, ankle mechanisms, foot mechanisms and lateral body displacement. These mechanisms were said to smooth the trajectory of a person's centre of mass (CM) and therefore reduce energy dissipation during walking. However, a number of experimental and mathematical based studies have since brought into question the validity of some of these determinants (Baker et al., 2004; Della Croce et al., 2001; Gard & Childress, 1997, 1999; Kerrigan et al., 2001; Kuo, 2007).

As gait analysis progressed, simple mathematical models of walking became more important. Unlike those concepts developed purely from observation, these studies provided mathematical evidence to justify their claims, which consequently carried more weight. The body would be approximated into a number of rigid body segments, joined together, that were assumed to have point masses and each was given appropriate geometric and inertial properties. These could then be used to investigate numerous

aspects of gait analysis but due to the many assumptions made, simple models were often purpose designed to only investigate one or two specific aspects of walking at a time.

However, the advent of more powerful computers and faster processors led to great advances in the sophistication of gait models. It made possible three-dimensional models with multiple bones, joints, muscles and degrees-of-freedom (DOF) accounted for. This made it possible to investigate many more of the kinematics and kinetics of walking in a single model, including the contributions of individual muscles, something that could not be done with the more simple models. Due to their complexity, they also required more sophisticated techniques to come to a solution. They are often indeterminate problems i.e. the number of variables is greater than the number of equations defining the movement. As a consequence, a desirable condition is often determined and optimisation approaches are used to produce a solution achieving it.

This development was undeniably progress but it was not natural progression. By going from simple link segment models to complex computer models in one step, the natural evolution of modelling has been omitted. Is there justification for investigating what happens in between? At what point can a model be considered 'appropriately complex' for the hypothesis it is being used to investigate? If we haven't tested the optimisation solution techniques on simple systems, how can we be confident in their application to systems we don't fully understand, such as the advanced models?

1.1 Definitions

Throughout this project, the following terminology will be used:

Gait Model: *This refers to the kinematic structure (segments and joints) that has been defined, the inertial parameters applied to it and the simplifications and assumptions that have been made.*

Modelling Framework: *This refers to the general methods used to derive mathematical models of the kinematics and kinetics of specific gait models.*

Simulation: *This refers to the generation of time-based results using the mathematical model, for a particular gait model, and other techniques such as numerical integration and optimisation, given a definition of certain input variables.*

In the general academic literature these terms are often used interchangeably but for clarity within this thesis, these definitions will be adhered to.

1.2 Chapter summary

In the following chapter, a comprehensive review of the relevant literature will be performed. This is to assess the current '*state-of-the-art*' and avoid simply repeating the work of other researchers. This review will indicate where there are gaps in our collective knowledge. Following this, appropriate and specific research questions and aims will be outlined.

Chapter 3 will look into the very simple models of gait that have only a single DOF and evaluate their benefits and shortcomings when compared to one another as well as experimental data.

Chapter 4 will advance the very simple models by sequentially adding extra DOF or other complexities. This will provide a good indication of a particular mechanism's effect on the kinematics and kinetics of the gait cycle and hopefully give an indication of why this is beneficial overall. Continuing the theme of starting at a fundamental level and building up, this chapter will consider the single support phase only.

Chapter 5 will look into double support phase models. This has the added complexity of having two points where the model interacts with external forces (i.e. the ground) which imposes additional kinematic constraints. Next, an amalgamation of the double and

single support simulations will allow half a gait cycle to be simulated, which, given a constraint of bilateral symmetry, may be considered to simulate a full gait cycle.

Chapter 6 will test the versatility of the models developed in the previous chapters. Gait data will be collected from a number of different people and the individual characteristics of each person will be used as inputs to the model. It will then be seen in what areas the model can make successful predictions and what areas it fails.

The final chapter will be a general discussion, summarising the findings of the project overall. How well the work was able to address the research questions will be examined and suggestions regarding future investigations, following on from these findings, will be considered.

A diagram outlining the contents of each chapter is shown in Figure 1.1.

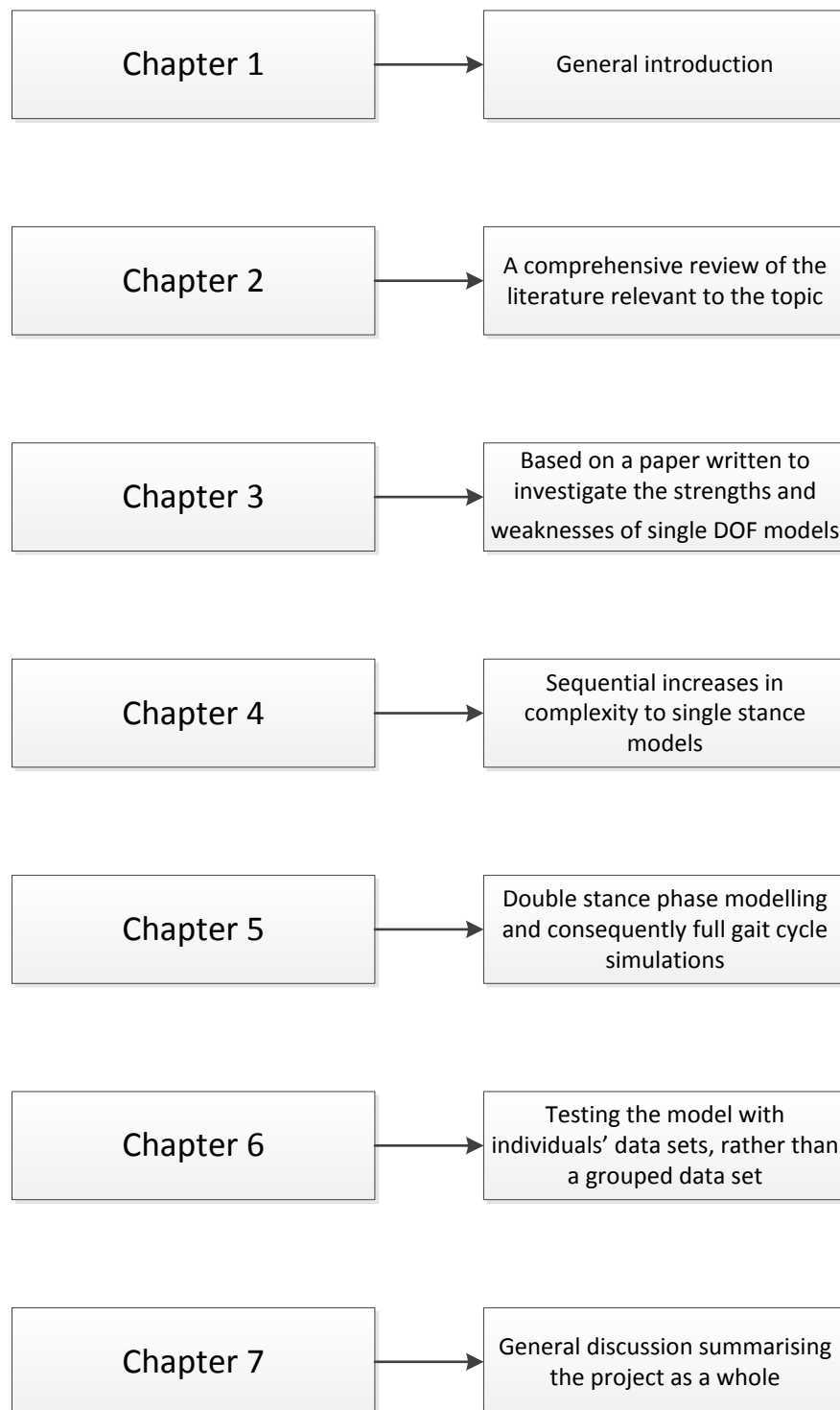


Figure 1.1: A summary of the proposed outline of the thesis

2 LITERATURE REVIEW

2.1 Simple models

Simple walking models can be very useful for investigating various features of gait. These models often consist of rigid body segments used to represent the different sections of the body or sometimes just the lower extremities. The entire mass of each segment acts at a single point on the segment (the CM), a given distance from the segment's end. The parameters defining each segment, such as length, mass, CM position, moment of inertia, etc., will have been taken from an anatomically reliable source. Many of these types of models will focus on the sagittal plane only.

The number of segments used is quite variable. The simplest model of walking is the Inverted Pendulum (IP) model (Baker et al., 2004; Buczek et al., 2006; Kuo, 2007). This model uses a single rigid segment representing the stance leg, pivoting about its distal end. The entire mass of the body acts at a single point at the proximal end and there is no moment of inertia (Figure 2.1). Although very primitive, the model can produce kinetic results similar to those found during empirical tests, particularly in the anterior-posterior direction. However, the predictions in the superior-inferior direction are less accurate with the curve of the ground reaction force (GRF) component failing to produce the double peak shape familiar to gait analysts.

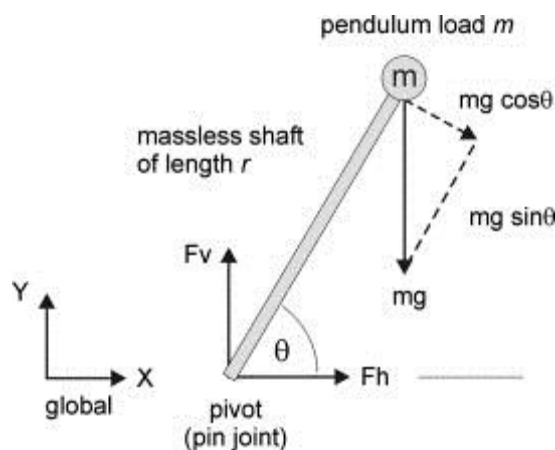


Figure 2.1: Inverted Pendulum model (Buczek et al., 2006)

This particular model has been shown to not require any external forces and can work purely on the principle of conservation of energy (Baker et al., 2004; Kuo, 2007). It has been postulated that the reason people do in fact expend energy during walking is because of the step-to-step transition. At the end of the step, the velocity of the CM of the IP is not travelling in the same direction as it does at the start of the step. This is a condition that needs to be met so that the process can be deemed cyclic, as walking is known to be. This would require either an infinite acceleration to change the mass' direction instantaneously, or other mechanisms that altered the mass' path during the step to ensure that its initial and terminal velocities were equal in magnitude and direction.

An alternative to the IP model is the spring loaded inverted pendulum (SLIP) model of locomotion (Bullimore & Burn, 2007; Hong et al., 2013; Millard et al., 2011; Poulakakis, 2010; Poulakakis & Grizzle, 2009; Soyguder & Alli, 2012). The structure of this model is the same except it incorporates a spring mechanism within the segment. The results for both GRF components match much better for this model as the vertical curve is now essentially a sine wave, thus achieving a double peak shape. This still does not nullify the problem of the step-to-step transition though.

Models incorporating more than a single segment often use hinge joints to represent the joints of the body (Figure 2.2). This forms what are known as multi-link inverted pendulums (Duan et al., 1997; Pandy & Berme, 1988a) which have an inherent instability. Some researchers have chosen to combat this problem by taking inspiration from the SLIP model and incorporating spring-damper mechanisms at certain joints within a multi-segment model (Pandy & Berme, 1988b; Siegler et al., 1982). An alternative method, which preserves biological accuracy better, is to actuate the joints. This means having the joints modelled as simple hinges but with joint moments applied, acting about these hinges. This can be achieved through dynamic structures, such as angular springs and dampers (Duan et al., 1997), or simply by applying joint moments when deriving the equations of motion (Pandy & Berme, 1988b).

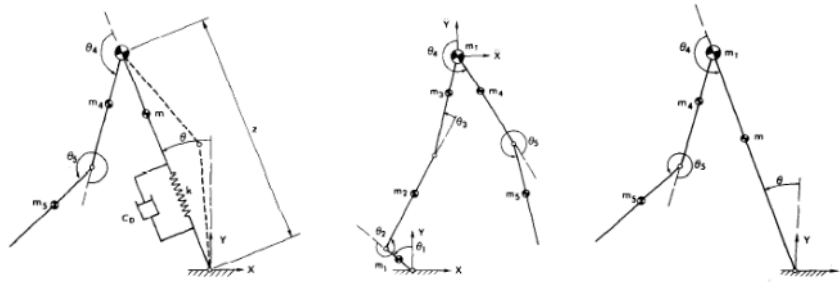


Figure 2.2: Examples of multi-segment models, incorporating springs and dampers (Pandy & Berme, 1988b)

The selection of these joint actuations and the initial conditions of the model are important factors that can have a large effect on the results of the simulation (Pandy & Berme, 1988b). Potentially, the trial and error method of exhaustive search could be used to select initial angles, velocities and spring/damping constants. This is understandable for the spring and damping coefficients because they have no anatomical equivalent and could potentially be non-linear. However, selecting the initial conditions of joint angles and angular velocities in this manner is very inefficient as data gathered from practical testing can be used (Siegler et al., 1982). This has the additional advantage of providing kinematic and kinetic data throughout the whole cycle, against which the model's performance can be judged. The best and most efficient way of determining these values however, is through the use of an optimising algorithm (Duan et al., 1997). Given an objective function to minimise/maximise, these algorithms will find the optimal values for the model parameters. A method of confirming that the most appropriate values for both initial states and actuations have been chosen is a sensitivity analysis (Pandy & Berme, 1988b). This is a systematic method that provides further confidence in the selections made.

A few studies have used pre-determined temporal functions to define how the joint actuations change over time, as they are observed to do so in gait laboratory experiments. One such study used basic step or ramp functions to do just this (Pandy & Berme, 1988b). Other methods of defining these curves, such as polynomials or Fourier series, may be able to achieve a moment profile curve closer to those recorded empirically.

Another feature of simple models is the necessity to make simplifications and assumptions. These are required in order to make the mathematics more tolerable but detrimentally affect the accuracy of the solution. This may include ignoring the effects of the swing leg (Siegler et al., 1982) or, if the swing leg is modelled, it might be decoupled from the stance leg (Pandy & Berme, 1988b). The justification for these assumptions is that the swing leg does not have a great effect on GRF.

A common problem seems to be how to model the foot. The foot-ground interaction has to be considered in order for the GRF is calculated correctly, and so does the pivoting mechanism to ensure that one or more of Perry's 'rockers' can be modelled correctly (Perry, 1992). These rockers are:

- Heel rocker: From the time of initial contact until foot flat.
- Ankle rocker: From the time of foot flat until heel rise.
- Forefoot rocker: From the time of heel rise until the metatarsal heads leave the ground.
- Toe rocker: From when the metatarsal heads leave the ground until toe off.

Many models have chosen to ignore the foot completely (Baker et al., 2004; Buczek et al., 2006; Duan et al., 1997; Kuo, 2007; Pandy & Berme, 1988b; Siegler et al., 1982) and hence they behave as if ankle rocker covers the whole cycle. Some have modelled feet as solid segments fixed perpendicular to the leg segments (Siegler et al., 1982) but this is still not very anatomically accurate. The best way to mimic the four rockers seems to be having separate models for each (Pandy & Berme, 1988b) and transition between them by taking the terminal state of the previous model as the initial state for the subsequent model.

One common use for simple models is inverse dynamics. This is the process of using kinematic and kinetic data recorded in practical experiments in order to calculate the joint forces and moments. This is done simply by way of Newton's laws.

There is some debate over the benefit of three-dimensional (3D) inverse dynamics when compared to the planar equivalent (2D). Some have observed little difference between the two methods, particularly when comparing '*inter-individual variation*', and hence

called for 2D to become the industry standard as this was the quicker and simpler of the two (Alkjaer et al., 2001). This opinion is directly contrasted by others who stress the benefits of the 3D method. It illustrates the importance of the work performed by the hip joint in the frontal plane to aid balance (Eng & Winter, 1995; Hardt & Mann, 1980) and gives the rotational patterns of the joints. That latter point is of particular importance to those studying and attempting to rehabilitate pathological gait. In cerebral palsy treatment, reducing rotational abnormalities is a priority so knowledge of this movement is paramount (Apkarian et al., 1989).

Although a conclusion to this debate has not been reached, the methods of investigation do add credence to the idea of sequentially increasing the complexity of subsequent models and analysing the perceived benefits.

A good judge of accuracy for a forward dynamics, simple model is to compare the results to those of practical experiments (Buczek et al., 2006; Pandy & Berme, 1988b; Siegler et al., 1982). This can be in terms of kinematics (joint angles etc.) or by calculating the kinetics (GRF). A good validation of the mathematics would be to then perform an inverse dynamics analysis to confirm that the calculated joint moments match the actuators applied. Often the comparison appears to be based purely on visual assessment of plots. A better gauge for a model's ability to simulate human walking would be to calculate numerical error values from the empirical data.

Other simple models can act simply as justification for developing a more complex one. Since complex models are more expensive, take longer to create and solve, and require much greater processing power, it is a good idea to develop a simpler model that can investigate a particular hypothesis and indicate whether it is an area worth exploring. Equally useful would be if the simple model refuted the hypothesis, thus saving time and money from being wasted.

The difficulty of deriving the equations of motion of a link segment system increases exponentially with the number of DOF accounted for. A generalised formula has been developed for an n-link open chain, using Newtonian mechanics (Pandy & Berme, 1988a). Constraints can also be added to the end effector of this chain in order to form a closed chain and model the double support phase of walking. A shortcoming of this formula is that it does not make concessions for either impact at the instant of foot contact or

branched segment chains, but this is not a problem with the mathematics, it is merely outside the scope of the algorithm. This particular technique will be discussed further in later chapters.

2.2 Complex models

The more complex models of walking provide a greater insight into the roles played by different muscles, muscle groups and tendons at different points in the gait cycle. From this information, stronger arguments can be made regarding the determinants of gait, thus helping to explain why people walk the way they do. With the ever-increasing power of computer processors, the length of time these types of models take to produce a solution will become much more manageable and they could potentially be used as an integral part of a patient's clinical assessment.

These are multi-segment, multiple DOF models that consider large numbers of individual muscle-like actuators, rather than just the joint actuations provided by the simple models. The difference is important as it illustrates how the joint moments were produced. For a participant with pathological gait, just knowing that they have a weak hip moment, for example, as a simple model could show, is not enough. A complex model could show which muscles were the cause of the weak hip moment and the appropriate treatment could be prescribed.

2.2.1 Muscle modelling

The involvement of muscles adds further to the complexity of the mathematics involved because now not only is an intricate dynamic system being accounted for but biological soft tissue behaviour must also be considered. Force-Length-Velocity relationships for each muscle must be represented so that the predicted performance of a given muscle is physically possible (Davy & Audu, 1987; Thelen & Anderson, 2006). Improvements have been shown when the same model evolves from treating muscle excitations as instantaneous (Thelen et al., 2003) to factoring in delays between activation and

excitation (Thelen & Anderson, 2006). Many models neglect to model the difference between fast and slow twitch muscles (Anderson & Pandy, 2003).

Some researchers have modelled the muscles using series-elastic springs, dampers and clutches (Davy & Audu, 1987; Endo & Herr, 2009), but the most common method is to use Hill-type '*musculotendon units*' (MTUs) (Anderson & Pandy, 2001a; Arnold et al., 2010; Endo & Herr, 2009; Jonkers et al., 2003; Yamaguchi & Zajac, 1990) as illustrated in Figure 2.3.

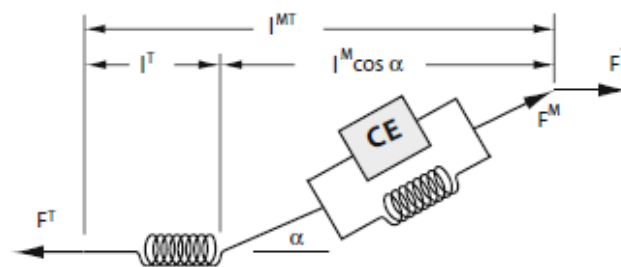


Figure 2.3: A Hill-type muscle model (Arnold et al., 2010)

In the same way that some models grouped together individual muscles into muscle groups (Davy & Audu, 1987; Yamaguchi & Zajac, 1990), it is also possible to divide the action of a single muscle into multiple actuators (Anderson & Pandy, 2001a). The benefit of this is that it provides a better anatomical representation of the muscle's geometry and the directions of the forces it produces.

The different methods of defining the muscle activation profiles are more numerous than those for the simple models. Some have used dynamic features, such as springs and series-elastic clutches (Endo & Herr, 2009), whereas other have defined the curves by functions. This has been attempted using a multitude of techniques including Fourier series, polynomials, first-order differential functions or a combination of discretisation and interpolation (Anderson & Pandy, 2001a, 2001b; Anderson & Pandy, 2003; Jonkers et al., 2003; Koh et al., 2009; Ren et al., 2007). The constants or coefficients required to define each of these representations are often selected by an algorithm built into the solution process.

2.2.2 Common assumptions

As with any type of modelling, simplifications and assumptions are often made. As with the simple models, a particularly troublesome area is the foot-ground contact. This has been approached by means of mass-spring-damper systems (Figure 2.4) being incorporated into the foot (Anderson & Pandy, 2001a; Yamaguchi & Zajac, 1990) or by carefully defining the shape of the foot (Ren et al., 2007) so that its rollover mechanism appears to mimic the four rockers (Perry, 1992).

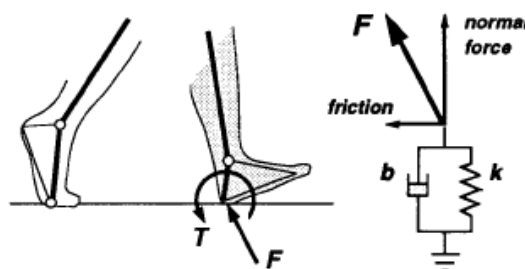


Figure 2.4: Example of mass-spring-damper mechanism to model foot contact (Yamaguchi & Zajac, 1990)

Whenever the head, arms and trunk (HAT) are modelled as a single segment, this nullifies any effect the swinging of the arms may have on the kinetics of walking. This is a widely used assumption in gait modelling (Anderson & Pandy, 2001b; Koopman et al., 1995; Ren et al., 2007; Yamaguchi & Zajac, 1990) where the focus is the lower extremities. Earlier investigations had been even simpler, ignoring HAT segments and the motion of the pelvis was predetermined by a fixed path (Davy & Audu, 1987).

Another common assumption is that of bilateral symmetry (Anderson & Pandy, 2001b; Ren et al., 2007). This means that only half a gait cycle need be simulated thus halving the processing required. In order to ensure this condition is met, constraints are often required so that the initial states of the right limbs are equivalent to the terminal states of the left limbs and vice versa.

When assumptions are made, Crowninshield (Crowninshield & Brand, 1981) emphasises the point that it is important to select the *'muscle prediction criteria based on physiological bases rather than on an arbitrary or mathematically convenient'* one.

2.2.3 Solution methods

Many different techniques have been used to solve complex walking models (Ren et al., 2006). Central Pattern Generators (CPG) have been used to mimic the interaction between the brain and the muscles/skeleton during walking (Ogihara & Yamazaki, 2001; Taga, 1995; Taga et al., 1991; Yamazaki et al., 1996). The state of the musculoskeletal system and its environment at a given time is sensed by the CPG. It will then produce the appropriate outputs that will activate the muscles in such a way so as to produce the desired motion. CPGs have associated values called '*connection weights*' that must be determined, either by trial and error (Taga et al., 1991) or optimisation (Taga, 1995). These types of models are exclusively forward dynamics problems and thus require large computational processing power. Whether or not this method is used by humans in reality is still debated (Duysens & Van De Crommert, 1998; Van De Crommert et al., 1998).

Another method is to use Control Engineering techniques. Popular in robotics studies, this can be used to track pre-determined joint trajectories (Hurmuzlu, 1993; Juang, 2000). The torque at the joints is adapted so as to produce the joint patterns. In practice, a drawback of this method is that it doesn't make any concessions for unexpected disturbances such as obstacles or external forces. By defining the controls to achieve a given performance criterion, rather than trajectory tracking, a quick controller has been shown to be able to overcome unexpected perturbations in practical robot experiments (Morimoto et al., 2003).

The idea that walking can be performed with zero joint moments, purely through ballistic behaviour is known as passive walking theory (McGeer, 1990; McMahon, 1984). This has been shown to be viable on a sloping floor (Garcia, Chatterjee, & Ruina, 1998; Goswami, 1999; Goswami et al., 1997; Goswami et al., 1998) but it has some shortcomings. The action of the HAT segment is not considered and all models are limited to the sagittal plane only. The argument of no muscle action also fails to explain how walking velocity can be determined (McMahon, 1984).

Another solution technique is to use an optimisation algorithm. After defining the initial conditions as the inputs to the algorithm, some parameters are chosen as the control variables. An objective function is also stated. The optimiser then uses an iterative

process, altering the control variables each time, to determine the values for which the objective function is at a minimum or maximum, depending upon the problem.

2.2.4 Static Optimisation

There are two different types of optimisation problem, known as static and dynamic. A static optimisation is one that occurs for a given time instant. At that time, given the data regarding joint angles and GRF, it is an indeterminate problem because there could be numerous muscle activation combinations that produce those results. The optimiser solves the indeterminate problem by calculating the kinetics according to an objective function, also known as cost functions.

The number of muscles a model replicates often depends upon the aims and solution techniques being used. Some solution methods, such as static optimisation, use little processing power and can solve quickly, meaning that it is possible to model large numbers of muscles without it being too detrimental to the solution time (Anderson & Pandy, 2001a). Such studies have previously considered anywhere between 30 and 50 different muscles and muscle groups (Arnold et al., 2010; Crowninshield & Brand, 1981; Glitsch & Baumann, 1997; Patriarco et al., 1981; Pedersen et al., 1997) as shown in Figure 2.5.

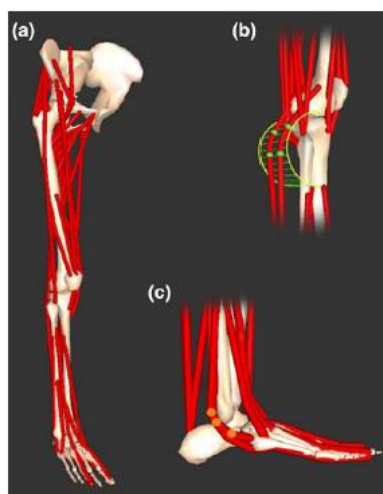


Figure 2.5: An example of a complex model incorporating a large number of individual muscles (Arnold et al., 2010)

A drawback of static optimisation, however, is that it is greatly dependent upon the accuracy of the input data, usually collected via gait lab tests. Another is that since the objective function for a static optimisation is inherently time-independent, this does not allow the overall aim of the entire walking cycle to be investigated (Anderson & Pandy, 2001b). In addition to these issues, if the problem is solved for a number of consecutive time instants, unrealistic discontinuities in muscle force could arise in the predictions as the solution is independent of those that have gone before it (Davy & Audu, 1987).

Static optimisation is common in inverse dynamics studies (Crowninshield & Brand, 1981; Glitsch & Baumann, 1997; Hardt, 1978; Pedersen et al., 1997; Röhrle et al., 1984). One investigation employed this method to examine the difference between 2D and 3D inverse dynamics using a complex walking model (Glitsch & Baumann, 1997). The findings of this study suggested that the 2D technique could underestimate total joint forces by up to 60%. This once more emphasises the point that increasing the complexity of consecutive models in small increments could provide knowledge that may otherwise be overlooked.

2.2.5 Dynamic optimisation

Dynamic optimisation is another method for gait simulation. This often involves forward dynamic techniques and is used to predict the motion of the model over a given time. Thus, in contrast to static optimising, the predictions made for late stance are dependent upon what has happened earlier in the cycle.

Since this method uses forward, rather than inverse dynamics, simulations require much more computational effort to achieve a solution and so large numbers of muscles would slow the process down considerably, making it impractical. These types of studies tend to use single actuations to represent the effort of muscle groups (e.g. iliopsoas, vasti, hamstrings, dorsiflexors etc.), which can still pinpoint a problem area for a participant, albeit not with the same precision. Typically these models will model ten or fewer muscle groups (Davy & Audu, 1987; Yamaguchi & Zajac, 1990) but more recent models have been able to utilise more powerful computers to consider over 20 individual muscles (Anderson & Pandy, 2001a; Jonkers et al., 2003).

They are predictive and have time-dependent objective functions. This means that novel movements can result and it is also possible to investigate the overall goal of a particular motor task (Ren et al., 2007; Thelen & Anderson, 2006). This can be particularly useful for those investigating motions other than walking (Hatze, 1981), where there is a more obvious measure of performance i.e. jumping higher, farther, etc.

This ability to produce novel motion can lead to physically impossible solutions being produced so it is often necessary to apply constraints to the joints of the model to avoid things like hyperextensions (Anderson & Pandy, 2001a, 2001b; Anderson & Pandy, 2003; Ren et al., 2007).

As mentioned, the types of objective functions differ between static and dynamic optimisations. Previous static optimisation works have used functions such as muscular endurance (Crowninshield & Brand, 1981), a fatigue criterion accounting for stride time, kinematics and joint forces and moments (Koopman et al., 1995), the sum of the squared muscle stresses (Glitsch & Baumann, 1997) or the sum of the cubed muscle stresses (Pedersen et al., 1997). Opinion seems to largely be in favour of the main goal of walking being to reduce the effort required from the muscles. A similar trend is apparent when the cost functions of dynamic optimisation studies are observed; metabolic expenditure per distance travelled (Anderson & Pandy, 2001a, 2001b; Anderson & Pandy, 2003), the sum of total work done by the muscles and enthalpy change during contraction (Davy & Audu, 1987), the mechanical energy cost (Channon et al., 1992; Marshall et al., 1989; Ren et al., 2007; Yen & Nagurka, 1987).

Other optimisations will be defined so that they track a data set gathered from laboratory testing and the judgement of performance will come from how well other predictions match another data set. For example, the muscle forces are controlled so that the kinematics of the joint angles correlate with their empirical counterparts. Then a comparison can be made between these predicted muscle forces and experiment EMG recordings (Thelen & Anderson, 2006). Equally, the EMG readings could be tracked to observe whether the correct kinematics result (Jonkers et al., 2003). There are many ways of comparing the tracking errors and quantifying the error for the performance criterion. Such examples include incorporating static optimisation within a dynamic one (Thelen & Anderson, 2006) or a simple least squares method (Cappozzo et al., 1975).

2.3 Validation

With any simulation it is important to provide validation so that the results can be considered accurate. The most common way to do this is by means of experimental data captured in a gait laboratory. In the world of gait modelling, a low number of participants is quite common, perhaps only five or six (Anderson & Pandy, 2001a, 2001b; Anderson & Pandy, 2003; Crowninshield et al., 1978; Patriarco et al., 1981). Some studies have only used a single participant (Glitsch & Baumann, 1997; Pedersen et al., 1997). The justification for these low numbers is that often it is the performance of the model that is being examined, as opposed to some hypothesis regarding a particular group of participants. In fact, it could be argued that a large number of participants could be detrimental to the simulations. Gait data is often captured and presented in terms of *'percentage of the gait cycle'* rather than in terms of absolute time. The instances at which certain gait events occur varies between participants so taking a data curve averaged across multiple participants could potentially be less representative than using a single person's data. In clinical applications, the model would only be used for an individual participant anyway.

Gait analysts used to capture the motion of the participant by attaching LEDs to specified anatomical landmarks and, from the path of these LEDs captured by cameras, the segment positions and joint angles could be calculated (Crowninshield et al., 1978; Röhrle et al., 1984). More recently, researchers have been able to use reflective markers that are tracked by infra-red cameras to perform this same task (Anderson & Pandy, 2001a; Anderson & Pandy, 2003; Glitsch & Baumann, 1997; Pedersen et al., 1997). For the kinetics, almost all studies will use a walkway instrumented with force plates to record the GRF and perform multiple trials per participant, although it is possible that even intra-participant averaging could lessen accuracy. Many will also record electromyographic (EMG) data to provide knowledge of the temporal changes in the activation of different muscles (Anderson & Pandy, 2001a; Anderson & Pandy, 2003; Crowninshield et al., 1978; Davy & Audu, 1987; Glitsch & Baumann, 1997; Patriarco et al., 1981; Pedotti, 1977;

Yamaguchi & Zajac, 1990). Information detailing the best ways to perform such experiments is readily available (Delagi & Perotto, 1980).

The anatomical parameters, such as segment lengths and the participant's height and weight can be measured in the gait lab, thus making the model participant specific. Generic values, as well as information gathered from cadaver studies regarding the inertial properties of different body segments, can be found in previous works (Crowninshield et al., 1978; Winter, 1979). These data sources are widely accepted and used in other works (Yamaguchi & Zajac, 1990) due to the difficulties and administrative processes involved in obtaining permission for cadaver studies.

2.4 Case study

A key body of work in the field of complex, dynamic optimisation modelling is that of Anderson and Pandy. A single complex model they developed has provided numerous insights in multiple studies (Anderson & Pandy, 2001a, 2001b; Anderson & Pandy, 2003; Pandy, 2003).

The model in question was a three-dimensional, 23 DOF model with 54 active MTUs (Figure 2.6). It was made up of ten segments. The pelvis was a single rigid segment with six DOF, the head, arms and torso were modelled as a single rigid body (HAT) and the other eight segments were divided evenly between the two legs. The feet consisted of hindfoot and forefoot segments. The muscles were defined appropriately to best represent the anatomical structure. The HAT segment was controlled by six back and abdominal muscles and each leg had 24 muscles to control it. Certain muscles, such as the gluteus maximus and gluteus medius/minimus, had to be separated into two separate actuators due to the complex geometry at their pelvic origin. This assumption meant the model could better replicate their actions.

metabolic energy divided by the anterior-posterior displacement of the CM. The energy used by each muscle was the sum of basal metabolic heat, shortening heat, activation heat, maintenance heat and mechanical work. A penalty function was included in the cost function to avoid joint hyperextension. The authors were keen to highlight that their model was not given a *'tracking'* problem; that is to say the kinematic motion was not strictly defined. Instead, only initial and final conditions were set.

One of its first uses was to investigate the differences between static and dynamic solutions and to justify the use of each for different scenarios (Anderson & Pandy, 2001b). Firstly, a dynamic simulation was performed. The cost function to be minimised was metabolic energy per unit of distance travelled with the constraint being that it had to produce a cyclic gait pattern. The activation profiles of the muscles were defined by first-order differential functions. There were two different static problems set up, relating to the way in which the muscles were modelled. In the first one, they behaved as ideal force generators; in the second they were constrained by their respective force-length-velocity profiles. In both cases, the joint moments produced by the forward dynamic solution were the inputs, the muscle activations were the variables and the sum of the squares of the muscle activations was the objective function to be minimised. The results showed a good agreement between all the models. This led the authors to conclude that, if the inverse dynamics problem can be solved accurately, the use of predictive dynamic optimisation over static is not justifiable. However in situations where accurate experimental data is unavailable or a time-dependent performance criterion is desired then it is very useful. The key conclusion the authors draw is that the two methods should complement one another.

The dynamic model was also compared to the gait lab data to see how well it was able to predict the basic kinematics and ground reaction forces (Anderson & Pandy, 2001a), as well as the individual muscle contributions to gait (Anderson & Pandy, 2003). Each muscle excitation history was defined by discretised *'control nodes'*. These were spread at equal time intervals across the excitation history and interpolated between. The values of all these nodes, as well as the initial values of each muscle excitation, were used as the control parameters in the dynamic optimisation. Once again, the cost function was minimising metabolic energy expenditure per unit distance travelled.

The results of this model were relatively close to the experimental data. In contrast to Pandy's double inverted pendulum model, which suggested that the first and second peaks in the vertical ground reaction force were caused by mechanisms at the knee and ankle respectively, the more complex model claimed it was hip and ankle mechanisms respectively (Pandy, 2003). This difference is explained by the increased complexity. Where the complex model is able to perform all six determinants of gait (Saunders et al., 1953), the double inverted pendulum can only reproduce three of them.

Upon closer inspection however there were some flaws. Although the predicted vertical component of GRF displayed the double peak shape, it contained a lot of spikes and was not a smooth curve like the empirical data. In addition to this, the contributions of "*inertial forces*", "*centrifugal forces*", "*muscle forces*" etc. appeared to rise or drop instantaneously at milestones such as heel rise and contralateral heel strike.

A large kinematic anomaly was the excessive transverse pelvic rotation around heel strike. The explanation for this is the heel-strike force required to decelerate the swing leg. The participants did not exhibit this behaviour in the practical testing which suggests there is a more sophisticated method used by humans than the model is able to replicate.

The explanation proffered for the spikes and discontinuities in ground reaction force components was due to the way in which the foot was modelled when in contact with the ground. A mass-spring-damper system was used. The model also predicted the metabolic energy consumption rate to be much greater than the results published elsewhere. This was explained by a lack of arm swing in the model and simplifications made in muscle modelling. For example, considerations of the difference between fast and slow twitch muscles were not made. They also state that, despite over 10,000 hours of processing time, it is possible that the solution hadn't completely converged.

In spite of these drawbacks, most of the kinematic behaviour of the simulation appeared close to reality. This suggested that minimum metabolic energy expenditure per distance travelled may indeed be a valid criterion for walking. They were also able to postulate the individual contributions of the different muscles of the lower limbs at different times in the gait cycle and although the magnitudes may not have been perfect due to spikes and step changes, the general proportions make good references for future work, particularly when EMG data is unavailable.

A slightly modified version of this model was used by Thelen and Anderson (2006) to investigate whether it could be solved within a more manageable time. The body was now modelled as an eight segment, 21 DOF structure, actuated by 92 MTUs. A number of extra considerations were made when solving the model. They state that due to measurement errors in practical data captured for comparison and modelling assumptions, kinematics and kinetics are often dynamically inconsistent. This means that models will predict extra, external forces known as residual forces. They hoped to produce a dynamically more consistent model by using a '*residual elimination algorithm (REA)*' and taking into consideration time delays between muscle excitation and activation.

The solving method was unique too. They used a '*computed muscle control (CMC)*' algorithm. This meant using the joint angle errors (when compared to those recorded from ten healthy male participants) at a given time to calculate the appropriate angular acceleration of the joint required, so as to match the joint angles at the next time instant. Muscle activation and contraction dynamics were integrated from the previous time step to work out the upper and lower bounds on the force that each muscle could produce at the current time step. A static optimisation was then used to calculate the appropriate muscle forces needed to achieve the necessary joint angular accelerations, by means of the equations of motion. This process was repeated for every time interval.

The results showed that the kinematic root mean-squared (RMS) errors were mostly less than 1° and the predicted muscle activation profiles, visually, appeared fairly consistent with the experimental data. It is important to highlight, however, that this method is a tracking problem, whereas the previous studies (Anderson & Pandy, 2001a; Anderson & Pandy, 2003) used a performance based dynamic optimisation which can produce novel motions.

2.5 Discussion

Simple mathematical models are good for giving generalised ideas of the purposes of different gait mechanisms. Also, by the absence of a mechanism, they can postulate the effects of these. Some good studies will postulate the effect of a mechanism and then

create a new model that incorporates it, validating the prediction (Pandy & Berme, 1988b). Where they struggle is in identifying the functions of specific muscles. The results are also affected by considerable assumptions.

Complex models give much clearer ideas of reality and are more anatomically representative. The results of complex model studies still have irregularities though and their causes are not fully understood. A good summary of their pros and cons, as well as the considerations they have to make, is given by Otten (2003).

Pandy quite nicely summarises the roles played by both simple and complex models in his paper comparing an inverted pendulum model, a double inverted pendulum model and a complex model (Pandy, 2003). It was stated that simple models "*identify basic features of muscle function*" and complex models "*discern the functional roles of specific muscles in movement*".

An interesting point to note is that the simple models of gait vary between active (Buczek et al., 2006) and passive (Garcia, Chatterjee, Ruina, et al., 1998; Siegler et al., 1982; Zhe et al., 2008), whereas the complex models are almost all active and require muscle action to be modelled. This is a strong indication that walking is in fact an active process but is performed in such a way that energy expenditure is minimal. This gives further credence to those studies that minimised the energy used to travel a given distance as their measure of performance (Anderson & Pandy, 2001a; Anderson & Pandy, 2003; Ren et al., 2007).

These different models employ different techniques as well. Inverse dynamics is very useful in both simple and complex numerical models, although there is some debate about the extent to which model complexity has an effect on the results given (Alkjaer et al., 2001; Apkarian et al., 1989; Eng & Winter, 1995).

The optimisation of kinematic and kinetic parameters is becoming a very popular method in gait analysis and it seems that future studies will become dependent upon it. This can be a time consuming process, particularly for the predictive, forward dynamics models, but produces worthwhile results.

It should be considered important to quantify the performance of a model so that fair comparisons can be made. One way to do this would be to make RMS comparisons

between the empirically captured data and the predictions of the simulation (Koh et al., 2009; Thelen & Anderson, 2006).

Very little work appears to have been done to transition from the simple to the complex models. This is true for both the complexity of the dynamics of the model and for the sophistication of the techniques used to provide the solutions. A gradual increase in the dynamic complexity would help highlight the effects that can be attributed to an individual mechanism, providing numerical justification for gait determinants. Advanced solution techniques applied to simple models could also potentially provide better solutions and provide insights previously unobserved.

2.6 Research questions and project aims

This project will begin by investigating the simplest model of normal human gait, the inverted pendulum, and incrementally augment the complexity of each subsequent model. This will be achieved by increasing the number of DOF accounted for and by incorporating complex modelling techniques, such as dynamic optimisation. The following questions are to be investigated:

1. *What are the strengths and weaknesses of the inverted pendulum for predicting the sagittal kinematics and kinetics of healthy human walking?*
2. *To what extent can a sequence of numerical models, incrementally increasing in complexity, highlight the effects of different gait mechanisms?*
3. *What is the minimum complexity required for a numerical model to predict the kinematics and kinetics of healthy sagittal bipedal gait, within a single standard deviation range*
 - a. *for one-legged single support?*
 - b. *for two-legged single support?*

c. for the full gait cycle?

4. Considering interpersonal differences, the time cost and the solution accuracy, how close is gait modelling to becoming a clinically usable tool?

For clarification, 'gait mechanisms', as referenced in Research Question 2, are defined as any traits, be they kinematic (e.g. knee flexion) or kinetic (e.g. the double peaks of the vertical GRF curve), that are characteristic of healthy human walking.

Figure 2.7 once more shows the outline for the thesis but now includes information on where each of the research questions will be addressed.

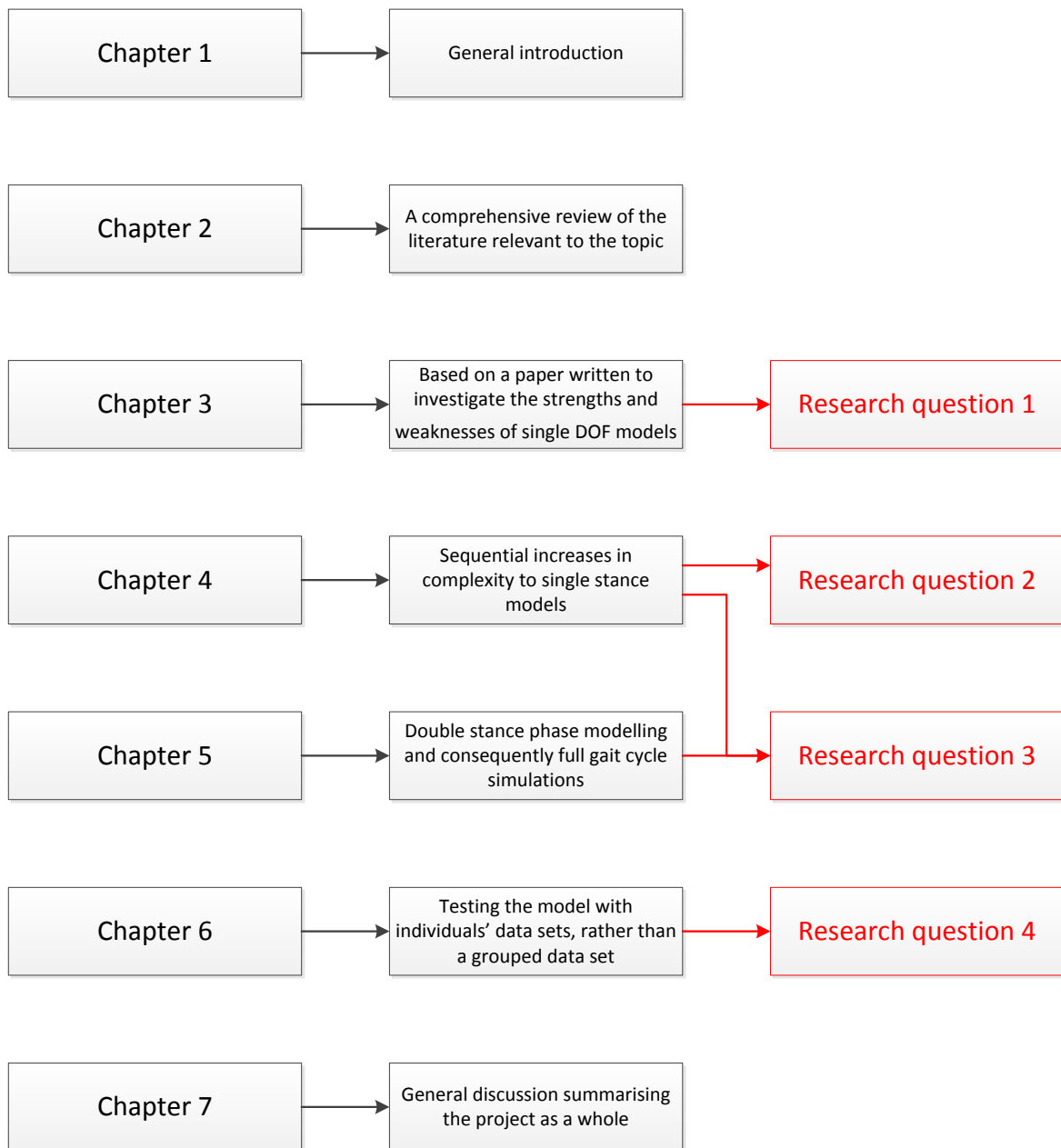


Figure 2.7: A summary of the outline of the thesis and where each research question will be addressed

3 SIMPLE MODELS

3.1 Introduction

The aim of this chapter is to answer the first research question regarding the advantages and disadvantages to approximating human walking to an inverted pendulum.

In terms of the thesis as a whole, the findings of this chapter will provide a good foundation for further chapters to build upon. The work here will highlight in what areas the simplest models of walking provide good approximations of reality, and in which areas they perform inadequately. This will provide a justifiable focus for future model development.

In addition, another outcome of the work with simple models will be to help establish a successful framework for further examination of more complex and unpredictable models. The second research question is regarding the effects of sequentially modelling and having a consistent investigation protocol for all models will also give credence to the findings. The framework proposed will start by outlining the specifics of the particular link-segment model being investigated, such as DOF, constraints etc. All models will have the foot-ground interaction as a workless constraint. Lagrangian mechanics will then be used to generate the equations of motion of that dynamic system. These equations of motion will be numerically integrated over a given time period during a simulation, tracking specific aspects of a clinical dataset (for this chapter, walking velocity is the focus). Finally, the outputs of the simulation will be compared to other aspects of the clinical dataset (e.g. kinematics and kinetics) to assess the ability of that model to predict healthy gait.

In this chapter, the approach will be to firstly appraise the relevant literature on the topic of inverted pendulum dynamics to develop an understanding of the current state of the art. Next the two models to be tested will be illustrated and described before the mathematical framework of the two models is outlined. This will include derivations of the equations of motion, an explanation of the numerical integration procedure and the relevant equations for calculating properties such as Ground Reaction Force (GRF). The simulation setup will be described next before the results for each of the simulations will

be given. Finally, there will be a discussion of what can be drawn from the results and some concluding remarks.

This chapter has been submitted for publication as a full paper to Gait and Posture.

3.2 Literature

One of the first mentions of the term “inverted pendulum” (IP) as a model of the stance phase of walking was by Cavagna et al. (1976) although similar concepts can be traced much earlier ((Alexander (1976); Elftman (1966); Saunders et al. (1953)). More recently the IP has formed the basis of a growing body of work associated with the Dynamic Walking movement (summarised by Kuo, 2007) which is based on principles first elucidated by Mochon and McMahon (1980) and subsequently by Tad McGeer (1990; 1993). Recent work of this group has tended to focus on the transitions from one step to the next (Donelan et al., 2002a; Donelan et al., 2002b; Kuo et al., 2005). The group, as well as other researchers, have presented several extended versions of IP models including springs, dampers, telescopic actuators, additional segments and joints. (Ankarali et al., 2012; Hong et al., 2013; Kim & Park, 2011; Koolen et al., 2012; O'connor & Kuo, 2007; Srinivasan, 2010).

This work has focussed on energetics and stability whereas the kinematics and kinetics of movement are more relevant to most clinical biomechanists and are less well understood. The mechanics of the IP itself (as opposed to the transitions) were presented briefly by Anderson and Pandy (appendix of 2003) who gave a brief description of the GRF. A more comprehensive comparison with gait data by Buczek et al. (2006) concluded that the IP predicts the anterior velocity of the whole body CM and anterior component of the GRF reasonably well but not the vertical components.

The aim of this chapter is thus to build on the work of Buczek et al (2006) in extending the ideas of the Dynamic Walking Group into the domain of clinical biomechanics. This includes extending their analysis to include fast and slow walking velocities and the IP model to include a hip joint controlled by a joint actuator in such a way as to maintain an upright trunk. Whilst this is unlikely to affect the overall dynamics of the system (it is still a one DOF system) it will allow an investigation of the extent to which hip flexor and

extensor activity measured using inverse dynamics during normal walking can be attributed to the requirements of an IP model. There is considerable current interest in the decomposition of the GRF to investigate the function of different muscles (Anderson & Pandy, 2003; Francis et al., 2013; Liu et al., 2006) and the analysis of the IP model has been extended to evaluate the contribution of the hip actuator to the GRF.

3.3 The Models

Figure 3.1a shows the free body diagram for Model 1. The inertial properties of the IP have been altered from the *'traditional'* IP models (Buczek et al., 2006). Previously the entire mass of the body acted at a single point at the end of the pendulum. For this model, the total mass has been redistributed to two separate points so now the *'leg'* has been assigned a mass (m_1), with the CM at a point a given distance (d_1) from the pivot, and moment of inertia (I_1). This change was motivated by the desire for the mass properties of the leg to be the same in both models to avoid an associated confounding effect. The mass of the rest of the body (m_2) acts at a single point at the *'hip joint'*, a given distance (l_1) from the pivot. The mass at the hip has zero moment of inertia. The anterior-posterior direction is defined as the x axis and the vertical direction is defined as the y axis.

Using information taken from Winter (1979, 1991), all data regarding lengths, distance and mass distributions were taken for a person of 1.80m height and 80 kg mass (Table 3.1; see also Appendix A.1). The position of the IP was specified by the angle that its axis of symmetry makes with the vertical (θ_1).

Figure 3.1b shows the free body diagram for Model 2 which consists of two segments of lengths l_1 and l_2 . The inertial properties of the two segments are specified by the respective masses (m_1 and m_2) and moments of inertia (I_1 and I_2) of the respective CMs, which are located at defined distances from the distal ends of the segments (d_1 and d_2). The positions of each segment are specified by the angles that their longitudinal axes make with the vertical (θ_1 and θ_2). A hip moment, M , is applied at the joint between the

two segments. The equations of motion for Model 2 can be derived, as can the formulae for the horizontal and vertical components of the GRF.

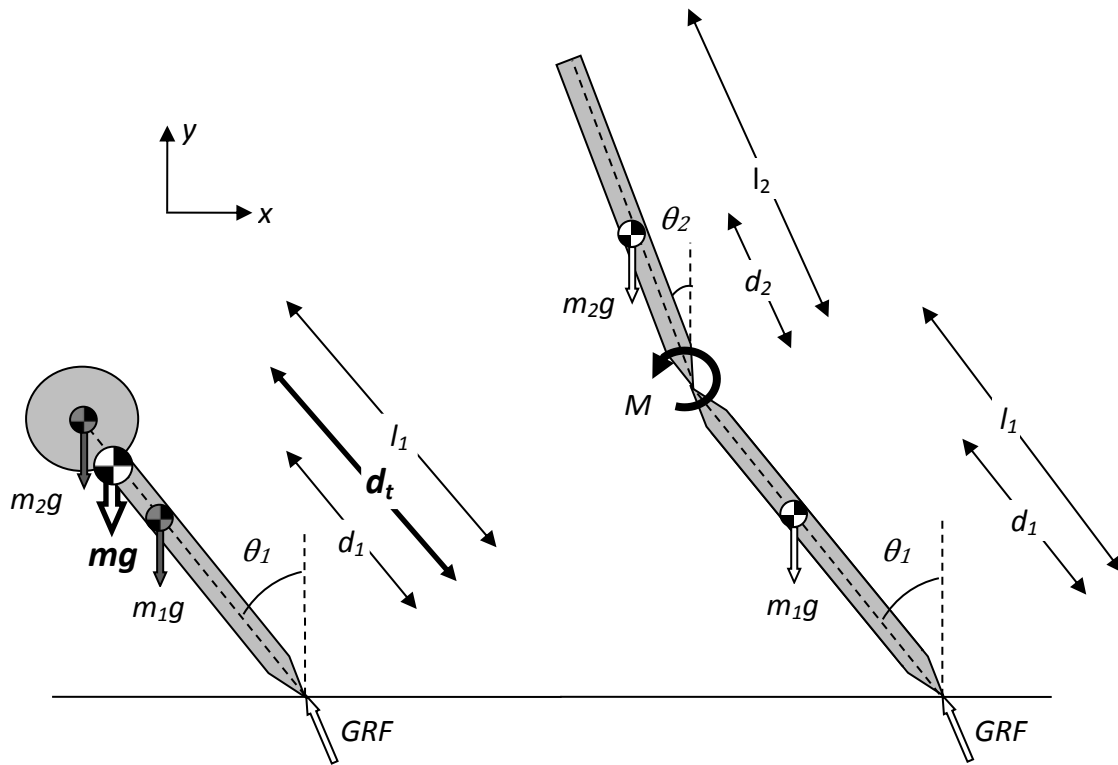


Figure 3.1: Free body diagrams for a) Model 1 (including the calculation approximations in bold) and b) Model 2.

3.4 The Modelling Framework

3.4.1 Lagrangian Dynamics

Lagrangian dynamics was selected to derive the equations of motion for the models in this study. This was deemed preferable to other methods, such as Newtonian dynamics, because it works independent of co-ordinate frame and uses energy calculations, as opposed to forces and moments, hence requiring less prior knowledge of the entire system. Previous studies that have detailed the Newtonian mechanics used, required the GRF to be measured or specified as a function of the kinematics (Pandy & Berme, 1988a,

1988b). This is avoided in Lagrangian mechanics as the ground contact is modelled as a workless constraint.

Equation 3.1 gives the governing equation for Lagrangian mechanics (Onyshko & Winter, 1980):

$$\frac{d}{dt} \frac{\partial L}{\partial \dot{\theta}} - \frac{\partial L}{\partial \theta} = 0$$

Equation 3.1

The term ' L ' is the Lagrange function and is defined as the difference between the kinetic energy of the system, T , and the potential energy, V . Calculating these values allows the equations of motion for a given system to be derived.

The equations of motion for Model 1 are derived first. In order for this to be done, the two masses are equated to a single mass (m) with a given moment of inertia (I), acting at a given distance from the pivot (d_t).

$$m = m_1 + m_2$$

$$d_t = \frac{(m_1 d_1 + m_2 l_1)}{(m_1 + m_2)}$$

$$I = (I_1 + m_1(d_t - d_1)^2) + (I_2 + m_2(l_1 - d_t)^2)$$

Equations 3.2, 3.3, 3.4

Next the kinetic and potential energy values of the system are calculated.

$$T = \frac{1}{2}mv^2 + \frac{1}{2}I\omega^2$$

$$V = mgh$$

$$L = T - V$$

$$\therefore L = \frac{1}{2}md_t^2\dot{\theta}^2 + \frac{1}{2}I\dot{\theta}^2 - mgd_t \cos \theta$$

Equation 3.5, 3.6, 3.7

Partial differentials of L with respect to $\dot{\theta}_i$, θ_i are taken in order to evaluate the variables in the Lagrange governing equation (Equation 3.1).

$$(md_t^2 + I)\ddot{\theta} - mgd_t \sin \theta = 0$$

$$\therefore \ddot{\theta} = \frac{mgd_t}{(md_t^2 + I)} \sin \theta$$

Equation 3.8

This is decomposed into two terms. These are the acceleration due to gravity, which is a function of angular position, and the acceleration due to centripetal effects, which is a function of angular position and velocity.

$$\ddot{\theta}_G = \frac{mgd_t}{(md_t^2 + I)} \sin \theta$$

$$\ddot{\theta}_C = 0$$

Equations 3.9, 3.10

The derivation of the equations of motion for Model 2 is slightly more complicated. Initially, it is treated as a two segment open chain, with two DOF. The addition of the hip joint moment later will reduce it to a one DOF system.

The governing Lagrange equation for a model with an actuated joint is shown below (Equation 3.11). Without any external input, the right hand side of the equation would be zero (as in Equation 3.1), but these models are to be actuated by joint moments, M_i , so the effects of these on the DOF must be incorporated.

$$\frac{d}{dt} \left(\frac{\partial L}{\partial \dot{q}_i} \right) - \frac{\partial L}{\partial q_i} = Q_i$$

Equation 3.11

Where Q_i are the generalised forces derived from a consideration of virtual work (δw):

$$\delta w = \sum_i Q_i \delta q_i$$

Equation 3.12

Where δq_i refers to the change in the state vector. The two obvious choices for q_i are joint angle (φ_i) or segment angle (θ_i) to the vertical.

$$\delta w = \sum_i -M_i \delta \varphi_i = \sum_i M_i (\theta_{i-1} - \theta_i) = \sum_i (M_{i+1} - M_i) \theta_i$$

Equation 3.13

This would mean Q_i is equal to $-M_i$ if joint angles are used or $M_{i+1} - M_i$ if the segment angles to the vertical are used. Although selecting the joint angles as the reference decouples the generalised force terms, it makes the functions for the energy calculations much more complex. Consequently, segment angles to the vertical are preferable and will be used throughout this thesis.

Now the derivation of the governing equation can begin by evaluating the kinetic and potential energy values. To do this, the cartesian coordinates of the masses are considered:

$$\begin{aligned} x_1 &= -d_1 \sin \theta_1, & y_1 &= d_1 \cos \theta_1 \\ x_2 &= -l_1 \sin \theta_1 - d_2 \sin \theta_2, & y_2 &= l_1 \cos \theta_1 + d_2 \cos \theta_2 \end{aligned}$$

Equations 3.14, 3.15, 3.16, 3.17

The linear velocities of the masses are defined by the first derivatives.

$$\begin{aligned}\dot{x}_1 &= -d_1 \cos \theta_1 \dot{\theta}_1, & \dot{y}_1 &= -d_1 \sin \theta_1 \dot{\theta}_1 \\ \dot{x}_2 &= -l_1 \cos \theta_1 \dot{\theta}_1 - d_2 \cos \theta_2 \dot{\theta}_2, & \dot{y}_2 &= -l_1 \sin \theta_1 \dot{\theta}_1 - d_2 \sin \theta_2 \dot{\theta}_2\end{aligned}$$

Equations 3.18, 3.19, 3.20, 3.21

The resultant velocities are calculated.

$$\begin{aligned}v_1^2 &= \dot{x}_1^2 + \dot{y}_1^2 = d_1^2 \dot{\theta}_1^2 \\ v_2^2 &= \dot{x}_2^2 + \dot{y}_2^2 = l_1^2 \dot{\theta}_1^2 + d_2^2 \dot{\theta}_2^2 + 2l_1 d_2 \dot{\theta}_1 \dot{\theta}_2 \cos(\theta_1 - \theta_2)\end{aligned}$$

Equations 3.22, 3.23

Kinetic and potential energy calculations allow the Lagrangian function to be evaluated.

$$\begin{aligned}T &= \frac{1}{2} m v^2 + \frac{1}{2} I \omega^2 \\ &= \frac{1}{2} m_1 v_1^2 + \frac{1}{2} I_1 \dot{\theta}_1^2 + \frac{1}{2} m_2 v_2^2 + \frac{1}{2} I_2 \dot{\theta}_2^2 \\ &= \frac{1}{2} m_1 d_1^2 \dot{\theta}_1^2 + \frac{1}{2} I_1 \dot{\theta}_1^2 + \frac{1}{2} m_2 (l_1^2 \dot{\theta}_1^2 + d_2^2 \dot{\theta}_2^2 + 2l_1 d_2 \dot{\theta}_1 \dot{\theta}_2 \cos(\theta_1 - \theta_2)) + \frac{1}{2} I_2 \dot{\theta}_2^2 \\ &= \frac{1}{2} \dot{\theta}_1^2 (m_1 d_1^2 + m_2 l_1^2 + I_1) + \frac{1}{2} \dot{\theta}_2^2 (m_2 d_2^2 + I_2) + \dot{\theta}_1 \dot{\theta}_2 (m_2 d_2 l_1 \cos(\theta_1 - \theta_2))\end{aligned}$$

$$V = mgh$$

$$\begin{aligned}&= (m_1 d_1 g \cos \theta_1) + (m_2 (l_1 g \cos \theta_1 + d_2 g \cos \theta_2)) \\ &= (m_1 d_1 + m_2 l_1) g \cos \theta_1 + (m_2 d_2) g \cos \theta_2\end{aligned}$$

$$\therefore L = T - V$$

$$\begin{aligned}&= \frac{1}{2} (m_1 d_1^2 + m_2 l_1^2 + I_1) \dot{\theta}_1^2 + \frac{1}{2} (m_2 d_2^2 + I_2) \dot{\theta}_2^2 + m_2 l_1 d_2 \cos(\theta_1 - \theta_2) \dot{\theta}_1 \dot{\theta}_2 - (m_1 d_1 + m_2 l_1) g \cos \theta_1 \\ &\quad - m_2 d_2 g \cos \theta_2\end{aligned}$$

Equations 3.24, 3.25, 3.26

Partial differentials of L with respect to $\dot{\theta}_i, \theta_i$ are taken in order to evaluate the variables in the Lagrange function.

$$\frac{\partial L}{\partial \dot{\theta}_1} = \dot{\theta}_1(m_1 d_1^2 + m_2 l_1^2 + I_1) + \dot{\theta}_2(m_2 d_2 l_1 \cos(\theta_1 - \theta_2))$$

$$\frac{d}{dt} \left(\frac{\partial L}{\partial \dot{\theta}_1} \right) = \ddot{\theta}_1(m_1 d_1^2 + m_2 l_1^2 + I_1) + \ddot{\theta}_2(m_2 d_2 l_1 \cos(\theta_1 - \theta_2)) - \dot{\theta}_2(\dot{\theta}_1 - \dot{\theta}_2)(m_2 d_2 l_1 \sin(\theta_1 - \theta_2))$$

$$\frac{\partial L}{\partial \theta_1} = -\dot{\theta}_1 \dot{\theta}_2(m_2 d_2 l_1 \sin(\theta_1 - \theta_2)) + (m_1 d_1 + m_2 l_1) g \sin \theta_1$$

Equations 3.27, 3.28, 3.29

$$\frac{\partial L}{\partial \dot{\theta}_2} = \dot{\theta}_2(m_2 d_2^2 + I_2) + \dot{\theta}_1(m_2 d_2 l_1 \cos(\theta_1 - \theta_2))$$

$$\frac{d}{dt} \left(\frac{\partial L}{\partial \dot{\theta}_2} \right) = \ddot{\theta}_2(m_2 d_2^2 + I_2) + \ddot{\theta}_1(m_2 d_2 l_1 \cos(\theta_1 - \theta_2)) - \dot{\theta}_1(\dot{\theta}_1 - \dot{\theta}_2)(m_2 d_2 l_1 \sin(\theta_1 - \theta_2))$$

$$\frac{\partial L}{\partial \theta_2} = \dot{\theta}_1 \dot{\theta}_2(m_2 d_2 l_1 \sin(\theta_1 - \theta_2)) + (m_2 d_2) g \sin \theta_2$$

Equations 3.30, 3.31, 3.32

From these calculations and Equation 3.11, the equations of motion can be written in matrix form.

$$B \cdot \ddot{\theta}_i = C \quad \text{where,} \quad \begin{pmatrix} b_{11} & b_{12} \\ b_{21} & b_{22} \end{pmatrix} \begin{pmatrix} \ddot{\theta}_1 \\ \ddot{\theta}_2 \end{pmatrix} = \begin{pmatrix} c_1 + M \\ c_2 - M \end{pmatrix}$$

Equation 3.33

Where:

$$b_{11} = (m_1 d_1^2 + m_2 l_1^2 + I_1)$$

$$b_{22} = (m_2 d_2^2 + I_2)$$

$$b_{12} = b_{21} = m_2 l_1 d_2 \cos(\theta_1 - \theta_2)$$

$$c_1 = -m_2 l_1 d_2 \sin(\theta_1 - \theta_2) \dot{\theta}_2^2 + (m_1 d_1 + m_2 l_1) g \sin \theta_1$$

$$c_2 = m_2 l_1 d_2 \sin(\theta_1 - \theta_2) \dot{\theta}_1^2 - m_2 d_2 g \sin \theta_2$$

From Equation 3.33, M is calculated so as to enforce the constraint that the angular acceleration of segment 2 is zero. When the value of M is known, this leads to a single equation of motion to calculate the angular acceleration of segment 1. Using the same method as Model 1, this acceleration is divided into gravity, centripetal and muscle terms.

3.4.2 Numerical integration

The equations of motion calculate the angular accelerations of each of the DOF to be calculated for a given time instant. For a forward dynamic simulation, these acceleration values must be used to calculate the subsequent angular position and velocity values for the next time instant. The new angular position and velocity values are then put into the equations of motion to calculate a new angular acceleration. This cycle is repeated iteratively for a desired number of time instants.

In this study, the method, by which the new angular positions and velocities are calculated, is a numerical integration, based on a Taylor expansion.

$$f(t + dt) = f(t) + f'(t)dt + \frac{1}{2!}f''(t)dt^2 + \frac{1}{3!}f'''(t)dt^3 \dots$$

Equation 3.34

$$\theta(t + dt) = \theta(t) + \dot{\theta}(t)\Delta t + \frac{1}{2}\ddot{\theta}(t)\Delta t^2 + \frac{1}{6}\ddot{\theta}(t)\Delta t^3 \dots$$

Equation 3.35

Given that:

$$\ddot{\theta}(t) \approx \frac{\ddot{\theta}(t) - \ddot{\theta}(t - \Delta t)}{\Delta t}$$

Equation 3.36

Therefore the following estimation of the next angular position is made.

$$\theta(t + dt) \approx \theta(t) + \dot{\theta}(t)\Delta t + \left(\frac{1}{2}\ddot{\theta}(t) + \frac{1}{6}(\ddot{\theta}(t) - \ddot{\theta}(t - \Delta t)) \right) \Delta t^2$$

Equation 3.37

Similarly, the next angular velocity value is evaluated.

$$\begin{aligned} \dot{\theta}(t + \Delta t) &= \dot{\theta}(t) + \ddot{\theta}(t)\Delta t + \frac{1}{2}\ddot{\theta}(t)\Delta t^2 \\ \dot{\theta}(t + \Delta t) &\approx \dot{\theta}(t) + \left(\ddot{\theta}(t) + \frac{1}{2}(\ddot{\theta}(t) - \ddot{\theta}(t - \Delta t)) \right) \Delta t \end{aligned}$$

Equations 3.38, 3.39

3.4.3 Ground reaction force calculations

In order to properly assess the kinetic performance of each simulation, the vertical and horizontal components of the GRF are to be evaluated and compared to experimental measurements.

Starting with Model 1 and taking inspiration from Anderson and Pandy (2003) who applied Newton's second law to determine the components of the ground reaction in the vertical direction, this approach can be extended to determine the horizontal component as well:

$$\begin{aligned} GRF_x &= m\ddot{x} \\ GRF_y &= mg + m\ddot{y} \end{aligned}$$

Equations 3.40, 3.41

Substituting expressions for \ddot{x} and \ddot{y} :

$$\begin{aligned} \ddot{x} &= -\ddot{\theta}d_t \cos\theta + \dot{\theta}^2 d_t \sin\theta \\ \ddot{y} &= -\ddot{\theta}d_t \sin\theta - \dot{\theta}^2 d_t \cos\theta \end{aligned}$$

Equations 3.42, 3.43

and for $\ddot{\theta}$ using Equation 3.8 and rearranging gives:

$$GRF_x = -g \frac{md_t^2}{(md_t^2 + I)} \cos\theta \sin\theta + m\dot{\theta}^2 d_t \sin\theta$$

$$GRF_y = mg - g \frac{md_t^2}{(md_t^2 + I)} \sin^2 \theta - m\dot{\theta}^2 d_t \cos\theta$$

Equation 3.44, 3.45

Anderson and Pandy (2003) grouped terms involving g and denoted these as ‘gravitational’ terms. All terms containing $\dot{\theta}_i$ were denoted as ‘centripetal’ terms.

$$GRF_{Gx} = -g \frac{md_t^2}{(md_t^2 + I)} \cos\theta \sin\theta$$

$$GRF_{Gy} = mg - g \frac{md_t^2}{(md_t^2 + I)} \sin^2 \theta$$

$$GRF_{Cx} = m\dot{\theta}^2 d_t \sin\theta$$

$$GRF_{Cy} = -m\dot{\theta}^2 d_t \cos\theta$$

Equations 3.46, 3.47, 3.48, 3.49

Model 2 is approached in the same way to calculate the GRF beneath it. The vertical component of GRF can be expressed in terms of linear vertical accelerations, and the horizontal component of GRF is calculated using the same method.

$$GRF_y - mg = m_1 \ddot{y}_1 + m_2 \ddot{y}_2$$

$$\ddot{y}_1 = d_1 \left(-\ddot{\theta}_1 \sin\theta_1 - \dot{\theta}_1^2 \cos\theta_1 \right)$$

$$\ddot{y}_2 = d_2 \left(-\ddot{\theta}_2 \sin\theta_2 - \dot{\theta}_2^2 \cos\theta_2 \right) + l_1 \left(-\ddot{\theta}_1 \sin\theta_1 - \dot{\theta}_1^2 \cos\theta_1 \right)$$

Equations 3.50, 3.51, 3.52

$$GRF_x = ma = m_1 \ddot{x}_1 + m_2 \ddot{x}_2$$

$$\ddot{x}_1 = d_1 \left(-\ddot{\theta}_1 \cos\theta_1 + \dot{\theta}_1^2 \sin\theta_1 \right)$$

$$\ddot{x}_2 = d_2 \left(-\ddot{\theta}_2 \cos\theta_2 + \dot{\theta}_2^2 \sin\theta_2 \right) + l_1 \left(-\ddot{\theta}_1 \cos\theta_1 + \dot{\theta}_1^2 \sin\theta_1 \right)$$

Equations 3.53, 3.54, 3.55

To decompose the GRF into gravitational, centripetal and muscular terms, the c_1 and c_2 terms from Equation 3.33 are separated:

$$\begin{aligned} c_{1G} &= (m_1d_1 + m_2l_1)g\sin\theta_1 & c_{2G} &= -m_2d_2g\sin\theta_2 \\ c_{2C} &= -m_2l_1d_2\sin(\theta_1 - \theta_2)\dot{\theta}_2^2 & c_{2C} &= m_2l_1d_2\sin(\theta_1 - \theta_2)\dot{\theta}_1^2 \\ c_{1M} &= M & c_{2M} &= -M \end{aligned}$$

Equations 3.56, 3.57, 3.58, 3.59, 3.60, 3.61

Using these variables in Equation 3.33 calculates the angular accelerations attributable to the respective source for the segment i . Substituting these values further into Equations 3.50-55 gives the GRF due to these accelerations.

3.5 Simulation Methods

The lengths l_1 and l_2 , the distribution of mass between m_1 and m_2 , the CM positions on their segments, d_1 and d_2 , and the moments of inertia, I_1 and I_2 , were all selected using Winter's data (1979, 1991). These are displayed in Table 3.1 (also see Appendix A.1).

i	m (kg)	d (m)	l (m)	I (kg.m ²)
1	12.88	0.53	0.95	1.25
2	67.12	0.32	0.85	18.53

Table 3.1: Values for model parameters

The same source was used for gait data against which the outputs of the simulations were judged. These covered a range of walking velocities and average temporal spatial parameters and are displayed in Table 3.2. The simulations were assumed to represent the half-gait cycle from the middle of one double support phase to the middle of the next. All Winter's data were thus time normalized to this definition of a step.

		Slow	Normal	Fast
Step length	m	0.69	0.75	0.82
	dimensionless	0.71	0.77	0.84
Cadence	steps/min	87	105	123
	dimensionless	0.46	0.55	0.65
Velocity	m/s	1.00	1.21	1.68
	dimensionless	0.32	0.42	0.54

Table 3.2: Average temporal spatial parameters for Winter's data

The equations of motion of the two models were integrated numerically over 10^{-3} s intervals. The leg segment in both models was assumed to move through an arc of 2θ symmetrical about the vertical and this was set to ensure the required average step length for the experimental data ($2l \sin \theta$). The initial angular velocity was then optimised to ensure that the time taken to swing through this arc resulted in the required cadence (note that this also constrains the average walking velocity). All graphical output was time normalized to step duration.

Inverse dynamics were subsequently performed using a standard Newton-Euler approach. This provided validation for the forward dynamic calculations, as well as allowing a comparison of the moments acting about the 'hip' in each of the models.

An examination of the GRFs constituent parts was also undertaken. The terms in the GRF equations were separated and the forces attributable to 'gravitational', 'centripetal' and 'muscular' effects were calculated.

3.6 Results

Figure 3.2 represents the components of hip velocity at the three different walking velocities for Models 1 and 2. Differences between the models are almost indiscernible graphically, particularly the vertical velocity curves, emphasising how close the results are

to one another. The RMS values in Table 3.3 confirm that differences are always less than or equal to 0.03m/s.

The way the horizontal velocity varied across the gait cycle followed the same patterns observed in the experimental data (see

Table 3.4). During mid-stance the vertical velocity also showed a good match between the predicted and experimental data (within 0.08m/s at all walking velocities). The predicted data differed from the experimental values over the first and last quarters of the step (half gait cycle). This showed that the models did not account for the mechanisms the body uses to ensure a zero vertical velocity at foot contact and thus avoid a discontinuity in velocity, allowing for a smooth cyclic pattern.

The RMS values in Table 3.3 showed that the two sets of predictions of hip velocity and the GRF were close to one another. As expected, the incorporation of joint actuation in this model made little difference to the overall dynamics of movement.

Figure 3.3 presents the GRFs at different walking velocities for the Models 1 and 2, in the horizontal and vertical directions. All plots include the decomposition into gravity and centripetal components for Model 1 and gravity, centripetal and muscle moment components for Model 2.

Again the total GRF components for Models 1 and 2 appeared similar and this was confirmed by the RMS values in Table 3.3. As expected the centripetal component varied minimally between the two models and the gravitational component differed by an RMS of 2.2% bodyweight (BW) with a maximum difference of 4.2% BW. This difference appeared to be accounted for by the component due to the hip muscles. There was a good match with the experimental data for the horizontal component of the total GRF predicted for both models (within 7.31% BW for all walking velocities). The match for the vertical component, however, varied up to 40.82% BW. It was still reasonable during mid-stance (within 15.36% BW) but poor over the first and fourth quarter of the step (up to 54.65% BW difference). Over these phases, as walking velocity increased, the match with experimental data became weaker.

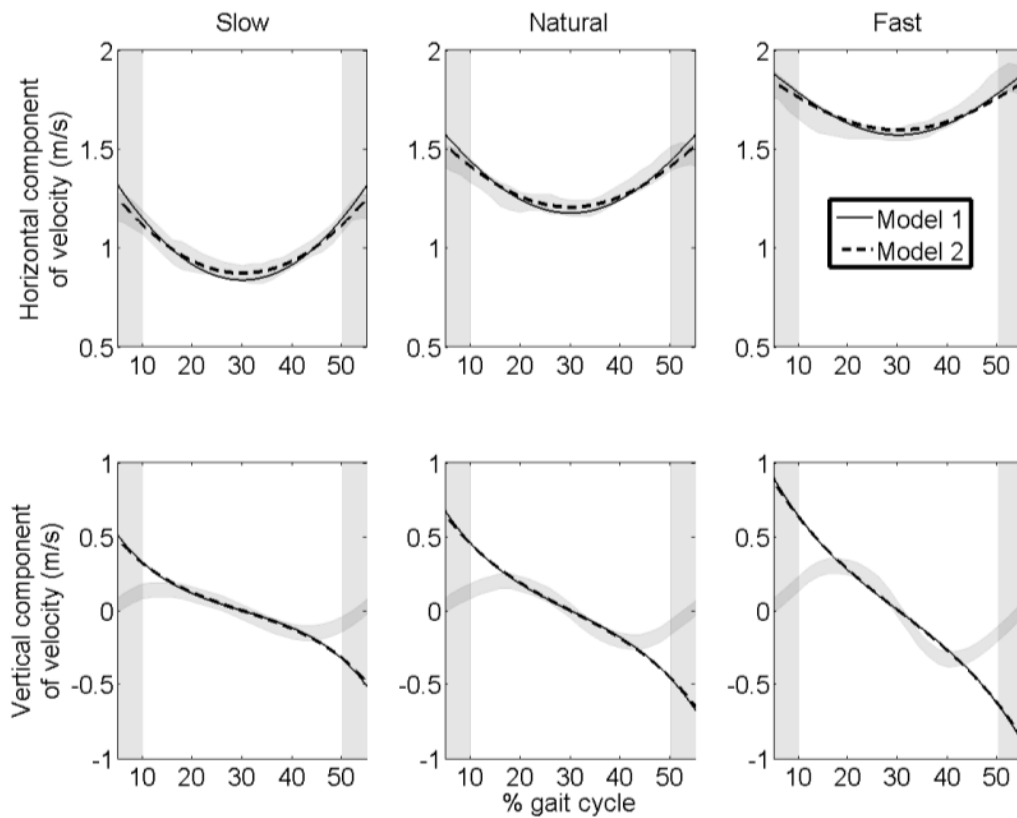


Figure 3.2: The linear velocity components for Models 1 and 2 at different walking velocities. The shaded areas indicate experimental data and double support periods. The line thicknesses of Model 2's velocity component curves have been increased so as to help distinguish between the two models' results. This is difficult, particularly for the vertical component of velocity, where the results were almost identical.

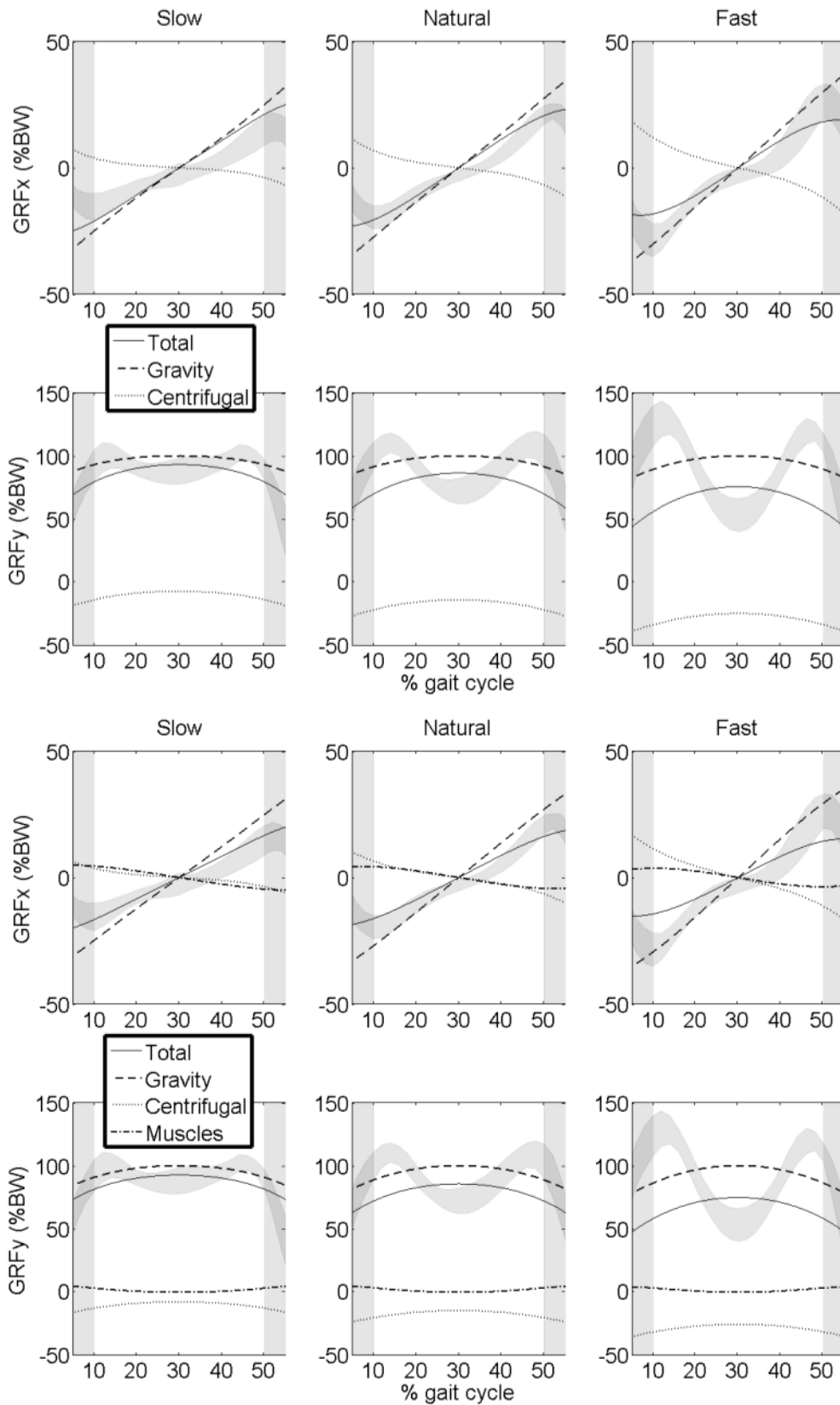


Figure 3.3: The GRF components for Models 1 (top six) and 2 (bottom six) models at different walking velocities

		Slow	Natural	Fast
Velocity (m/s)	x	0.03	0.03	0.02
	y	0.01	0.01	0.01
Ground Reaction Force (%BW)	x	3.18	3.16	2.83
	y	1.50	1.61	1.57
Gravitational component of GRF (%BW)	x	0.38	0.45	0.62
	y	1.60	1.86	2.16
Centripetal component of GRF (%BW)	x	0.26	0.36	0.52
	y	0.90	1.14	1.50

Table 3.3: The RMS of the difference between Models 1 and 2 predictions

		Model 1			Model 2		
		Slow	Natural	Fast	Slow	Natural	Fast
Velocity (m/s)	x	0.03	0.04	0.04	0.01	0.02	0.04
	y	0.17	0.25	0.34	0.17	0.24	0.34
Ground Reaction Force (%BW)	x	5.96	3.63	5.34	3.26	3.25	7.31
	y	9.82	21.05	40.82	9.72	19.91	39.56
Hip Moment (Nm)		11.92	19.66	39.48	16.96	13.06	31.52

Table 3.4: The RMS of the differences between the models' predictions and the experimental data

Hip joint moment graphs can be produced for both models by applying inverse dynamics and they can be compared to experimental data (Figure 3.4). For all walking velocities, the IP model had zero moment about the hip. This is because the mass at the hip had zero rotary moment of inertia. For the Model 2, the moment varied from an extensor moment at the start of the cycle to a flexor moment of equal magnitude at the end. This matched the broad pattern seen in the experimental data with the magnitude at natural velocity with an RMS error of only 13.06Nm.

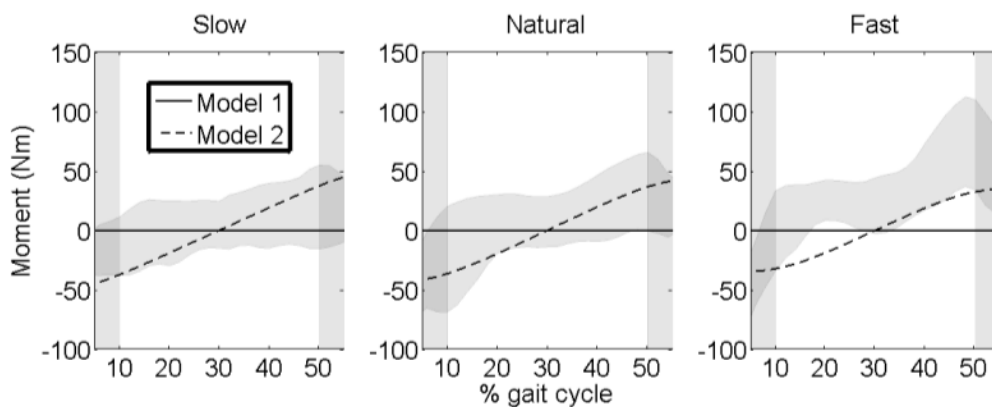


Figure 3.4: The hip joint moments (flexion positive) for Models 1 (red) and 2 (blue) models at different walking velocities

3.7 Discussion

The aim of this study was to further investigate what insights simple IP based models can give into the mechanisms that drive human walking. The IP model of walking has been described as the “simplest walking model” (Garcia, Chatterjee, Ruina, et al., 1998). Despite this only one previous paper has set out to describe the biomechanical characteristics of the IP and then only at a single walking velocity (Buczek et al., 2006). Adding a HAT segment held upright by an actuator (representing the hip extensor musculature) was a simple modification that could make the model more physiologically representative of human walking and allow a calculation of the hip muscle activity required to support the trunk. The simulation still had just one DOF and it was thus

possible to compare this with the first model to give an understanding of how much this muscle activity affects movement in simple models.

The horizontal component of GRF was predicted well by both models throughout the stance phase. Researchers often make the assumption that in early stance and particularly in the push-off phase, muscle activity is required to generate the horizontal component of the GRF (Perry & Burnfield, 2010). The results of the IP model show that these are a natural consequence of the body's posture and muscle forces are not necessarily required.

Model 2 was able to predict the hip moment curves well (less than 32Nm for all walking velocities), particularly at natural walking velocity (RMS error of 13.06Nm). This provides evidence for the primary purpose of the hip moment being to maintain the upright posture of the trunk and therefore illustrating how even a simple anatomical extension to the IP model can provide extra insight into gait mechanics.

One of the biggest failures of these two models is that they are not inherently cyclic. A symmetrical IP inevitably results in a motion in which the vertical component of velocity is equal and opposite at either end of the step cycle. It is thus clearly not possible to simply string together IP steps sequentially to model walking. Although vertical and horizontal components of velocity match experimental data over the middle 50% of the step the modelled vertical velocity differs markedly from experimental data over the first and last 25%. This suggests that whilst the IP may be regarded as a good model of single support (particularly the middle part) it is not a good model of double support.

A number of studies have addressed the step-to-step transition issue. There are numerous examples of such modelling in the literature, a particular strand of this associates energy loss with the "collision" that is inevitable at the transition from one IP step to the next (Adamczyk & Kuo, 2009; Donelan et al., 2001; Donelan et al., 2002a; Donelan et al., 2002b; Kuo, 2007; Kuo et al., 2005; Srinivasan & Ruina, 2006). The analysis in this chapter, however, highlights the inadequacies of modelling double support as a simple transition between consecutive IP steps and questions whether such modelling of energy loss based on these assumptions is reasonable.

This model failing was also implicit in a vertical component of the GRF which was always below bodyweight (essentially the CM has a negative acceleration throughout the gait cycle). The IP thus fails the first pre-requisite of normal walking – adequately supporting bodyweight. The average vertical force under either foot is about 10% less than bodyweight. Empirical data show the characteristic double bump of the vertical component of the GRF which IP models cannot predict (Anderson & Pandy, 2003). It is interesting that even this data however gives an average force under each limb of below bodyweight over each step. This emphasizes the importance of double support, during which the forces under both limbs add to give the highest overall force on the body at any time during the gait cycle, as a mechanism for ensuring bodyweight is supported. Differences between the IP model and empirical data increased with increasing walking velocity suggesting that the IP performs worse at higher walking velocities.

The predicted contribution of hip musculature to the GRF was quite different to the findings of Anderson and Pandy (2003). They stated that hip extensors contributed up to 40% BW in early single support, considerably more than Model 2. On the other hand they found that the hip flexors provided minimal contribution, anywhere throughout single support in agreement with the Model 2. The differences may be attributed to the model dependency of '*induced accelerations*' as highlighted by Chen (2006).

Decomposing the GRF into its constituent parts is a relatively new technique (Anderson & Pandy, 2003) and is still poorly understood. This study has analysed this for two very simple models and it is here where the largest differences are observed between the two models with the "gravitational" GRF differing at the beginning and end of the step (the vertical component is up to 4.2% BW larger for Model 1). This difference is almost exactly that which is attributed to the hip muscles in the HAT model (the centrifugal component and total force are very nearly identical). Considering the free body diagram and the similarity in the way the two models move, gravity would appear to have an extremely similar effect on both models and it may be that labelling this as the "gravity" component is misleading. The difference is attributable to the different structures of the models (one has a hip joint, the other doesn't). This component is that which would be exerted by the structure in the absence of movement or muscular action and "structural support" might be considered a better label than "gravity". The explanation of the analytical results is

then that the jointed HAT structure is inherently less resistant to collapse under the same gravitational forces as the IP and muscle activity is required to allow it to move similarly.

In summary, consideration of these two models suggests that IP based models appear to give valuable insights into the fundamental mechanisms by which the body moves through single support. They are not cyclically consistent, however, and cannot serve as reliable models for the transition from one step to the next. Incorporation of an actuated hip joint identifies the primary role of the hip musculature in stance as that of keeping the HAT upright. Alternative explanations for the role of this muscle function during walking have been offered, such as support of bodyweight (Anderson & Pandy, 2003; Liu et al., 2006; Liu et al., 2008).

3.8 Conclusions

Overall this study has been very useful for laying the foundations for further models to build upon. The IP model of walking has been shown to produce a fairly good approximation of walking during single support but cannot replicate double support. The addition of an actuated hip joint has given mathematical evidence towards the hypothesis that hip muscle action is focussed on maintaining an upright trunk. These conclusions directly address the first Research Question. In addition, the framework implemented for this investigation has been shown to produce results effectively.

With these observations in mind, the next chapter of this thesis will focus on fine-tuning the accuracy of the single support phase. This will be approached by producing a sequence of models that incrementally increase in complexity. It is hoped that, just like the addition of the hip joint moment, each new element will provide mathematical evidence for what its role in walking might be.

Chapter 5 will investigate double support and what extra considerations need to be accounted for in order to produce an adequate solution.

4 SINGLE SUPPORT MODELS

4.1 Introduction

In this chapter, the simple models addressed previously will be advanced by the inclusion of extra DOF and additional complexities. There are previous studies in the same vein as this but there are a number of considerations that set this particular investigation apart from those, as described in Section 4.2. The goal of this work was to address Research Question 2: to see what can be learnt from sequential increases in model complexity.

The simulations discussed in this chapter focus solely on the single support phase of walking thus avoiding the step-to-step transition problems discussed in Chapter 3 and addressed in Chapter 5. This will help to address the first parts of Research Question 3: what is the minimum level of complexity required to adequately model one-legged and two-legged single support?

The structure of the chapter will be much the same as the previous one. An appraisal of the relevant literature will be given first. Following that, the modelling framework will be laid out. This explains the mathematics used to produce a model capable of making predictions and why certain choices were taken. The next step will be to outline the models themselves. This will include a free body diagram of each structure and explanations of their intricacies. The simulation procedure will then be considered. This covers any restrictions or constraints put on the motion and how the best prediction was discovered. The results of the simulations will be given and discussed, highlighting any evidence for the effects caused by additional complexities. The chapter will end with some concluding remarks about what has been learnt and what this means for the project as a whole.

4.2 Literature

The work of the Dynamic Walking group and others that champion the Spring Loaded Inverted Pendulum (SLIP) model (Bullimore & Burn, 2007; Hong et al., 2013; Millard et al., 2011; Poulakakis, 2010; Poulakakis & Grizzle, 2009; Soyguder & Alli, 2012) was discussed

in the previous chapters. While this does produce a realistic CM motion, and hence better GRF curves, it considers neither anatomical accuracy nor how its parameters translate to reality. The SLIP model replaces the knee joint mechanism with a telescopic, straight leg containing a spring of defined stiffness. It is unable to predict joint angle time-histories or joint moment time-histories since it is only the whole body CM that behaves as it does in healthy walking. If it were used to simulate experimental data it may be found that a given stiffness, k N/m, produces the optimum correlation but how can this information be used when the human knee does not contain a spring mechanism?

Another aspect of these types of models also seems to be that they tend to ignore the kinetic results (Duan et al., 1997). Even those that give GRF curves are unable to predict joint moment time-histories (Siegler et al., 1982) or use very simple approximations, such as step or ramp functions (Pandy & Berme, 1988a). Kinetic results not only provide information regarding the accuracy and validity of simulations but are also useful in a clinical environment.

One of the major focuses of this project, as stated in Research Question 2, is to develop a sequence of models that incrementally augments complexity so that the effect of a particular additional mechanism or DOF on the kinematics and/or kinetics of walking can be observed. This would illustrate the benefit of each additional complexity included in a gait model and also provide mathematical evidence for or against *'The Determinants of Gait'*. These are six properties of healthy human walking (pelvic rotation, pelvic obliquity, knee flexion, lateral displacement of the CM, and knee and ankle mechanisms) first proposed by Saunders et al. (Saunders et al., 1953), as ways that the body minimises energy consumption by translating the CM *"through a sinusoidal pathway of low amplitude in which the deflections are gradual"*. There have been numerous experimental based studies to test this idea (Della Croce et al., 2001; Gard & Childress, 1997, 1999; Kerrigan et al., 2000; Kerrigan et al., 2001; Ortega & Farley, 2005), as well as conceptual ones (Kuo, 2007) but a mathematically based examination would provide the strongest evidence for their validity.

4.3 The Modelling Framework

4.3.1 Introduction

Lagrangian dynamics was once more used to derive the equations of motion for all models. As mentioned in the previous chapter, Lagrange's equation for the derivation of the equations of motion of an actuated, open-link chain is:

$$\frac{d}{dt} \left(\frac{\partial L}{\partial \dot{q}_i} \right) - \frac{\partial L}{\partial q_i} = Q_i$$

Equation 4.1

This gives one equation for every DOF of the system. Instantaneously for a known state vector (q_i, \dot{q}_i) , each equation is linear with respect to the generalised accelerations (\ddot{q}_i) . This means the set of equations of motion can be put into matrix form and easily inverted so as to give the accelerations, as a function of the state vector (q_i, \dot{q}_i) and the applied moments (M_i) , at any given time instant. Knowing the values of these accelerations allows for the numerical integration over time.

One unknown, that has a large impact on the acceleration values, is the time-history profiles of the joint moment activations. The solution is to use an optimisation procedure with these joint moments as the input parameters and a cost function that quantifies the error of the predicted state vectors over time from those of the measured data.

Once the generalised accelerations, velocities and positions are known, over the given time period, inverse dynamics can be used to equate the vertical and horizontal components of the GRF and how they change over time.

4.3.2 Generalised formula for n-link chain equations of motion

A generalised formula for the equations of motion of a link model of n segments has been previously developed for use in gait modelling, using a Newtonian approach (Pandy & Berme, 1988a). This project repeated this investigation but instead, used Lagrangian mechanics to develop the formula. A great advantage of this generalised formula is the

time saved in developing the equations of motion for models with a large number of DOF, where a manual approach would be unmanageable.

The following derivation is for an open-link chain consisting of n rigid, straight segments, where the ground acted as a workless constraint at one end of the chain and the other end was free. Each segment has the following characteristics (Figure 4.1). The angular position of 'segment i ' is defined as the angle the segment makes with the vertical. The right hand rule is used for angles, angular velocities, accelerations and moments (i.e. anticlockwise is positive). The total length of the segment is l_i . The position of the CM of the segment is defined by two values, d_i and e_i . These values operate within the segment coordinate frame, rather than a global one, where d_i is parallel to the length of the segment and e_i is perpendicular. The force due to gravity acting at the CM is $m_i g$. The direction of progression is in the positive x direction and upwards is the positive y direction.

For these generalised formulae to be valid, a number of assumptions are made. There is no branching and each segment is connected to any adjacent segments by frictionless hinge joints. The model is 2D, in the sagittal plane, and the hinge joints are the only DOF. For each segment, there are two controlled muscle moments acting directly on the proximal and distal ends respectively.

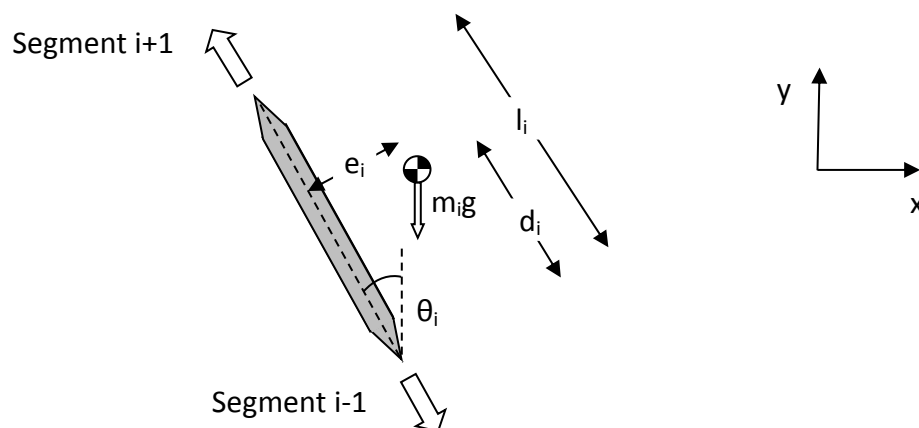


Figure 4.1: The geometry of any given segment

Firstly, the coordinates of the masses are considered:

$$x_i = \sum_{h=1}^{i-1} (-l_h \sin \theta_h) - d_i \sin \theta_i + e_i \cos \theta_i$$

$$y_i = \sum_{h=1}^{i-1} (l_h \cos \theta_h) + d_i \cos \theta_i + e_i \sin \theta_i$$

Equations 4.2, 4.3

The linear velocities of the masses are defined by the first derivatives.

$$\dot{x}_i = \sum_{h=1}^{i-1} (-l_h \cos \theta_h \dot{\theta}_h) - d_i \cos \theta_i \dot{\theta}_i - e_i \sin \theta_i \dot{\theta}_i$$

$$\dot{y}_i = \sum_{h=1}^{i-1} (-l_h \sin \theta_h \dot{\theta}_h) - d_i \sin \theta_i \dot{\theta}_i + e_i \cos \theta_i \dot{\theta}_i$$

Equations 4.4, 4.5

The resultant velocities are calculated for each mass.

$$v_i^2 = \dot{x}_i^2 + \dot{y}_i^2 =$$

$$\sum_{h=1}^{i-1} (l_h^2 \dot{\theta}_h^2) + d_i^2 \dot{\theta}_i^2 + e_i^2 \dot{\theta}_i^2 + \sum_{h=1}^{i-1} (2l_h d_i \dot{\theta}_h \dot{\theta}_i \cos(\theta_h - \theta_i)) + \sum_{h=1}^{i-1} (2l_h e_i \dot{\theta}_h \dot{\theta}_i \sin(\theta_i - \theta_h))$$

$$+ \sum_{h=1, f=1}^{\{i-1|h \neq f\}} \left(l_h l_f \dot{\theta}_h \dot{\theta}_f \cos \left(\begin{cases} \theta_h - \theta_f & \text{if } h < f \\ \theta_f - \theta_h & \text{otherwise} \end{cases} \right) \right)$$

Equation 4.6

Where the sigma notation $\sum_{h=1, f=1}^{\{i-1|h \neq f\}}$ means h and f cover all of the values from 1 to $(i - 1)$, but are never the same as one another. To give a simple example, say $(i - 1)$ equals 3, and the summation is of the function hf , then:

$$\sum_{h=1, f=1}^{\{3|h \neq f\}} hf = (1 \times 2) + (1 \times 3) + (2 \times 1) + (2 \times 3) + (3 \times 1) + (3 \times 2) = 22$$

Equation 4.7

In order to calculate the equations of motion of a system using Lagrangian mechanics, the kinetic energy, T , and the potential energy, V , of the system must be calculated.

$$\begin{aligned}
T &= \frac{1}{2}mv^2 + \frac{1}{2}I\omega^2 \\
&= \sum_{i=1}^n \left(\frac{1}{2}m_i v_i^2 + \frac{1}{2}I_i \dot{\theta}_i^2 \right) \\
&= \sum_{i=1}^n \left(\frac{1}{2}m_i \left(\sum_{h=1}^{i-1} (l_h^2 \dot{\theta}_h^2) + d_i^2 \dot{\theta}_i^2 + e_i^2 \dot{\theta}_i^2 + \sum_{h=1}^{i-1} (2l_h d_i \dot{\theta}_h \dot{\theta}_i \cos(\theta_h - \theta_i)) + \sum_{h=1}^{i-1} (2l_h e_i \dot{\theta}_h \dot{\theta}_i \sin(\theta_i - \theta_h)) \right. \right. \\
&\quad \left. \left. + \sum_{h=1, f=1}^{\{i-1|h \neq f\}} \left(l_h l_f \dot{\theta}_h \dot{\theta}_f \cos \left(\begin{cases} \theta_h - \theta_f & \text{if } h < f \\ \theta_f - \theta_h & \text{otherwise} \end{cases} \right) \right) + \frac{1}{2}I_i \dot{\theta}_i^2 \right) \\
&= \sum_{i=1}^n \left(\frac{1}{2} \dot{\theta}_i^2 \left(m_i d_i^2 + m_i e_i^2 + \sum_{j=i}^n (m_{j+1}) l_j^2 + I_i \right) \right) \\
&\quad + \frac{1}{2} \sum_{h=1, i=1}^{\{n|h \neq i\}} \left(\dot{\theta}_h \dot{\theta}_i \left(\left(\left(\left(m_i d_i + \sum_{j=i}^n (m_{j+1}) l_j \right) l_h \cos(\theta_h - \theta_i) \right) \right) \right) \right. \\
&\quad \left. \left(\left(\left(m_h d_h + \sum_{j=h}^n (m_{j+1}) l_j \right) l_i \cos(\theta_i - \theta_h) \right) \right) \right) \\
&\quad \left. + \left(\begin{cases} (m_i e_i l_h) \sin(\theta_i - \theta_h) & \text{if } h < i \\ (m_h e_h l_i) \sin(\theta_h - \theta_i) & \text{otherwise} \end{cases} \right) \right)
\end{aligned}$$

Equation 4.8

$$\begin{aligned}
V &= mgh \\
&= \sum_{i=1}^n \left(m_i \left(\sum_{h=1}^{i-1} (l_h g \cos \theta_h) + d_i g \cos \theta_i + e_i g \sin \theta_i \right) \right) \\
&= \sum_{i=1}^n \left(\left(m_i d_i + \sum_{j=i}^n (m_{j+1}) l_j \right) g \cos \theta_i + m_i e_i g \sin \theta_i \right)
\end{aligned}$$

Equation 4.9

The Lagrangian function is calculated by subtracting the potential energy from the kinetic.

$$\begin{aligned}
L &= T - V = \\
&= \sum_{i=1}^n \left(\frac{1}{2} \dot{\theta}_i^2 \left(m_i d_i^2 + m_i e_i^2 + \sum_{j=i}^n (m_{j+1}) l_j^2 + I_i \right) \right) \\
&+ \frac{1}{2} \sum_{h=1, i=1}^{\{n|h \neq i\}} \left(\dot{\theta}_h \dot{\theta}_i \left(\left(\left(\left(m_i d_i + \sum_{j=i}^n (m_{j+1}) l_j \right) l_h \cos(\theta_h - \theta_i) \quad \text{if } h < i \right) \right. \right. \right. \\
&\left. \left. \left. \left(m_h d_h + \sum_{j=h}^n (m_{j+1}) l_j \right) l_i \cos(\theta_i - \theta_h) \quad \text{otherwise} \right) \right) \right) \\
&\left. + \left(\left(\left(m_i e_i l_h \right) \sin(\theta_i - \theta_h) \quad \text{if } h < i \right) \right. \right. \\
&\left. \left. \left(m_h e_h l_i \right) \sin(\theta_h - \theta_i) \quad \text{otherwise} \right) \right) \\
&- \sum_{i=1}^n \left(\left(m_i d_i + \sum_{j=i}^n (m_{j+1}) l_j \right) g \cos \theta_i + m_i e_i g \sin \theta_i \right)
\end{aligned}$$

Equation 4.10

Partial differentials of L with respect to $\dot{\theta}_i$ and θ_i are taken in order to evaluate the variables in the Lagrange function.

$$\begin{aligned}
\frac{\partial L}{\partial \dot{\theta}_i} = & \sum_{i=1}^n \left(\dot{\theta}_i \left(m_i d_i^2 + m_i e_i^2 + \sum_{j=i}^n (m_{j+1}) l_j^2 + I_i \right) \right. \\
& + \frac{1}{2} \sum_{h=1, h \neq i}^n \left(\dot{\theta}_h \left(\left(\left(\left(m_i d_i + \sum_{j=i}^n (m_{j+1}) l_j \right) l_h \cos(\theta_h - \theta_i) \quad \text{if } h < i \right) \right. \right. \right. \\
& \left. \left. \left(\left(m_h d_h + \sum_{j=h}^n (m_{j+1}) l_h \right) l_i \cos(\theta_i - \theta_h) \quad \text{otherwise} \right) \right) \right. \\
& \left. \left. + \left(\begin{cases} (m_i e_i l_h) \sin(\theta_i - \theta_h) & \text{if } h < i \\ (m_h e_h l_i) \sin(\theta_h - \theta_i) & \text{otherwise} \end{cases} \right) \right) \right)
\end{aligned}$$

$$\begin{aligned}
\frac{d}{dt} \left(\frac{\partial L}{\partial \dot{\theta}_i} \right) = & \sum_{i=1}^n \left(\ddot{\theta}_i \left(m_i d_i^2 + m_i e_i^2 + \sum_{j=i}^n (m_{j+1}) l_j^2 + I_i \right) \right. \\
& + \frac{1}{2} \sum_{h=1, h \neq i}^n \left(\ddot{\theta}_h \left(\left(\left(\left(m_i d_i + \sum_{j=i}^n (m_{j+1}) l_j \right) l_h \cos(\theta_h - \theta_i) \quad \text{if } h < i \right) \right. \right. \right. \\
& \left. \left. \left(\left(m_h d_h + \sum_{j=h}^n (m_{j+1}) l_h \right) l_i \cos(\theta_i - \theta_h) \quad \text{otherwise} \right) \right) \right. \\
& \left. \left. + \left(\begin{cases} (m_i e_i l_h) \sin(\theta_i - \theta_h) & \text{if } h < i \\ (m_h e_h l_i) \sin(\theta_h - \theta_i) & \text{otherwise} \end{cases} \right) \right) \right) \\
& - \dot{\theta}_h \left(\left(\left(\left((\dot{\theta}_h - \dot{\theta}_i) \left(m_i d_i + \sum_{j=i}^n (m_{j+1}) l_j \right) l_h \sin(\theta_h - \theta_i) \quad \text{if } h < i \right) \right. \right. \right. \\
& \left. \left. \left((\dot{\theta}_i - \dot{\theta}_h) \left(m_h d_h + \sum_{j=h}^n (m_{j+1}) l_h \right) l_i \sin(\theta_i - \theta_h) \quad \text{otherwise} \right) \right) \right. \\
& \left. \left. + \left(\begin{cases} (\dot{\theta}_i - \dot{\theta}_h) (m_i e_i l_h) \cos(\theta_i - \theta_h) & \text{if } h < i \\ (\dot{\theta}_h - \dot{\theta}_i) (m_h e_h l_i) \cos(\theta_h - \theta_i) & \text{otherwise} \end{cases} \right) \right) \right)
\end{aligned}$$

$$\begin{aligned}
& \frac{\partial L}{\partial \theta_i} \\
&= \frac{1}{2} \sum_{h=1, i=1}^{\{n|h \neq i\}} \left(\begin{matrix} 1 & \text{if } h < i \\ -1 & \text{otherwise} \end{matrix} \right) \dot{\theta}_h \dot{\theta}_i \left(\begin{matrix} \left(\begin{matrix} (\dot{\theta}_h - \dot{\theta}_i) \left(m_i d_i + \sum_{j=i}^n (m_{j+1}) l_j \right) l_h \sin(\theta_h - \theta_i) & \text{if } h < i \\ (\dot{\theta}_i - \dot{\theta}_h) \left(m_h d_h + \sum_{j=h}^n (m_{j+1}) l_h \right) l_i \sin(\theta_i - \theta_h) & \text{otherwise} \end{matrix} \right) \\
&+ \left(\begin{matrix} (\dot{\theta}_i - \dot{\theta}_h) (m_i e_i l_h) \cos(\theta_i - \theta_h) & \text{if } h < i \\ (\dot{\theta}_h - \dot{\theta}_i) (m_h e_h l_i) \cos(\theta_h - \theta_i) & \text{otherwise} \end{matrix} \right) \\
&+ \sum_{i=1}^n \left(\left(m_i d_i + \sum_{j=i}^n (m_{j+1}) l_j \right) g \sin \theta_i + m_i e_i g \cos \theta_i \right)
\end{matrix} \right)
\end{aligned}$$

Equations 4.11, 4.12, 4.13

From these calculations, the equations of motion can be written in matrix form.

$$B \cdot \ddot{\theta}_i = C \quad \text{where, } \begin{bmatrix} b_{1,1} & \cdots & b_{1,n} \\ \vdots & \ddots & \vdots \\ b_{n,1} & \cdots & b_{n,n} \end{bmatrix} \begin{bmatrix} \ddot{\theta}_1 \\ \vdots \\ \ddot{\theta}_n \end{bmatrix} = \begin{bmatrix} c_1 \\ \vdots \\ c_n \end{bmatrix}$$

Equation 4.14

For a given row, p , and a given column, q , the following formulae are used:

$$b_{p,q} = \begin{cases} \left(m_p d_p^2 + m_p e_p^2 + \left(\sum_{j=p}^n m_{j+1} \right) l_p^2 + I_p \right) & \text{if } p = q \\ \left(\left(m_p d_p + \left(\sum_{j=p}^n m_{j+1} \right) l_p \right) l_q \cos(\theta_q - \theta_p) \right) + (m_p e_p l_q \sin(\theta_p - \theta_q)) & \text{if } p > q \\ \left(\left(m_q d_q + \left(\sum_{j=q}^n m_{j+1} \right) l_q \right) l_p \cos(\theta_p - \theta_q) \right) + (m_q e_q l_p \sin(\theta_q - \theta_p)) & \text{if } q > p \end{cases}$$

Equation 4.15

$$c_p = \sum_{h=1}^{\{n|p \neq h\}} \left(\begin{matrix} 1 & \text{if } h < p \\ -1 & \text{otherwise} \end{matrix} \right) \dot{\theta}_h^2 \left(\begin{matrix} \left((\dot{\theta}_h - \dot{\theta}_p) \left(m_p d_p + \sum_{j=i}^n (m_{j+1}) l_p \right) l_h \sin(\theta_h - \theta_p) \right) & \text{if } h < p \\ \left((\dot{\theta}_p - \dot{\theta}_h) \left(m_h d_h + \sum_{j=h}^n (m_{j+1}) l_h \right) l_i \sin(\theta_p - \theta_h) \right) & \text{otherwise} \end{matrix} \right) \\ + \left(\begin{matrix} ((\dot{\theta}_p - \dot{\theta}_h)(m_p e_p l_h) \cos(\theta_p - \theta_h)) & \text{if } h < p \\ ((\dot{\theta}_h - \dot{\theta}_p)(m_h e_h l_p) \cos(\theta_h - \theta_p)) & \text{otherwise} \end{matrix} \right) \\ + \left(m_p d_p + \left(\sum_{j=p}^n m_{j+1} \right) l_p \right) g \sin \theta_p - m_p e_p g \cos \theta_p + M_{p+1} - M_p$$

Equation 4.16

Matrix B can then be inverted and used to produce the vector $\ddot{\theta}_i$, which gives the angular acceleration for each of the segments of the chain.

A MATLAB (v 2011a, The MathWorks Inc., Natick, MA, 2011) script was written that, given the model parameters and DOF as inputs, automated the coding of these equations of motion (see Appendix A.2).

4.3.3 Numerical integration

The equations of motion were numerically integrated for each time instant using the same Taylor expansion method used in the previous chapter (Section 3.4.2).

4.3.4 Ground reaction force calculations

In order to properly assess the kinetic performance of each simulation, the vertical and horizontal components of the ground reaction force were to be evaluated and compared to experimental measurements.

By considering the vertical direction first, Newton's second law of motion is used:

$$GRF_y - mg = ma = \sum_{i=1}^n m_i \ddot{y}_i$$

Equation 4.17

Where:

$$\begin{aligned} \ddot{y}_i &= r\alpha_{y,i} + r\omega_{y,i}^2 \\ &= \left(\sqrt{d_i^2 + e_i^2} \right) \left(-\ddot{\theta}_i \sin \left(\theta_i - \left(\tan^{-1} \frac{e_i}{d_i} \right) \right) - \dot{\theta}_i^2 \cos \left(\theta_i - \left(\tan^{-1} \frac{e_i}{d_i} \right) \right) \right) \\ &\quad + \sum_{h=1}^{i-1} l_h \left(-\ddot{\theta}_h \sin \theta_h - \dot{\theta}_h^2 \cos \theta_h \right) \end{aligned}$$

Equation 4.18

Similarly, for the horizontal direction:

$$GRF_x = ma = \sum_{i=1}^n m_i \ddot{x}_i$$

Equation 4.19

Where:

$$\begin{aligned} \ddot{x}_i &= r\alpha_{x,i} + r\omega_{x,i}^2 \\ &= \left(\sqrt{d_i^2 + e_i^2} \right) \left(-\ddot{\theta}_i \cos \left(\theta_i - \left(\tan^{-1} \frac{e_i}{d_i} \right) \right) + \dot{\theta}_i^2 \sin \left(\theta_i - \left(\tan^{-1} \frac{e_i}{d_i} \right) \right) \right) \\ &\quad + \sum_{h=1}^{i-1} l_h \left(-\ddot{\theta}_h \cos \theta_h + \dot{\theta}_h^2 \sin \theta_h \right) \end{aligned}$$

Equation 4.20

4.4 Sequential Model development

Initial model development focussed exclusively on the single support phase of walking. The approach was to add extra mechanisms and DOF one by one so that the complexity of the model increases sequentially. The differences between the results the models produce would then indicate which characteristics of walking can be attributed to which mechanisms.

Another area of interest was how additional complexities in the model dynamics affected the kinematic and kinetic predictions it would make. It was possible that a higher number of DOF would mean the model was able to produce a more accurate GRF but equally it could mean that the kinematic accuracy, for a given segment, would be compromised as a larger number of segment angles would have to be considered in the cost function and thus trade-offs would be required.

4.4.1 Three degrees-of-freedom (Model 3)

Augmenting Model 2 of walking (from Section 3.3) by separating the leg into thigh and shank/foot segments, a three DOF model was developed (Figure 4.2). No foot mechanism was used so the model pivots about a workless constraint at a point on the ground. The respective values for m , d , e and l for the thigh and shank/foot segments were assigned using Winter's formulae (1979, 1991) for a person of 80kg mass and 1.8m height (see Table 4.1 and Appendix A.1).

Actuation moments were applied at the hip and knee joints. However, unlike Model 2, where the size of the joint moment was that which resulted in zero acceleration for the HAT segment, all joint moment trajectories were defined by a number of optimisation variables (this is described more in-depth in Section 4.5.1).

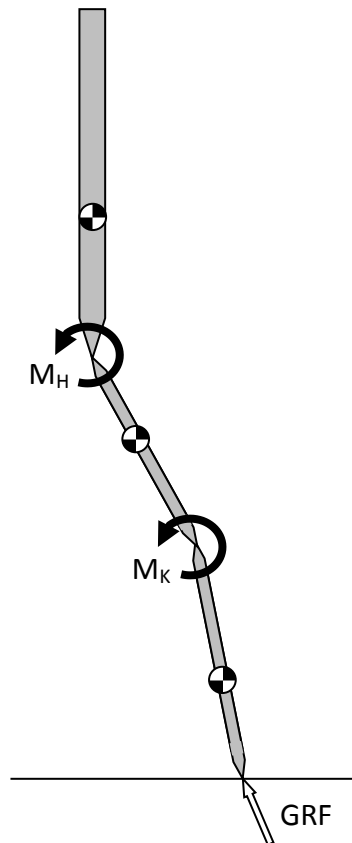


Figure 4.2: Model 3: A three degrees-of-freedom model of human walking

i	m (kg)	d (m)	e (m)	l (m)	I (kg.m ²)
1	4.880	0.201	0.000	0.510	0.220
2	8.000	0.233	0.000	0.410	0.140
3	67.120	0.337	0.000	0.900	13.375

Table 4.1: Values for model parameters of Model 3

4.4.2 Four degrees-of-freedom (Model 4)

The next mechanism to be added was a stance foot. This took more consideration than simply adding an extra segment. In all previous models, the GRF had acted at a single point, where the first segment met the ground. This is known to not be the case in reality. The point of application of the GRF is called the centre of pressure (COP) and moves along the long axis of the foot during stance (Figure 4.3).

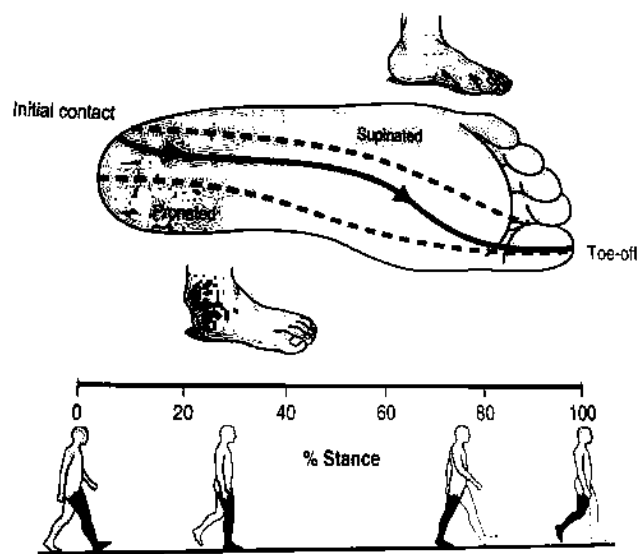


Figure 4.3: Centre of pressure motion during stance (Whittle, 2007)

Another issue arises when the kinematics of the foot during single support are considered. At the start of the single support phase, the foot is often flat on the ground. The segment defining the foot extends from the pivot with the ground (at the metatarsal head) to the ankle joint. At this angle and with zero initial velocity, the weight of the foot and other segments will accelerate it downwards, causing the model to collapse through the ground. A constraint is required to stop the downward motion of the foot and represent the action of the ground.

Both of these issues, the COP movement and the ground action, are effectively the same problem and consequently they can both be solved by a single solution. In dynamics, a

force offset from a point (in this case, the pivot at the metatarsal heads) can be equated to the same force acting at that point plus a moment about the point (Figure 4.4).

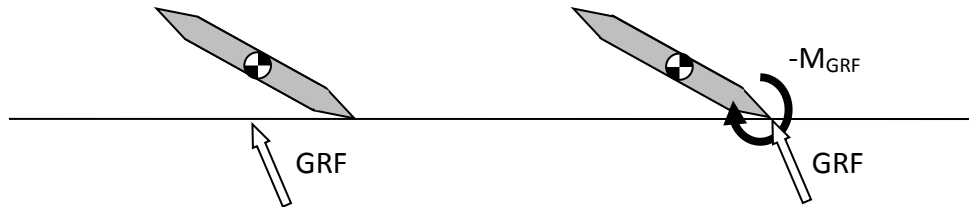


Figure 4.4: The real-life position of the GRF (left) and how it is approximated by the model (right)

The value of this moment is calculated so as to produce zero angular acceleration for the foot segment, using the same method as Model 2 did for its HAT segment. Dividing the moment by the vertical component of GRF gives the horizontal distance between the COP and the pivot point. When this distance reaches zero, i.e. the COP has reached the pivot point, M_{GRF} is set to stay at zero, and the foot segment is now free to move and begins to rise. This is likely to cause a gradient discontinuity in M_{GRF} and hence the GRF curves. Unfortunately, this could not be avoided.

The foot mechanism was added to the previous model so as to create a four DOF model (Figure 4.5). This meant that the model was essentially divided into two 'submodels', foot flat and heel rise, with the difference between the two being the constraint on the foot segment's motion. These submodels would be run sequentially so the final state of the foot flat phase would be the initial state of the heel rise phase. Importantly, a single optimisation would cover both phases.

The mass of the shank segment was divided between the tibia and foot segments and each was given the appropriate moment of inertia (Winter, 1979, 1991). An actuating moment was added at the ankle joint. The pivot point was defined as the metatarsal head and therefore the foot length is defined as the distance from the ankle joint to the metatarsal head. A full set of the model parameters is shown in Table 4.2 (see also Appendix A.1).

i	m (kg)	d (m)	e (m)	l (m)	I (kg.m ²)
1	1.160	0.075	0.000	0.150	0.060
2	3.720	0.247	0.000	0.435	0.064
3	8.000	0.233	0.000	0.410	0.140
4	67.120	0.337	0.000	0.900	13.375

Table 4.2: Values for model parameters of Model 4

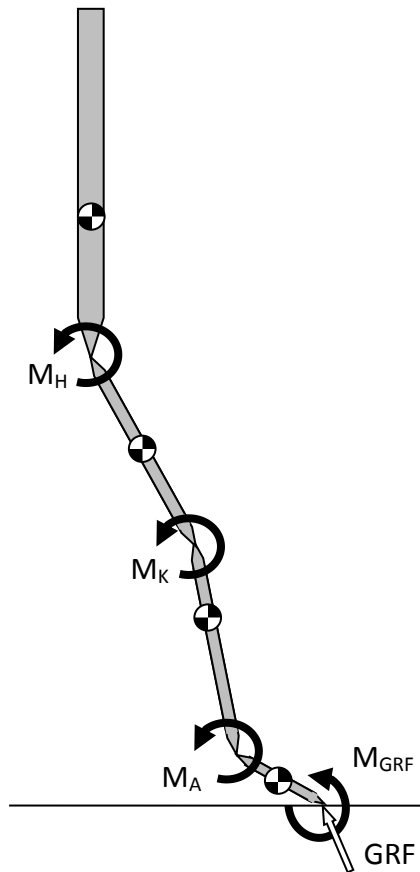


Figure 4.5: Model 4: A four degrees-of-freedom model of human walking

4.4.3 Seven degrees-of-freedom (Model 5)

The final single support model added a swing leg (shown in red in Figure 4.6) to the stance leg (blue) and HAT (grey) segments. Since the generalised formula could not model branched chains, the HAT segment was modelled horizontally but given zero length. The

CM of the segment was positioned correctly and the moment of inertia was calculated in terms of the participant's height. This also allowed the two legs to interact dynamically, while maintaining two separate hip joints and hip joint moments. A full set of the model parameters is given in Table 4.3 (see also Appendix A.1).

i	m (kg)	d (m)	e (m)	l (m)	I (kg.m ²)
1	1.160	0.075	0.000	0.150	0.006
2	3.720	0.247	0.000	0.435	0.064
3	8.000	0.233	0.000	0.410	0.140
4	54.240	0.000	0.337	0.000	10.809
5	8.000	0.178	0.000	0.410	0.140
6	3.720	0.188	0.000	0.435	0.064
7	1.160	0.075	0.000	0.150	0.006

Table 4.3: Values for model parameters of Model 5

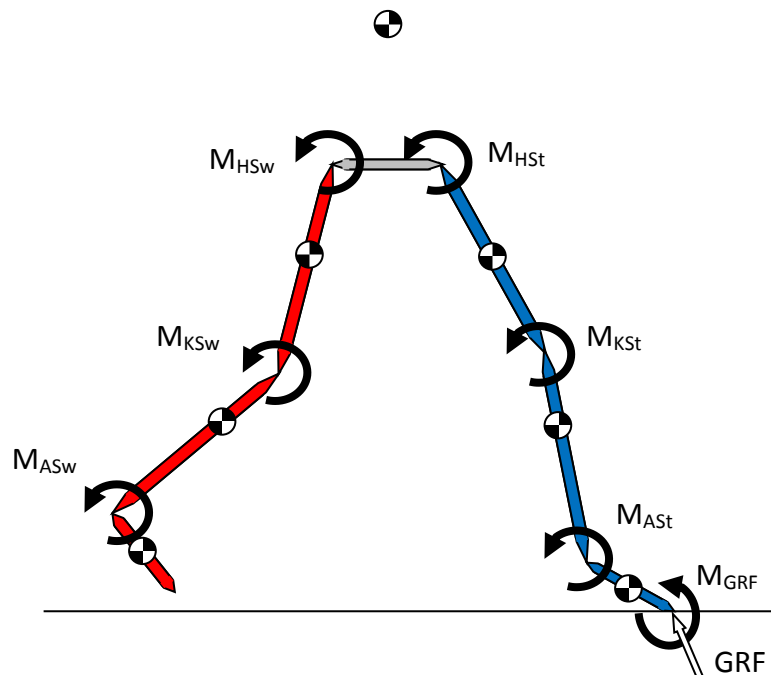


Figure 4.6: Model 5: A seven degrees-of-freedom model of human walking

This model also incorporated the use of two submodels, defining foot flat and heel rise respectively. They were run sequentially with a single optimisation, exactly like Model 4.

4.5 Simulation methods

To ensure a fair comparison between the different models, the method used to perform simulations was the same for each one. The natural walking velocity of 1.2m/s was taken from Winter's data (1979, 1991), a single gait cycle was calculated to take approximately 0.9 seconds. Many sources cite a single support period as being approximately 40% of the full gait cycle (Kirtley, 2006; Perry, 1992; Rose & Gamble, 1994; Whittle, 2007) and so the time for which the simulations were run was to be 0.36 seconds. All the initial conditions were taken from the experimental data and anthropometric measures mentioned by Winter (1979, 1991).

4.5.1 Joint moments

Each joint moment was defined by 21 nodes starting at $t=0$, and then at evenly spaced intervals until $t=0.36$. These nodes defined the magnitude of the moment at that given time instant. The moment values between the nodes were determined using spline interpolation function in MATLAB. The spline function uses piecewise cubic polynomials to create the interpolated values (De Boor, 1978). Using cubics means that there are no discontinuities in the first derivative of moment.

Figure 4.7 shows the moment definition procedure. In the first plot on the left, a range of one standard deviation either side of the experimental mean value for a particular knee moment is shown. Continuing to the top row, the next plot (top centre) shows the positions of the moment nodes if they were to define a curve equivalent to the experimental mean. To the right of that (top right) is a plot showing how interpolating between these nodes produces this curve with a value calculated for every single time instant. The bottom row of plots illustrates how altering these node values affects the resulting moment curve. This allows the user or optimisation algorithm to investigate the effects of increasing or decreasing joint moments at a given time period in the gait cycle.

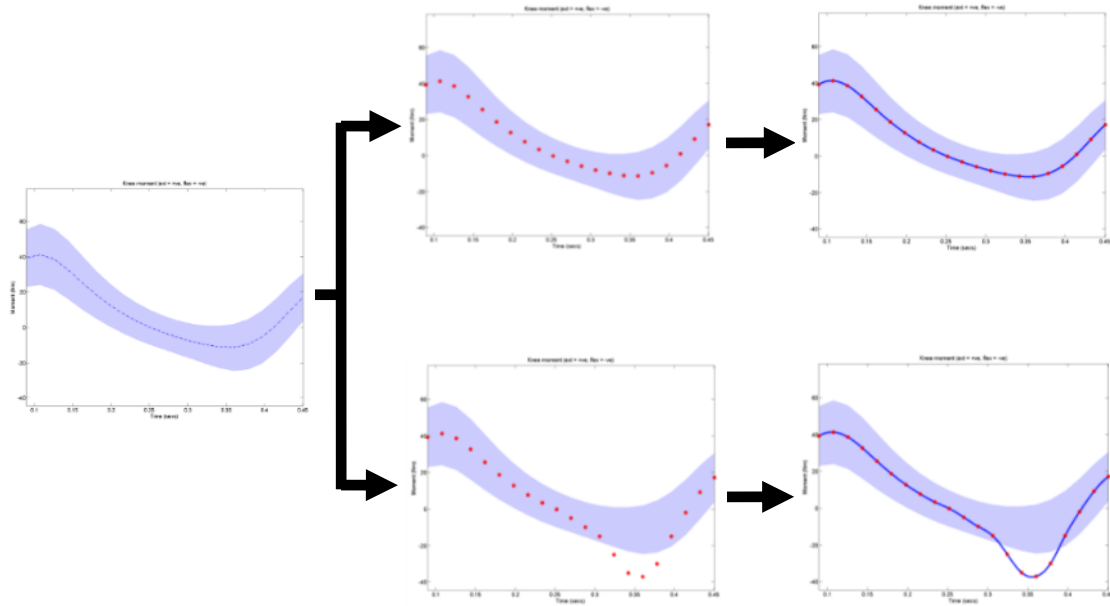


Figure 4.7: Moment nodes and interpolation

4.5.2 Optimisation parameters

The models in this project are all forward dynamics simulations, meaning that, given an initial starting point, the kinematics are determined from kinetic inputs (in this case joint moments). Firstly, the optimisation parameters were chosen to include the initial angular positions (from the vertical axis) and angular velocities of the body segments. This information could have been taken from the experimental data but preliminary testing showed that relatively minor changes in these values could have large effects on the simulation results, so it was considered preferable that the optimiser select the precise values. In addition to the initial state, the moment nodes were also deemed to be optimised parameters. This is necessary since these are unknown quantities that had the most control over the resulting movement of the model. The initial estimates for all these values were taken from the experimental data.

4.5.3 Cost function

One of the ideas behind this study has been stated as the application of complex solution techniques to simple models (Section 2.5). An optimisation approach has often been applied to complex dynamic models, but rarely to simple models. Often the cost functions used are specific to complex models, relating to muscle fatigue and stress (Glitsch & Baumann, 1997; Koopman et al., 1995; Pedersen et al., 1997), factors which aren't considered by the simpler mechanical models. Tracking kinematics and/or kinetics (Thelen & Anderson, 2006) is a possible solution technique that could be applied to the simpler models.

For this study, the chosen cost function was the kinematic match with the experimental data, as determined by a number of root mean square (RMS) error calculations (Equations 4.21, 4.22). For a thorough comparison, the experimental data was interpolated using the spline fit function in MATLAB (as explained in Section 4.5.1) so that error could be calculated for every available time instant.

For segment i , at each time instant, t , the difference between the predicted segment angle ($\theta_{i_{sim,t}}$) and the mean experimental value ($\bar{\theta}_{i_{exp,t}}$) was calculated. These values were then divided by their respective experimental standard deviation values, for that segment, at that given time instant ($\sigma_{i_{exp,t}}$). The results were then squared. The mean value of these squares was taken and then square rooted to produce the RMS error value for that particular segment. The sum of the RMS error values for each of the segments was the cost function (CF).

$$RMS_i = \sqrt{\frac{\sum_t \left(\left(\frac{\theta_{i_{sim,t}} - \bar{\theta}_{i_{exp,t}}}{\sigma_{i_{exp,t}}} \right)^2 \right)}{n}}$$
$$CF = \sum_i RMS_i$$

Equations 4.21, 4.22

The reason each of the difference calculations was divided by the appropriate standard deviation value was to ensure a fair weighting for each of the segment angles. For example, an angular difference of 5° would be of greater significance for the foot segment than it would for the femur segment, so incorporating standard deviations takes this into account. It also meant that if the cost function was changed and incorporated properties with different SI units, it wouldn't be a problem since all RMS errors would be in terms of standard deviations.

This cost function was chosen to see both how well the model could match the desired kinematic motion. Once the simulation result was given, observations of how well the resulting kinetics agreed with reality were made. Some models required further constraints but these are detailed in the respective results sections.

Winter's data (1979, 1991) were used as the input (joint moment trajectories) to the model and for comparison (segment angle trajectories), as an assessment of its success. Kinematic data for a single HAT segment was not available from this source however. Instead, guidance was taken from a number of studies (Ceccato et al., 2009; Krebs et al., 1992; Opila-Correia, 1990; Thorstensson et al., 1982). Based on the data given by these studies, it seemed a fair approximation was a mean value of zero throughout the whole gait cycle (i.e. vertical HAT segment), with a consistent standard deviation range of $\pm 5^\circ$.

4.5.4 Algorithms

The final consideration is the algorithm used to solve the optimisation problem. Simulations in this project used MATLAB to perform parameter optimisation and achieve the best results given the desired cost function. There are two *'toolboxes'* that contain built in optimisation algorithms; the *'OPTIMISATION TOOLBOX'* and the *'GLOBAL OPTIMISATION TOOLBOX'*.

The solvers in the MATLAB OPTIMISATION TOOLBOX are all what are known as *'local optimisation'* algorithms (Lagarias et al., 1998; Nocedal & Wright, 2006). What this means is that if a function has more than one minimum point then the closest one to the initial estimate will be found. Obviously, this may not be the absolute minimum point for the function (see Figure 4.8).

Global optimisation is a technique that is used to calculate the highest or lowest values of a non-linear function that has multiple maxima and minima. This is a much better method of optimisation because it doesn't require as much knowledge about the initial estimate or the function domain as local optimisation does.

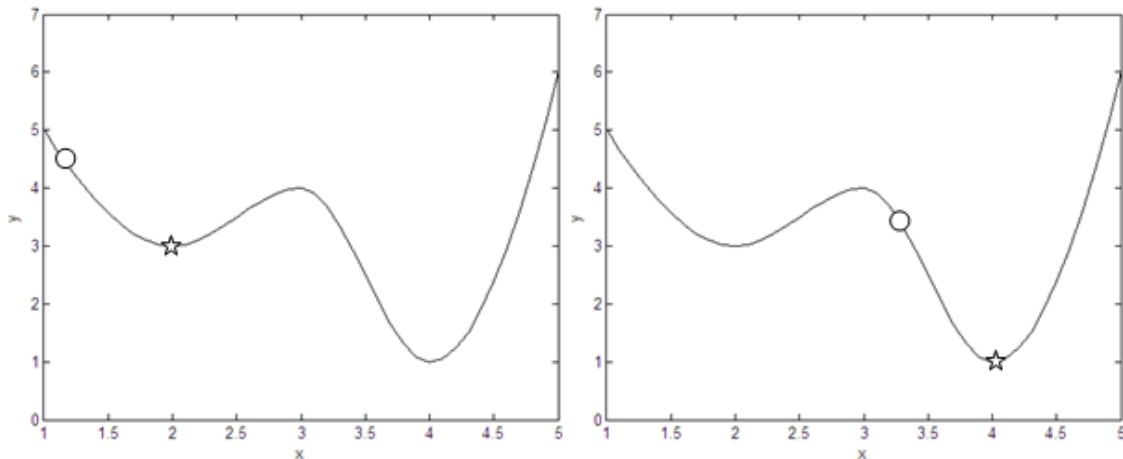


Figure 4.8: Illustration of Local Optimisation behaviour. The dots indicate the initial estimate and the stars show the solutions the solver found.

In practice, it is used to find optimal, often novel and counter-intuitive designs for products and is especially good when a compromise is required between certain design parameters. It is also faster at finding these solutions than exhaustive search methods.

There are many different solvers that can be used in the MATLAB GLOBAL OPTIMISATION TOOLBOX, each using different algorithms and resulting in differing levels of precision, depending upon the type of problem being solved. It is recommended that a solver is run more than once on the same problem to determine the reliability of the result and that once an output is gained, a local solver is used, with this output as the initial estimate, to obtain the required degree of accuracy.

The 'Global search' function in MATLAB, using an interior-point algorithm, was chosen for use in this study (Ugray et al., 2007). It is a type of multi-start algorithm but incorporates a heuristic aspect. The random start points generated are assigned penalty values depending upon their respective cost function value and their adherence to any problem constraints. Any points with too high a penalty value are ignored.

Figure 4.9 shows a three-dimensional representation of how a cost function may change against two variables. To find the global minimum, the first step is for multiple random start points to be generated. The point with the lowest penalty value is selected and the local minimum is found. The vector from the start point to the minimum is then taken as the radius of a 'basin' around the minimum. It is then assumed that any further start points within this basin will find this minimum and so don't need evaluating (Figure 4.10). Next, a new random start point is chosen. Assuming it is still below the threshold value it is selected, if not it is rejected. If a new start point finds a minimum that already has a basin, the basin radius is expanded to that start point (Figure 4.11).

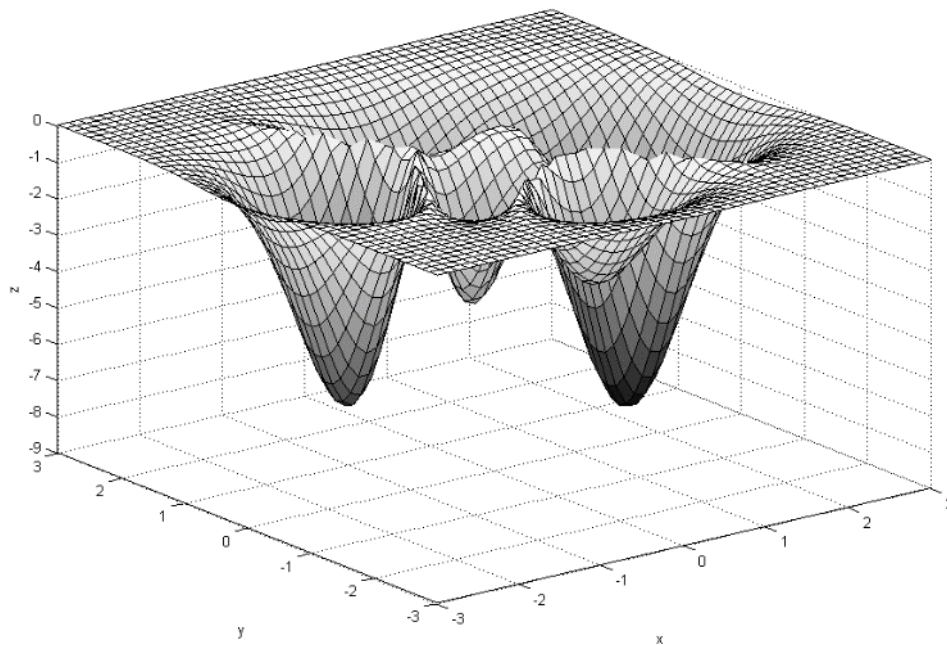


Figure 4.9: 3D plot of a cost function

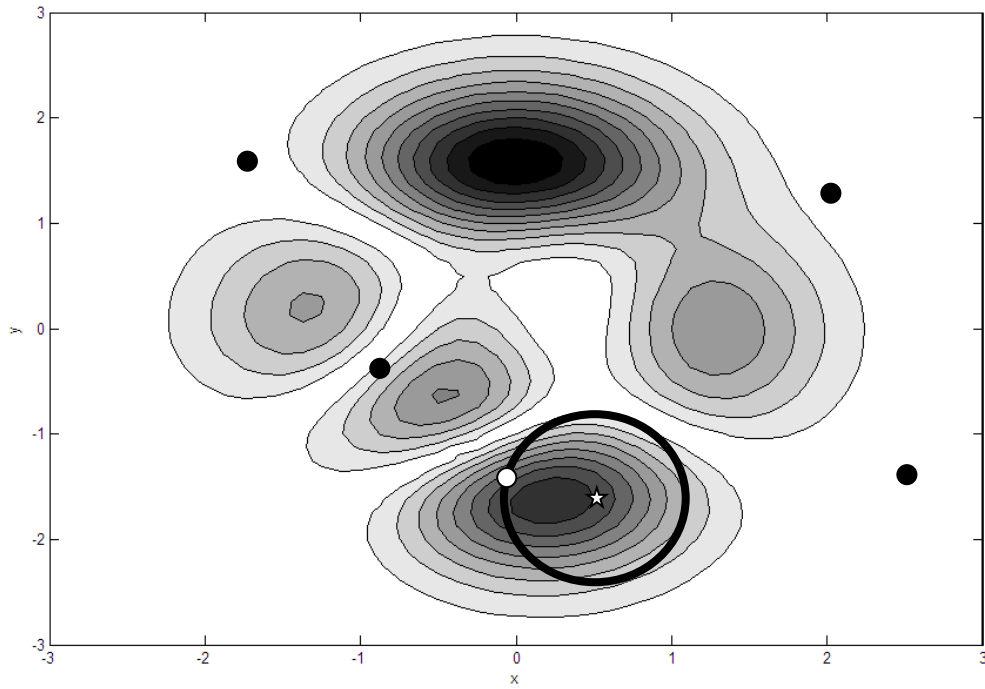


Figure 4.10: From multiple random start points, the chosen first start point finds a local minimum (the star) creating the first basin (the ring)

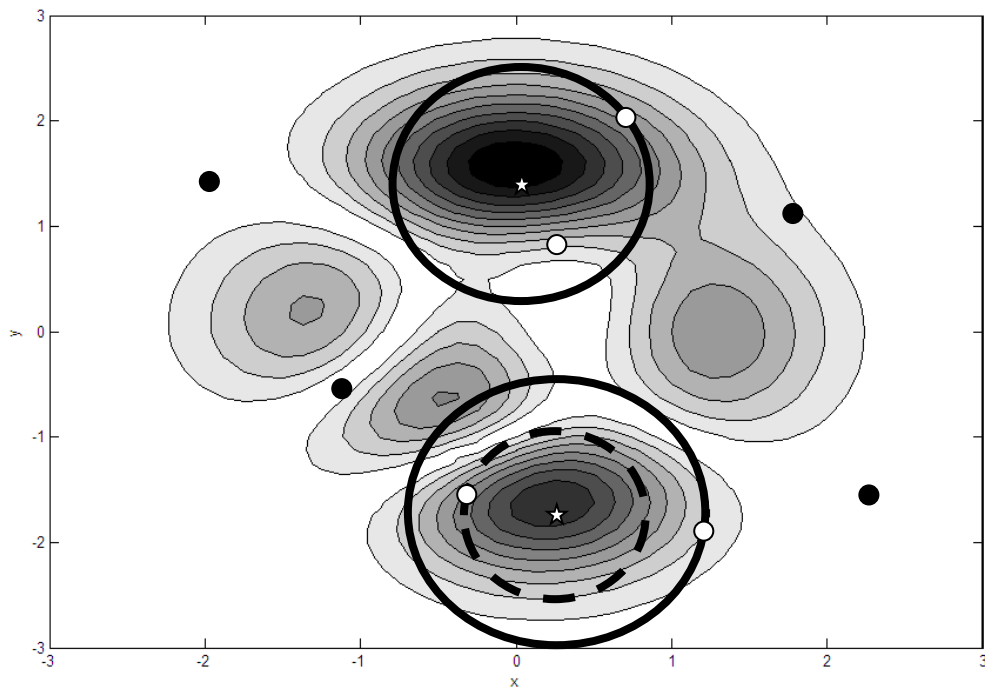


Figure 4.11: Basin expansion (bottom) and a new start point within an existing basin (top)

Eventually, the lowest value of the local minima found is taken to be the absolute minimum.

Each simulation in this study consisted of a global optimiser being employed multiple times, with the same start point, so as to investigate its repeatability. Next, the optimum global output was then fed as the input into a local optimiser (Lagarias et al., 1998; Nocedal & Wright, 2006) to increase the accuracy of the result. This was implemented as an automated process in MATLAB.

4.6 Results

The shaded areas on each of the following plots show the values covered by ± 1 standard deviation from the experimental mean. The solid lines show the results predicted by simulations.

The moment graphs are oriented so that anticlockwise is positive, as according to the right hand rule for moments, as opposed to gait analysis conventions.

4.6.1 Model 3 – Three degrees-of-freedom

An extra penalty function was added to the optimiser to prevent knee hyperextension. Bearing in mind the right hand rule was used for positive segment angles, if the femur segment angle became less than that of the shank/foot segment (rotated further clockwise), the cost function was set to 9999. This meant the optimiser would avoid all solutions that included hyperextension.

The plots in Figure 4.13 show a comparison between the predicted motion and empirical data at equally spaced time intervals between the beginning (top left) and end (bottom right) of single stance. The experimental angular position data of the tibia is used for comparison with the simulation results for the angular position of the shank/foot segment.

The results of this simulation looked encouraging for the first half of single support but the kinematics showed that the leg, particularly the shank/foot segment, has rotated too far forward by the end of single stance (Figure 4.12 and Figure 4.13). Similarly, the kinetic

correlation looked good during the first half of stance with both moment curves within their respective standard deviation ranges of their experimental data (Figure 4.14) and the vertical GRF curve appearing to show the peak, dropping to a mid-stance trough (Figure 4.15). However, these predictions deteriorated during the second half of the simulation.

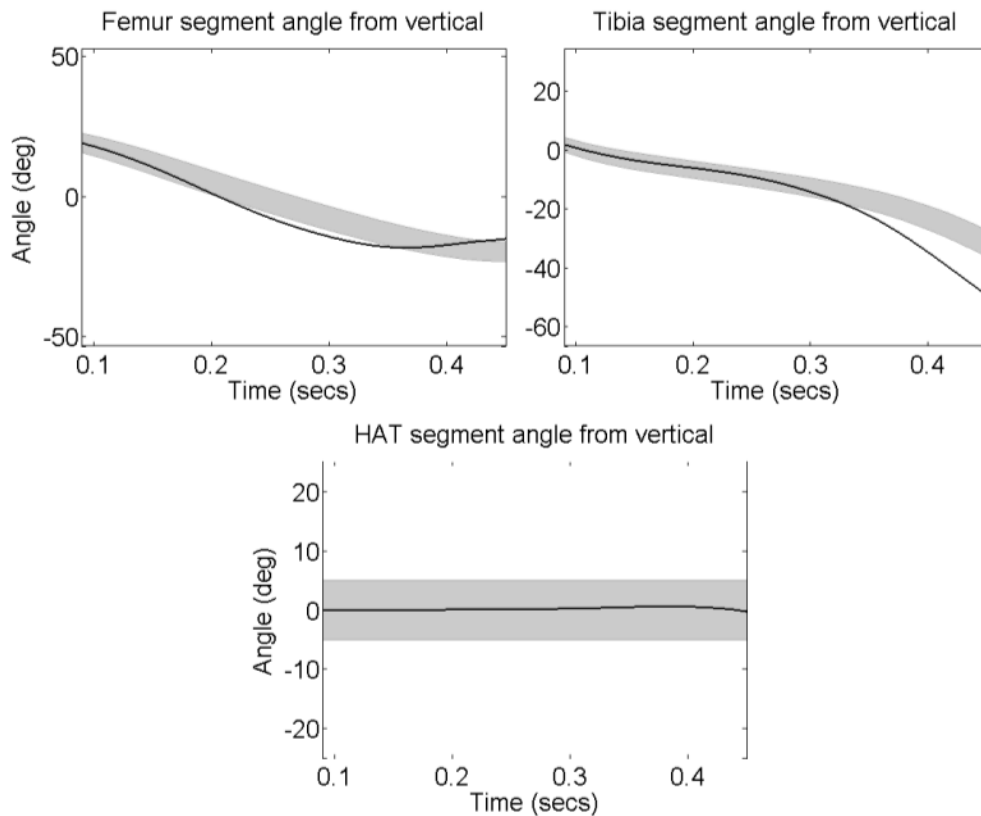


Figure 4.12: The kinematic predictions for Model 3

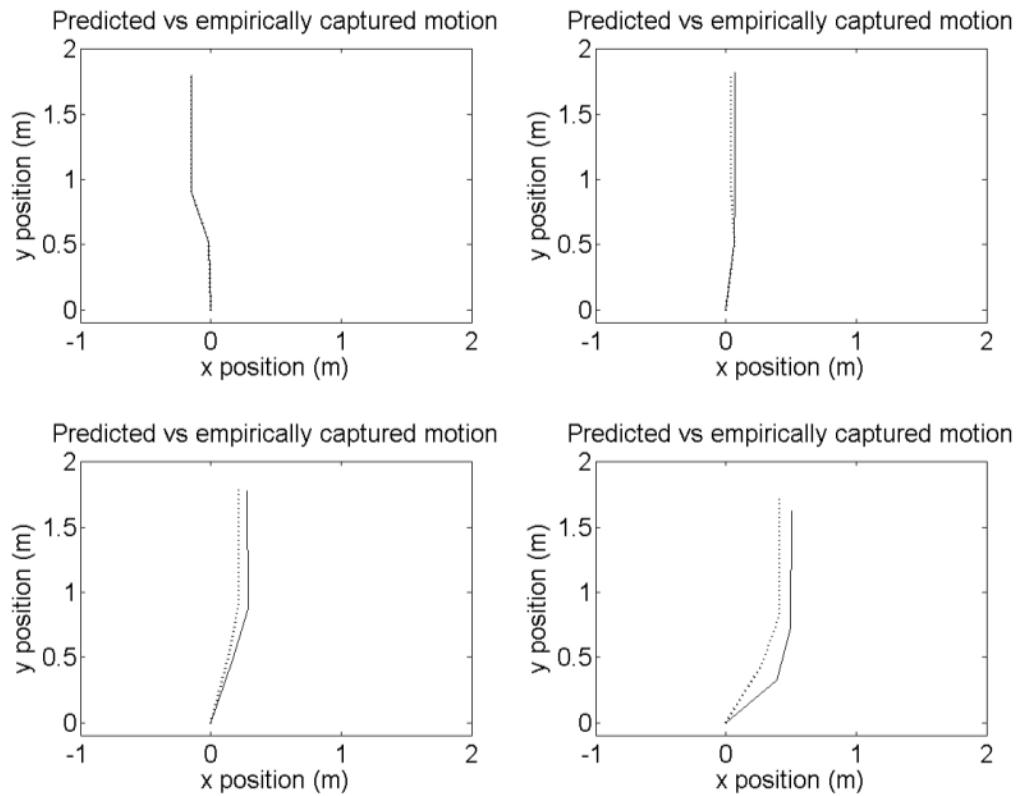


Figure 4.13: The kinematic predictions (solid) vs the empirical means (dotted) for Model 3

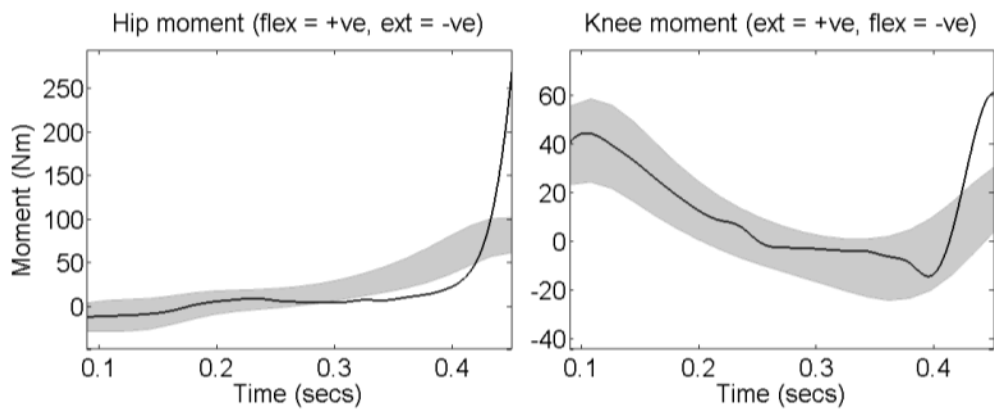


Figure 4.14: The joint moment predictions for Model 3

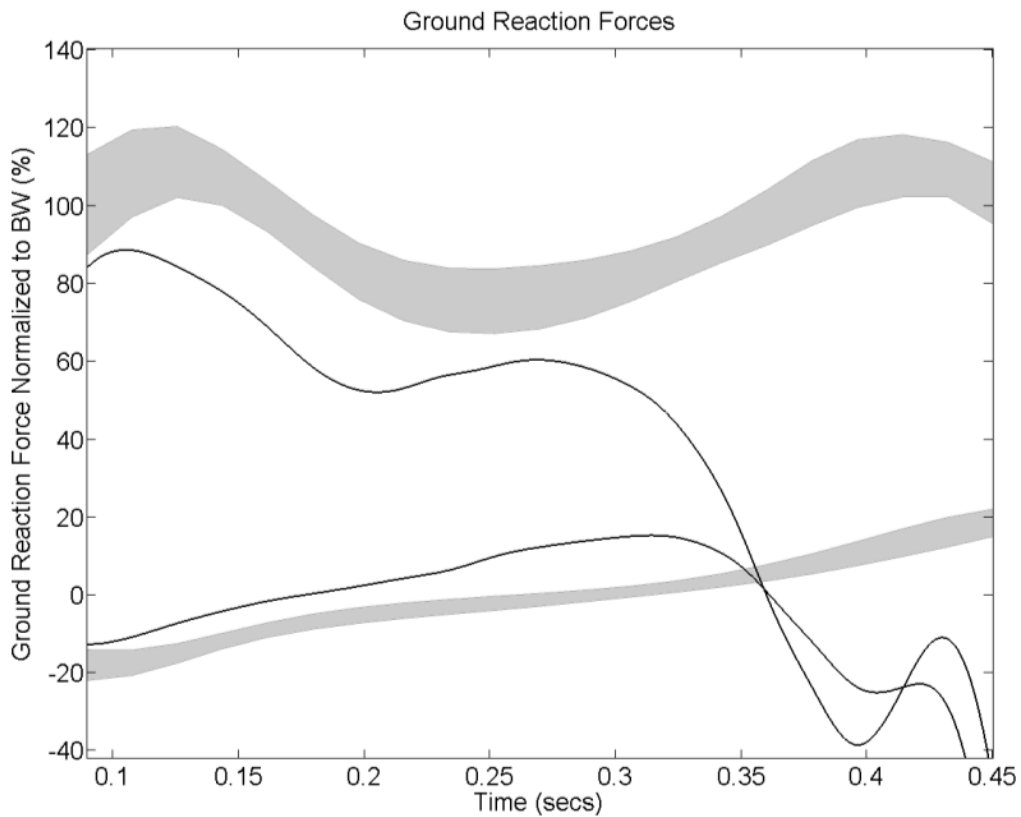


Figure 4.15: The GRF predictions for the Model 3

There were two explanations for the poor predictions in the second half of the simulation. The first was the lack of ankle moment and as a consequence there was less control over the shank/foot segment as there would be in reality. In addition to this, the foot is not modelled as a separate segment and hence the contact with the ground is a single point rather than distributed under the sole of the foot. Nor is the forward motion of the COP modelled, which would affect support, particularly in late stance, where the errors are occurring.

Consequently, it was proposed that an alternative three DOF model be used. This time, instead of treating the first segment as a shank/foot combination, it was treated as solely a tibial segment. This, however, raised another issue over where the mass of the stance foot would be incorporated. The model displayed in Figure 4.16 was the solution. This model was named Model 3.1 and a full set of model parameters is given in Table 4.4 (see also Appendix A.1)

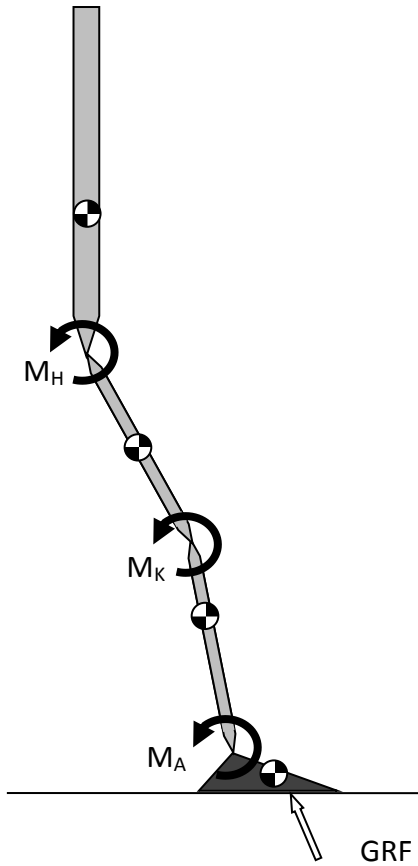


Figure 4.16: Model 3.1: A three degrees-of-freedom model of human walking with a static foot

i	m (kg)	d (m)	e (m)	l (m)	I (kg.m ²)
1	1.160	0.075	0.000	0.150	0.006
2	3.720	0.247	0.000	0.435	0.064
3	8.000	0.233	0.000	0.410	0.140
4	67.120	0.337	0.000	0.900	13.375

Table 4.4: Values for model parameters of Model 3.1

This model incorporated a foot segment but it remained static (indicated on the free body diagram by its darker colour). This retained three DOF but provided a better support mechanism and mass distribution. An extra moment was added to the ankle joint. All other aspects of the simulation were kept the same. Figure 4.17-Figure 4.20 are the simulation results for this model.

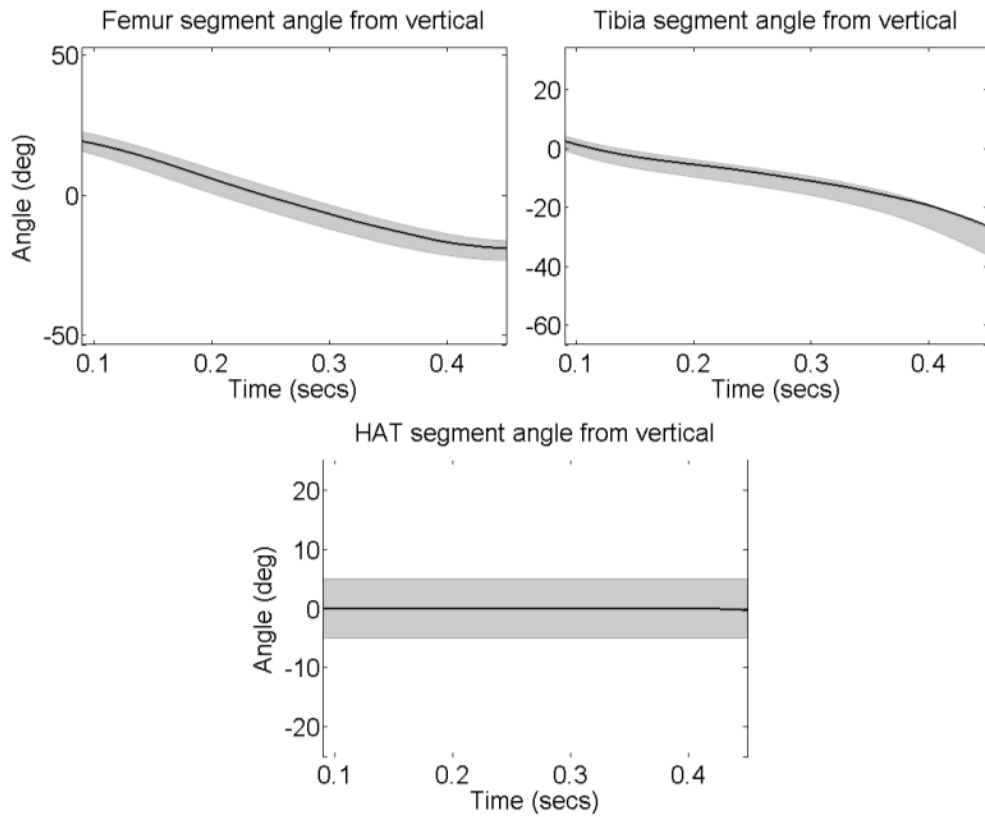


Figure 4.17: The kinematic predictions for Model 3.1

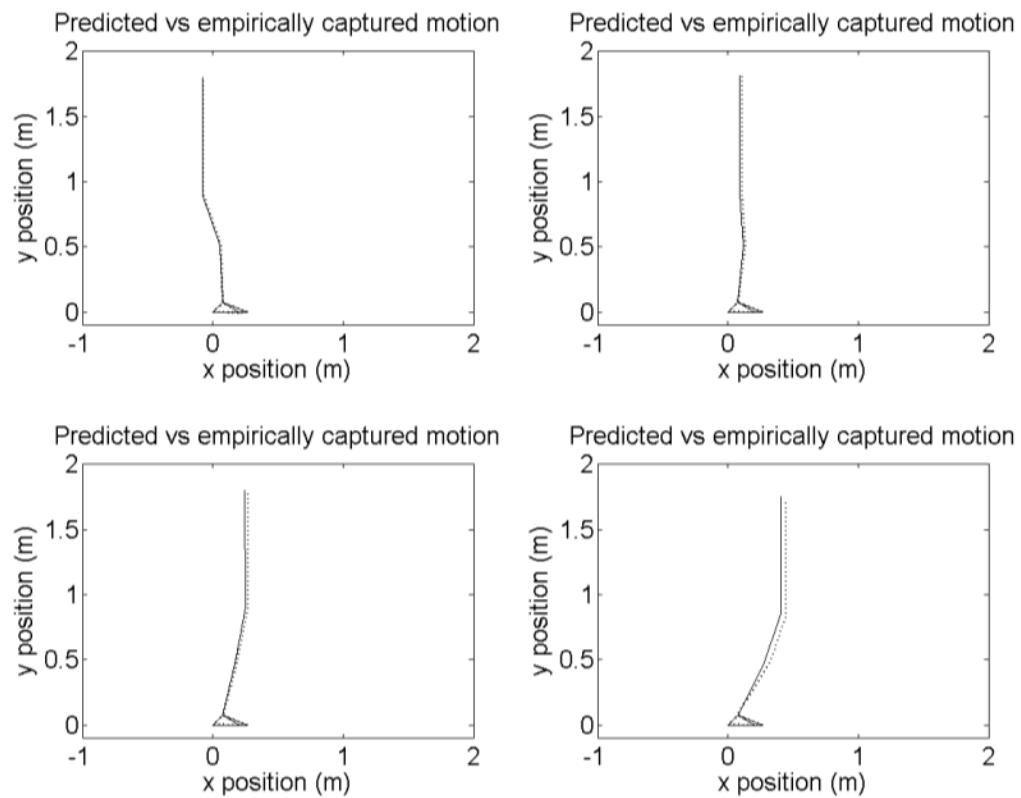


Figure 4.18: The kinematic predictions (solid) vs the empirical means (dotted) for Model 3.1

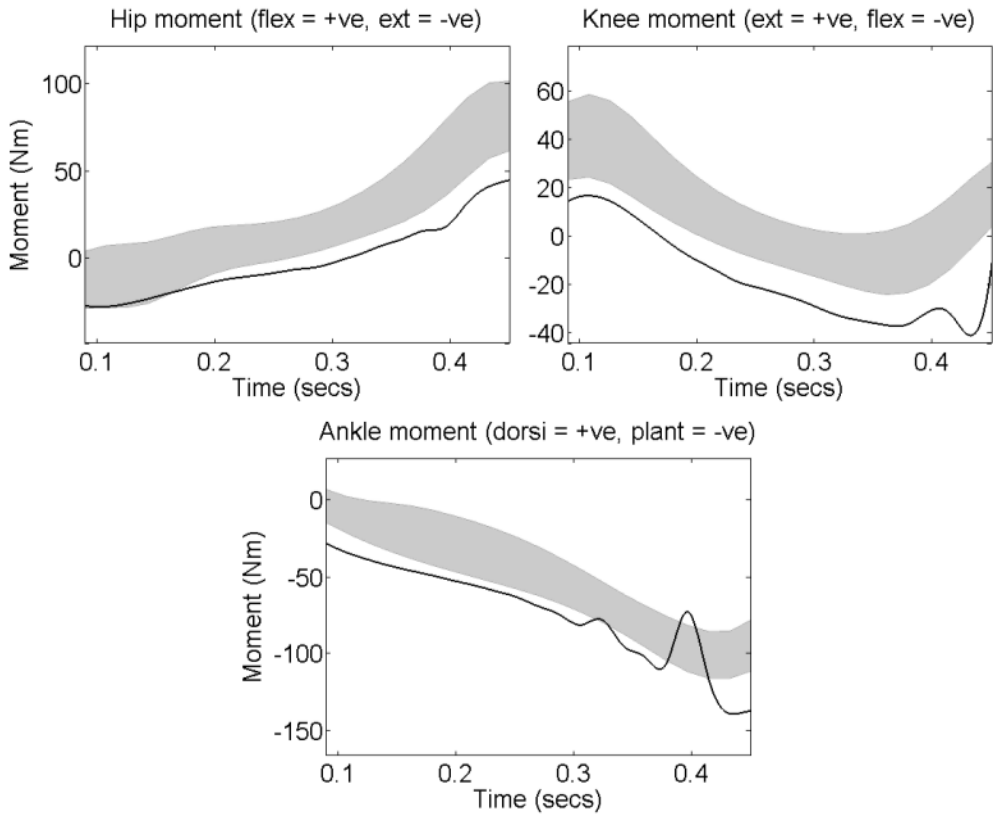


Figure 4.19: The joint moment predictions for Model 3.1

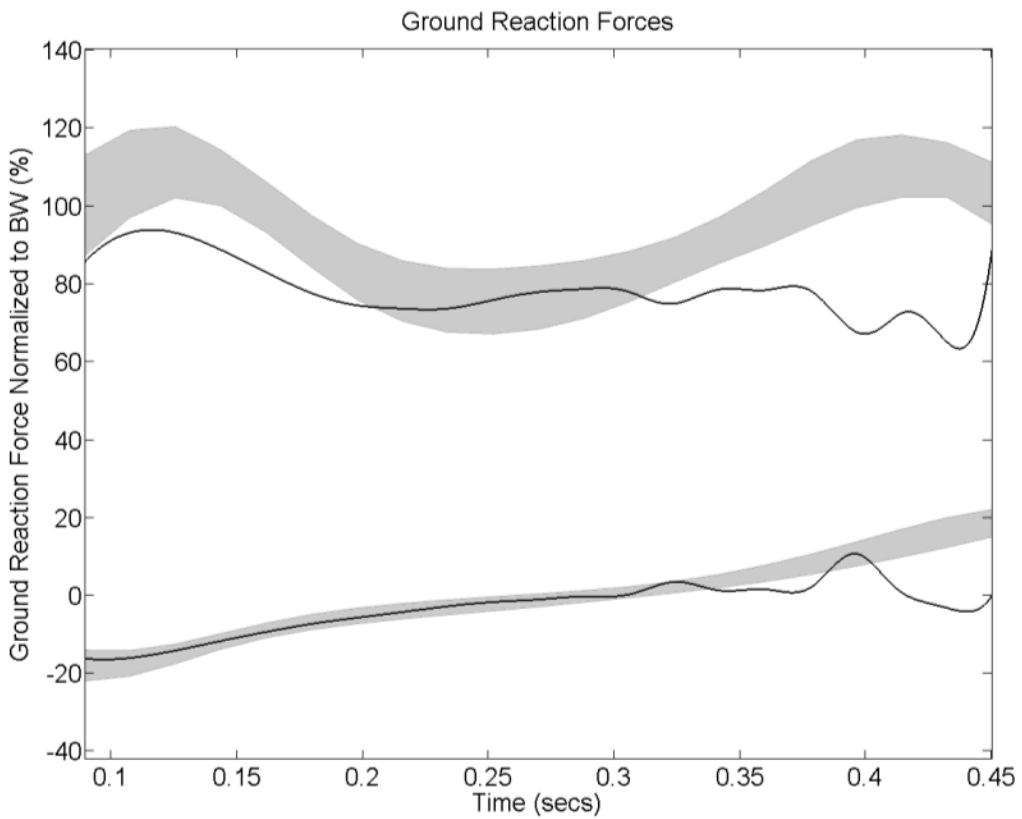


Figure 4.20: The GRF predictions for Model 3.1

As the model did not have a moving foot, the empirical kinematic data was plotted as if the foot didn't move in Figure 4.18. The simulation was able to achieve a result where all segment angles remained within the standard deviation ranges throughout the entirety of single support.

The joint moment time-histories gave interesting results (Figure 4.19). Each curve exhibited the appropriate shape, as given by the experimental results, but was translated just outside its standard deviation range; the hip showed more extension, the knee more flexion and the ankle more plantarflexion.

The vertical GRF curve clearly showed a distinct initial peak and mid-stance trough, although the peak was not as high in magnitude as the experimental data had suggested (Figure 4.20). The horizontal GRF improved in the first half of stance, staying within the standard deviation range. Both curves strayed from the empirical data in the second half of stance, although not quite as drastically as the previous model.

A numerical comparison of the two models' simulation results (Table 4.5) highlights the improvements achieved by separating the tibia and foot segments, even though the number of DOF remained constant. The kinematic errors decreased by approximately 70% from the original model and the GRF error reduced by over 70%.

It should be noted that although the cost functions, used in this study, normalised the RMS errors by each parameters respectively standard deviation values, the data is given here in appropriate units. This is to help conceptualise the error in terms of *'real world'* measures.

		Model 3	Model 3.1
Segment angles (°)	Tibia	6.67	2.36
	Femur	4.18	0.93
	HAT	0.31	0.06
Joint moments (Nm)	Ankle	N/A	23.63
	Knee	48.11	26.52
	Hip	34.80	24.24
GRF (%BW)	y	71.91	20.32
	x	22.89	6.38

Table 4.5: The prediction RMS errors with the experimental data for Models 3 and 3.1

4.6.2 Model 4 - Four degrees-of-freedom

Two penalty functions were added to the optimiser; one to prevent knee hyperextension and one to ensure heel rise achieved a sufficient angle. Both of these conditions were applied in the same way as the Model 3 constraint. The cost function would be set to 9999 should either one of two constraints not be met. Bearing in mind the right hand rule was used for positive segment angles, if the femur angle was less than (rotated further clockwise) than the tibia angle at any point during the simulation, then the penalty was applied. If the final value of the foot segment angle was not less than 55° from the vertical (approximately two standard deviations from the experimental mean) then the penalty was applied. This meant the optimiser would avoid all solutions where such results occurred.

The dotted vertical line on each of the plots indicates the time at which heel rise began.

The kinematic results for Model 4 all remained within the single standard deviation range of the experimental mean values, apart from the foot segment which rose too slowly in the second half of stance (Figure 4.21 and Figure 4.22).

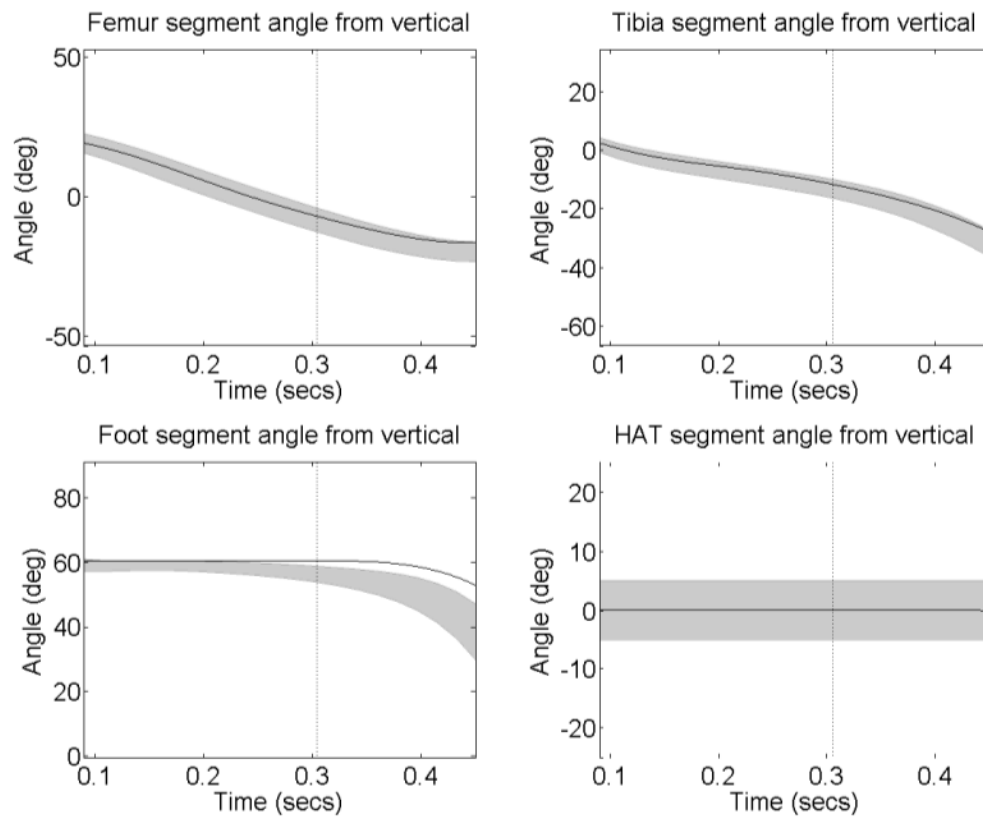


Figure 4.21: The kinematic predictions for Model 4

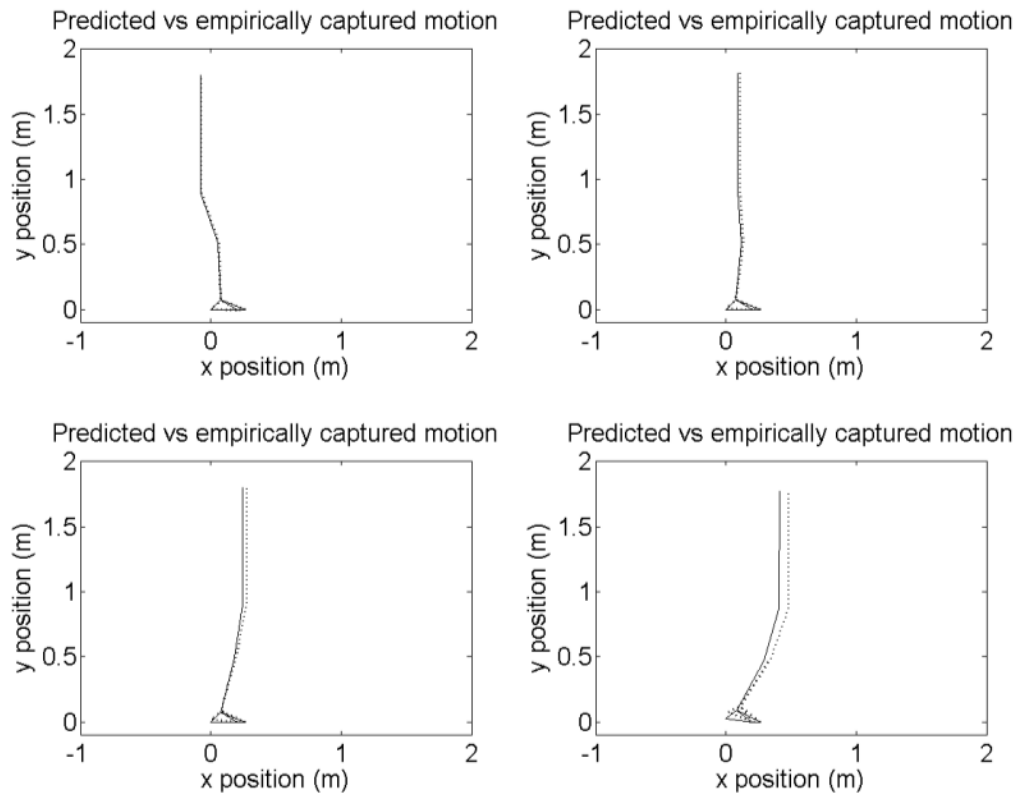


Figure 4.22: The kinematic predictions (solid) vs the empirical means (dotted) for Model 4

The moment curves all followed the correct patterns but were once again translated outside of the standard deviation ranges, in the same way as they were for Model 3.1 (Figure 4.23).

In Figure 4.24, the first peak of the vertical GRF component, while present, was once again lower than the experimental data measurements but this was the only time at which either vertical or horizontal values were outside the standard deviation range. For the first time, the second vertical GRF peak was present.

Table 4.6 shows, for each parameter of the simulation, the RMS error from the experimental data mean values.

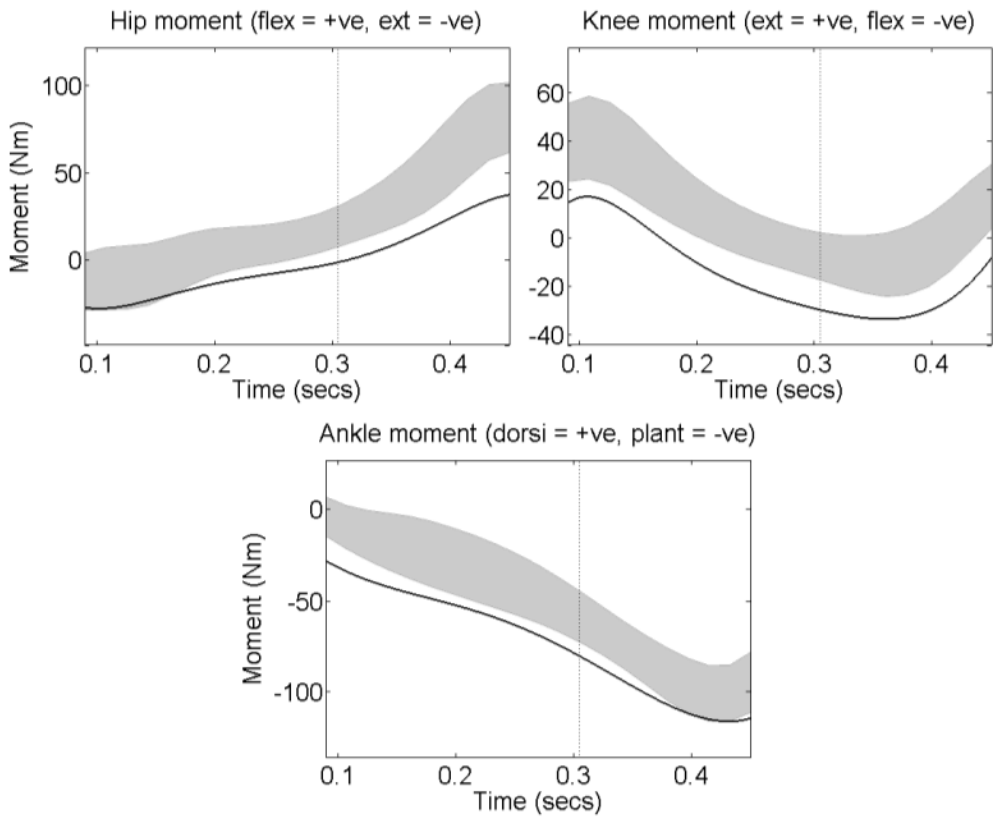


Figure 4.23: The joint moment predictions for Model 4

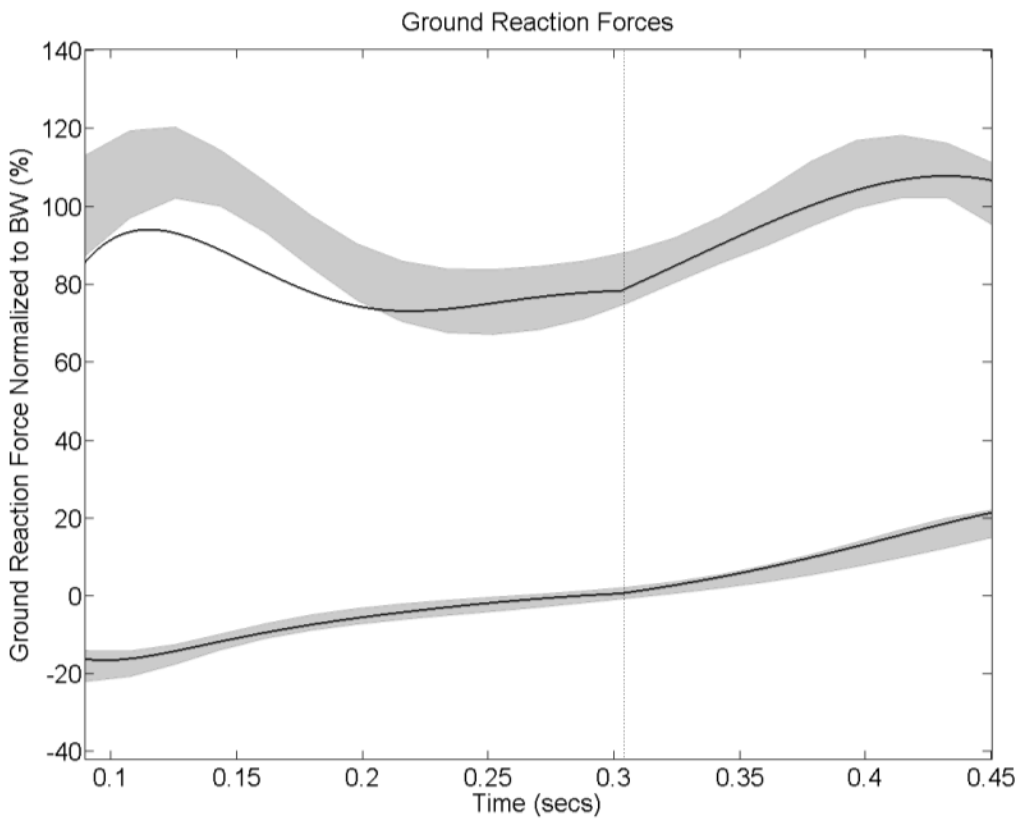


Figure 4.24: The GRF predictions for Model 4

		Model 4
Segment angles (°)	Foot	5.62
	Tibia	1.84
	Femur	1.64
	HAT	0.02
Joint moments (Nm)	Ankle	21.41
	Knee	23.50
	Hip	24.84
GRF (%BW)	y	8.91
	x	1.28

Table 4.6: The RMS errors from the experimental means for Model 4

4.6.3 Model 5 - Seven degrees-of-freedom

No extra penalty functions were required for this model. The dotted vertical line on each of the plots indicates the time at which heel rise began.

Table 4.7 shows, for each parameter of the simulation, the RMS error from the experimental data mean values.

		Model 5	
		Stance	Swing
Segment angles (°)	Foot	4.65	0.40
	Tibia	1.00	0.93
	Femur	2.14	0.63
	HAT	0.02	
Joint moments (Nm)	Ankle	10.06	1.07
	Knee	5.63	8.07
	Hip	31.16	15.63
GRF (%BW)	y	9.45	
	x	0.64	

Table 4.7: The RMS errors from the experimental means for Model 5

This model was able to produce a very strong kinematic match with a mean segment angle RMS error of 1.4°. The stance foot was once again slow to rise in late stance but its final angular position was just on the edge of the desired range (Figure 4.25 and Figure 4.26).

The moment curves stayed mostly within the experimental ranges for the first half of stance (Figure 4.27). There were a number of spikes in the curves in the second half of stance (notably swing knee and both hips) but the general patterns exhibited were close to the empirical measurements.

The GRF component curves in Figure 4.28 were quite similar to those produced by Model 4 except with more obviously visible gradient change at the transition between the foot-

flat and heel rise phases of single support. After heel rise, both curves are closer to the experimental means than their equivalents for Model 4.

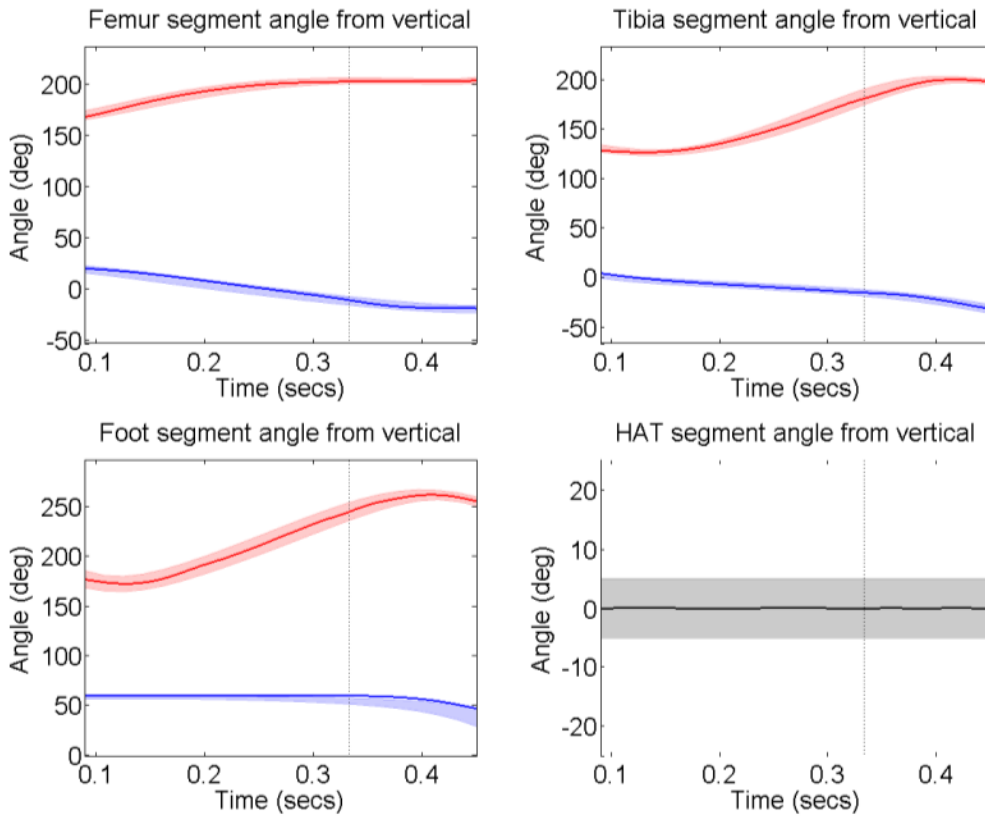


Figure 4.25: The segment angle predictions for Model 5. Blue is stance leg; red is swing leg.

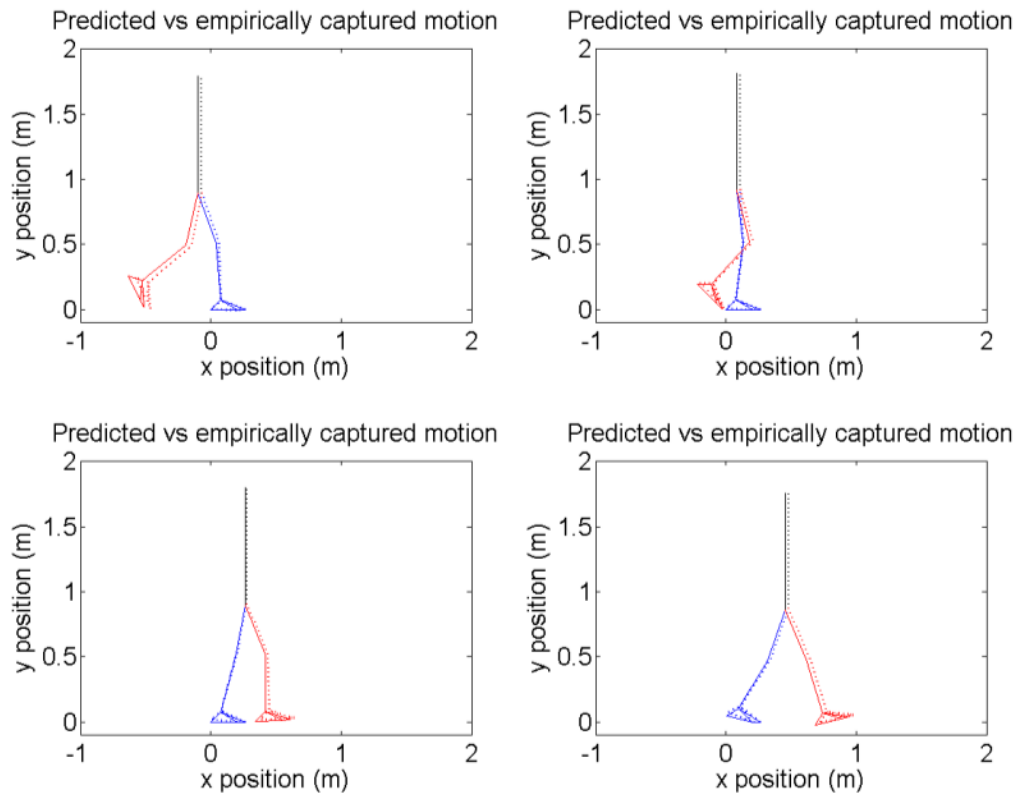


Figure 4.26: The kinematic predictions (solid) vs the empirical means (dotted) for Model 5

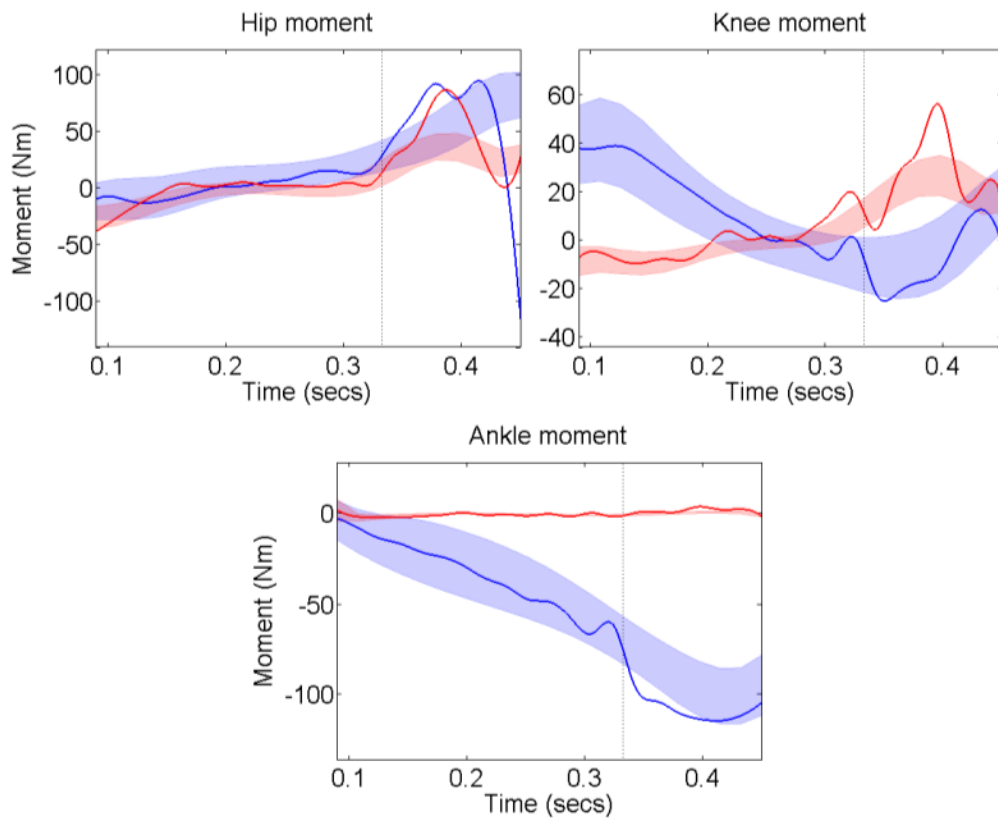


Figure 4.27: The joint moment predictions for Model 5. Blue is stance leg; red is swing leg.

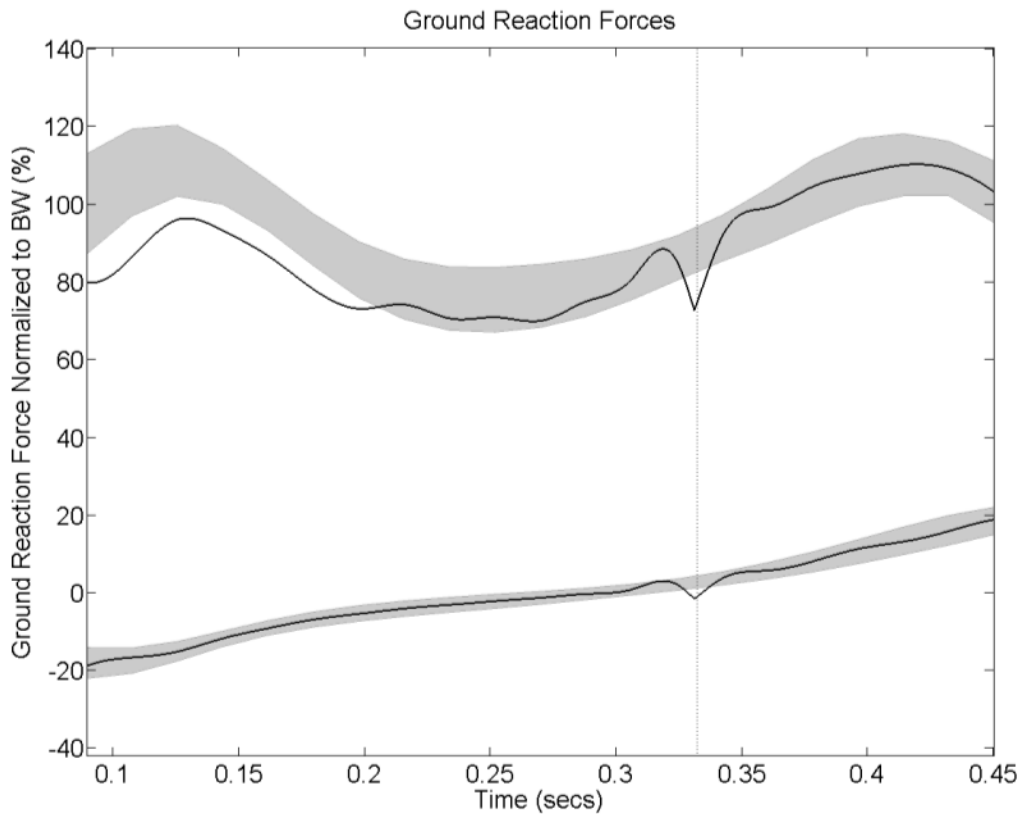


Figure 4.28: The GRF predictions for Model 5

4.7 Discussion

The main aim of this study was to investigate how incremental increases in model complexity affected the simulation results produced. This was considered in terms of both the kinematic and kinetic correlations with an experimental data set. It was hoped that from these results, new evidence for the causes of, and reasons for, different gait mechanisms, could be inferred. The models in this chapter sequentially added a knee joint, an ankle/foot mechanism and a swing leg and observed the consequences of doing so.

Model 3 was conceived as being only slightly more complex than Model 2 from the previous chapter. A knee joint was added to the leg, dividing it into femur and shank/foot segments. This knee joint was controlled by the optimiser defined moment. The only other change from Model 2 was that the hip joint moment was now also defined by the optimiser, rather than calculated so as to maintain an upright trunk segment. Although

this model strayed badly from the experimental data in the second half of stance, both in terms of kinematics and kinetics, during the first half of stance the characteristic initial peak and mid stance trough of the vertical GRF curve were observed (Figure 4.15). This is something that was not seen in Model 2 (Figure 3.3). Although there have been two changes from Model 2, since the trunk remains vertical throughout this simulation, as it did for Model 2, the appearance of the initial peak and mid-stance trough has to be attributable to the presence of an actuated knee joint. The peak, however, was lower in magnitude than the experimental data so it is possible that in reality, there is another mechanism during walking, not modelled in this simplified design, which helps augment this peak.

Model 3.1 was similar to Model 3 except an ankle joint moment was incorporated. In order to do this, a static foot segment was used to provide a joint, and this also had the consequence of providing a more true-to-life geometry and mass distribution. Fairly intuitively, this addition stopped the model *'falling'* too far forward during late stance due to a wider base of support and a control moment at the pivot (compare Figure 4.18 with Figure 4.13). Changes that were more difficult to predict beforehand were the improvements to both vertical and horizontal GRF component curves in early single support (Figure 4.20). It can be inferred from this that ankle moment is one of the mechanisms that contributes to the initial vertical GRF peak, in addition to the presence of the knee joint. However, once more the peak is lower than the experimental data so these cannot be considered the only contributing factors.

It was observed, however, that the moment curves were translated outside of the standard deviation range, despite following the correct shape. This only happens after the ankle moment has been added but before the swing leg is added (i.e. only for Models 3.1 and 4). So it seems that the optimiser is using the ankle moment to compensate for the lack of a swing leg. The offset is towards plantarflexion moment, which suggests that the ankle moment is being used to resist forward motion which otherwise would have been resisted by the action of the swing leg in the last half of single support.

Model 4 advanced the static foot model (Model 3.1) so as to allow heel rise to occur when the point at which the ground reaction vector acted (the COP) reached the anterior pivot at the metatarsal heads. Aside from this, everything else remained the same. The

results of this simulation, prior to the point of heel rise, were very similar to those of Model 3.1. This is to be expected because before that point they are equivalent models. After that point, key differences were observed. Both the vertical and horizontal components of GRF improved to the point that they were both within the respective standard deviation ranges of the empirical data. This was the first model to show the second peak in the vertical GRF force so this is evidence to suggest that the second peak is created by the presence of the ankle/foot mechanism (compare Figure 4.24 with Figure 4.20). It is hypothesised that the behaviour of the horizontal GRF component illustrates the '*push-off*' action and hence shows walking to be an active process, rather than mainly passive.

The most obvious shortcoming of Model 4 was the fact that the heel did not rise fast enough or achieve a final angle within the experimental standard deviation range. It could have been the case that this was a problem inherent within the framework of the model; a consequence of the simple constraint restricting the foot's motion. Another explanation could be that, due to the lack of a swing leg, mass that would have otherwise been much further forward and decelerating had just been incorporated into the HAT segment mass. This meant it was much further back and moving much more slowly.

The moment curves in Model 4 were like those observed in Model 3.1; the correct shape but translated outside of the standard deviation range. Again this may be attributable to the optimiser using the ankle moment to compensate for the lack of a swing leg.

The additional complexity of including swing leg segments in Model 5 provided further improvements to mass distribution and also the accelerations of the different masses. This did indeed increase the amount of heel rise, albeit only just into the standard deviation range of the empirical measurements. Interestingly, this improved heel rise was achieved despite starting at a later point than it did in Model 4.

The joint moments for Model 5 were mostly within the standard deviation ranges, unlike Models 3.1 and 4 where the moment curves appeared to follow the correct patterns except they were translated outside of the standard deviation ranges. After heel rise however, the behaviour of the some moments became more erratic, with a number of spikes appearing. This may be attributed to the simple fact that the model still lacks some

important complexities and the optimiser has been able to compensate for this by making many small adjustments to the joint moment trajectories.

Table 4.8 displays all the results of the different models and their simulations. It is very easy to compare Models 3 (3 DOF) and 3.1 (3 DOF with ankle moment), in terms of kinematics and GRF, as their error calculations were the same. It can be seen that Model 3.1 was a vast improvement, decreasing both these error values to approximately 30% of their original values.

It is, however, very difficult to fairly compare between the other different models and say definitively that one performs better than another. It could be argued that even using the mean values is unfair. Model 4 has a foot segment, the movement of which is restricted by a constraint, so it may be that achieving a good kinematic match for this segment is much more difficult. This would skew the mean error value. Even if the mean kinematic RMS error for Model 4 was worked out without taking the foot segment into account, the result would not be fair to compare against that of Model 3.1, even though the calculation used to evaluate these error values would be exactly the same for both models. This is because Model 4 will have had to make compromises with the accuracy of the HAT, femur and tibia segment kinematics, in order to achieve improved foot segment kinematics.

Another limitation of Model 3.1, that actually gives it an unfair advantage in comparisons with other models, is that there was no restriction on COP position. The moment constraining the foot segment to remain static was calculated as whatever value was necessary to maintain zero angular acceleration. As a result, the COP was able to move in front of the pivot point, and that's exactly what happened for this simulation. This effectively permitted non-physiological ankle moment behaviour and this may go some way to explain why the segment angle RMS error was lower for this model than for Model 4 (Table 4.8).

Despite having almost double the number of segments, and therefore theoretically requiring greater compromise, Model 5 has a lower mean kinematic RMS error than Model 4. Both models have the same constraint of motion on the stance foot so that cannot be considered unfair weighting for this comparison. Whereas the improved mass distribution between Models 3 and 3.1 was relatively small, there is a much more

significant redistribution of mass between Models 4 and 5. This relates directly to the position of the COP as the mass of the swing leg is no longer incorporated into the HAT segment mass but is further forward instead, thus allowing a more realistic COP progression. This, in turn, means that the constraint on the stance foot is less detrimental to the kinematics of Model 5 than it was to Model 4.

Model	3	3.1	4	5
Mean segment angle RMS error (°)	3.72	1.12	2.28	1.40
Mean joint moment RMS error (Nm)	41.46	24.80	23.25	11.94
Mean GRF RMS error (%BW)	47.40	13.35	5.09	5.04

Table 4.8: The RMS errors from the experimental means for all models

A comparison of the moment RMS error values is similarly difficult due to different numbers of joint moments being used in different models. In addition to this, the moment time-histories are '*controlled*' by the optimiser and are unconstrained so as to maximise the chance of finding an optimum kinematic match. A fair assessment of a model's performance should be a parameter that is independent of the simulation setup and an output of the solution, whereas the joint moments are an input.

The only fair comparison seems to be the mean GRF RMS error values because they are calculated the same way for all the models and are independent of the simulation process. They are also an output; they are not being optimised at all. Figure 4.29 illustrates how the mean GRF RMS error changed with increasing complexity. The general trend is that as complexity increases, GRF RMS error decreases. It can also be observed that the rate at which this error decreases, from one model to the next more complex

one, is reducing. This means that the extra complexity is resulting in smaller increases in accuracy. This suggests that there may in fact be a level of complexity that can be deemed 'appropriate' i.e. the optimum trade-off between accuracy of predictions and the time costs to produce a solution. This is however, a small sample number, so this conclusion cannot be drawn with any conviction.

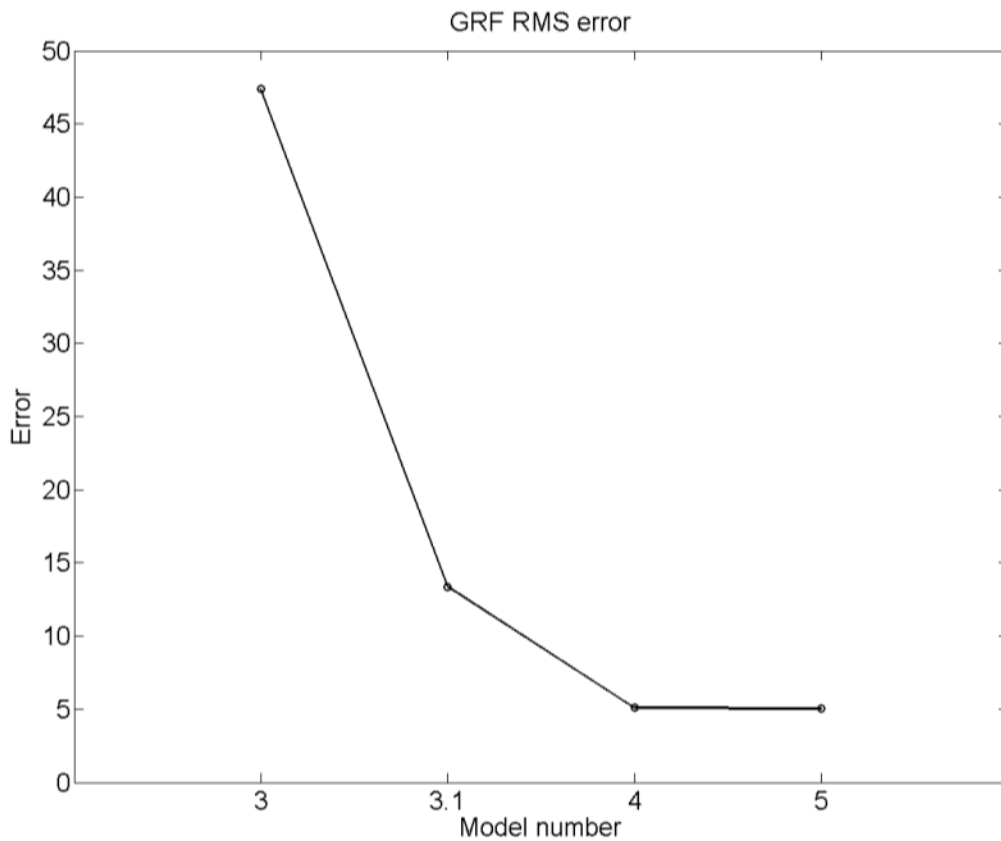


Figure 4.29: The mean GRF RMS error with increasing model complexity from left to right

4.8 Conclusions

Following on from the work in Chapter 3, the modelling of the single support phase was refined by sequentially increasing model complexity. The next chapter examines double support modelling before unifying the best single and double support models to fully simulate a gait cycle and thus directly addresses the final part of Research Question 3: *“What is the minimum complexity required for a numerical model to predict the*

kinematics and kinetics of healthy sagittal bipedal gait, within a single standard deviation range, for the full gait cycle?”

The sequential addition of extra complexities showed that the presence of a knee joint and an active ankle moment both contribute greatly to achieving the initial peak in the vertical GRF component curve. The curves observed were too low however, so these are not the sole contributors. The action of heel rise is largely responsible for producing the second peak in the vertical GRF component curve. The accuracy of this second peak is further improved by the presence of a swing leg as it permits a more realistic mass distribution and acceleration behaviour. These observations directly answer Research Question 2: *“To what extent can a sequence of numerical models, incrementally increasing in complexity, highlight the effects of different gait mechanisms?”*

It has been shown that a seven DOF model of walking achieves a simulation where the predicted kinematics and GRF curves are within the single standard deviation range for the vast majority of the simulation time. This goes some way to answering the first two parts of Research Question 3: *“What is the minimum complexity required for a numerical model to predict the kinematics and kinetics of healthy sagittal bipedal gait, within a single standard deviation range, for one-legged (first part) and two-legged (second part) single support?”*

5 DOUBLE SUPPORT AND FULL GAIT CYCLE MODELS

5.1 Introduction

This project has already observed the shortcomings of simple walking models when it comes to modelling double support and step-to-step transitions (Chapter 3). Discontinuities will often arise in the velocity of the system's CM and the GRF that is produced. Better double support modelling will help move the system CM along a more anatomically accurate path and adding constraints to try to achieve bilateral symmetry will minimise step-to-step discontinuities.

As the previous chapter highlighted, this project aims to encompass all aspects of healthy walking, and this includes the resulting kinetics. A difficulty that arises with double support modelling is how to distribute the GRF between the two ground contact points. There are more unknowns than defining equations, thus creating an indeterminate problem. Ren et al. (2007) used a smooth transition assumption to combat this problem. It may be possible to utilise an optimisation function also but this study found a novel way to calculate these forces using the underlying mechanics, the details of which are described in this chapter.

This work will be focussed on attempting to answer Research Question 3c: *what is the minimum complexity required for a numerical model to predict the kinematics and kinetics of healthy sagittal bipedal gait, within a single standard deviation range, for a full gait cycle?* An important part of this is achieving good double support results. This again contributes to the clinical relevance of the simulations.

In terms of the wider project aims, the work in this chapter will allow simulations of full gait cycles to be performed. In the next chapter, where data will be collected from a number of different subjects, the simulations can be individualised with each person's data. This would be a fundamental requirement for any clinically applicable gait model.

The structure of this chapter will be much the same as the previous. Firstly the modelling framework will be described. This will describe where these models are different, mathematically, from the single support ones and what this means for the results

produced. Next, the specifics of the different models and their dynamics will be laid out in free body diagrams before the setup for the simulation will be outlined.

5.2 The Modelling Framework

5.2.1 Lagrangian multipliers and constraints

The mathematics that will be used in this chapter is an extension of the Lagrange mechanics used in the previous one. Whereas the last chapter was concerned with open-link chains, double support models require closed-link chains. Further considerations regarding the appropriate constraints to achieve this goal must be made. An advantage of Lagrange mechanics is that it is possible to apply constraints relatively simply using ‘Lagrange multipliers’.

In order to apply a constraint, the j^{th} constraint function (f_j) is defined such that:

$$f_j = 0$$

Equation 5.1

Therefore, the governing Lagrange equation is modified to include the Lagrange multipliers:

$$\frac{d}{dt} \left(\frac{\partial L}{\partial \dot{q}_i} \right) - \frac{\partial L}{\partial q_i} - \sum_j \left(\lambda_j \frac{\partial f_j}{\partial q_i} \right) = Q_i$$

Equation 5.2

For a given number of constraint equations, m , the same number of new unknown variables need to be solved. This is done by incorporating the constraint equations into the matrix formulation of the equations of motion, thus solving for \ddot{q}_i and λ_j simultaneously. If the constraint equations are purely position (only contain q_i terms),

they need to be differentiated twice so that they contain \ddot{q}_i terms. This new equation then needs to be separated into two functions, one that contains only the \ddot{q}_i terms and one that contains the rest of the terms (see Equation 5.3). These terms can now be incorporated into the matrix formulation (Equation 5.4).

$$\frac{d^2 f_j}{dt^2}(\ddot{q}_i, \dot{q}_i, q_i, t) = g_j(\ddot{q}_i, t) + h_j(\dot{q}_i, q_i, t)$$

Equation 5.3

$$\begin{bmatrix} b_{i,i} & -\frac{\partial f_j}{\partial q_i} \\ g_j(\ddot{q}_i, t) & 0 \end{bmatrix} \begin{bmatrix} \ddot{q}_i \\ \lambda_j \end{bmatrix} = \begin{bmatrix} c_i \\ -h_j(\dot{q}_i, q_i, t) \end{bmatrix}$$

Equation 5.4

It's important to note that \ddot{q}_i is no longer independent. For a chain with n DOF and m constraint equations, only $n-m$ are independent. In theory, computing \ddot{q}_i for all DOF should still produce solutions which are consistent with the constraint equations. However, it is possible that computational rounding errors may occur, which over the course of a whole simulation, would accumulate. Consequently, for this study, the numerical integration of the angular positions and angular velocities will be performed, in the same way as previous chapters, for the first $n-m$ links in the chain and the constraint equations will be used for the final m segments (Ülker, 2010).

The Lagrange multipliers are also useful in another way. It is possible to calculate the force required to maintain a given constraint and this can be very useful in understanding the system dynamics. In the case of this study, the forces required to hold the trailing foot to the ground can be used to calculate the GRF under that foot. By using inverse dynamics, in the same way as before, to calculate the total GRF, a simple subtraction can be used to assess the GRF distribution. This process is detailed in Section 5.2.4.

Aside from these changes, the rest of the simulation procedure will be the same. The same optimisation framework is applied to determine the moment actuations required for driving the model to track the measured generalised coordinates.

5.2.2 Four-chain example

The following is a worked example (Ülker, 2010) of how Lagrange multipliers and constraints can be incorporated so as to constrain the end of a four-segment chain to the ground (Figure 5.1). This requires the application of two constraint equations, f_1 and f_2 , to restrict motion in the horizontal and vertical directions respectively, in order to hold the end of the chain to a point on the ground, a given distance, S , from the start of the chain:

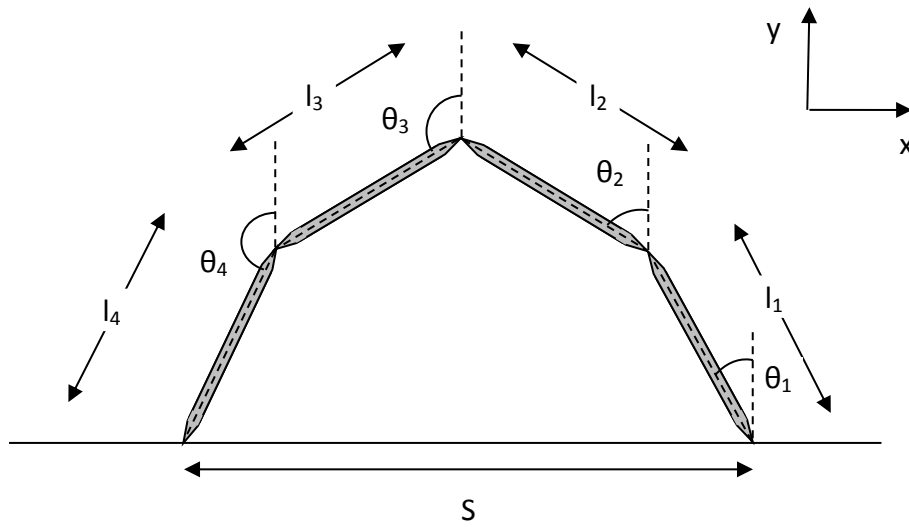


Figure 5.1: A four segment closed chain

$$f_1 = \left(\sum_{i=1}^n (-l_i \sin \theta_i) \right) + S = 0$$

$$\therefore -l_1 \sin \theta_1 - l_2 \sin \theta_2 - l_3 \sin \theta_3 - l_4 \sin \theta_4 + S = 0$$

Equation 5.5

$$f_2 = \sum_{i=1}^n (l_i \cos \theta_i) = 0$$

$$\therefore l_1 \cos \theta_1 + l_2 \cos \theta_2 + l_3 \cos \theta_3 + l_4 \cos \theta_4 = 0$$

Equation 5.6

These are combined and rearranged to give:

$$\begin{aligned}
 l_3^2 &= (-l_1 \sin \theta_1 - l_2 \sin \theta_2 - l_4 \sin \theta_4 + S)^2 + (l_1 \cos \theta_1 + l_2 \cos \theta_2 + l_4 \cos \theta_4)^2 \\
 &= l_1^2 + l_2^2 + l_4^2 + S^2 - 2Sl_1 \sin \theta_1 - 2Sl_2 \sin \theta_2 - 2Sl_4 \sin \theta_4 + 2l_1l_2(\sin \theta_1 \sin \theta_2 + \cos \theta_1 \cos \theta_2) \\
 &\quad + 2l_1l_4(\sin \theta_1 \sin \theta_4 + \cos \theta_1 \cos \theta_4) + 2l_2l_4(\sin \theta_2 \sin \theta_4 + \cos \theta_2 \cos \theta_4)
 \end{aligned}$$

Equation 5.7

The following trigonometric identities are substituted into Equation 5.7 and $\tan\left(\frac{\theta_4}{2}\right) = X$ is assumed.

$$\sin \theta_4 = \frac{2 \tan\left(\frac{\theta_4}{2}\right)}{1 + \tan^2\left(\frac{\theta_4}{2}\right)}$$

$$\cos \theta_4 = \frac{1 - \tan^2\left(\frac{\theta_4}{2}\right)}{1 + \tan^2\left(\frac{\theta_4}{2}\right)}$$

Equations 5.8, 5.9

$$\begin{aligned}
 0 &= l_1^2 + l_2^2 + l_4^2 + S^2 - l_3^2 - 2Sl_1 \sin \theta_1 - 2Sl_2 \sin \theta_2 - 2Sl_4 \left(\frac{2X}{1 + X^2}\right) \\
 &\quad + 2l_1l_2(\sin \theta_1 \sin \theta_2 + \cos \theta_1 \cos \theta_2) + 2l_1l_4 \sin \theta_1 \left(\frac{2X}{1 + X^2}\right) + 2l_1l_4 \cos \theta_1 \left(\frac{1 - X^2}{1 + X^2}\right) \\
 &\quad + 2l_2l_4 \sin \theta_2 \left(\frac{2X}{1 + X^2}\right) + 2l_2l_4 \cos \theta_2 \left(\frac{1 - X^2}{1 + X^2}\right)
 \end{aligned}$$

Equation 5.10

A number of terms are grouped to make the expression more manageable:

$$K_1 = l_1^2 + l_2^2 + l_4^2 + S^2 - l_3^2$$

$$K_2 = -2Sl_1 \sin \theta_1 - 2Sl_2 \sin \theta_2$$

$$K_3 = 4Sl_4$$

$$K_4 = 2l_1l_2(\sin \theta_1 \sin \theta_2 + \cos \theta_1 \cos \theta_2)$$

$$K_5 = 4l_1l_4 \sin \theta_1 + 4l_2l_4 \sin \theta_2$$

$$K_6 = 2l_1l_4 \cos \theta_1 + 2l_2l_4 \cos \theta_2$$

Equations 5.11, 5.12, 5.13, 5.14, 5.15, 5.16

A quadratic equation can now be evaluated, solved for X and hence give θ_4 .

$$aX^2 + bX + c = 0$$

where:

$$a = K_1 + K_2 + K_4 - K_6$$

$$b = K_3 + K_5$$

$$c = K_1 + K_2 + K_4 + K_6$$

Equation 5.17

Once θ_4 is known, the constraint equations are used to calculate θ_3 . To calculate the velocities of these two dependent segments, the constraint equations are differentiated.

$$-\dot{\theta}_1l_1 \cos \theta_1 - \dot{\theta}_2l_2 \cos \theta_2 - \dot{\theta}_3l_3 \cos \theta_3 - \dot{\theta}_4l_4 \cos \theta_4 = 0$$

Equation 5.18

$$-\dot{\theta}_1l_1 \sin \theta_1 - \dot{\theta}_2l_2 \sin \theta_2 - \dot{\theta}_3l_3 \sin \theta_3 - \dot{\theta}_4l_4 \sin \theta_4 = 0$$

Equation 5.19

Equation 5.18 is divided by $\cos \theta_3$ and Equation 5.19 is divided by $\sin \theta_3$, then the latter is subtracted from the former:

$$\frac{\dot{\theta}_1l_1 \sin \theta_1 + \dot{\theta}_2l_2 \sin \theta_2 + \dot{\theta}_4l_4 \sin \theta_4}{\sin \theta_3} - \frac{\dot{\theta}_1l_1 \cos \theta_1 + \dot{\theta}_2l_2 \cos \theta_2 + \dot{\theta}_4l_4 \cos \theta_4}{\cos \theta_3} = 0$$

$$\begin{aligned} \therefore \dot{\theta}_1 l_1 (\sin \theta_1 \cos \theta_3 - \cos \theta_1 \sin \theta_3) + \dot{\theta}_2 l_2 (\sin \theta_2 \cos \theta_3 - \cos \theta_2 \sin \theta_3) \\ + \dot{\theta}_4 l_4 (\sin \theta_4 \cos \theta_3 - \cos \theta_4 \sin \theta_3) = 0 \end{aligned}$$

$$\therefore \frac{\dot{\theta}_1 l_1}{l_4} \left(\frac{\sin(\theta_1 - \theta_3)}{\sin(\theta_3 - \theta_4)} \right) + \frac{\dot{\theta}_2 l_2}{l_4} \left(\frac{\sin(\theta_2 - \theta_3)}{\sin(\theta_3 - \theta_4)} \right) = \dot{\theta}_4$$

Equation 5.20

The other dependent angular velocity can be calculated from Equation 5.18 and Equation 5.19.

Now that all the angular position and angular velocity values are known, the equations of motion can be evaluated. As mentioned before, the constraint equations are incorporated into the same matrix formulation that is used to calculate \ddot{q}_i . Since neither f_1 nor f_2 contain any of the unknowns, they are differentiated twice by time, before being incorporated into the matrix formulation. This gave:

$$\begin{bmatrix} b_{1,1} & b_{1,2} & b_{1,3} & b_{1,4} & l_1 \cos \theta_1 & l_1 \sin \theta_1 \\ b_{2,1} & b_{2,2} & b_{2,3} & b_{2,4} & l_2 \cos \theta_2 & l_2 \sin \theta_2 \\ b_{3,1} & b_{3,2} & b_{3,3} & b_{3,4} & l_3 \cos \theta_3 & l_3 \sin \theta_3 \\ b_{4,1} & b_{4,2} & b_{4,3} & b_{4,4} & l_4 \cos \theta_4 & l_4 \sin \theta_4 \\ l_1 \cos \theta_1 & l_2 \cos \theta_2 & l_3 \cos \theta_3 & l_4 \cos \theta_4 & 0 & 0 \\ l_1 \sin \theta_1 & l_2 \sin \theta_2 & l_3 \sin \theta_3 & l_4 \sin \theta_4 & 0 & 0 \end{bmatrix} \begin{bmatrix} \ddot{\theta}_1 \\ \ddot{\theta}_2 \\ \ddot{\theta}_3 \\ \ddot{\theta}_4 \\ \lambda_{f_1} \\ \lambda_{f_2} \end{bmatrix} = \begin{bmatrix} c_1 \\ c_2 \\ c_3 \\ c_4 \\ \sum_{i=1}^4 l_i \dot{\theta}_i \sin \theta_i \\ \sum_{i=1}^4 -l_i \dot{\theta}_i \cos \theta_i \end{bmatrix}$$

Equation 5.21

The unknowns can be solved by way of matrix algebra.

5.2.3 Numerical integration

The equations of motion were numerically integrated for each time instant using the same Taylor expansion method used in the previous chapters (Section 3.4.2), except for

the two dependent segments which are calculated for each time step by the method outlined in the constrained four segment chain example (Section 5.2.2).

5.2.4 Ground reaction force calculations

During double support, since both feet are in contact with the ground, the GRF can be calculated but there is an infinite number of ways this can be distributed between the two feet. Previous models have made a smooth transition assumption (Ren et al., 2007) but there is another way, specific to the models in this project, that is preferred. The Lagrangian multipliers provide constraint forces that restrict motion for the point of contact between the trailing foot and the ground. Since the constraint forces are acting upon the trailing foot and it is stationary, it can be assumed that the GRF components beneath it are equal to these constraint forces. The forces the constraints produce can be expressed:

$$F_{q_i} = \lambda \frac{\partial f}{\partial q_i}$$

Equation 5.22

For this model $q = \theta$. However, it was preferable to have the forces in the x and y directions. Therefore:

$$F_x = \lambda_{f_1} \left(\frac{\partial f_1}{\partial \theta_i} \frac{\partial \theta_i}{\partial x} \right) = \lambda_{f_1} \left(-l_i \cos \theta_i \cdot \frac{1}{-l_i \cos \theta_i} \right) = \lambda_{f_1}$$

Equation 5.23

$$F_y = \lambda_{f_2} \left(\frac{\partial f_2}{\partial \theta_i} \frac{\partial \theta_i}{\partial y} \right) = \lambda_{f_2} \left(-l_i \sin \theta_i \cdot \frac{1}{-l_i \sin \theta_i} \right) = \lambda_{f_2}$$

Equation 5.24

The GRF components are calculated in the same way as they were for the single support models. This gives the total force underneath both feet so these values are then subtracted from the relevant total GRF component value in order to give the force beneath the leading foot.

5.3 Double support model

The double support model was originally designed using the same seven DOF model as for Model 5 single support. However, it was discovered that using the experimental data segment angles with the model's proportions, both feet did not remain on the ground throughout. This was because the feet of the seven DOF model extended from ankles to metatarsal head only. A toe segment was added to the trailing foot, hence creating a closed chain of eight segments and the ground but, because of the dependent segments, it only had seven DOF. This toe segment had no mass so did not affect the mass distribution of the system.

Three different phases of double support were defined as submodels. The differences between these phases were to do with the designated pivot points and the constraints applied. These submodels were run sequentially i.e. the final conditions of Phase 1 were the initial conditions of Phase 2 and the final conditions of Phase 2 were the initial conditions of Phase 3. This meant all three were grouped into a single simulation and therefore, a single optimisation procedure. Collectively, they were named the DS model.

5.3.1 Phase 1: Lead heel contact to lead foot flat

The first phase to be modelled began at the exact instant that the lead foot made contact with the ground. The lower limb and HAT segments were represented by eight rigid links. Unlike the previous seven segment model that was used for single support, the lead foot segment extended from the ankle to the point of contact with the ground at the heel. The d and e distances for the foot were chosen so as to keep the mass in the same position as it was for single support, relative to the ankle joint (dashed lines on Figure 5.2). At the other end of the chain, the end of the trailing toe segment was constrained to a fixed

point on the ground. There was also a moment acting about the end of the toe segment, constraining it to remain flat until said moment reached zero (as indicated on Figure 5.2 by the darker colouring). This constraint worked in the exact same way as for the transition in single support between foot flat and heel rise. It was effectively tracking the COP underneath the toe segment. The dependent segments were the trailing foot and tibia. Phase 1 ended when the lead foot became flat on the ground.

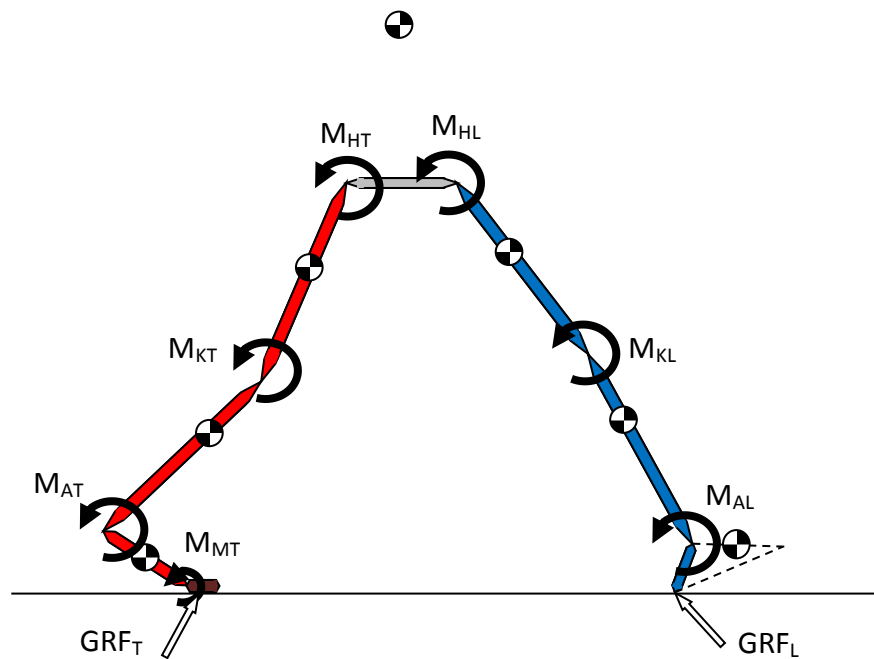


Figure 5.2: DS model, phase 1: A free body diagram

5.3.2 Phase 2: Lead foot flat to trail foot toe-rise

Phase 2 began at the point where the lead foot became flat on the ground. In this model, the leading foot and trailing toe segments were stationary (indicated by the darker colouring on the diagram Figure 5.3) so there were only six moving segments. The dependent segments were the trailing foot and tibia. The simulation continued until trail foot toe-rise.

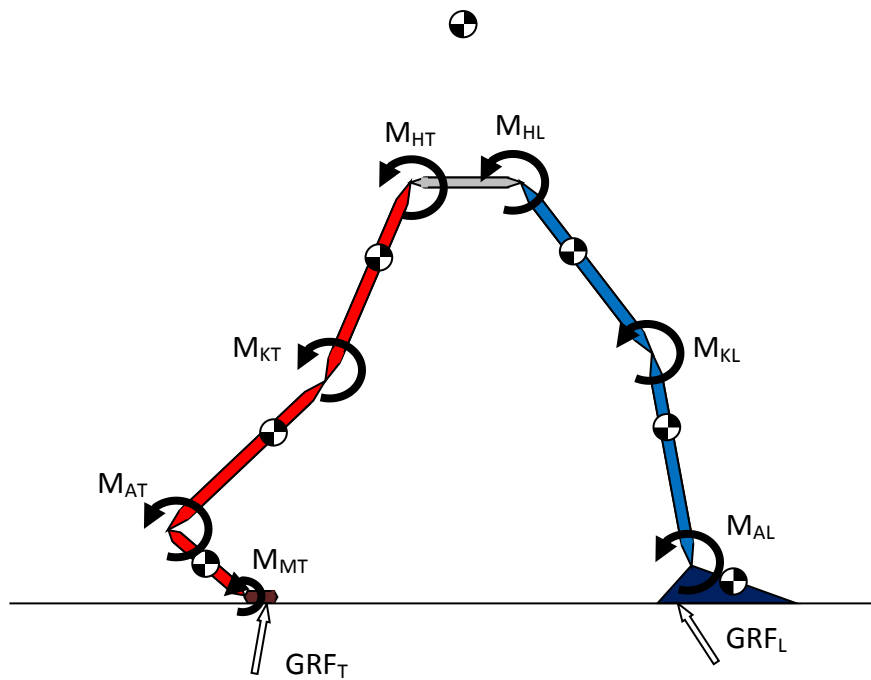


Figure 5.3: DS model, phase 2: A free body diagram

5.3.3 Phase 3: Trail foot toe-rise to trail foot toe-off

Phase 3 began at the point where the metatarsal head of the trailing foot left the ground. In this model, the lead foot was stationary (hence the dark colouring on the diagram in Figure 5.4) so there were only seven moving segments. For this phase of the model, the dependent segments were the trailing foot and trailing toe segments.

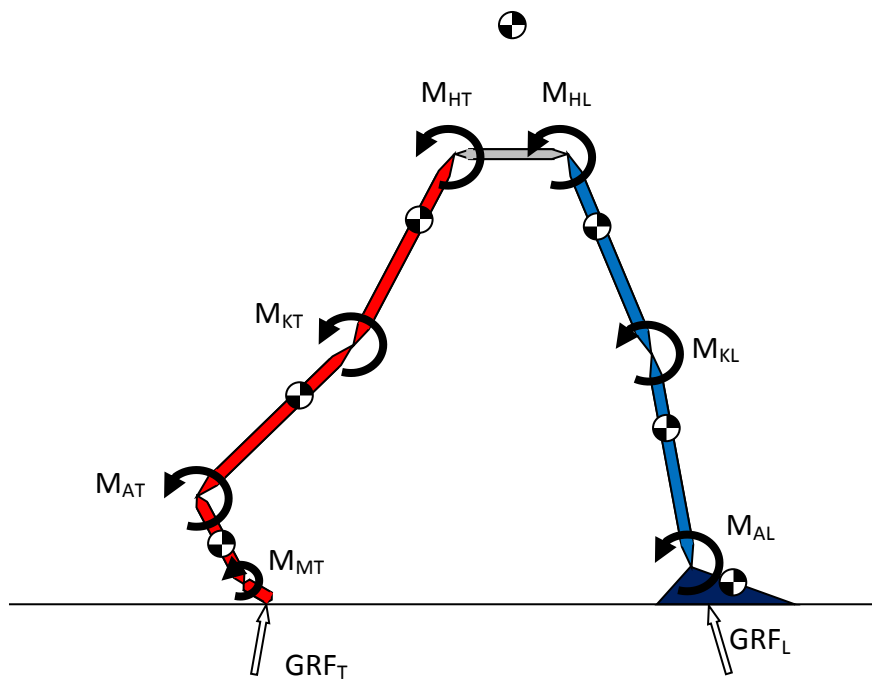


Figure 5.4: DS model, phase 3: A free body diagram

5.4 Simulation methods

A single simulation ran all three double support submodels consecutively, where the terminal state of one was the initial state of the next. The time for which the simulations were run was chosen to be 0.09 seconds. This time span covered 10% of a full gait cycle at the chosen walking velocity. Many sources cite approximately 10% as the length of the double support phase (Kirtley, 2006; Perry, 1992; Rose & Gamble, 1994; Whittle, 2007). All the initial conditions were taken from the experimental data mentioned by Winter (1979, 1991). The anthropometric measures were the same as those for Model 5 (Table 4.3).

5.4.1 Joint moments

Each joint moment was defined by 6 nodes starting at $t=0$, and then at evenly spaced intervals until $t=0.09$. These points represented 2% instants between 0-10% of the gait cycle because these were the points for which experimental data were available.

5.4.2 Optimisation parameters

The optimised parameters were the initial angular positions (from the vertical axis), initial angular velocities of the body segments, and the moment nodes (see Section 4.5.1). The initial estimates for all these values were taken from the experimental data.

5.4.3 Cost function

The chosen cost function was the kinematic RMS error from the experimental data. This was calculated in the same way as the previous study (Section 4.5.3).

Winter's data (1979, 1991) and the HAT kinematic approximation (see Section 4.5.3) were used as the input to the model and for comparison, as an assessment of its success, just like for the single support models. For each parameter, there were 6 data points from the experimental data (the final time instant being the same as the initial time instant in the single support simulations). The experimental data was interpolated in MATLAB, using the spline function (Section 4.5.1), and comparisons were made at every 10^{-3} seconds time interval. A Root Mean Squared (RMS) error comparison, normalised by the parameter's standard deviation, was used to give a single numerical value of the error between simulation and experimental results.

5.4.4 Algorithms

For all double support simulations, the GlobalSearch MATLAB (Section 4.5.4) function was used and then followed with a local optimisation function (Lagarias et al., 1998; Nocedal & Wright, 2006) in order to find a more accurate solution.

5.5 Results

The shaded areas on each of the following plots show the values covered by ± 1 standard deviation from the experimental mean. The solid lines show the results predicted by simulations. The dotted lines on the graphs below indicate the time at which the lead foot flat and trailing foot toe-rise events occurred.

The only extra constraint for this simulation was one to ensure the solution was not complex. For complex solutions, the cost function was set to 9999 so that the optimiser would avoid these results.

The kinematic results for the DS model were all within their respective experimental data standard deviation ranges for almost the entirety of the simulation. Only the lead foot was slightly outside the standard deviation range (4.45°) in early stance (RMS error of 5.29°).

The moment curves were more erratic with only one (trailing ankle joint moment) remaining within the standard deviation range for the full simulation time. The mean error of 16.46Nm appeared to be in a similar range to the single support models (Table 4.8) but, considering that this simulation ran for a quarter of the time of the single support ones, the error would be expected to be lower.

The GRF curves were predicted well, remaining within the experimental data range throughout the simulation. There were slight discontinuities in the gradient of the GRF curves at the point of foot flat (the first dotted line). This is because at this point, the foot segment goes from having an angular velocity to having zero velocity in a single time instant. This was unavoidable given the dynamics of the model.

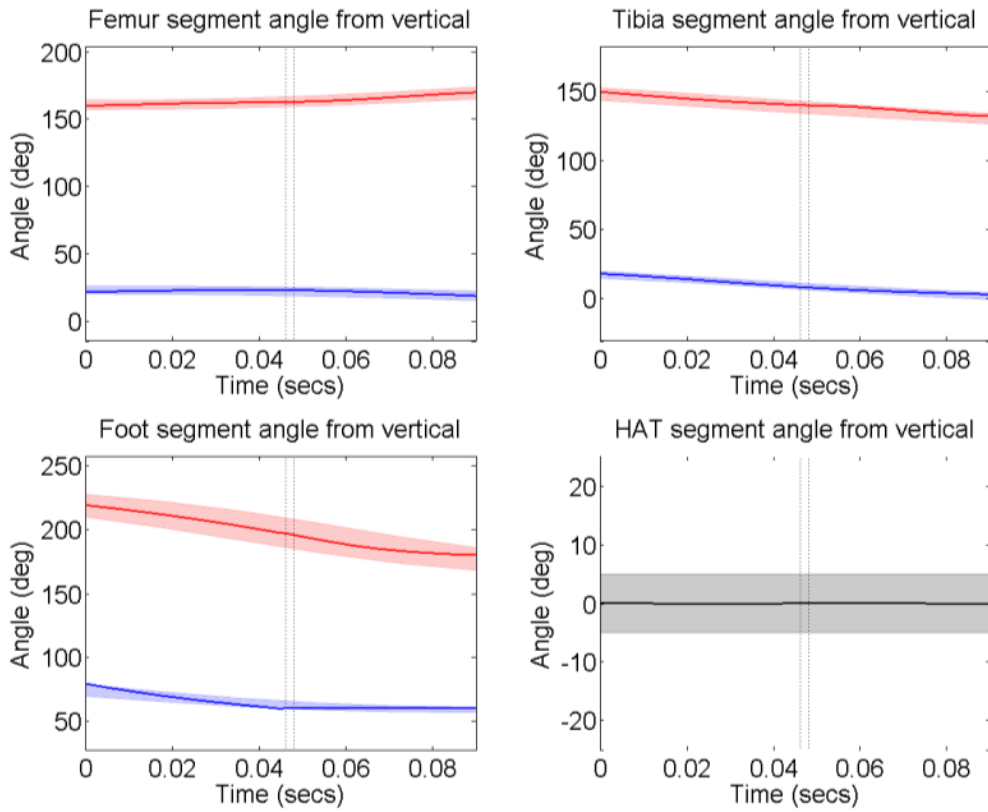


Figure 5.5: The segment angle predictions for the DS model. Blue is lead leg; red is trail leg.

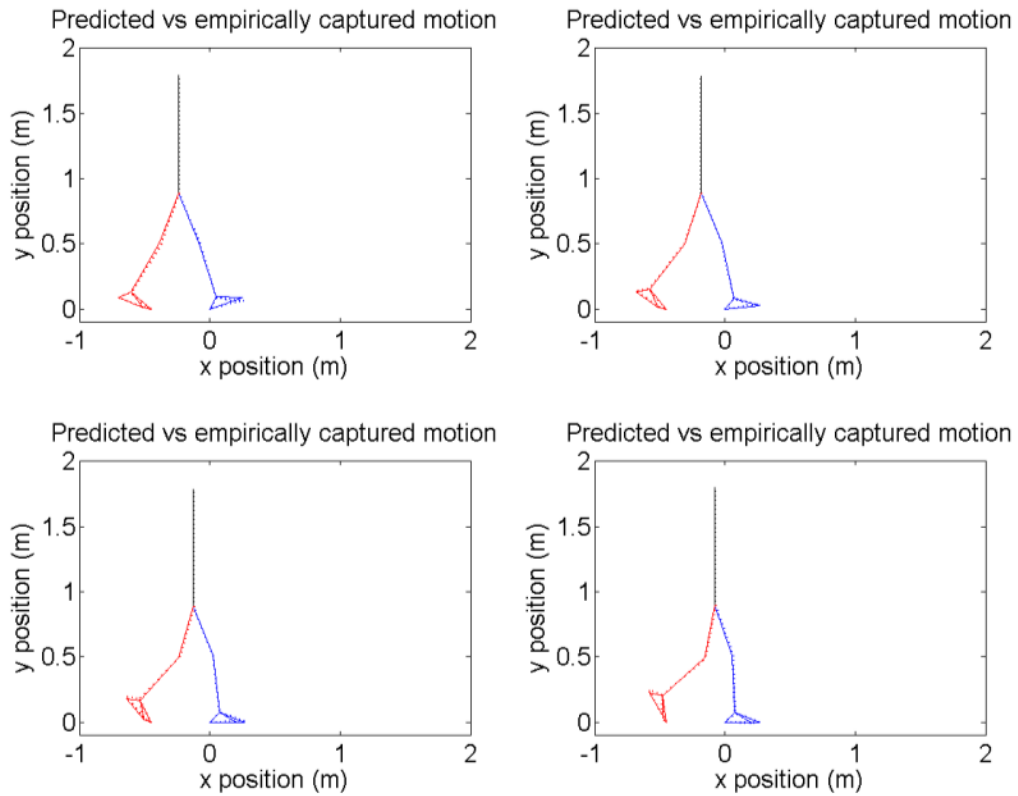


Figure 5.6: The kinematic predictions (solid) vs the empirical means (dotted) for the DS model

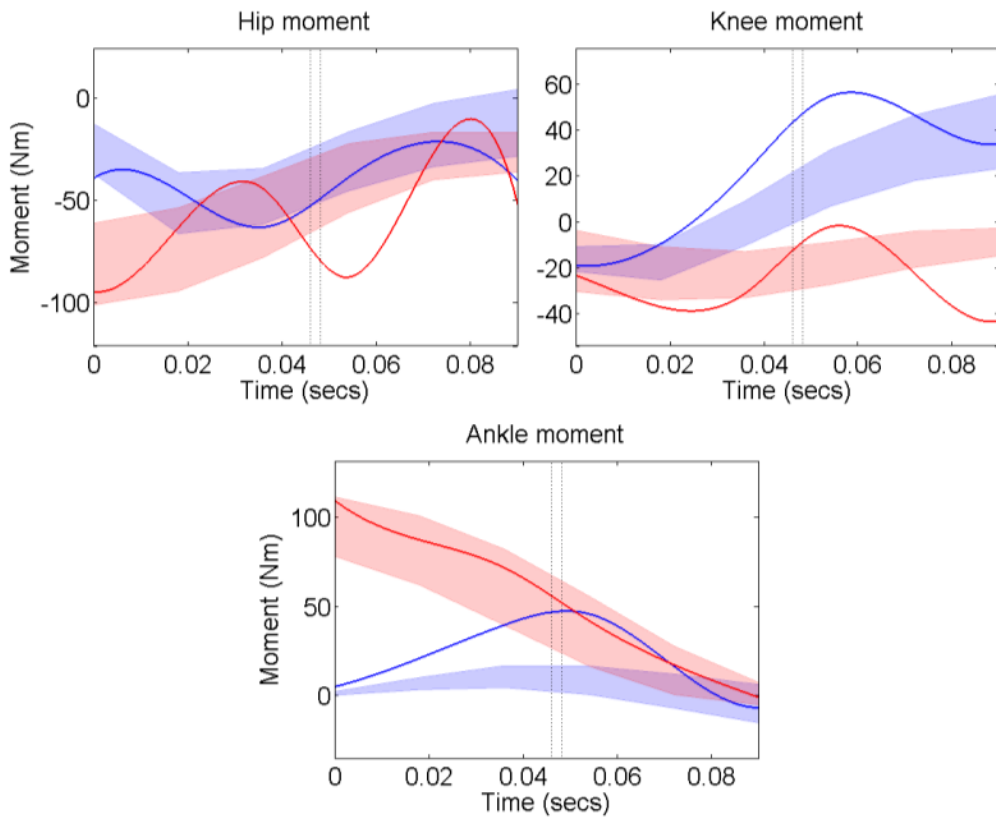


Figure 5.7: The joint moment predictions for the DS model. Blue is lead leg; red is trail leg.

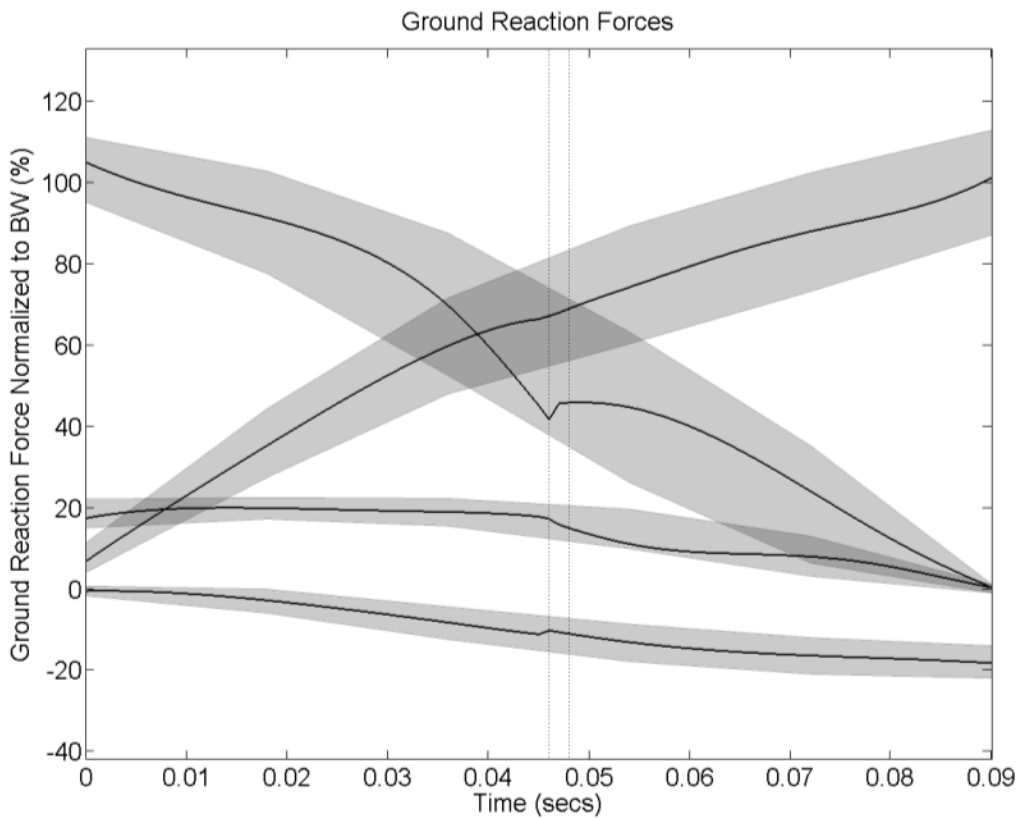


Figure 5.8: The GRF moment predictions for the DS model

		DS Model	
		Leading	Trailing
Segment angles (°)	Foot	1.85	1.11
	Tibia	0.55	1.70
	Femur	0.76	0.39
	HAT	0.03	
Joint moments (Nm)	Ankle	22.66	7.04
	Knee	19.87	16.04
	Hip	10.53	22.64
GRF (%BW)	y	0.67	3.76
	x	0.25	1.51

Table 5.1: The RMS error values for the DS model

5.6 Full gait cycle simulation

To simulate a full gait cycle, the double support simulation results were plotted in conjunction with the single support ones. No extra simulation or optimisation procedure was performed and there was no continuation enforced between the final state of the DS model and the initial state of Model 5 (and vice versa). This meant that discontinuities were possible at the transitions between double and single support.

The following plots illustrate what happened when the best results for each were added together; the DS model followed by Model 5 of single support. This meant no continuity of angular positions, velocities, accelerations or moments were enforced at the transition from double to single support. This was referred to as the ‘*Sum*’ model.

5.6.1 Sum model

The layouts of the following plots are slightly different to previous models. The plots have been designed to show behaviour over a full gait cycle. For example, for a given segment, the plot will track its behaviour starting as part of the leading leg in double support, then the stance leg in single support, then the trailing leg in double support, and finally the swing leg in single support (Figure 5.10). The same thing is done for the joint moments (Figure 5.11) and GRF (Figure 5.12). The purpose of this is to give a clearer idea of how the model can handle step-to-step transition.

The plot showing the kinematic comparison with the experimental means (Figure 5.9), however, is shown at equalled spaced time instants starting at $t=0$ and ending at the end of the first half gait cycle. This provides a better idea of how the two compare and avoids repetition.

The dotted lines on plots indicate the transitions between the different model phases.

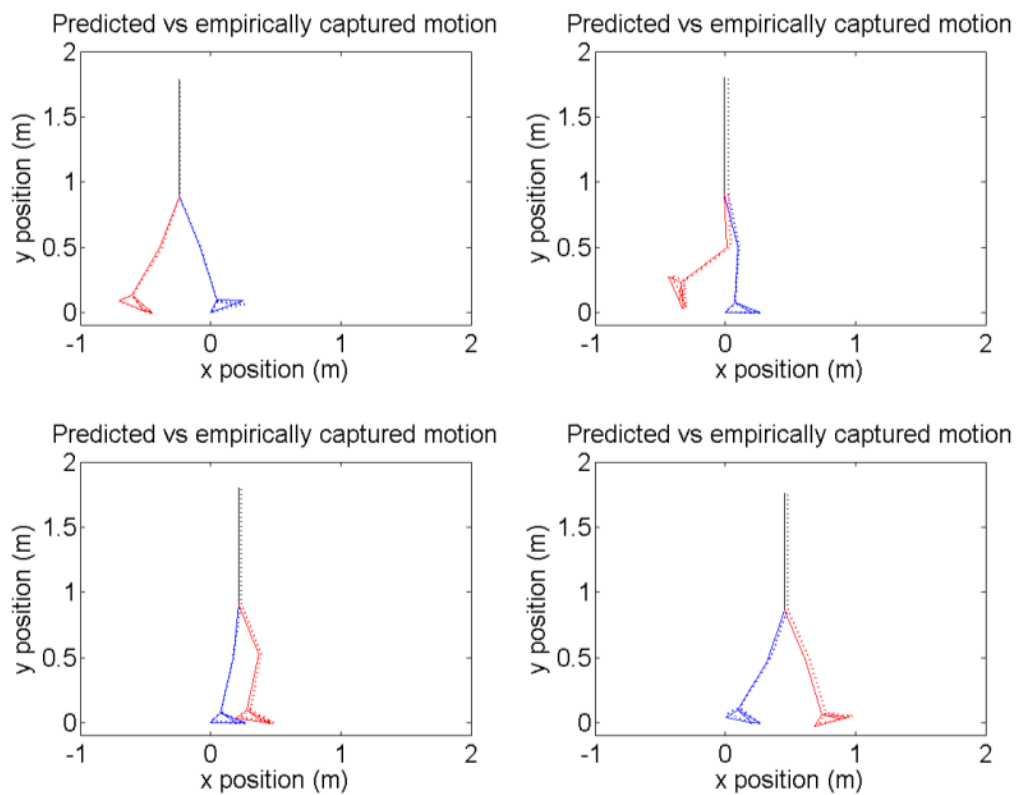


Figure 5.9: The kinematic predictions (solid) vs the empirical means (dotted) for the Sum model

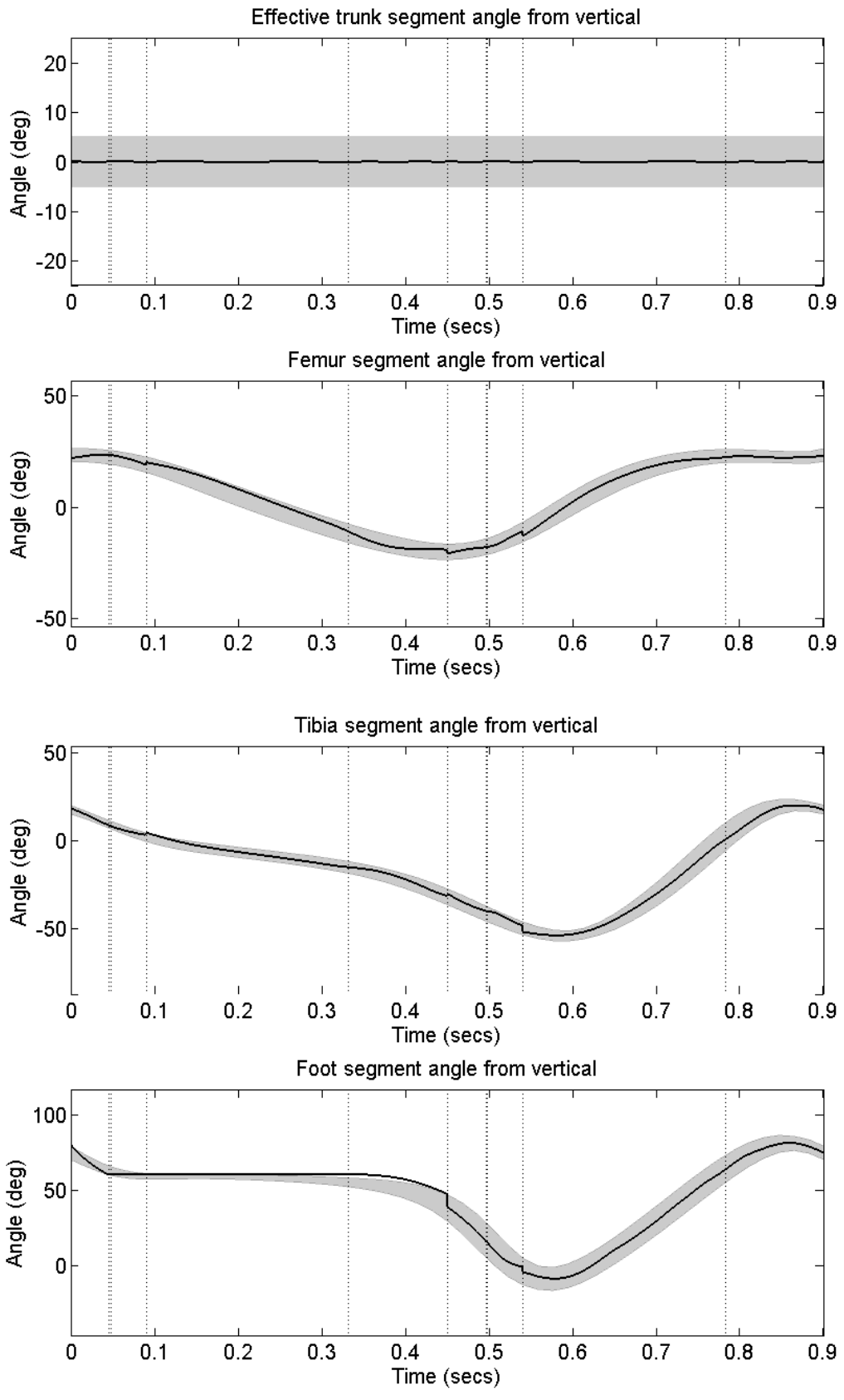


Figure 5.10: The segment angle predictions for the Sum model

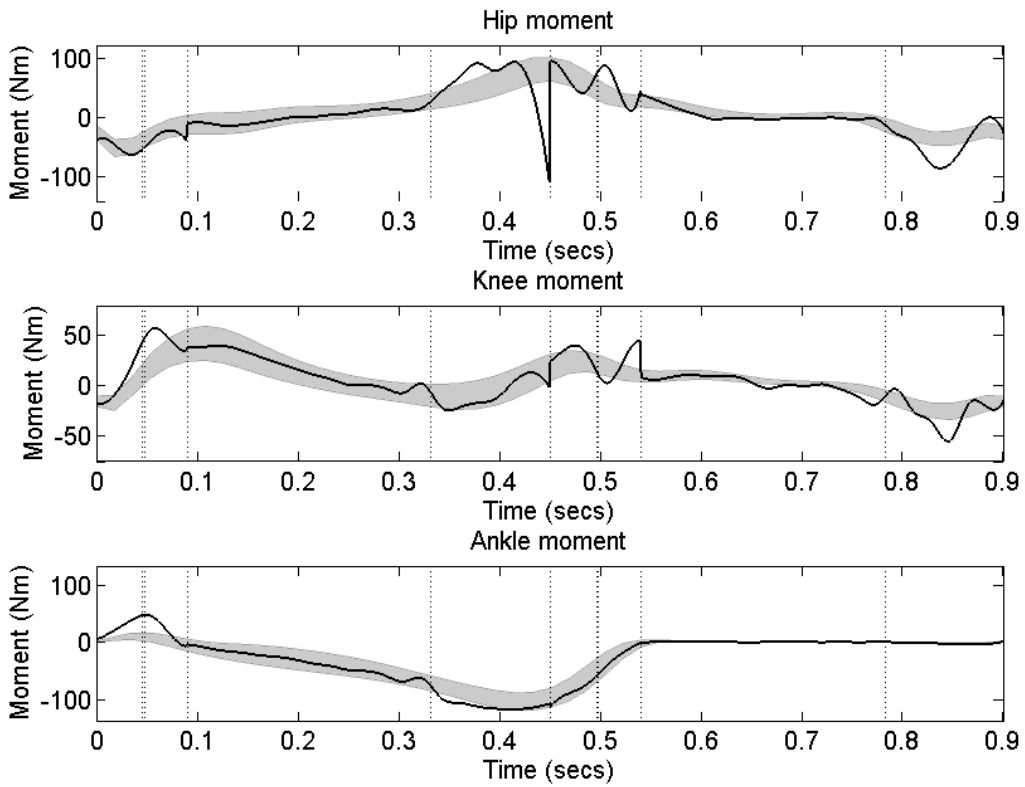


Figure 5.11: The joint moment predictions for the Sum model

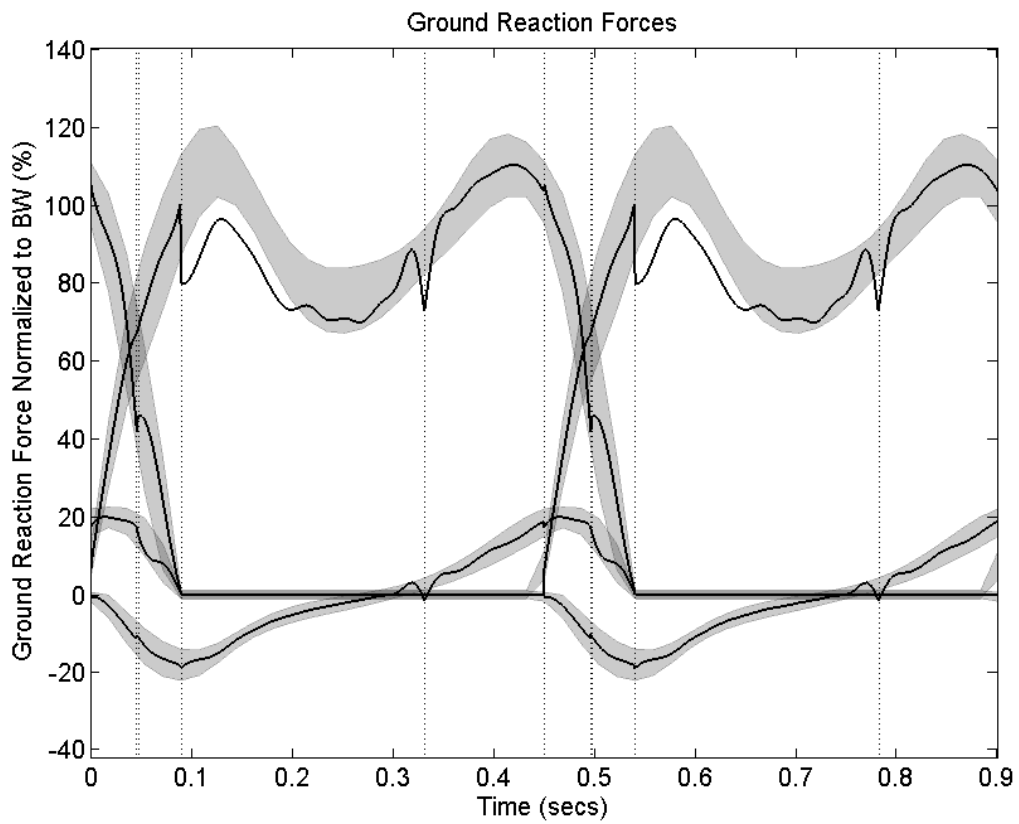


Figure 5.12: The GRF moment predictions for the Sum model

The numerical error values (Table 5.2) also only consider the first half of the gait cycle so as to separate the results for equivalent parameters on opposite legs.

		Sum Model	
		Leading/Stance	Trailing/Swing
Segment angles (°)	Foot	4.24	0.59
	Tibia	0.93	1.13
	Femur	1.94	0.59
	HAT	0.02	
Joint moments (Nm)	Ankle	13.59	3.30
	Knee	10.24	10.05
	Hip	28.24	17.25
GRF (%BW)	y	8.47	1.86
	x	0.58	0.73

Table 5.2: The RMS error values for the Sum model

The strengths and weaknesses of the predictions of the different kinematic and kinetic parameters in this model have already been described separately in the sections detailing the single and double support models. What have not been addressed are the discontinuities in these parameters at the transitions from double to single support and from the first half of the gait cycle to the second (Table 5.3). No constraints had been added to minimise these discontinuities but in terms of kinematics, they were relatively small. The mean kinematic discontinuity was 1.93° which was skewed by the foot segment which had an individual mean error of 3.04° . This segment was expected to have the largest errors since it is the segment that has constraints applied to it.

The joint moment discontinuities were much wider ranging from as little as 1.32Nm to 215.66Nm. These were in no way optimised so this explains why they had much greater discontinuities than the kinematics.

The horizontal GRF component performed very well with a mean discontinuity less than 1% of bodyweight. The vertical component had a large drop of approximately 20% of bodyweight at the first double to single support transition.

	TO1	FC1	TO2	FC2	Mean
Segment angles (°)	0.03	8.96	1.97	1.21	3.04
	1.37	1.03	3.83	1.03	1.81
	0.98	1.25	4.03	5.07	2.83
	0.03	0.02	0.03	0.02	0.02
Joint moments (Nm)	3.13	5.16	1.32	2.90	3.13
	3.95	27.57	35.72	5.92	18.29
	27.64	215.66	5.31	10.82	64.86
GRF (%BW)	20.05	1.95	1.36	6.70	7.52
	0.70	1.52	0.75	0.55	0.88

Table 5.3: Discontinuities at both toe-off and foot contact events, during the full gait cycle, for the Sum model

5.7 Discussion

This work has shown that it is possible to model double support, rather successfully, with a sagittal, eight segment chain. The only drawback of this simulation was that the predicted joint moments did not match the experimental data as well as the kinematics

and GRFs did. It may be possible that a solution existed that whereby the joint moments' collective error was much less but this required a trade-off that compromised the kinematic match. The optimisation algorithm would have dismissed this solution as it was concerned only with minimising the kinematic error.

An interesting factor of the DS model was that it required a moment about the trailing foot metatarsal in order to achieve a workable solution. This moment was in the range of 0-25Nm so was far from trivial. It is hypothesised that this is present so as to assist the push-off mechanism used during walking.

The application of Lagrange multipliers to provide the necessary constraints was very successful. Not only did they restrict the motion of the trailing foot but using the constraint forces to calculate the GRF distribution was shown to be a very effective method, for both horizontal and vertical directions, with a mean GRF RMS error of only 2.91% BW.

The moment curves for the DS model were the only area where large RMS errors occurred. As mentioned, the mean RMS error was similar to that of the single stance Model 5 (16.46Nm compared to 11.94Nm) but over a shorter simulation time it is much more noticeable. These errors could be a result of the chain being closed, rather than having a free end. However, it is difficult to be too critical of the moment curves since they were not optimised in any way.

Both the DS model and single support Model 5 have been shown to simulate their respective stages of walking with a good degree of success so it stands to reason that the Sum model for a full gait cycle would also produce strong results. What was less obvious, though, was that most of the discontinuities between these models would be relatively small. This did mean, however, that the larger discontinuities stood out more.

In terms of kinematics, the largest errors were for the foot segment. This is understandable as it is the only segment (for which kinematic errors are calculated) upon which constraints are placed. Aside from the foot, the only other error that is of concern is that of the tibia segment, when it is on the trailing limb, at the second toe off event. This can be explained by the fact that this is the point at which this segment goes from

being dependent, during double support, to independent, during single support. Such a change in the governing dynamics of a segment is likely to produce error.

There was one joint moment discontinuity that eclipsed the rest and that was the stance hip moment at the transition from single to double support. The error arises in the single support phase as the moment value at the start of double support is within the experimental standard deviation range. In terms of model dynamics, it makes sense that the largest error is at the end of the half gait cycle simulation, because in forward dynamics, errors accumulate from earlier in the simulation. A possible explanation for this behaviour could be because this moment has a direct effect on the HAT segment mass, which is the largest of the system's masses. With the opposite leg in front, it may be that the standing hip moment has to make this large adjustment so as to keep the HAT segment from tipping forwards, holding it upright. This concurs with the conclusion drawn in Chapter 3 that maintaining an upright trunk is a key role for the hip moments during walking.

The other large joint moment discontinuities are of the knee joint moment. These are at the first transition from single to double support (27.57Nm) and at the second transition from double to single (35.72Nm). Both of these discontinuities occur when this knee moment is on the trailing limb. The key to these errors again is the difference between dependent and independent segments. At the transitions named, the tibia segment adjacent to these knee moments is changing between being dependent and independent. As discussed before, this can cause kinematic discontinuities which would almost certainly have a large effect on the required knee joint moment.

Despite these large discontinuities in moment curves, the GRF curves' discontinuities are relatively small. The horizontal GRF, in particular, has a mean discontinuity of only 0.88% BW. The largest error was that of the vertical GRF under the lead foot at the transitions from double to single stance. It is hypothesised that, once again, the fact that this point is the point at which the trailing tibia and foot segments went from having dependent angular positions and angular velocities, to having them independently defined, is highly significant here.

A suggestion for potential future work would be to eliminate or reduce these discontinuities as much as possible. This would require starting Model 5 from the

terminal state of the DS model to eliminate errors at the double to single support transitions and then adding some kind of constraint to ensure that the terminal state of Model 5 was as close as possible to the initial state of the DS model.

Throughout this discussion, a repeated source of error has been the change of the tibia and foot segments from dependent to independent and vice versa. It would be interesting to investigate the effects of choosing two different dependent segments, e.g. the femur segments. A small error in angle for the femur would have less of an effect on the system overall than the same error for the foot, say. This is because its length, it would mean that the CM displacement caused by this angle error would be much smaller than it would be for the foot.

Focussing on the limitations of this model will help to assess where further improvements could be made but it is important that the success of the current model's performance is not overlooked. Firstly, the gauge of success of the model has been based on a tolerance of one standard deviation either side of the experimental mean value, and has been deemed to have performed well. It is known that this accounts for approximately 68% of the population. There is great variation in the way different people walk so one standard deviation either way may even be too stringent. Two standard deviations either side of the experimental mean constitutes approximately 95% of the population and when the results of the Sum model are reassessed with these criteria, it can be seen just how well the model performs. The RMS error values for every parameter fall within this range. Some kinetic parameters do stray out of this range but only for short times. The horizontal and vertical GRF components beneath the lead/stance limb are within this range for 99% and 97% of the simulation, respectively. The ankle, knee and hip moments of the same limb are within this range for 84%, 93% and 92% of the simulation, respectively. All other predictions are within the two standard deviation range for 100% of the simulation.

5.8 Conclusions

An eight segment model has been shown to effectively model the double support stage of walking. The use of Lagrange multipliers also proved to be a reliable method to apply

the necessary constraints, as well as assess the GRF distribution when there were two contact points with the ground. The fact that a trailing foot metatarsal moment was required gives further credence to the hypothesis of an active push-off action in walking.

A combination of this model with the best single support walking model provided good predictions over the complete gait cycle. There were, however, some discontinuities at the transitions from one stage to the next. Suggestions for further investigations to attempt to eliminate or reduce these discontinuities have been put forward.

With an acceptable model of a full gait cycle, data can now be collected for a number of different subjects and applied to the model. Individualised simulations of each person's walking will be performed, in order to test the versatility of the model when it comes to different geometries, walking patterns, heights, weights, etc.

6 DATA COLLECTION AND ANALYSIS

6.1 Introduction

The real essence of clinical gait analysis is to provide insight into the differences between individuals. The previous chapters in this project have used averaged data from the literature (1979, 1991) and this method has been a good standard against which to gauge the success of simulations, proving the general applicability of the modelling approach. However, this does not give any information regarding the differences from one person to the next. This is an important distinction that must be considered when addressing Research Question 4: *'considering interpersonal differences, the time cost and the solution accuracy, how close is gait modelling to becoming a clinically usable tool?'*

To rigorously test the capabilities of a given model, individuals' measurements and proportions should be used as inputs. Common anthropometric measures and proportions are detailed numerically in Winter's data set (1979, 1991) but once again these are averages and may not be accurate for all people (see Appendix A.1). If the model is equally successful for a variety of different individuals with various weights, heights, proportions and walking velocities, it will make it more appropriate for use in clinical diagnostics.

The study in this chapter will collect gait data from ten healthy participants, five male and five female, with a range of heights, weights and walking velocities. Healthy individuals were chosen because inter-individual differences are small and if these can be detected, then larger differences, between patients and healthy people, should be even easier to demonstrate. These data will be applied to the Sum model for each person and a simulation of a full gait cycle will be performed. Each person's simulation will be compared to their own experimental data.

In this chapter, firstly, an appraisal of relevant literature will be undertaken. This will highlight the issues faced by previous investigations in this area. Next, the process for capturing personalised individual data will be outlined. This involves recruitment of participants, the laboratory set up, the software used, the experimental method and post-processing. Following this, a description of how the data were imported into

MATLAB will be given. The results of simulations attempting to match these data will be given, with the best and worst matches described and analysed.

6.2 Literature

The kinematics and kinetics of healthy adults walking are illustrated in many text books (Kirtley, 2006; Perry, 1992; Whittle, 2007). As one would expect from such publications though, it is generic behaviour and always in relation to percentage of gait cycle rather than time. Another shortcoming of these books is that they display their data in graphical form only, making numerical comparisons difficult and inaccurate.

There have been journal papers that have used computer models to predict healthy adult walking (Anderson & Pandy, 2001a; Anderson & Pandy, 2003) but again they do not publish their data numerically.

There are studies that have applied advanced models to individualised datasets, with the widely used freeware *OpenSim* (Delp et al., 2007) now allowing this function. However, clinically useful insights are difficult to interpret from these investigations (Gerus et al., 2013; Liu et al., 2008; Reinbolt et al., 2011; Steele et al., 2013; Steele et al., 2010; Van Der Krogt et al., 2013).

There seems to be a problem with complex walking models, which is widely acknowledged informally but rarely published in the literature. This is that they are particularly sensitive to the model parameter selection and a large amount of time can be spent adjusting these parameters so as to produce a convergent solution. This can sometimes even require values beyond a sensible physiological range (Arnold et al., 2010). This is somewhat intuitive as these models are essentially large non-linear dynamic systems and consequently small changes to the inputs can have a large effect on the solution. It can be hypothesised, therefore, that the less complex models, while still dependent upon non-linear dynamics, will produce more stable solutions because they rely upon fewer input parameters.

However, very simple models are not the obvious solution either. Taking Model 2 (Section 3.3) from this project as an example, sensible customisation of the model to a

given person's data seems nigh on impossible. Firstly, there is the problem of anthropometry and which measurements should be used for the mass, length, moment of inertia and CM position of the single leg segment, since some of these values will vary over time. Then, there is the issue of how to optimise the leg's trajectory. Would the hip joint centre be the only consideration? As was shown in Chapter 3, this model does not adequately simulate double stance either so comparisons during that phase would have large errors.

6.3 Method

The purpose of the practical experimentation was to produce person-specific data, some of which could be used as the input to the model and some which could be used to assess the strength of a simulation's kinematic and kinetic predictions.

Firstly, anthropometric measurements were needed in order for the model to accurately replicate the specific person. These included the lengths of all the different segments used in the Sum model, the person's height and their total mass. From the total mass and segment lengths, the approximate mass, moment of inertia, and the position of the CM of any given segment could be evaluated. These still relied on formulae outlined in Winter's books (1979, 1991) and shown in Appendix A.1.

The data collected during the walking trials provided all of the kinematic and kinetic curves that were previously taken from the *normal set*, for example, the time history of a given segment angle. These could be used to calculate the RMS error values for each comparison parameter.

6.3.1 Participant recruitment

Ethical approval for the study was granted by the University of Salford, School of Health Sciences Research Ethics Panel (Appendix A.3).

The participants were volunteers and were recruited using posters (Appendix A.4) on University noticeboards, in accordance with the University of Salford ethical procedure.

The inclusion criteria were for adults (over 18 years old) who could walk unaided, with no illness or pathology that affected their gait. There was no upper bound on their age.

Upon expressing interest, each person was supplied with a participant information sheet (Appendix A.5) and an appointment time to come to the University gait lab was arranged. Upon arrival, each was again supplied with a copy of the information sheet and was able to ask any questions they may have had. Next, they were asked to complete and sign a participant consent form (Appendix A.6).

6.3.2 The research environment

The data collection took place in the University of Salford's purpose-built Brian Blatchford Gait Laboratory (Figure 6.1). Within the floor of the 10m walkway are mounted six force plates (two portable Kistler 9286aa, four fixed Kistler 9281b). Force plates 1 to 5 are in a line, along the direction of progression of walking, and force plate 6 is to the right of force plate 3. Mounted to the walls are 12 Vicon T40 infra-red cameras. There are no windows in the laboratory so there was no chance of external light interference.



Figure 6.1: The University of Salford's Brian Blatchford Lab

6.3.3 Calibration

The software used for the data collection was Vicon (Vicon Motion Systems Ltd, Oxford, UK). Before any data collection could take place, the cameras needed to be calibrated to the capture volume. Each camera only sees a 2D image, but with a combination of 12 2D images from different angles, the position of a given marker can be identified, relative to a designated origin. For reference, the x direction will describe the anterior-posterior axis (the direction of progression during the walking trials), y will describe the superior-inferior axis and z will describe the medial-lateral axis, in keeping with the terminology of the models.

A T-shaped wand with infra-red LEDs on was waved within the desired volume (approximately 5m by 1.2m by 1.5m). Since the LEDs are a known distance apart from one another, the software can work out the positions and orientations of the cameras, relative to one another. The origin was chosen to be the first right corner of the force plate (that is to say all the other force plates had positive x position values) and was defined by placing the wand so that junction of the T-shape was at this corner (Figure 6.2). This allowed the software to orient the cameras, relative to the force plates.

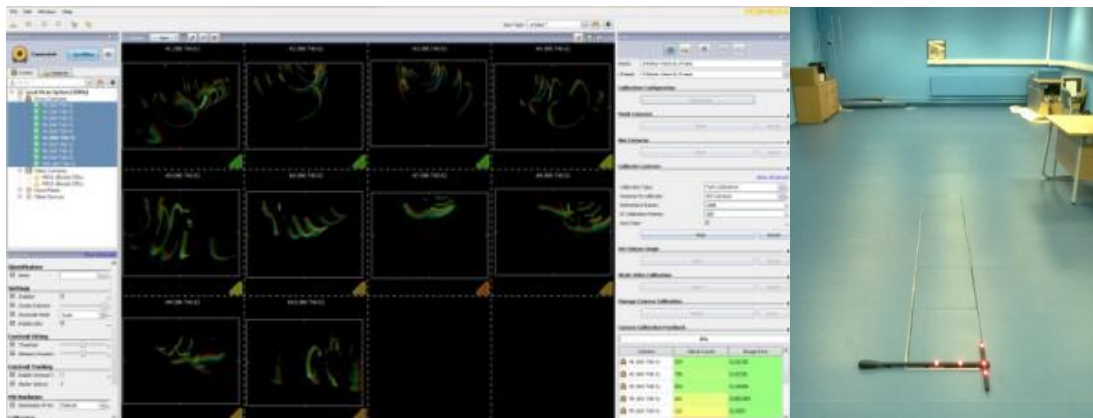


Figure 6.2: Camera calibration and setting the origin

6.3.4 Marker positioning

The marker setup used was the Vicon lower body Plug-in Gait model. This model is very widely used in the gait analysis community (Benedetti et al., 2011; Bonnefoy-Mazure et al., 2013; Davis et al., 1991; Ferrari et al., 2008; Gutierrez-Farewik et al., 2006; Horsak & Baca, 2013; Kadaba et al., 1989; Raspovic, 2013; Riley et al., 2007; Rueda et al., 2013; Syczewska et al., 2010; Thummerer et al., 2012). An advantage of this model was that it allowed the software to perform an inverse dynamics algorithm and give time-histories for the joint moments which could then be compared to those predicted by the Sum model.

Segments are created for the pelvis, thighs, shanks and feet. These segments are triangles defined by three points determined by the marker positions. For this study, wand markers were used for the thigh and shank markers. The theory behind this idea was that if the marker were on the skin, the triangles created would be narrow and as such, a small skin artefact could result in a large change in segment angle. When the wand was used, any artefact movement of that marker would have a less drastic effect on the segment angle, thus minimising measurement error.

In addition to the Plug-in Gait marker set, there were extra markers added so as to provide all the necessary information for the MATLAB simulation. Since it was planned to track joint centres, it was decided that including medial knee and ankle markers would simplify calculating these joint centres. Markers were also placed on the first metatarsal head, on the instep of the foot, and on the nail of the hallux.

In order for these markers to be recognised by the Vicon software, they had to be given marker names. To do this a customised version of the Plug-in Gait model was coded by editing the .vst file in an XML writing program.



Figure 6.3: The marker placement

6.3.5 Anthropometric measurements

Several anthropometric measurements were necessary for the purposes of the Plug-in Gait model. Each participant had their height and weight taken. The right and left leg lengths were measured from the anterior superior iliac spine (ASIS) to the medial malleolus. A pair of callipers was used to measure the medial-lateral knee and ankle widths.

Along with the height and weight, some further measurements were taken for use as inputs to the MATLAB simulations. The femur length was taken as the distance from greater trochanter to lateral knee epicondyle and tibia length was taken as the distance from lateral knee epicondyle to lateral malleolus. The distance between the medial malleolus and the first metatarsal head was taken as foot length and that between the first metatarsal head and the tip of the hallux was taken as the toe length. Since the Sum model was bilaterally symmetrical, these measurements were taken on both legs and mean values were used.

6.3.6 Experimental method

Data was collected for 10 subjects (5 male and 5 female) aged 25.5 ± 2.5 years, with masses of 70.5 ± 15.5 kg and heights of 1.725 ± 0.105 m. Once the anthropometric measurements were taken and the markers were placed correctly, each subject was asked to stand as still as possible, with their arms folded across their chest, on the first force plate, to perform a static trial. It was important that all the markers could be seen by the cameras. The purpose of the static trial was to calculate certain calibration quantities. The angle between the posterior and anterior pelvis markers or between the feet markers, for example, gave the '*offset*' angles of these segments, during the '*neutral*' position. Further calculations regarding joint centre positions were also performed at this stage.

Next the dynamic trials were performed. Each participant started at one end of the lab's walkway. This meant at least three steps were taken before they were in the recording region, allowing them to get into their natural rhythm before recordings were made. They were asked to walk, as naturally as possible, with a self-selected velocity, to the other end of the walkway. Their walk was observed so as to make sure that '*clean contacts*' were made with the first, second and third force plates. A clean contact was defined as one where the landing foot contacted exclusively one force plate. The reason clean contacts were required on each of these force plates was because the double support data (for use in model simulations) were taken from force plates 1 and 2, and the single support data was defined from the moment the trailing foot left force plate 1, until

the moment it contacted force plate 3. Little instruction was given so that the subject didn't alter their natural gait pattern in order to achieve clean hits on the force plates. When clean contacts were made with the first three force plates it was defined as a 'good trial'. Each subject was asked to keep on traversing the walkway until five good trials were achieved. Between each trial, the force plates were set to a zero level.

6.3.7 Post-processing

Once the trials had been recorded in Vicon, some post-processing was required to export the necessary information. All of the data (marker positions, GRF and joint moments) were exported as an ASCII file so as to provide numerical values to import into MATLAB for comparison with the project's models.

A MATLAB script was coded to import the ASCII files and extract the necessary numerical values. The data chosen were from the first time frame where a force value was registered on force plate 2 and continued until the final time frame before a force value was recorded on force plate 3. This meant that the data would start with a double support period (on force plates 1 and 2) followed by a single support period (on force plate 2), giving the same half gait cycle as is simulated by the Sum model. In accordance with the simulation, bilateral symmetry was assumed.

Using the time frames defined by the force plate data, the marker data were selected. These gave the x, y and z coordinates of each of the markers, relative to the origin at the corner of force plate 1. In order to make this raw data usable for the simulations, the joint centre coordinates had to be calculated. All of the following calculations were taken from previous research into the topic of hip joint centre position prediction (Davis lii et al., 1991; Harrington et al., 2007). For these calculations, all lengths were in millimetres.

To calculate the hip joint centre, firstly, the pelvic origin, \mathbf{O}^P , must be defined. This is taken as the midpoint of the left and right ASIS marker vectors:

$$\mathbf{O}^P = \frac{lASIS + rASIS}{2}$$

Equation 6.1

The posterior pelvis point, or sacrum, is defined as the midpoint of the posterior superior iliac spine (PSIS) markers:

$$S = \frac{lPSIS + rPSIS}{2}$$

Equation 6.2

Next, the axes of the pelvic coordinate system are defined. It should be noted at this point that the x, y and z axes' definitions are not the same for the Vicon system as they are for the MATLAB models. The medio-lateral axis, \hat{y}^P , is taken as the vector from the left ASIS to the right ASIS. The proximal axis, \hat{z}^P , is taken as being perpendicular to the medio-lateral axis and the vector between the pelvic origin and the sacrum. Finally, the anterior axis, \hat{x}^P , is taken as perpendicular to the medio-lateral and proximal axes.

$$\hat{y}^P = \frac{rASIS - lASIS}{|rASIS - lASIS|}$$

$$\hat{z}^P = \frac{\hat{y}^P \times (O^P - S)}{|\hat{y}^P \times (O^P - S)|}$$

$$\hat{x}^P = \hat{z}^P \times \hat{y}^P$$

Equations 6.3, 6.4, 6.5

By consolidating these three axes into a single matrix, the direction cosine matrix for the pelvis (DCM^P) is formed.

$$DCM^P = \begin{pmatrix} \hat{x}_x^P & \hat{y}_x^P & \hat{z}_x^P \\ \hat{x}_y^P & \hat{y}_y^P & \hat{z}_y^P \\ \hat{x}_z^P & \hat{y}_z^P & \hat{z}_z^P \end{pmatrix}$$

Equation 6.6

The vector, H^P , gave the positions of the hip joint centres within the pelvic coordinate frame. The \pm symbol in the y direction indicates whether it is the left or right hip joint centre being calculated.

$$H^P = \begin{pmatrix} -0.24PD - 9.9 \\ 0.33PW - 10.9 \\ \pm(0.30PW + 10.9) \end{pmatrix}$$

Equation 6.7

Where PD, pelvic depth, is “the distance between the midpoints of the line segments connecting the two ASIS and the two PSIS” (Harrington et al., 2007) and PW, pelvic width, is the distance between the left and right ASIS markers. The latter is a constant value calculated during the static trial (see Section 6.3.6).

Finally, the hip joint centre coordinates, relative to the global axis are calculated.

$$H = O^P + DCM^P H^P$$

Equation 6.8

Since the model assumes that the left and right hips have the same coordinates, the mean values of the left and right hip joint centres’ positions were taken.

The knee and ankle joint centre calculations were much simpler. The mean of the lateral and medial markers’ coordinates, for the respective leg and joint, were taken.

The position of the HAT segment mass was taken as having the same x position as the combined hip joint and a y position was calculated using the static trial data and formulae from Winter (1979, 1991) detailed in Appendix A.1.

In the Sum model, the origin of the Cartesian coordinates was defined as the point at which the heel of the lead foot contacts the ground. The coordinate origin defined for the Vicon system was the front right corner of force plate 1, as viewed by the walker. In order to equate the Vicon data to fit the model, all the marker data were offset in relation to the lead foot heel marker position at the start of the gait cycle.

For comparison with previous models, the segment angles were computed. For segment i , the following calculation was used for the segment angle:

$$\theta_i = \tan^{-1} \left(\frac{x_i - x_{i+1}}{y_{i+1} - y_i} \right)$$

Equation 6.9

Where x_i and y_i are the coordinates of the end of the segment closest to the start of the chain and x_{i+1} and y_{i+1} are the coordinates of the other end of the segment.

Once all the relevant data had been imported and extra calculations had been made for each trial, for a given subject, the following statistic data for that person were evaluated. Firstly, the data from each trial were normalised and interpolated to cover from 0% to 50% of a gait cycle, in 1% steps, in order to make trials of different time lengths more comparable. Next, from each percentage value, the mean magnitude over the five trials was taken for each kinematic and kinetic parameter. This allowed the calculation of a standard deviation value for each percentage of the gait cycle.

6.3.8 Simulation setup

Simulations were run for each of the subjects. The dimensions and inertial properties of the Sum model were adapted to represent those of each person. The setups for the single support, double support and full gait cycle simulations were the same as those described for Model 5, the DS model and the Sum model respectively (see Chapters 4 and 5). The only differences were that for the single and double support simulations, the timings were changed to those recorded for the particular trial being studied. Each double support simulation had six equally-spaced moment nodes for each joint moment, and each single support simulation had 21 equally-spaced moment nodes for each joint moment, regardless of total time taken.

For each of the simulations, the cost function was designed to minimise the RMS error between the predicted joint centre kinematics and those measured during the experiment, for that specific person.

Since joint centres were used for kinematic comparisons with experimental data, a datum had to be defined for the trunk segment. A formula was used from Winter's data (1979, 1991) to calculate the position of the HAT CM and this was used as the point of comparison (see Appendix A.1). This has been illustrated on the figures displaying the body segment kinematics against trial data (see Sections 6.4.3 and 6.4.4).

For each person, a single trial was chosen. The reason for this was that using the mean of all five trials would create "averaged" data, just like Winter's dataset (1979, 1991) that had been used previously. Using a single trial would give the most accurate representation of how that person walked. The values from that particular trial were taken as the kinematic and kinetic experimental data, against which the simulation predictions would be compared, and the simulations' time lengths were adapted accordingly. However, the standard deviation range values were those evaluated from all five of that subject's trials, which were given in terms of percentage gait cycle (as described in Section 6.3.7). These were adapted to apply to the time length of the chosen trial.

6.3.9 Statistical Analysis

In order to assess if the success of the model, as determined by the RMS error values, was affected by subject characteristics (such as height, mass, gait cycle time etc.) Pearson's correlation coefficients (ρ) were calculated (Equation 6.10).

$$\rho = \frac{\left(\frac{\sum (x - \bar{x})(y - \bar{y})}{n - 1} \right)}{\sigma_x \sigma_y}$$

Equation 6.10

In the equation, x and y are the values in the two sets of data, \bar{x} and \bar{y} are the respective mean values of these two sets, σ_x and σ_y are the respective standard deviation values of these two sets, and n is the number of values in the sets.

The MATLAB function ‘*corr*’, part of the STATISTICS TOOLBOX, was used to calculate this value and also gave the associated ‘*p-value*’ (Best & Roberts, 1975; Gibbons, 1985; Hollander & Wolfe, 1973; Kendall, 1970). This determines the probability that the null hypothesis occurred by chance, with a value of less than 0.05 being widely accepted as meaning that the correlation given is a significant one (Breakwell et al., 2012).

It was also useful to investigate correlations in the RMS error values when ranked over the ten subjects. For this purpose, Spearman’s rank correlation coefficients (ρ_s) were evaluated (Equation 6.11).

$$\rho_s = 1 - \frac{6 \sum d^2}{n(n^2 - 1)}$$

Equation 6.11

When the two sets of n values being compared are ranked in order, d is a set of n values, formed by the differences in the two rankings for each subject.

6.4 Results

The following tables provide a summary of the performance of the Sum model when customised to specific people’s data. The full data can be found in Appendix A.7.

6.4.1 RMS errors

Table 6.1 shows, for each subject, the mean RMS error in their predicted segment angles (includes all segments), joint centre positions (includes both x and y direction errors), moments (at all joints) and GRFs (both x and y components). Although the cost function was calculated by normalising these errors by experimental standard deviation, the

values are given here in terms of units relevant to each parameter group to make their interpretation easier. It should also be noted that the mean RMS error for joint centre position considers only errors in the linear x and y directions, not absolute displacement. For example, if the predicted position of a joint was 3mm to the right and 4mm higher than the experimental position, this would be treated as two separate errors, rather than the absolute distance error of 5mm.

Subject	Segment Angle (°)	Mean RMS error		
		Joint centre position (mm)	Moments (Nm)	GRF (%BW)
1	1.86	13.07	18.64	3.64
2	1.33	9.30	20.82	2.91
3	3.09	20.97	12.97	3.10
4	3.51	21.85	13.95	3.36
5	1.63	9.33	14.79	2.08
6	4.23	19.79	10.03	5.07
7	2.75	21.67	12.06	2.90
8	1.71	13.79	18.56	2.55
9	2.74	28.29	17.99	2.11
10	3.49	15.51	21.05	3.56
Mean	2.64	17.36	16.09	3.13

Table 6.1: The mean RMS error values for each subject, for the different kinematic and kinetic values

Table 6.2 shows a breakdown of all the predicted values that were compared to experimental data, and the mean RMS error for each, across all ten subjects. The errors are separated into the results for each leg, during the first half of the gait cycle.

			Lead/stance	Trail/swing
Joint centre positions (mm)	Met	x	0.40	30.33
		y	2.27	22.02
	Ankle	x	8.24	31.26
		y	7.38	22.95
	Knee	x	18.61	24.08
		y	11.68	17.81
	Hip	x	22.84	22.84
		y	13.44	13.44
	HAT	x		28.88
		y		13.94
Segment angles (°)	Foot		4.00	2.90
	Tibia		2.94	3.23
	Femur		1.87	1.73
	HAT			1.78
Joint moments (Nm)	Ankle		14.45	5.51
	Knee		14.82	9.09
	Hip		25.85	26.79
GRF (%BW)		y	7.57	1.98
		x	2.21	0.76

Table 6.2: The mean RMS error values for each comparison parameter, across all subjects

6.4.2 Discontinuities

The concept of discontinuities in simulations was introduced and discussed in Chapter 5. These occur when the terminal state of the double support phase is not exactly equal to the initial state of the single support phase, and vice versa.

Table 6.3 shows the mean discontinuity values, for each subject, in their predicted segment angles, joint centre positions, moments and GRFs. The values are given in the unit of measurement specific to that parameter group.

Subject	Mean discontinuities			
	Segment Angle (°)	Joint centre position (mm)	Moments (Nm)	GRF (%BW)
1	2.50	17.39	51.33	3.67
2	2.32	11.43	71.81	5.42
3	3.10	19.77	21.57	3.13
4	4.02	21.86	20.13	7.91
5	2.17	13.68	27.72	2.63
6	5.09	20.38	15.81	8.36
7	3.52	13.53	20.79	5.12
8	1.73	10.82	50.37	5.00
9	3.24	18.62	50.10	4.47
10	4.98	18.25	68.96	6.76
Mean	3.27	16.57	39.86	5.25

Table 6.3: The mean discontinuity values for each subject, for the different kinematic and kinetic values

Table 6.4 shows all the measured parameters and the mean discontinuities, calculated across all subjects. Data from the both legs have been combined so as to represent the behaviour a single limb, moving through a full gait cycle simulation. Discontinuity values are given for the first and second toe-off events (TO1 and TO2) and the first and second foot contact events (FC1 and FC2).

			TO1	FC1	TO2	FC2	
Joint centre positions (mm)	Met	x	0.00	0.00	32.00	0.00	
		y	0.00	15.40	28.73	35.39	
	Ankle	x	0.07	0.00	35.65	0.00	
		y	0.20	22.76	27.31	21.85	
	Knee	x	20.28	0.00	29.78	0.00	
		y	1.25	21.67	22.60	20.86	
	Hip	x	45.54	0.00	45.54	0.00	
		y	13.58	22.34	13.58	22.34	
	HAT	x	44.91	0.00	44.91	0.00	
		y	13.60	23.59	13.60	23.59	
	Segment angles (°)	Foot		0.08	5.49	6.22	2.44
		Tibia		2.85	2.16	4.56	3.22
Femur			5.35	4.02	4.65	2.19	
HAT			1.18	3.33	1.18	3.33	
Ankle			6.43	8.47	7.55	2.20	
Joint moments (Nm)	Knee		11.54	18.25	25.50	5.46	
	Hip		46.51	169.57	142.05	34.77	
		y	12.78	10.28	2.58	6.72	
GRF (%BW)		x	3.31	3.53	0.92	1.84	

Table 6.4: The mean discontinuity values for each comparison parameter, across all subjects

6.4.3 The best results

The following results describe the best performer for each parameter group (i.e. segment angles, joint centre positions, GRF). These are not necessarily the same subject throughout. The lowest segment angle RMS error and the lowest GRF RMS error, for example, could be for different subjects.

The best joint centre position and segment angle predictions

Figure 6.4-Figure 6.6 show the kinematic predictions of the simulation for Subject #2, which had the lowest mean RMS error for joint centre positions (9.30mm) and segment angles (1.33°). From observation alone, it can be seen on the graphs of joint centre positions that the largest deviations from the experimental data come at the end of the swing phase. Throughout the first half of the gait cycle, most joint centres stayed within their respective standard deviation ranges.

The greatest deviations from the experimental data, in terms of segment angles, were during the first double support phase and towards the end of the first single support phase. The segment angles during swing phase were mostly within their standard deviation ranges.

The mean discontinuity over all joint centre positions was 11.43mm; the second lowest of all the subjects (only Subject #8 was less at 10.82). The largest error was that of the metatarsal joint, at the second foot contact event in the gait cycle, in the y direction (45.73mm)

The largest segment angle discontinuities were both for the foot segment at first foot contact (6.74°) and second toe-off (6.30°). For both of these events it was the trailing foot. The mean segment angle discontinuity (2.32°) was below the inter-subject mean (3.27°).

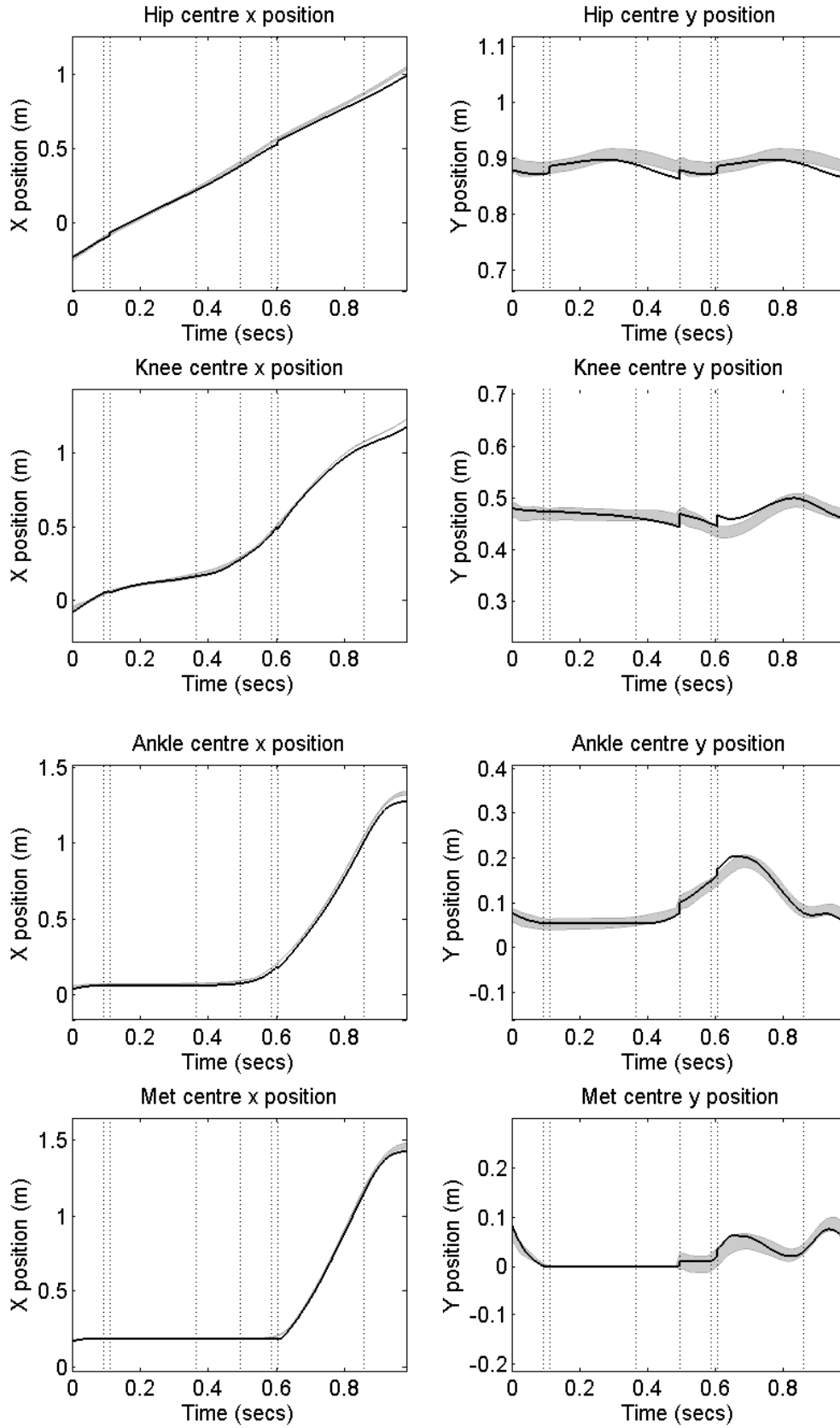


Figure 6.4: The joint centre predictions for Subject #2

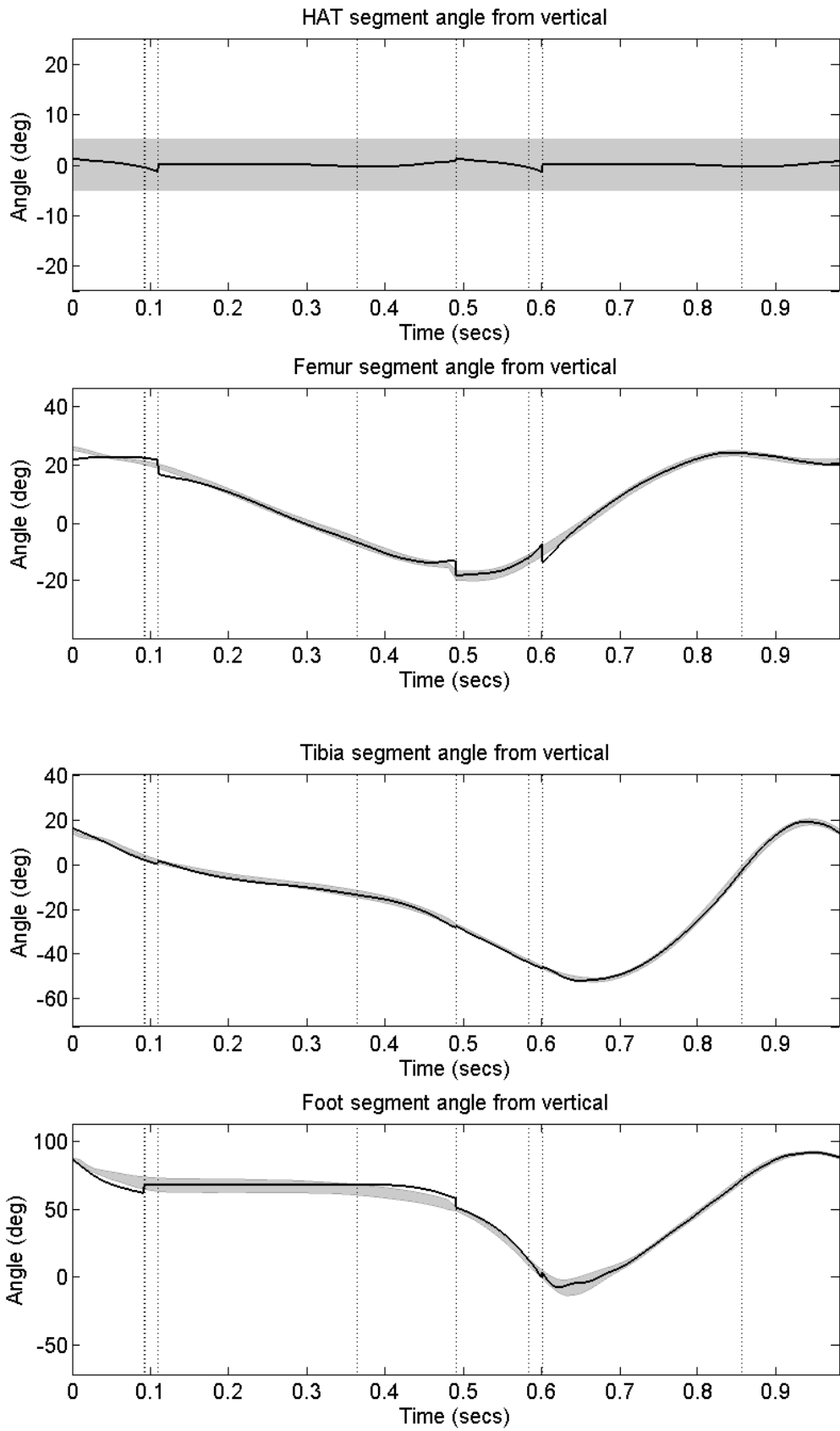


Figure 6.5: The segment angle predictions for Subject #2

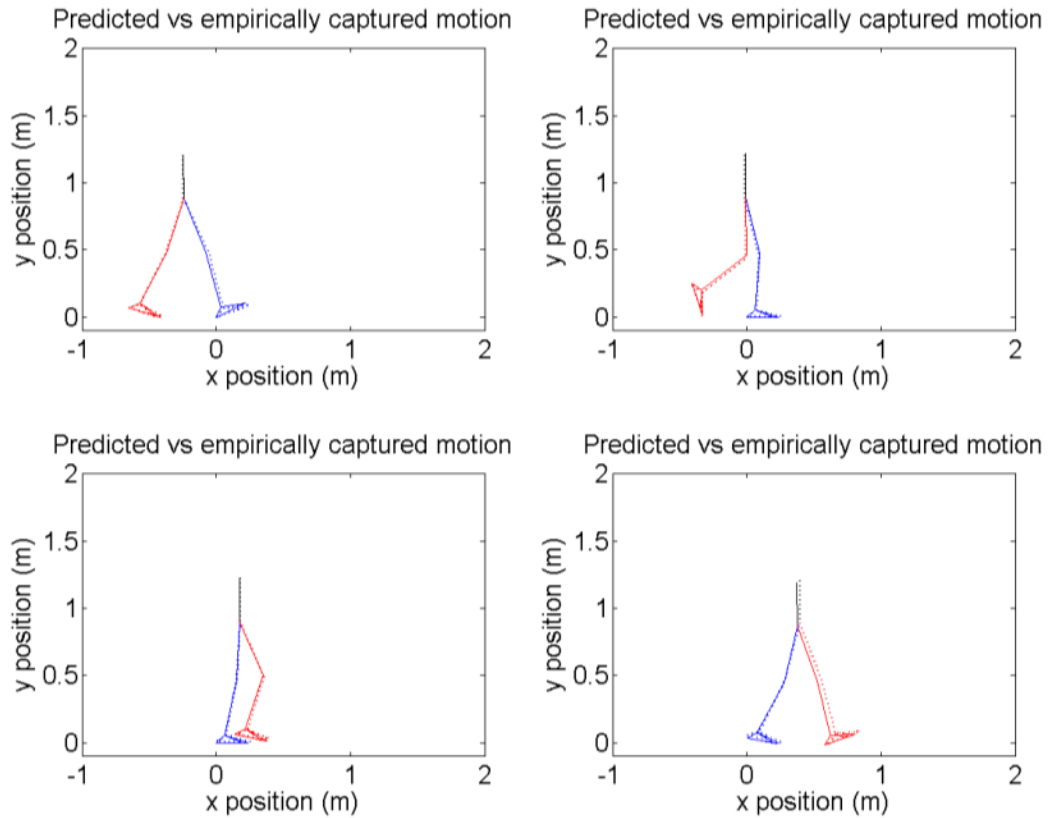


Figure 6.6: The kinematic predictions (solid) vs the experimental trial data (dotted) for Subject #2

The best GRF predictions

Figure 6.7 shows the GRF predictions of the simulation for Subject #5, which had the lowest RMS error for GRF (2.08% BW).

The resulting GRF curves do have discontinuities, the greatest of which occurs for the vertical component, at the transition from single to double support (7.70% BW). However, the mean GRF discontinuity for this subject was only 2.63% BW; the lowest of all the subjects.

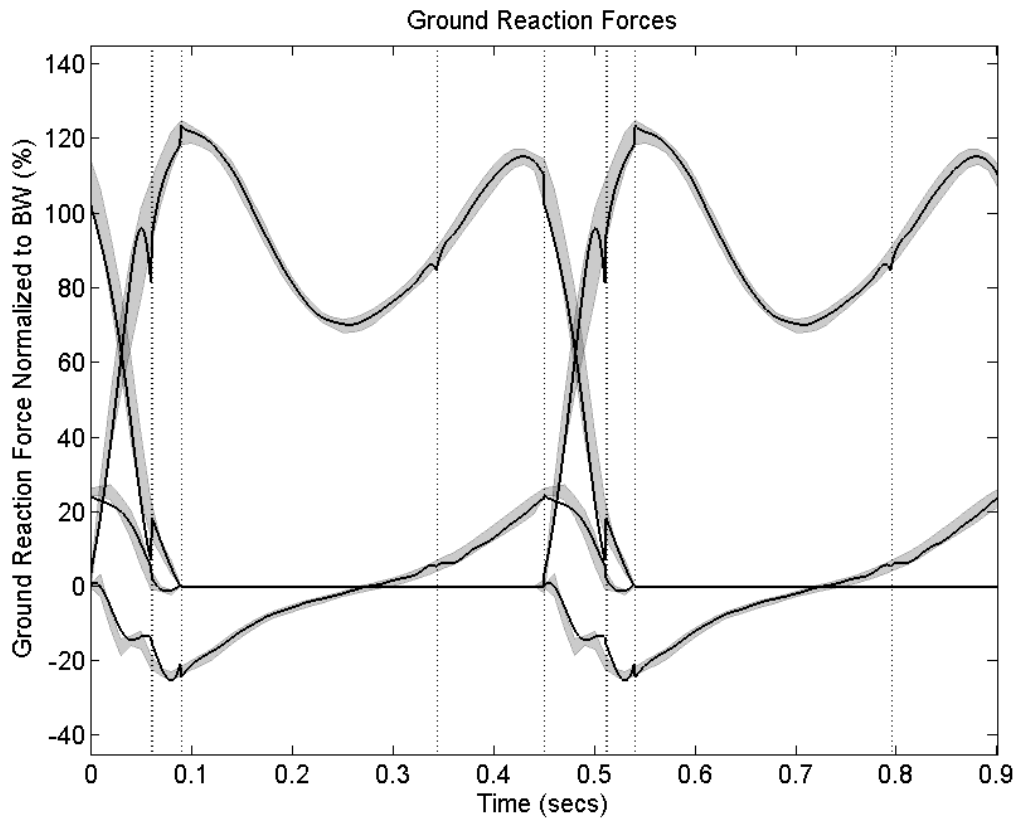


Figure 6.7: The GRF predictions for Subject #5

The best joint moment predictions

Figure 6.8 shows the joint moment predictions for Subject #6, which had the lowest mean RMS error for joint moments (10.03Nm).

The mean discontinuity over all joint moments for this subject (15.81Nm) was the lowest of all the subjects.

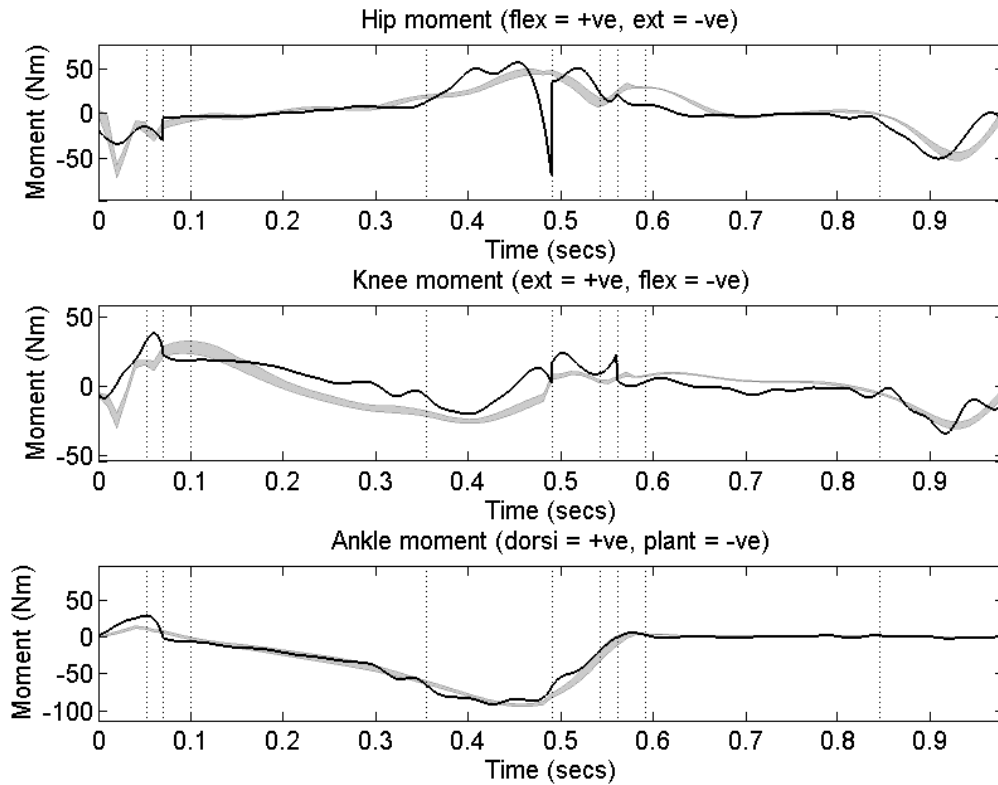


Figure 6.8: The joint moment predictions for Subject #6

6.4.4 The worst results

The following results describe the worst performer for each parameter group (i.e. segment angles, joint centre positions, GRF). These are not necessarily the same subject throughout. The highest segment angle RMS error and the highest GRF RMS error, for example, could be for different subjects.

The worst joint centre position predictions

Figure 6.9 and Figure 6.10 show the kinematic predictions of the simulation for Subject #9, which had the highest mean RMS error for joint centre positions (28.29mm).

The mean discontinuity over all joint centre positions for this subject (18.62mm) was greater than the mean across all subjects (16.57mm).

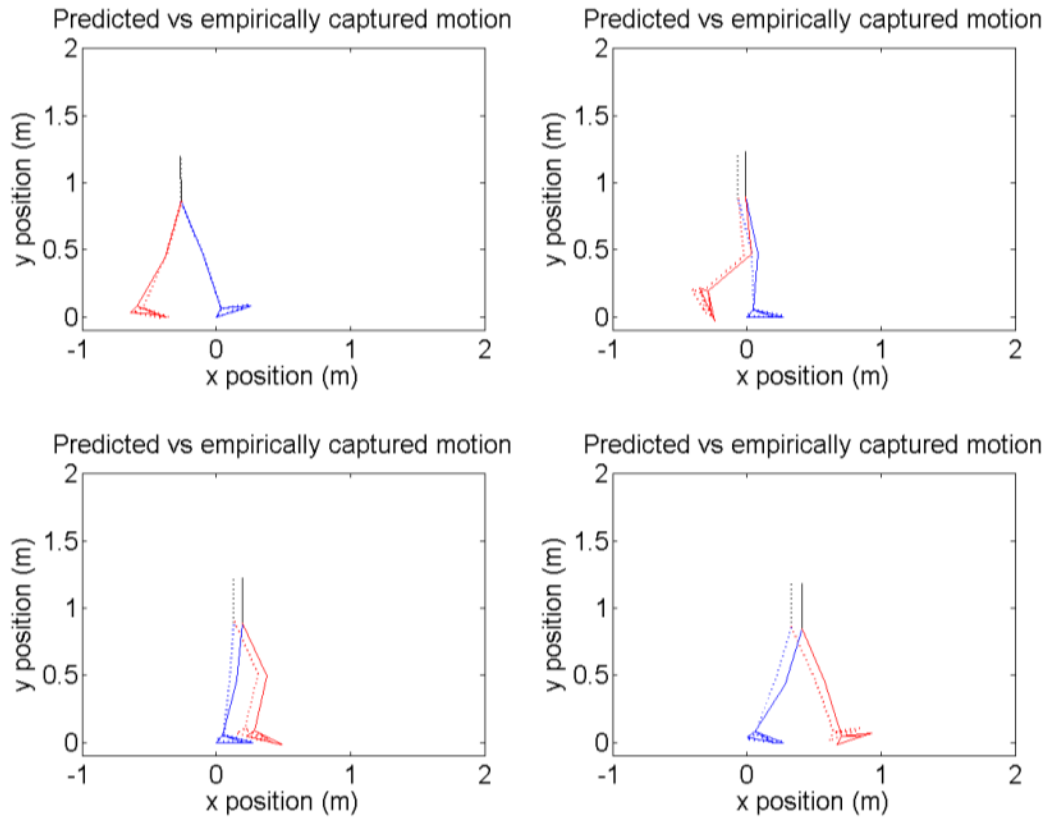


Figure 6.9: The kinematic predictions (solid) vs the experimental trial data (dotted) for Subject #9

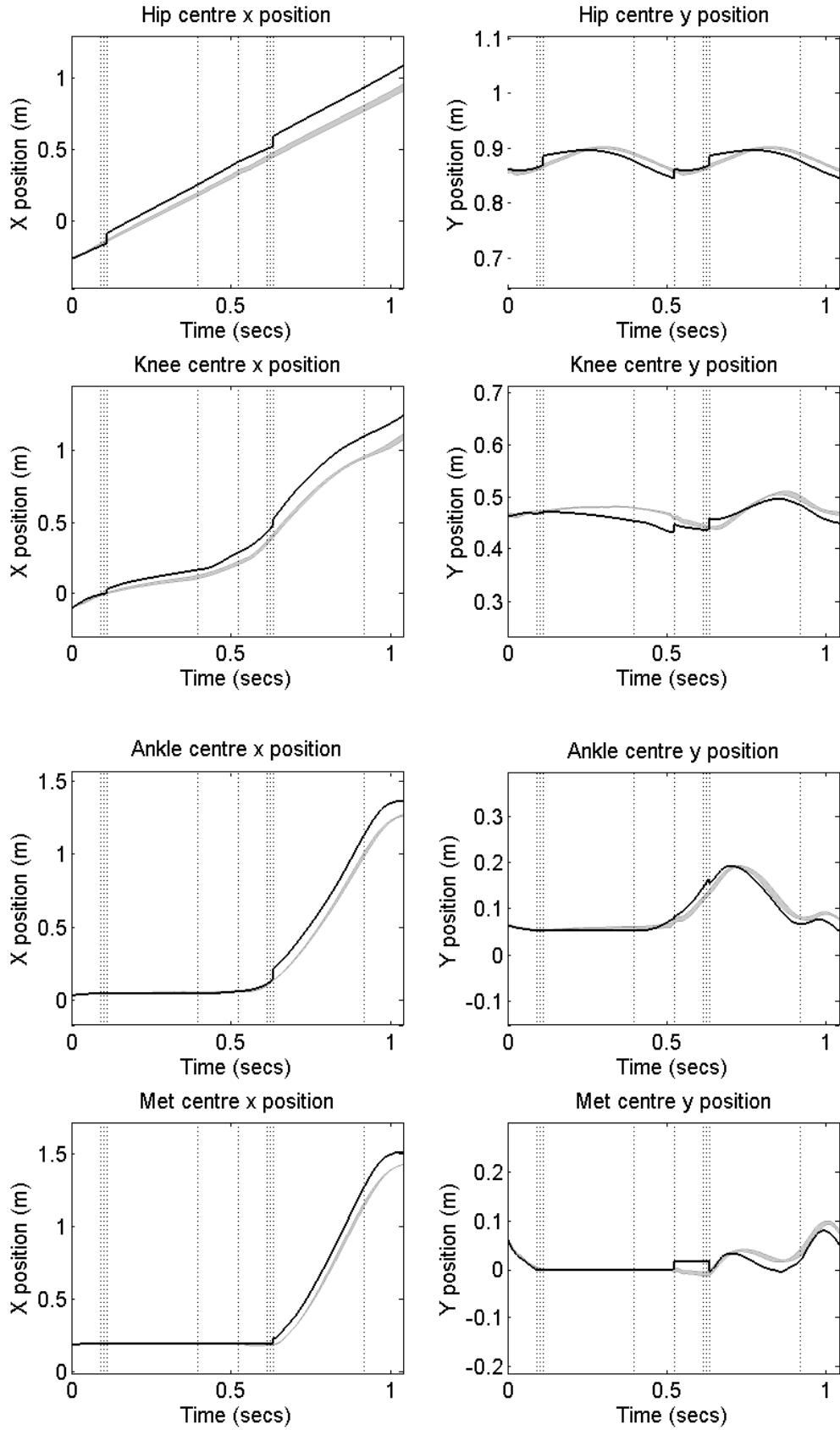


Figure 6.10: The joint centre predictions for Subject #9

The worst segment angle predictions

Figure 6.11 and Figure 6.12 show the kinematic predictions of the simulation for Subject #6, which had the highest mean RMS error for segment angles (4.23°). This subject also had the highest mean discontinuity value for segment angles (5.09°), attributable mainly to the trail/swing leg femur and foot segments at the second double to single support transition (13.17° and 15.71° respectively).

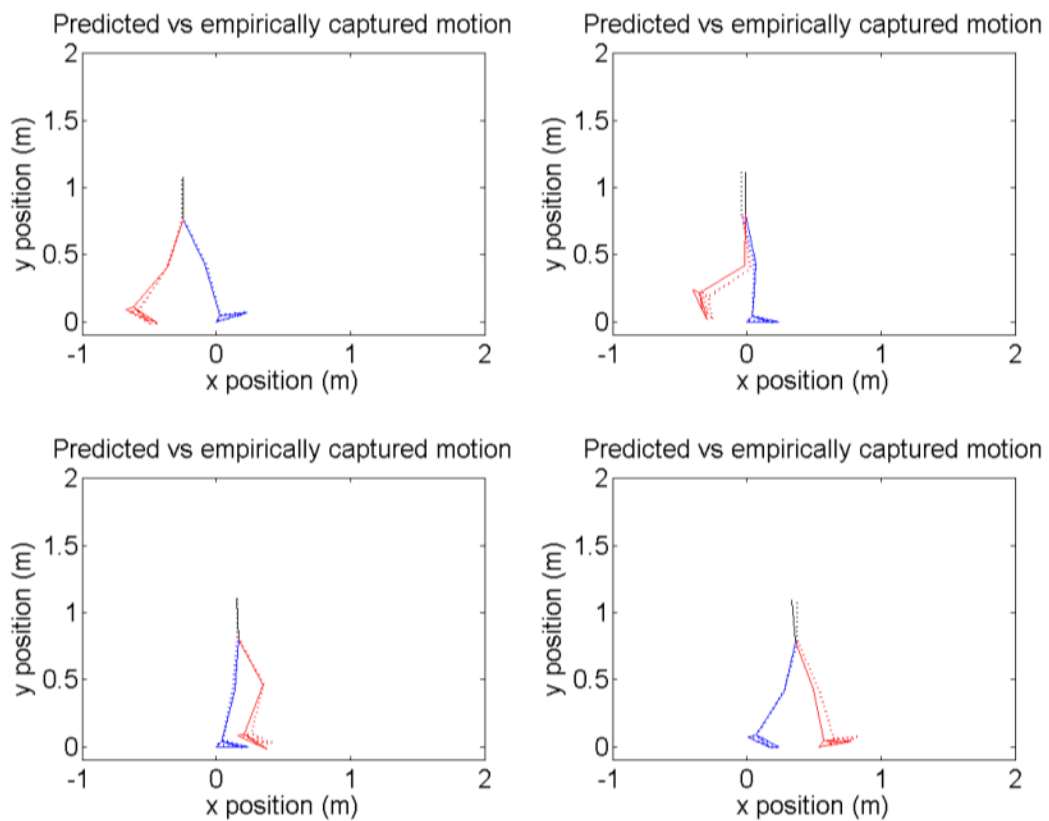


Figure 6.11: The kinematic predictions (solid) vs the experimental trial data (dotted) for Subject #6

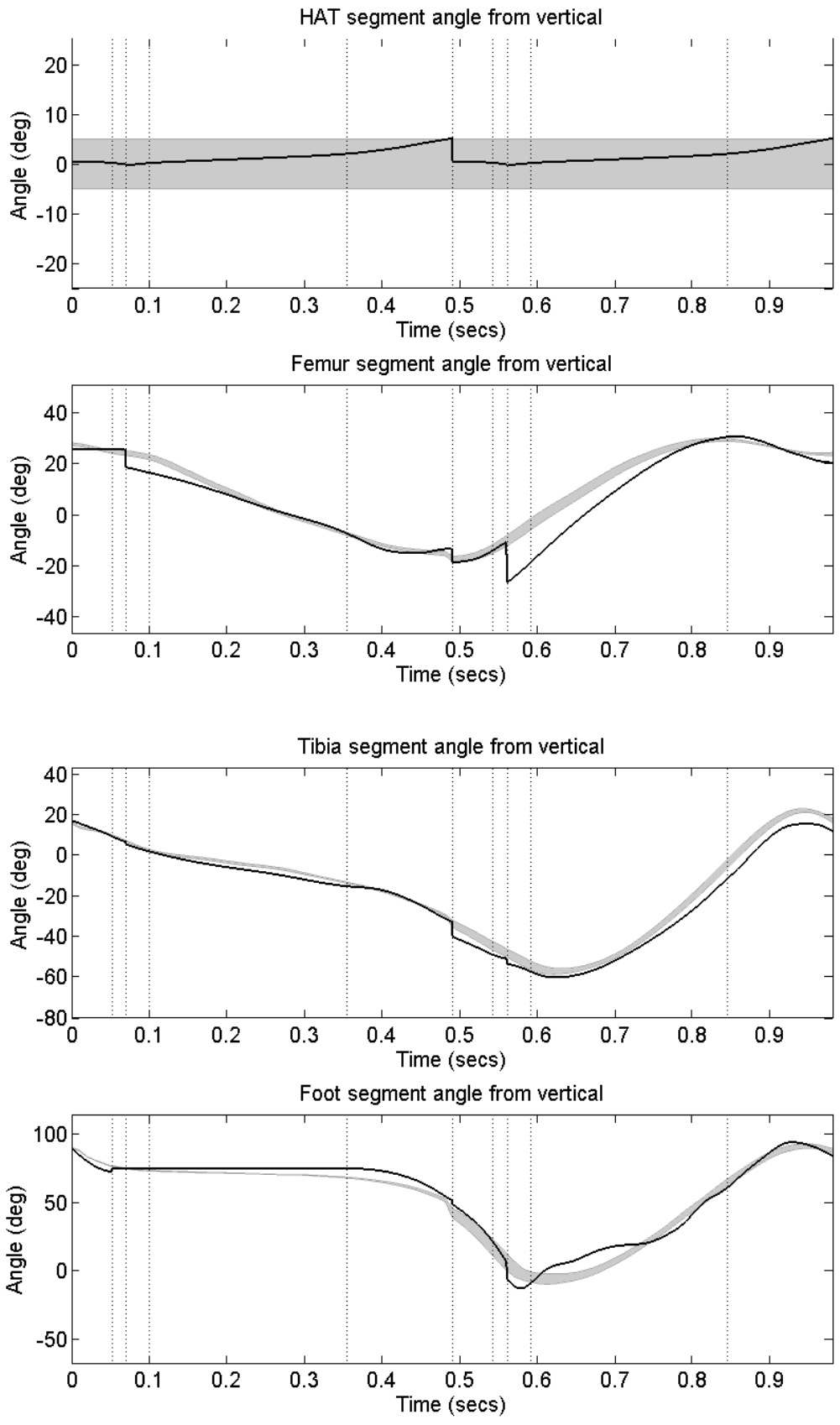


Figure 6.12: The segment angles predictions for Subject #6

The worst GRF predictions

Figure 6.13 shows the GRF predictions of the simulation for Subject #6, which also had the highest mean RMS error for GRF (5.07% BW). From the graph it is clear that the main problem was during single support but particularly the transition to it, from double support, where the vertical component under the leading foot displays a discontinuity of almost 25% BW.

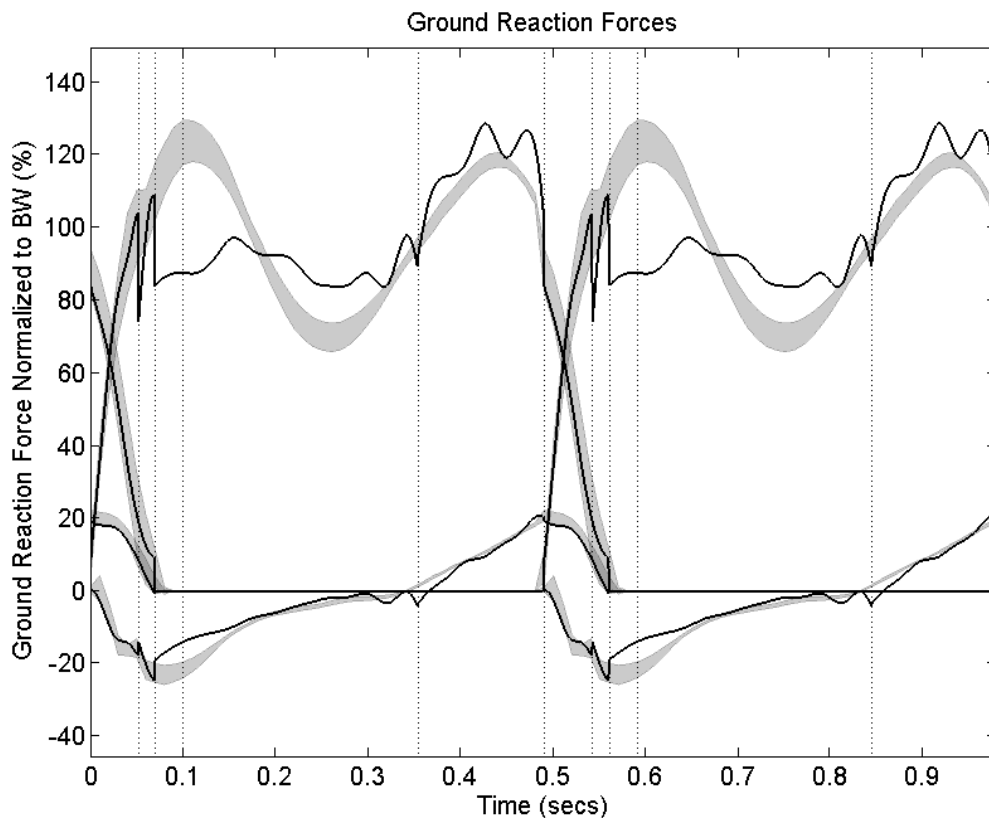


Figure 6.13: The GRF predictions for Subject #6

The worst joint moment predictions

Figure 6.14 shows the joint moment predictions for Subject #10, which had the highest mean RMS error for joint moments (21.05Nm).

The mean discontinuity over all joint moments for this subject (68.96Nm) was the highest of all the subjects.

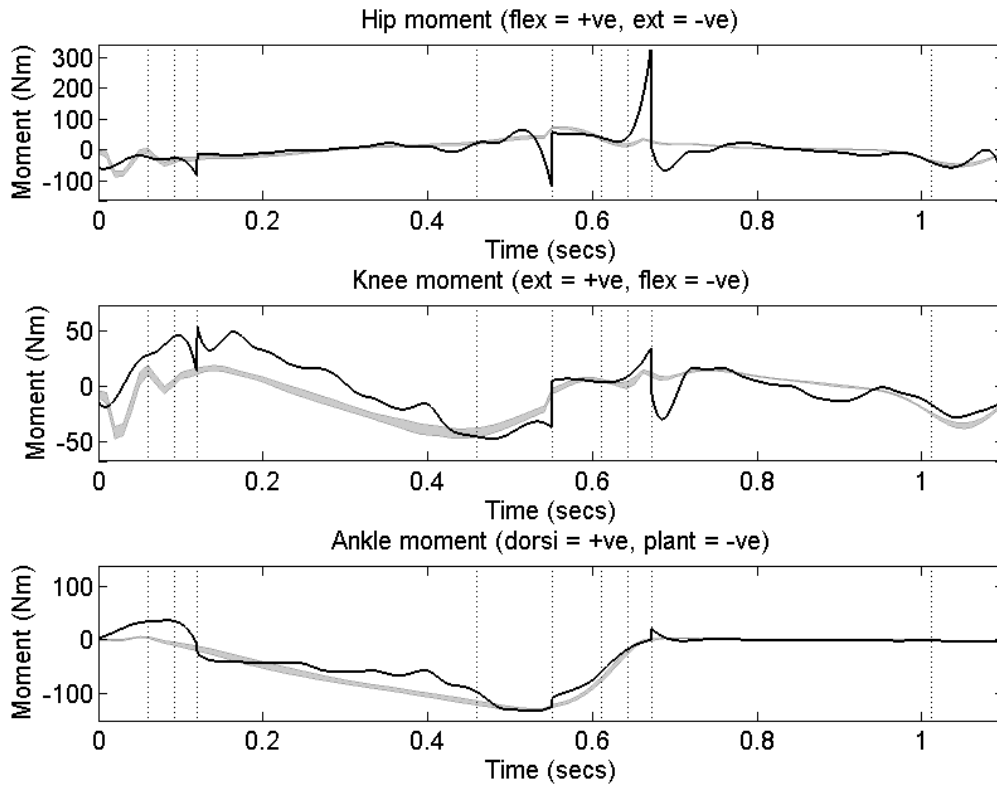


Figure 6.14: The joint moment predictions for Subject #10

6.4.5 Inter-subject comparisons

Table 6.5 shows the correlation coefficients for certain person-specific characteristics (height, mass and gait cycle time) and the RMS error values for the different kinematic and kinetic parameters. These are given in terms of both Pearson's correlation and Spearman's ranked correlation. The associated p-values are also shown. Figure 6.15- Figure 6.17 illustrate these correlations graphically.

Significant correlations ($p < 0.05$) were only found between the height of the participant and the RMS error of the predicted joint moments, and between the mass of the participant and the RMS error of the predicted joint moments.

There were other weak correlations observed. These were segment angle to height, segment angle to mass and GRF to mass.

		RMS error			
		Segment angles	Joint centre positions	Joint moments	GRF
Height	ρ	-0.31	-0.05	0.76	-0.21
	p-value	0.38	0.89	0.01	0.56
	ρ_s	-0.22	-0.11	0.67	0.04
	p-value	0.54	0.76	0.03	0.92
Mass	ρ	-0.43	0.02	0.77	-0.45
	p-value	0.22	0.96	0.01	0.19
	ρ_s	-0.52	-0.18	0.77	-0.28
	p-value	0.13	0.63	0.01	0.43
Gait cycle time	ρ	0.15	0.28	0.26	0.10
	p-value	0.68	0.43	0.48	0.78
	ρ_s	0.21	0.23	0.21	0.25
	p-value	0.55	0.52	0.57	0.49

Table 6.5: The Pearson's Correlation Coefficients (ρ) with their respective p-values, and Spearman's rank correlation coefficient (ρ_s) with their respective p-values, for comparisons of RMS errors and certain subject characteristics

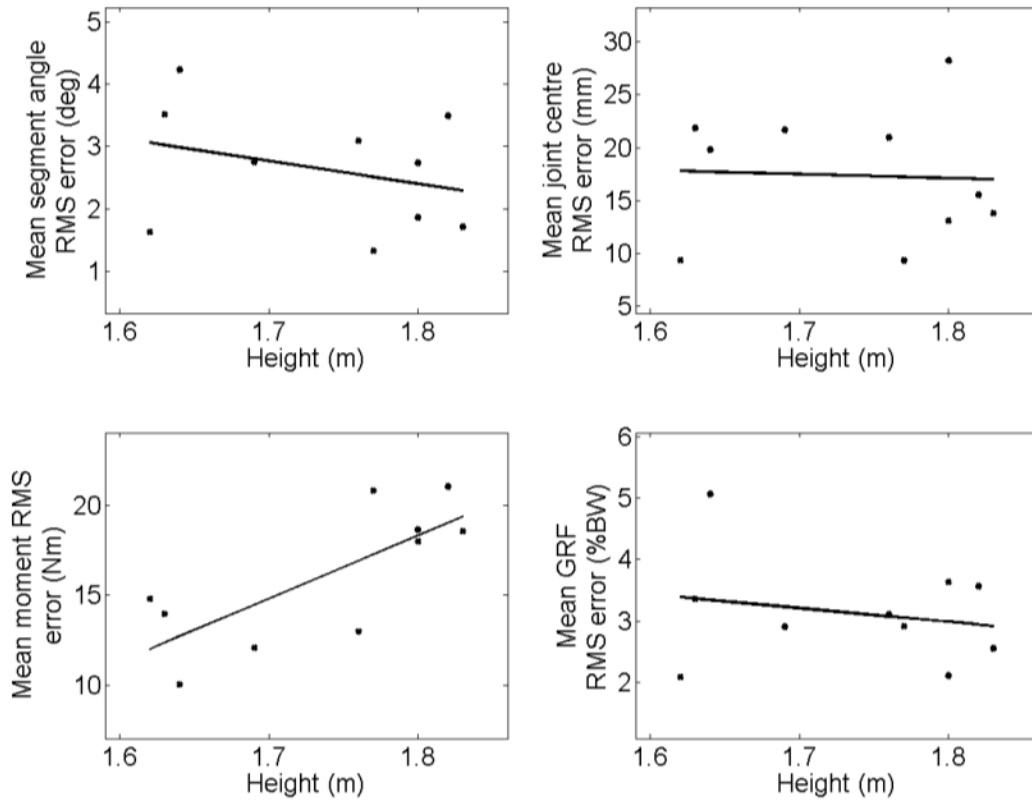


Figure 6.15: Comparison of RMS errors against height for all subjects

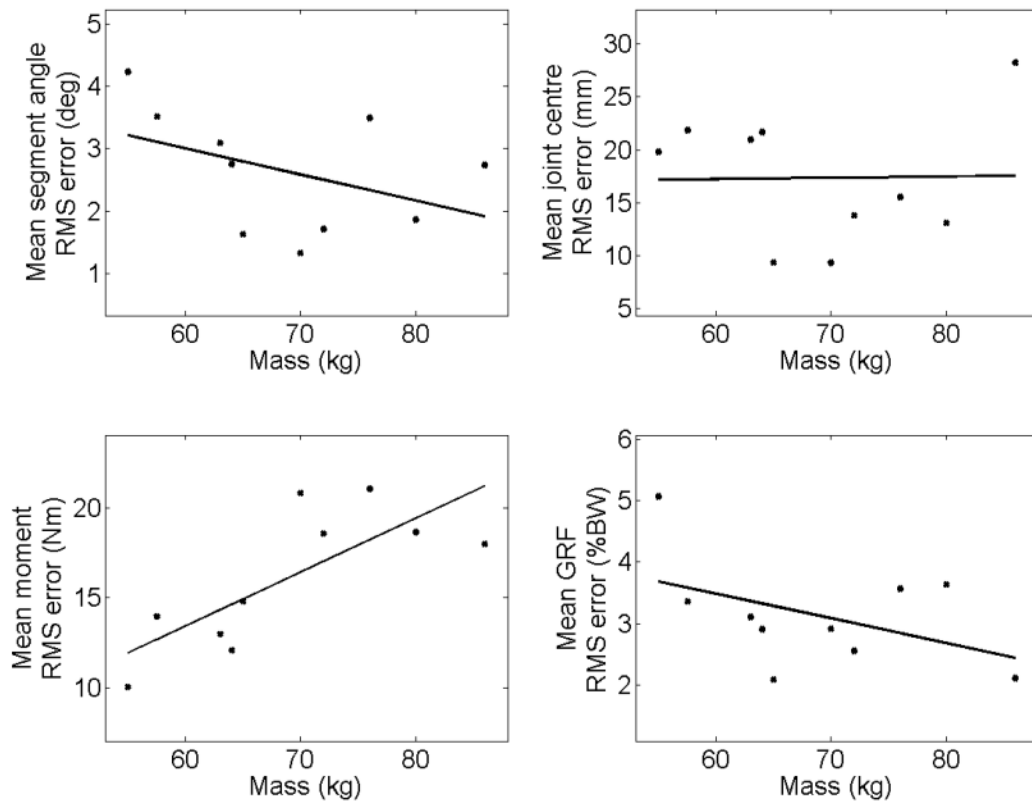


Figure 6.16: Comparison of RMS errors against mass for all subjects

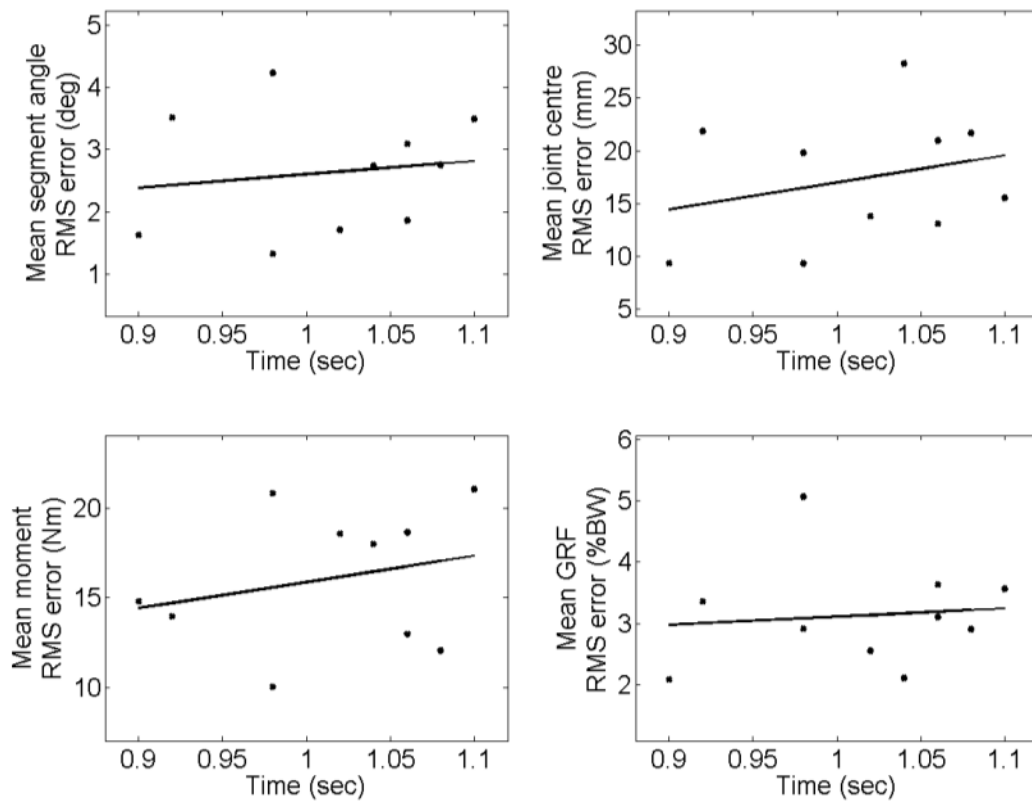


Figure 6.17: Comparison of RMS errors against gait cycle time for all subjects

6.5 Discussion

The big change from previous modelling work that this study incorporated was the ‘personalisation’ of each simulation. For each person tested, the model was adapted to their specific dimensions and inertial properties, and was compared to their particular data set, rather than the general data used during model development. The necessity for this change was to test the adaptability of the model; a characteristic it would require to become useful in a clinical environment.

Another change from the previous simulation setup was the use of joint centre positions as a measure of the kinematic error. The segment angle RMS errors were still calculated for comparison. It was observed that, when ranked in order of joint centre position RMS error and then by segment angle RMS error, there was a positive correlation with a Spearman’s rank correlation coefficient of 0.66 ($p=0.04$). The fact that this wasn’t a perfect correlation shows that optimising for joint centre position does give different

results to optimising for segment angle, and hence provides justification for the decision to assess kinematic error in this new way.

Something that was discussed in detail during the model development was the presence of discontinuities between single and double support stages of the model. These were also still present for all of these person-specific simulations. Those discontinuities observed in the original model were compared to the results from the subject specific simulations. In terms of segment angles, there was only one subject that had smaller discontinuities than the original model (Subject #8). There were five subjects that had smaller discontinuities in their moment curves (Subject #s 3, 4, 5, 6 & 7) and three with smaller discontinuities in their GRF curves (Subject #s 1, 3 & 5).

Table 6.5 shows the Pearson's correlation coefficient when the errors of each of the subjects were compared against height (Figure 6.15), mass (Figure 6.16) and gait cycle time (Figure 6.17). Significant correlations were observed between joint moment RMS error and both the height and the mass of the subject. A quick calculation shows the Pearson's correlation coefficient between height and mass was 0.79 ($p=0.01$) so it would be fair to say that joint moment RMS error increases for 'larger' people. A possible explanation for this could be that larger people require generally larger moments in order to move their longer, heavier body segments. Therefore, the absolute error value in newton-metres may be larger than that of a smaller person but proportionally, as a percentage of the total moment produced, the error may be equivalent. This is confirmed when using the error values normalised by standard deviations, since no significant correlations are found.

There were some weak correlations observed that, despite having p-values greater than 0.05, are still worthwhile discussing. The height of a participant had a weak negative correlation with segment angle error. Assuming that taller people have longer body segments helps to explain this phenomenon. Consider the example of a tall and a short person. The optimiser was coded to minimise joint centre position error so let's assume that for a given joint, the knee say, the RMS error is 5mm for both participants. The taller person will have a longer tibial segment and therefore the 5mm error causes a smaller change in segment angle than it does for the short person's tibial segment.

The mass of the person also weakly correlated with segment angle and GRF. It has already been shown that mass correlated with height so it stands to reason that it would also appear to correlate with segment angles. In terms of the mass and GRF connection, better segment angle predictions would suggest more accurate segment angular accelerations. These accelerations, along with the segment masses, are the basis for calculating the GRF.

The correlations for the other measured kinematic and kinetic values with these subject-specific variables were mostly quite low suggesting that the model is not unjustly biased towards one type of subject. Also, the p-values are all quite high. Most authors cite a p-value of less than 0.05 as evidence that there is a significant correlation (Breakwell et al., 2012) so the high p-values here are an indication that a significant correlation does not exist.

Aside from a low number of subjects, there were other limitations to this method as a means of investigating the model. The preparation of the data collected from the gait lab tests, for example, was not perfect. There were six force plates in the laboratory. The data for comparison was taken from the first instant of double support of force plates 1 and 2, and continued until the first instant of interaction with force plate 3. This meant that the data collected would show one double support stage, followed by a single support stage, in the same way that the model behaved. As with the model, bilateral symmetry was assumed. The fault with this assumption is that there could be a discontinuity in the experimental data between the end of the first half of the gait cycle and the start of the second half, or at the transition from one gait cycle to another. This did not seem to have too much of an adverse effect on the results, however.

Another limitation was with the model itself. Assuming bilateral symmetry meant that the respective segments on each leg were modelled the same length as one another i.e. both femurs were the same length. This is not necessarily the case in reality and small differences could potentially make large differences to the simulation results. If this model were ever used in a clinical setting for people with pathologies or prostheses, this issue would have to be addressed as their walking patterns, geometries and mass distributions would not necessarily be bilaterally symmetrical.

6.6 Conclusions

The full gait cycle model of healthy human walking was shown to have versatility when it came to use with different people. Preliminary tests explored any bias in terms of patient height, mass or walking velocity, and explanations were proposed. Some of the limitations of this model and this study's method have been discussed.

The experimental data gathered here showed much greater variation than was allowed by the '*normal*' data set used in the model development. This showed that what is considered the '*normal*' way to walk does not necessarily apply to everyone and there is a necessity for subject-specific modelling.

The final chapter in this thesis will take the findings here, and in previous chapters, and summarise the '*bigger picture*'. The conclusions that each of these investigations has drawn, and hypotheses that have been suggested as a result, will be analysed in further detail. The benefits and drawbacks of these kinds of studies will be addressed and suggestions for improvements and future work will be considered.

7 GENERAL DISCUSSION

7.1 Introduction

Musculoskeletal modelling has gained considerable momentum in the gait analysis field as it is very useful in providing insight into why we walk the way we do, which is not immediately obvious from observation alone. *In silico* experimentation also permits investigations that would be difficult to perform in practice, providing knowledge that was previously unavailable.

The overall purpose of this thesis was to investigate the progress of these types of models. Incorporating extra DOF and muscles in a model allows more realism but can blur cause and effect relationships in gait that provide an understanding of why we have developed to use specific mechanisms. In addition to this, with increasing complexity there is often an increasing dependence upon assumptions. Less complex models, with fewer considerations, make these relationships more easily observable and thus are worthwhile exploring.

After a short introduction in the first chapter, Chapter 2 explored the current state-of-the-art of modelling through an appraisal of the relevant literature. From this, areas of interest that warranted further investigation were highlighted and specific research questions were outlined.

Chapter 3 examined the strengths and weaknesses of forward dynamic IP models, comparing them to one another, as well as a '*normal*' set of experimental walking data. This was done for three different walking velocities.

Chapter 4 focussed on the single stance period of gait. A generalised Lagrange formulation for a joint actuated, open chain, dynamic system was developed and used to produce four models, each incorporating more complexity than the previous one. An optimisation procedure was performed in an attempt to track the '*normal*' kinematic data. After a solution was given, the resulting kinetics were observed and used as a comparative measure of model performance. The effects of each of the individual complexities were highlighted.

Chapter 5 focussed on the double stance period of gait. A framework was developed, employing Lagrange Multipliers to augment the previous generalised formulation (Chapter 4), giving a new one for joint actuated, closed chain, dynamic systems. This was not only a method of applying the necessary constraints, but also aided the calculation of the GRF distribution between the two ground contact points. The same optimisation procedure was used to develop a double support solution. The amalgamation of the double support solution and the single support solution produced results for a whole gait cycle.

Chapter 6 took the model of the full gait cycle and tested its versatility. The anthropometric measurements and gait data of ten participants were collected in practical experiments. These data were then input into the model and the optimisation procedure was used once more to produce a solution that matched that individual's kinematic data by minimising the RMS error between predicted and experimental data. The variables that affected model performance were examined.

In this discussion, each of the research questions will be reviewed. The extent to which the various studies in this thesis were able to answer each of these questions, will be considered. Following this, the general limitations of the methods and models used throughout these studies will be analysed. This will lead on to a section proposing how this work could be taken further and what such work might discover. Finally, the conclusions of the thesis, as a whole, will be outlined.

7.2 Research question 1

What are the strengths and weaknesses of the inverted pendulum for predicting the sagittal kinematics and kinetics of healthy human walking?

This research question was explored exclusively in Chapter 3 of this thesis. Two different IP models, one incorporating a HAT segment, were compared to each other and experimental data. In terms of strengths, the IP models were able to show a good prediction of linear CM velocity, in both x and y directions, during the single support

phase of gait. Also, during single support, the x and y components of GRF were close to that of the experimental data. The y component curve was not the right shape, but the magnitude was close. The weaknesses of IP models of gait were most apparent during the double support phase. The vertical linear velocity and vertical GRF component curves had large errors from their experimental data counterparts during this period. It was also noted that these discrepancies tended to increase with walking velocity. These errors were greatest at the transition from one step to the next. This led to the conclusion that IP models cannot adequately model the double support phase of walking.

7.3 Research question 2

To what extent can a sequence of numerical models, incrementally increasing in complexity, highlight the effects of different gait mechanisms?

This phenomenon can be observed across several different chapters in this thesis. Firstly, in Chapter 3, the traditional IP model (Model 1) was extended to include a HAT segment and a hip moment (Model 2), the value of which is calculated so as to keep the HAT segment upright, maintaining only a single DOF. The predictions of the two models were very similar in terms of kinematics and GRF. The point of interest was that the predicted hip moment curve of Model 2, was very similar to that of the experimental data. This suggested that maintaining an upright trunk during walking was a key role of the hip joint moment. In Chapter 4, the addition of a knee joint was shown to be the primary contributor to the first peak in the vertical GRF component curve by allowing a better representation of the whole body CM motion in the first half of single support. The addition of a static foot and ankle moment improved the GRF component curves in the second half of single support but the action of heel rise in the next model was shown to be the major contributing factor towards achieving the second peak in the vertical GRF component curve. It was hypothesised that this is evidence for an active '*push-off*' mechanism from the trailing foot at the end of single support. The addition of a swing leg increased the realism of the mass distribution and refined the second peak further.

The process of incrementally increasing the complexity from one model to the next meant that hypotheses could be proposed regarding the roles of different muscle actions and kinematic movements made during gait. It was able to provide mathematical evidence for the true '*determinants of gait*', rather than just basing ideas on observation.

7.4 Research question 3

What is the minimum complexity required for a numerical model to predict the kinematics and kinetics of healthy sagittal bipedal gait, within a single standard deviation range

- a) for one-legged single support?*
- b) for two-legged single support?*
- c) for the full gait cycle?*

One-legged single support models were examined in both Chapter 3 and Chapter 4. The most complex of these models was Model 4, incorporating knee and ankle joints and permitting heel rise, with four DOF. The curves for Model 4's predicted kinematics and GRF components fell outside the ± 1 standard deviation range for parts of the single support period. This was most notable for the foot segment angle during the heel rise stage and the vertical GRF component curve during the first half of single support. However, when the errors were normalised by the experimental data standard deviations, this was the only single-legged model for which the mean segment angle RMS error (0.59σ) and the mean GRF RMS error (0.98σ) were both less than one. This was deemed within the acceptable criteria of part '*a*' of this research question.

There was only one two-legged model of single support: Model 5, which had seven DOF. Once again, the predicted kinematics and kinetics fell outside the single standard deviation range of the normal data for parts of the gait cycle. As with Model 4 though, when the errors were normalised by the experimental data standard deviations, both mean segment angle RMS error (0.37σ) and mean GRF RMS error (0.94σ) were less than one, hence making it acceptable for part '*b*' of this research question.

In order to get a workable model for the double support period, it was necessary to add a toe segment to the trailing foot, so there were eight segments but the presence of two dependent segments meant there were still only seven DOF in total. The Sum model of a full gait cycle was formed by combining the seven DOF double support model with the seven DOF single support model. The mean values of both segment angle RMS error and GRF RMS error, when normalised by standard deviation, were both less than one (0.35σ and 0.5σ , respectively).

However, there were some weaknesses. As well as the periods at which some predictions strayed from the experimental standard deviation range, there were discontinuities at the transitions between double and single support stages. In spite of these drawbacks, this model was acceptable under the criteria of part 'c' of this research question.

It should be noted that for all these 'accepted' models, the mean moment RMS error values, when normalised by standard deviation, were not less than one. However, since the moment actuations were the optimisation variables, it was highly likely that these could drift from their experimental values so it was decided not to use these in the measure of performance of the models.

7.5 Research question 4

Considering interpersonal differences, the time cost and the solution accuracy, how close is gait modelling to becoming a clinically usable tool?

For predictive gait modelling to become a clinically useful tool, any model used would have to be able to adapt to the characteristics of a wide variety of people. The adaptability of the Sum model was tested in Chapter 6. Data was collected for ten different participants, input into the model and optimisation was used to minimise the joint centre position RMS error from that specific subject's gait data. The results showed varying degrees of accuracy but were definitely promising. There are limitations and potential areas for improvement with this model, which are discussed in detail in Section 7.6.

In terms of time cost however, these models achieve a solution in a much more manageable time than the very complex models cited in the literature. Whereas Anderson and Pandy's complex model used 10,000 hours of processing time (Anderson & Pandy, 2003), the most complex simulations in this study took approximately 8-12 hours. This implies that clinical application is a much more realistic prospect.

Realistically, in order to provide all the data that a clinician might need, a more complex model than this would be necessary. It is recommended that the engineers developing the models liaise with clinical staff to identify which data they require and thus which complexities are essential to incorporate in a model. However, with the rate at which computer processing power is increasing and the rate at which the cost of such processors is decreasing, it won't be long before computational modelling is an integral part of the clinical analysis and diagnostics.

7.6 General limitations

There are a number of limitations with the models used throughout this study. Firstly, all the models were 2D, sagittal plane only. This meant that subtleties such as hip rotation were not accounted for, which could have an effect on quantities like step length. Other actions and motions that could have affected the model results, such as arm swing, were omitted because the head, arms and trunk were all grouped together in a single segment. Some researchers have previously modelled just the trunk itself using multiple segments (Ceccato et al., 2009) so a single HAT segment assumption could have a great effect.

In terms of a clinical environment, it is likely that modelling would be used to help diagnose and treat people with some kind of pathology. The fact that this model only considers healthy human walking is therefore a limitation. Many assumptions were possible for a healthy model that would have to be changed in order to produce one that works with pathological or prosthetic gait. The first example of this is the bilateral symmetry assumption. This means that the properties of a given segment on one leg are identical to its equivalent on the other leg. They are the same length, mass, have the same moment of inertia and behave the same way as each other over the gait cycle, except in anti-phase. Obviously, this will not necessarily be the case for pathological

walking. Asymmetrical gait is common, particularly in patients with cerebral palsy (CP) or similar conditions (Dobson et al., 2011; Rodda et al., 2004).

Some pathological conditions mean that the first contact with the ground is with the forefoot or toe and sometimes the foot will never be flat on the ground (Dobson et al., 2011; Rodda et al., 2004). A weakness of these models when it comes to modelling pathologies is that the foot interaction with the ground is rather restricted. All of the different '*rockers*' (Perry & Burnfield, 2010) are modelled by different submodels, but the order in which they occur is determined before the start of a simulation.

The discontinuities between the double and single support stages have been discussed at length throughout this thesis. This is caused because both the double and single support models have their initial state defined by the optimiser, so when they are run concurrently, the initial state of one will not necessarily be the same as the terminal state of the previous. The best way to combat this would be to force the initial state of one simulation to be equal to the terminal state of the previous. This is discussed further in Section 7.7 and some preliminary results are shown in Appendix A.8.

The fact that the actuations in these models were defined by actuated joint moments is another simplification. Some muscles and tendon are '*biarticular*' (cross two or more joints) so their action is not highlighted when overall moment is the only consideration.

Throughout the model development process, a normal dataset, taken from Winter's work (1979, 1991), was used as a comparison to measure each model's performance. Not only that, but many of the properties such as segment mass, length, moment of inertia, CM position etc. were all taken from generic proportions based on height or simple formulae based on segment length. These were developed from previous studies (Dempster, 1955; Dempster et al., 1959; Drillis & Contini, 1966), some of which had used cadavers. But why was this taken as a '*gold standard*'? The reason was because there are so few of these types of studies. This is because they are very difficult to reproduce and ethical approval is difficult to attain. Just the three studies referenced by Winter (Dempster, 1955; Dempster et al., 1959; Drillis & Contini, 1966), have over 2000 citations between them. Essentially, these are the data that are available. They may not be perfect for every subject but they provide a good approximation.

Where possible, the study in Chapter 6 collected individualised data to reduce the use of approximations, but some were still necessary, for example to calculate the moment of inertia of a segment.

The data collection is prone to error also. There is measurement error of equipment such as tape measures, cameras and force plates, and marker error caused by placement and skin artefact. There are also calculations based on generalities. The joint centre positions, for example, involved calculations based on the subjects's proportions, as did the HAT segment CM position.

The inverse dynamics used by the Vicon software to calculate the joint moments, rely on sections of the body being approximated into three-dimensional segments and thus maybe under- or overestimate the true value.

Despite these limitations, the Vicon system for gait data capture is one of the most widely used and trusted systems throughout the gait analysis community and was thus considered acceptable for this particular study.

7.7 Future work

Throughout this thesis there have been discussions regarding the failings and limitations of the models used, as well as the potential reasons for them. From these a number of suggestions for future development have been proposed.

Firstly, in order to thoroughly investigate the bias of the model to a particular characteristic of the subject being modelled, a study with a larger number of people should be performed. This would make the statistical analysis more persuasive.

An asymmetric model with fewer constraints on foot behaviour would be required so that pathological gaits could be modelled. This would necessitate a new solution to the COP motion when the foot is in contact with the ground, possibly requiring a multi-segment foot. This simulation might also consider incorporating a decision tree to determine which submodel would be most appropriate to use at a given time.

Other changes that could aid the modelling of pathological gait include expanding to three dimensions or using a multi-segment trunk, with a more realistic mass distribution, to investigate what effect this would have on the posture of the simulated gait pattern.

In order for a model to become clinically useful, it needs to provide as much information as possible. An issue highlighted in the discussion of the limitations of this model was that it only considers overall joint moment and makes no concessions for biarticular muscles. A future extension of this work could be to model muscles and muscle groups, and use these to provide the necessary actuation. Static optimisation could be incorporated to determine the contribution of biarticular muscles. In addition to this, geometric means could be used to determine the potential force generation of different muscles and muscle groups.

A particular problem for the Sum model was the behaviour of the segments that were dependent during the double support phase and then independent during the single support phase. An investigation is proposed to study the effects of changing dependency on different segments. It is hypothesised that for larger segments with lower rotational velocities, such as the femur segments, this change will have a less significant effect.

Another drawback of the Sum model was the problem of discontinuities between double and single support phases. In order to combat this, the terminal state of the first double support period would need to be used as the initial state for the first single support period. With the bilateral symmetry assumption still in place, hence only half the gait cycle is modelled, there is still the problem over ensuring the terminal state of the single support period is equal, or as close as possible to, the initial state of the double support period. This could perhaps be done by incorporating a penalty condition into the optimiser's cost function.

An interesting result of the study was how the model solutions reflect on the original '*Determinants of Gait*' (Saunders et al., 1953). In order to develop their hypotheses, Saunders et al. started with a '*compass gait*', much like an IP, and added features one by one. The models in this study started with the IP and added different gait features one by one (the rationale for each subsequent addition can be found in Appendix A.9). The focus of this investigation was the effects of these mechanisms on gait kinetics, as opposed to how well they helped the whole body CM achieve a smooth sinusoidal pathway, as

Saunders et al. stated. However, it is logical to assume that this motion is what helps us produce these kinetic profiles. This project has shown the importance of stance phase knee flexion, and foot and ankle mechanisms but the addition of further complexities would be required to investigate how important hip rotation, pelvic obliquity and lateral CM displacement are to the walking process. Clearly, this would require the model to be extended to 3D.

7.8 General conclusions

- The very simple models do not adequately simulate gait.
- For forward dynamic simulations, the sequential addition of extra complexities highlights '*cause and effect*' relationships, helping to identify the true determinants of gait.
- Lagrangian mechanics and Lagrange Multipliers have many advantages when it comes to equation of motion development, constraint application and force distribution in gait models.
- Computational predictive modelling is set to play a key role in the future of gait analysis and rehabilitation.

APPENDICES

A.1 Formulae for generalised body parameters

Segment	Segment mass /Total body mass	CM position /Segment length		Radius of gyration /Segment length
		From proximal end	From distal end	About CM
Foot	0.0145	0.5	0.5	0.475
Shank	0.0465	0.433	0.567	0.302
Thigh	0.1	0.433	0.567	0.323
Foot and shank	0.061	0.606	0.394	0.416
Total leg	0.161	0.447	0.553	0.326
HAT	0.678	0.626	0.374	0.496

Table A.1: The formulae for calculating generalised body parameters as functions of a person's height and weight (Winter, 1979, 1991)

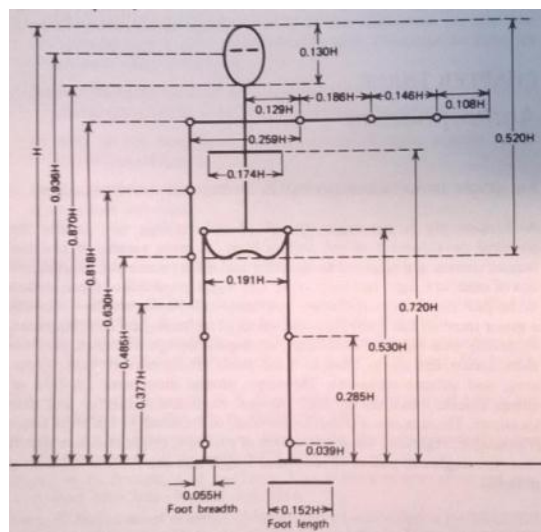


Figure A.1: Body proportions based on height (Winter, 1979, 1991)


```

elseif h==j

    B{h,j}={'(m(' int2str(h) ').*(d(' int2str(h) ').^2))+(m('
int2str(h) ').*(e(' int2str(h) ').^2))+sum(m(' int2str(h+1)
':end)).*(l(' int2str(h) ').^2))+I(' int2str(h) ')'};

elseif h>j

    B{h,j}={'((cos(theta((i+1),' int2str(j) )-theta((i+1),' int2str(h)
'))).*((m(' int2str(h) ').*d(' int2str(h) '))+((sum(m('
int2str(h+1) ':end))).*l(' int2str(h) '))).*l(' int2str(j)
')))+((sin(theta((i+1),' int2str(h) )-theta((i+1),' int2str(j)
'))).*((m(' int2str(h) ').*e(' int2str(h) '))).*l(' int2str(j)
')))}';
    C{h}={C{h} '+((vel((i+1),' int2str(j) ').^2).*(sin(theta((i+1),'
int2str(j) )-theta((i+1),' int2str(h) '))).*((m(' int2str(h)
').*d(' int2str(h) '))+((sum(m(' int2str(h+1) ':end))).*l('
int2str(h) '))).*l(' int2str(j) ')))+((vel((i+1),' int2str(j)
').^2).*(cos(theta((i+1),' int2str(h) )-theta((i+1),' int2str(j)
'))).*((m(' int2str(h) ').*e(' int2str(h) '))).*l(' int2str(j)
')))}';

    C{h}=cell2mat(C{h});

end

B{h,j}=cell2mat(B{h,j});

end

C{h}={C{h} '+Mom(i+1,' int2str(h+1) )-Mom(i+1,' int2str(h) )'};

C{h}=cell2mat(C{h});

end

```

For $n=3$, the B and C matrices produced are shown on the next pages. The strings that make up the individual elements of these matrices were evaluated, for each time step, as part of the numerical integration procedure (Section 4.3.3).

<pre> C= '(((g.*sin(theta((i+1),1)))).*(m(1).* d(1))+((sum(m(2:end)).*1(1)))))- ((g.*cos(theta((i+1),1)))).*(m(1).*e (1)))))- ((vel((i+1),2).^2.*(sin(theta((i+1), 1))- theta((i+1),2))).*((m(2).*d(2))+((su m(m(3:end)).*1(2)).*1(1))))- ((vel((i+1),2).^2.*(cos(theta((i+1), 2))- theta((i+1),1))).*((m(2).*e(2)).*1(1))))- ((vel((i+1),3).^2.*(sin(theta((i+1), 1))- theta((i+1),3))).*((m(3).*d(3))+((su m(m(4:end)).*1(3)).*1(1))))- ((vel((i+1),3).^2.*(cos(theta((i+1), 3))- theta((i+1),1))).*((m(3).*e(3)).*1(1)))+Mom(i+1,2)-Mom(i+1,1)'</pre>	<pre> '(((g.*sin(theta((i+1),2))).*(m(2).*d (2))+((sum(m(3:end)).*1(2)))))- ((g.*cos(theta((i+1),2))).*(m(2).*e(2)))))+((vel((i+1),1).^2.*(sin(theta(i+1),1)- theta((i+1),2))).*((m(2).*d(2))+((sum (m(3:end)).*1(2)).*1(1)))+(vel((i+1),1).^2.*(cos(theta((i+1),2))- theta((i+1),1))).*((m(2).*e(2)).*1(1)))- ((vel((i+1),3).^2.*(sin(theta((i+1),2))- theta((i+1),3))).*((m(3).*d(3))+((sum (m(4:end)).*1(3)).*1(2))))- ((vel((i+1),3).^2.*(cos(theta((i+1),3))- theta((i+1),2))).*(m(3).*e(3)).*1(2)))+Mom(i+1,3)-Mom(i+1,2)'</pre>	<pre> '(((g.*sin(theta((i+1),3))).*(m(3) .*d(3))+((sum(m(4:end)).*1(3)))))- ((g.*cos(theta((i+1),3))).*(m(3).* e(3)))))+((vel((i+1),1).^2.*(sin(theta((i+1),1)- theta((i+1),3))).*((m(3).*d(3))+((sum(m(4:end)).*1(3)).*1(1)))+(ve l((i+1),1).^2.*(cos(theta((i+1),3) - theta((i+1),1))).*(m(3).*e(3)).* 1(1)))+(vel((i+1),2).^2.*(sin(the ta((i+1),2)- theta((i+1),3))).*((m(3).*d(3))+((sum(m(4:end)).*1(3)).*1(2)))+(ve l((i+1),2).^2.*(cos(theta((i+1),3) - theta((i+1),2))).*(m(3).*e(3)).* 1(2)))+Mom(i+1,4)-Mom(i+1,3)'</pre>
--	---	---

A.3 Letter confirming ethical approval



Research, Innovation and Academic
Engagement Ethical Approval Panel

College of Health & Social Care
AD 101 Allerton Building
University of Salford
M6 6PU

T +44(0)161 295 7016
r.shuttleworth@salford.ac.uk

www.salford.ac.uk/

12 June 2013

Dear Mike,

RE: ETHICS APPLICATION HSCR13/18 – The kinematics and kinetics of healthy human walking

Following your responses to the Panel's queries, based on the information you provided, I am pleased to inform you that application HSCR13/18 has now been approved.

If there are any changes to the project and/ or its methodology, please inform the Panel as soon as possible.

Yours sincerely,

Rachel Shuttleworth

Rachel Shuttleworth
College Support Officer (R&I)

A.4 Recruitment poster

University of
Salford
MANCHESTER

School of
Health Sciences

Volunteers needed!



Are you over 18?

Are you healthy and able to walk unaided?

Participants are required for a study collecting healthy walking kinematics and kinetics for use in predictive computer simulations.

For more information, please email m.p.mcgrath@edu.salford.ac.uk

A.5 Participant Information Sheet

Study Title: The Kinematics and Kinetics of Healthy Human Walking

I would like to invite you to take part in a research study. Please take time to read this information sheet thoroughly. Please feel free to then ask any questions you may have and decide whether or not you wish to take part. Once you completely understand the study, you will be asked to sign a consent form in order to take part. From that point on, your participation is entirely voluntary and you may withdraw at any time, without giving a reason.

All information collected in this study is confidential and if you choose to withdraw, all your data will be deleted.

What is the purpose of the study?

The main purpose of this study is to gather data that can be used to test the reliability of a computer simulation that aims to predict how a person walks. Using measurements of the size of a subject's limbs, their height and their weight, predictions can be made about how that subject's body will move over time, along with the forces and torques required to produce that motion. This prediction will be compared to the same data, as measured in the laboratory.

Why have I been invited?

You have been invited because you are a healthy adult. The group of subjects will consist of an even spread of males and females, as well as a variety of heights, weights and ages.

Do I have to take part?

Participation is voluntary and you can choose to withdraw at any time.

What will happen to me if I take part?

If you choose to partake you will need to attend the gait laboratory at the University of Salford for a single session of approximately two hours.

During this session, you will be required to wear shorts and a t-shirt and be barefooted. The researcher will firstly take measurements of your height, weight and the distances between the joints of your legs. These are common measurement procedures used by physiotherapists/biomechanists etc. Next, retro-reflective markers will be placed (using double-sided tape and/or bandages) at certain positions on your feet, legs and hips. You will then be asked to walk along a track approximately 10m in length. Infra-red cameras positioned around the gait lab will record the motion of these markers in three dimensions. You will be asked to repeat these walks until five successful trials have been recorded.

All data and recordings are confidential and will not identify the subject.

What will I have to do?

The only requirement is that you attend the prearranged appointment time and perform the walking task.

What are the possible disadvantages and risks of taking part?

Since this test only involves barefoot walking, realistically, the potential for injury is very low.

What if there is a problem?

If you have a concern about any aspect of this study, you should ask to speak to the researcher who will do their best to answer your questions (email: m.p.mcgrath@edu.salford.ac.uk).

If you remain unhappy and wish to complain formally you can do this through the University complaints procedure by contacting the supervision team of the primary

researcher, who will follow the University Procedure for Allegations of Scientific or Ethical Misconduct.

Will my taking part in the study be kept confidential?

All information collected is kept confidential. All data and recordings made will be kept secure and password protected, with no personal identifying markers whatsoever. The data will only be used by the primary researcher for their PhD studies.

What will happen if I don't carry on with the study?

If you decide to withdraw from the study, you have the right to request that all data relating to you be deleted.

What will happen to the results of the research study?

The results of this study will be used for testing the reliability of computer simulations of walking, which make up a PhD project.

Further information and contact details:

Primary researcher: Michael McGrath

Supervisors: Dr Richard Baker and Dr David Howard

Information Sheet based on: COREC/NHS National Patient Safety Agency. *Information Sheets and Consent Forms – Guidance for Researcher and Reviewers* Version 3.0 Dec 2006.
Link to IRAS website - [IRAS](#)

A.6 Research Participant Consent Form

Title of Project: The Kinematics and Kinetics of Healthy Human Walking

Ethics Ref No: HSCR13/18

Name of Researcher: Michael McGrath

(Delete as appropriate)

I confirm that I have read and understood the information sheet for the above study and what my contribution will be.

Yes	No
-----	----

I have been given the opportunity to ask questions (face to face, via telephone and e-mail)

Yes	No
-----	----

I agree to digital images being taken during the research exercises

Yes	No
-----	----

I understand that my participation is voluntary and that I can withdraw from the research at any time **without giving any reason**

Yes	No
-----	----

I understand how the researcher will use my results, who will see them and how the data will be stored.

Yes	No
-----	----

I agree to take part in the above study

Yes	No
-----	----

Name of participant

Signature

Date

Name of researcher taking consent Michael McGrath

Researcher's e-mail address m.p.mcgrath@edu.salford.ac.uk

A.7 All practical data

Subject	Gender	Characteristics					
		Age	Height	Mass	DS time	SS time	Total time
1	M	25	1.8	80	0.10	0.43	0.53
2	F	27	1.77	70	0.11	0.38	0.49
3	F	27	1.76	63	0.10	0.43	0.53
4	F	25	1.63	57.5	0.07	0.39	0.46
5	F	28	1.62	65	0.09	0.36	0.45
6	F	24	1.64	55	0.07	0.42	0.49
7	M	27	1.69	64	0.10	0.44	0.54
8	M	26	1.83	72	0.11	0.40	0.51
9	M	27	1.8	86	0.11	0.41	0.52
10	M	23	1.82	76	0.12	0.43	0.55

Table A.2: Characteristics of each of the subjects

The following tables show, for each participant, the overall RMS errors for different kinematic and kinetic parameters, as well as the discontinuities at the transitions between double and single support. Note that although the cost functions used error values normalised by standard deviation, the errors here are quoted in terms of the unit of measurement, specific to that parameter. The RMS error values also only consider the first half of the gait cycle so as to separate the results for equivalent parameters on opposite legs. For the discontinuity tables, data from the both legs have been combined so as to represent the behaviour a single limb, moving through a full gait cycle simulation.

A.7.1 Subject 1

			Lead/stance	Trail/swing
Joint centre positions (mm)	Met	x	0.36	0.76
		y	0.51	8.50
	Ankle	x	3.40	0.83
		y	4.47	4.38
	Knee	x	1.33	1.32
		y	11.73	4.25
	Hip	x	2.47	2.47
		y	3.66	3.66
	HAT	x		3.29
		y		3.69
Segment angles (°)	Foot		4.51	0.64
	Tibia		1.58	1.12
	Femur		2.65	0.68
	HAT			0.28
Joint moments (Nm)	Ankle		8.11	8.38
	Knee		3.76	6.82
	Hip		8.68	5.10
GRF (%BW)		y	2.25	0.44
		x	2.86	1.00

Table A.3: The RMS error values for Subject 1

			TO 1	FC 1	TO 2	FC 2	Mean
Joint centre positions (mm)	Met	x	0.00	0.00	50.56	0.00	12.64
		y	0.00	15.29	22.46	62.13	24.97
	Ankle	x	0.06	0.00	44.48	0.00	11.13
		y	0.15	7.64	21.53	7.83	9.29
	Knee	x	6.03	0.00	39.54	0.00	11.39
		y	0.35	9.82	27.75	13.52	12.86
	Hip	x	63.33	0.00	63.33	0.00	31.67
		y	24.31	0.57	24.31	0.57	12.44
	HAT	x	70.32	0.00	70.32	0.00	35.16
		y	23.98	0.67	23.98	0.67	12.32
Segment angles (°)	Foot		0.06	3.29	3.20	4.21	2.69
	Tibia		0.82	0.55	1.09	2.45	1.23
	Femur		8.28	4.15	2.20	1.98	4.15
	HAT		1.20	2.65	1.20	2.65	1.93
	Ankle		2.06	12.40	0.67	1.14	4.07
Joint moments (Nm)	Knee		11.50	18.86	63.42	9.78	25.89
	Hip		40.04	215.06	227.46	13.56	124.03
GRF (%BW)	y		3.57	3.11	2.53	7.59	4.20
	x		6.51	2.78	0.66	2.57	3.13

Table A.4: The discontinuity values for Subject 1

A.7.2 Subject 2

			Lead/stance	Trail/swing
Joint centre positions (mm)	Met	x	0.49	0.55
		y	0.67	0.57
	Ankle	x	3.43	0.69
		y	0.51	0.76
	Knee	x	0.83	0.90
		y	0.60	1.15
	Hip	x	0.73	0.73
		y	1.07	1.07
	HAT	x		0.72
		y		1.67
Segment angles (°)	Foot		1.20	0.64
	Tibia		1.16	0.65
	Femur		1.60	0.53
	HAT			0.08
Joint moments (Nm)	Ankle		7.71	4.90
	Knee		4.91	7.52
	Hip		14.51	19.24
GRF (%BW)		y	1.99	2.28
		x	0.50	3.75

Table A.5: The RMS error values for Subject 2

			TO 1	FC 1	TO 2	FC 2	Mean
Joint centre positions (mm)	Met	x	0.00	0.00	9.78	0.00	2.45
		y	0.00	10.58	16.25	45.73	18.14
	Ankle	x	0.01	0.00	17.15	0.00	4.29
		y	0.03	23.97	15.98	24.09	16.02
	Knee	x	9.81	0.00	21.41	0.00	7.80
		y	0.12	25.97	20.44	19.07	16.40
	Hip	x	25.09	0.00	25.09	0.00	12.55
		y	11.98	16.26	11.98	16.26	14.12
	HAT	x	16.82	0.00	16.82	0.00	8.41
		y	12.07	16.21	12.07	16.21	14.14
Segment angles (°)	Foot		0.01	6.74	6.30	1.04	3.52
	Tibia		1.34	0.58	0.84	2.67	1.36
	Femur		4.92	4.81	3.02	0.89	3.41
	HAT		1.46	0.50	1.46	0.50	0.98
	Ankle		5.78	1.32	2.03	1.99	2.78
Joint moments (Nm)	Knee		0.28	12.11	66.72	8.32	21.86
	Hip		109.26	184.53	449.75	19.57	190.78
GRF (%BW)	y		19.21	3.67	1.28	14.03	9.55
	x		1.03	0.72	2.31	1.13	1.30

Table A.6: The discontinuity values for Subject 2

A.7.3 Subject 3

			Lead/stance	Trail/swing
Joint centre positions (mm)	Met	x	0.81	1.80
		y	1.06	4.85
	Ankle	x	3.58	2.54
		y	3.81	5.74
	Knee	x	3.11	2.19
		y	5.96	10.17
	Hip	x	3.77	3.77
		y	6.92	6.92
	HAT	x		4.41
		y		8.70
Segment angles (°)	Foot		6.77	0.85
	Tibia		4.08	2.05
	Femur		2.26	1.98
	HAT			0.18
Joint moments (Nm)	Ankle		7.33	5.17
	Knee		3.11	3.04
	Hip		6.91	3.77
GRF (%BW)		y	1.78	1.19
		x	2.37	1.05

Table A.7: The RMS error values for Subject 3

			TO 1	FC 1	TO 2	FC 2	Mean
Joint centre positions (mm)	Met	x	0.00	0.00	31.52	0.00	7.88
		y	0.00	16.46	1.29	22.64	10.10
	Ankle	x	0.02	0.00	54.54	0.00	13.64
		y	0.07	29.99	0.36	32.17	15.65
	Knee	x	24.03	0.00	21.30	0.00	11.33
		y	1.31	31.22	31.58	32.68	24.20
	Hip	x	70.67	0.00	70.67	0.00	35.33
		y	16.94	25.38	16.94	25.38	21.16
	HAT	x	74.50	0.00	74.50	0.00	37.25
		y	16.82	25.41	16.82	25.41	21.12
Segment angles (°)	Foot		0.03	6.63	6.95	2.76	4.09
	Tibia		3.24	0.32	6.22	0.22	2.50
	Femur		6.63	2.23	9.44	0.96	4.82
	HAT		0.68	1.30	0.68	1.30	0.99
	Ankle		2.06	9.76	0.75	0.97	3.38
Joint moments (Nm)	Knee		4.56	12.62	6.29	4.72	7.05
	Hip		27.28	164.65	23.23	2.01	54.29
GRF (%BW)	y		0.78	13.54	1.70	5.11	5.28
	x		2.54	0.80	0.04	0.54	0.98

Table A.8: The discontinuity values for Subject 3

A.7.4 Subject 4

			Lead/stance	Trail/swing
Joint centre positions (mm)	Met	x	0.12	2.81
		y	0.28	24.06
	Ankle	x	5.56	1.20
		y	3.82	4.51
	Knee	x	2.61	2.28
		y	12.46	15.52
	Hip	x	3.78	3.78
		y	8.47	8.47
	HAT	x		4.18
		y		8.83
Segment angles (°)	Foot		4.43	0.47
	Tibia		4.03	2.30
	Femur		5.06	2.27
	HAT			0.15
Joint moments (Nm)	Ankle		5.20	4.64
	Knee		6.99	7.55
	Hip		10.27	9.37
GRF (%BW)		y	3.62	0.58
		x	4.12	1.75

Table A.9: The RMS error values for Subject 4

			TO 1	FC 1	TO 2	FC 2	Mean
Joint centre positions (mm)	Met	x	0.00	0.00	18.91	0.00	4.73
		y	0.00	14.11	99.82	20.43	33.59
	Ankle	x	0.01	0.00	16.66	0.00	4.17
		y	0.02	29.07	99.91	24.76	38.44
	Knee	x	29.53	0.00	30.63	0.00	15.04
		y	2.28	17.05	24.74	11.87	13.98
	Hip	x	70.58	0.00	70.58	0.00	35.29
		y	17.58	23.00	17.58	23.00	20.29
	HAT	x	65.37	0.00	65.37	0.00	32.68
		y	17.71	22.99	17.71	22.99	20.35
Segment angles (°)	Foot		0.01	8.54	6.20	4.01	4.69
	Tibia		4.47	3.00	13.42	8.40	7.32
	Femur		6.70	2.72	0.95	2.15	3.13
	HAT		0.97	0.88	0.97	0.88	0.93
	Ankle		2.55	15.32	1.93	4.13	5.98
Joint moments (Nm)	Knee		9.63	10.74	2.20	15.78	9.59
	Hip		39.44	97.78	29.06	13.02	44.83
GRF (%BW)		y	15.59	26.14	4.63	0.53	11.72
		x	2.79	2.11	0.70	10.84	4.11

Table A.10: The discontinuity values for Subject 4

A.7.5 Subject 5

			Lead/stance	Trail/swing
Joint centre positions (mm)	Met	x	0.84	0.50
		y	1.19	2.99
	Ankle	x	2.28	0.81
		y	2.83	5.97
	Knee	x	0.84	1.16
		y	3.38	3.95
	Hip	x	0.88	0.88
		y	4.26	4.26
	HAT	x		1.13
		y		5.26
Segment angles (°)	Foot		2.67	0.50
	Tibia		1.22	1.78
	Femur		2.00	0.29
	HAT			0.14
Joint moments (Nm)	Ankle		6.47	6.72
	Knee		4.15	4.41
	Hip		5.22	3.36
GRF (%BW)		y	0.39	1.17
		x	0.82	1.09

Table A.11: The RMS error values for Subject 5

			TO 1	FC 1	TO 2	FC 2	Mean
Joint centre positions (mm)	Met	x	0.00	0.00	35.75	0.00	8.94
		y	0.00	14.11	7.26	53.55	18.73
	Ankle	x	0.04	0.00	37.23	0.00	9.32
		y	0.10	25.17	7.35	11.86	11.12
	Knee	x	13.29	0.00	28.58	0.00	10.47
		y	0.52	22.57	18.53	13.79	13.85
	Hip	x	31.61	0.00	31.61	0.00	15.80
		y	18.11	10.24	18.11	10.24	14.18
	HAT	x	40.58	0.00	40.58	0.00	20.29
		y	17.94	10.31	17.94	10.31	14.12
Segment angles (°)	Foot		0.04	5.88	0.47	1.35	1.94
	Tibia		1.99	0.68	2.10	0.92	1.42
	Femur		7.53	6.86	0.63	1.25	4.07
	HAT		1.68	0.79	1.68	0.79	1.24
	Ankle		12.57	2.37	22.05	1.02	9.50
Joint moments (Nm)	Knee		7.65	9.64	21.43	3.36	10.52
	Hip		18.35	145.48	13.70	75.07	63.15
GRF (%BW)	y		4.87	7.70	0.09	3.53	4.05
	x		3.67	0.53	0.50	0.16	1.22

Table A.12: The discontinuity values for Subject 5

A.7.6 Subject 6

			Lead/stance	Trail/swing	
Joint centre positions (mm)	Met	x	0.70	3.12	
		y	0.97	7.62	
	Ankle	x	7.36	3.70	
		y	9.06	9.91	
	Knee	x	2.35	2.24	
		y	6.10	6.08	
	Hip	x	3.10	3.10	
		y	12.12	12.12	
	HAT	x		3.31	
		y		11.02	
	Segment angles (°)	Foot		13.48	2.28
		Tibia		3.62	3.21
Femur			2.54	3.94	
HAT				0.41	
Joint moments (Nm)	Ankle		3.53	15.19	
	Knee		4.78	11.19	
	Hip		9.22	12.95	
GRF (%BW)		y	4.11	0.47	
		x	3.62	1.03	

Table A.13: The RMS error values for Subject 6

			TO 1	FC 1	TO 2	FC 2	Mean
Joint centre positions (mm)	Met	x	0.00	0.00	35.75	0.00	8.94
		y	0.00	14.11	7.26	53.55	18.73
	Ankle	x	0.04	0.00	37.23	0.00	9.32
		y	0.10	25.17	7.35	11.86	11.12
	Knee	x	13.29	0.00	28.58	0.00	10.47
		y	0.52	22.57	18.53	13.79	13.85
	Hip	x	31.61	0.00	31.61	0.00	15.80
		y	18.11	10.24	18.11	10.24	14.18
	HAT	x	40.58	0.00	40.58	0.00	20.29
		y	17.94	10.31	17.94	10.31	14.12
Segment angles (°)	Foot		0.04	5.88	0.47	1.35	1.94
	Tibia		1.99	0.68	2.10	0.92	1.42
	Femur		7.53	6.86	0.63	1.25	4.07
	HAT		1.68	0.79	1.68	0.79	1.24
	Ankle		12.57	2.37	22.05	1.02	9.50
Joint moments (Nm)	Knee		7.65	9.64	21.43	3.36	10.52
	Hip		18.35	145.48	13.70	75.07	63.15
GRF (%BW)	y		4.87	7.70	0.09	3.53	4.05
	x		3.67	0.53	0.50	0.16	1.22

Table A.14: The discontinuity values for Subject 6

A.7.7 Subject 7

			Lead/stance	Trail/swing
Joint centre positions (mm)	Met	x	0.01	0.82
		y	0.71	3.43
	Ankle	x	0.87	0.86
		y	0.28	1.14
	Knee	x	1.07	0.41
		y	0.11	0.22
	Hip	x	1.21	1.21
		y	0.18	0.18
	HAT	x		4.54
		y		33.38
Segment angles (°)	Foot		1.87	1.53
	Tibia		3.35	2.00
	Femur		1.45	2.73
	HAT			0.50
Joint moments (Nm)	Ankle		11.59	9.47
	Knee		5.20	8.18
	Hip		10.09	5.58
GRF (%BW)		y	1.92	0.71
		x	2.80	2.04

Table A.15: The RMS error values for Subject 7

			TO 1	FC 1	TO 2	FC 2	Mean	
Joint centre positions (mm)	Met	x	0.00	0.00	18.36	0.00	4.59	
		y	0.00	16.46	7.43	14.82	9.68	
	Ankle	x	0.04	0.00	23.39	0.00	5.86	
		y	0.09	29.91	7.13	48.37	21.37	
	Knee	x	33.11	0.00	26.63	0.00	14.94	
		y	3.54	20.84	11.06	37.80	18.31	
	Hip	x	20.43	0.00	20.43	0.00	10.22	
		y	0.87	41.11	0.87	41.11	20.99	
	HAT	x	15.41	0.00	15.41	0.00	7.71	
		y	0.85	42.44	0.85	42.44	21.64	
	Segment angles (°)	Foot		0.04	6.54	7.33	1.40	3.83
		Tibia		4.90	2.39	0.75	4.67	3.18
Femur			2.02	7.22	1.92	3.94	3.78	
HAT			0.89	5.68	0.89	5.68	3.28	
Joint moments (Nm)	Ankle		1.99	3.77	1.16	0.18	1.78	
	Knee		13.30	11.67	5.18	1.93	8.02	
	Hip		23.68	148.63	25.84	12.10	52.56	
GRF (%BW)	y		16.14	12.65	0.85	0.40	7.51	
	x		3.73	5.96	0.81	0.40	2.72	

Table A.16: The discontinuity values for Subject 7

A.7.8 Subject 8

			Lead/stance	Trail/swing
Joint centre positions (mm)	Met	x	0.39	0.73
		y	0.65	5.69
	Ankle	x	5.10	1.29
		y	11.63	6.43
	Knee	x	1.16	1.44
		y	10.09	7.54
	Hip	x	0.59	0.59
		y	5.56	5.56
	HAT	x		0.58
		y		5.66
Segment angles (°)	Foot		2.29	0.45
	Tibia		0.48	0.88
	Femur		0.66	0.56
	HAT			0.06
Joint moments (Nm)	Ankle		4.63	4.34
	Knee		6.14	7.38
	Hip		5.77	8.85
GRF (%BW)		y	0.49	0.84
		x	0.35	1.80

Table A.17: The RMS error values for Subject 8

			TO 1	FC 1	TO 2	FC 2	Mean
Joint centre positions (mm)	Met	x	0.00	0.00	1.97	0.00	0.49
		y	0.00	15.29	3.90	28.17	11.84
	Ankle	x	0.35	0.00	1.20	0.00	0.39
		y	0.97	17.24	3.70	27.67	12.40
	Knee	x	0.90	0.00	19.53	0.00	5.11
		y	0.93	28.73	17.33	32.03	19.76
	Hip	x	15.44	0.00	15.44	0.00	7.72
		y	6.51	39.45	6.51	39.45	22.98
	HAT	x	9.10	0.00	9.10	0.00	4.55
		y	6.53	39.46	6.53	39.46	23.00
Segment angles (°)	Foot		0.40	0.84	4.88	2.02	2.03
	Tibia		0.07	3.11	3.81	2.30	2.32
	Femur		2.39	3.49	0.30	1.00	1.79
	HAT		1.04	0.48	1.04	0.48	0.76
Joint moments (Nm)	Ankle		11.99	14.40	20.91	2.49	12.45
	Knee		9.34	41.21	22.06	5.52	19.53
	Hip		37.20	185.83	184.72	68.80	119.14
GRF (%BW)	y		3.49	8.73	3.29	7.44	5.74
	x		0.04	14.18	0.79	2.06	4.26

Table A.18: The discontinuity values for Subject 8

A.7.9 Subject 9

			Lead/stance	Trail/swing
Joint centre positions (mm)	Met	x	0.63	3.00
		y	0.91	4.76
	Ankle	x	4.57	3.21
		y	3.75	4.17
	Knee	x	4.46	5.66
		y	19.50	3.93
	Hip	x	4.80	4.80
		y	4.30	4.30
	HAT	x		4.76
		y		5.40
Segment angles (°)	Foot		4.60	1.42
	Tibia		5.31	3.06
	Femur		3.43	0.92
	HAT			0.11
Joint moments (Nm)	Ankle		7.63	4.90
	Knee		3.72	2.70
	Hip		6.44	4.62
GRF (%BW)		y	1.85	0.39
		x	1.78	0.76

Table A.19: The RMS error values for Subject 9

			TO 1	FC 1	TO 2	FC 2	Mean
Joint centre positions (mm)	Met	x	0.00	0.00	36.96	0.00	9.24
		y	0.00	16.46	20.71	47.07	21.06
	Ankle	x	0.02	0.00	72.11	0.00	18.03
		y	0.06	3.66	9.50	15.70	7.23
	Knee	x	27.96	0.00	43.40	0.00	17.84
		y	1.95	14.60	20.34	13.12	12.50
	Hip	x	72.12	0.00	72.12	0.00	36.06
		y	17.26	16.80	17.26	16.80	17.03
	HAT	x	60.13	0.00	60.13	0.00	30.07
		y	17.51	16.82	17.51	16.82	17.17
Segment angles (°)	Foot		0.02	5.14	3.85	1.27	2.57
	Tibia		3.83	2.91	5.65	1.16	3.39
	Femur		6.23	1.04	13.24	1.03	5.38
	HAT		2.05	1.18	2.05	1.18	1.61
	Ankle		2.89	9.55	3.77	3.91	5.03
Joint moments (Nm)	Knee		15.32	6.82	10.33	1.43	8.47
	Hip		78.14	256.13	156.20	56.74	136.80
GRF (%BW)	y		15.01	2.52	1.41	10.86	7.45
	x		3.80	0.37	1.33	0.42	1.48

Table A.20: The discontinuity values for Subject 9

A.7.10 Subject 10

			Lead/stance	Trail/swing
Joint centre positions (mm)	Met	x	0.50	4.10
		y	0.96	11.16
	Ankle	x	7.96	5.27
		y	3.99	8.16
	Knee	x	4.98	2.45
		y	14.34	11.11
	Hip	x	2.95	2.95
		y	4.01	4.01
	HAT	x		9.90
		y		7.28
Segment angles (°)	Foot		6.49	1.30
	Tibia		3.22	7.16
	Femur		3.71	2.43
	HAT			1.63
Joint moments (Nm)	Ankle		7.90	10.10
	Knee		7.34	8.98
	Hip		5.09	16.77
GRF (%BW)		y	5.57	2.09
		x	3.48	1.93

Table A.21: The RMS error values for Subject 10

			TO 1	FC 1	TO 2	FC 2	Mean	
Joint centre positions (mm)	Met	x	0.00	0.00	27.06	0.00	6.77	
		y	0.00	18.81	43.92	32.73	23.86	
	Ankle	x	0.13	0.00	31.62	0.00	7.94	
		y	0.36	39.68	43.09	21.57	26.18	
	Knee	x	49.12	0.00	19.48	0.00	17.15	
		y	0.83	37.17	3.77	29.96	17.93	
	Hip	x	34.97	0.00	34.97	0.00	17.49	
		y	4.68	32.15	4.68	32.15	18.42	
	HAT	x	44.03	0.00	44.03	0.00	22.02	
		y	5.08	44.42	5.08	44.42	24.75	
	Segment angles (°)	Foot		0.14	8.64	7.26	1.04	4.27
		Tibia		6.49	0.70	9.14	3.72	5.01
Femur			1.93	2.34	1.66	3.33	2.31	
HAT			1.55	15.12	1.55	15.12	8.34	
Ankle			18.71	14.90	21.42	4.40	14.86	
Joint moments (Nm)	Knee		38.28	42.72	39.73	2.16	30.72	
	Hip		66.80	184.89	308.32	85.19	161.30	
GRF (%BW)	y		24.29	7.95	1.00	8.72	10.49	
	x		3.31	7.16	1.38	0.30	3.04	

Table A.22: The discontinuity values for Subject 10

A.8 Preliminary investigation of future work

Preliminary work on a 'Continuous' model was done. The initial state of the single support phase was defined by the terminal state of the double support phase. A penalty function observed the RMS error for each segment angle for the final time instant. If the error was greater than a single standard deviation, a penalty of 500 was added to the cost function. This value weighted the optimisation in favour of reducing discontinuities. The transition from double to single support was defined by the instant the vertical GRF component under the trailing foot reached zero, rather than by a specific time.

The results are shown below.

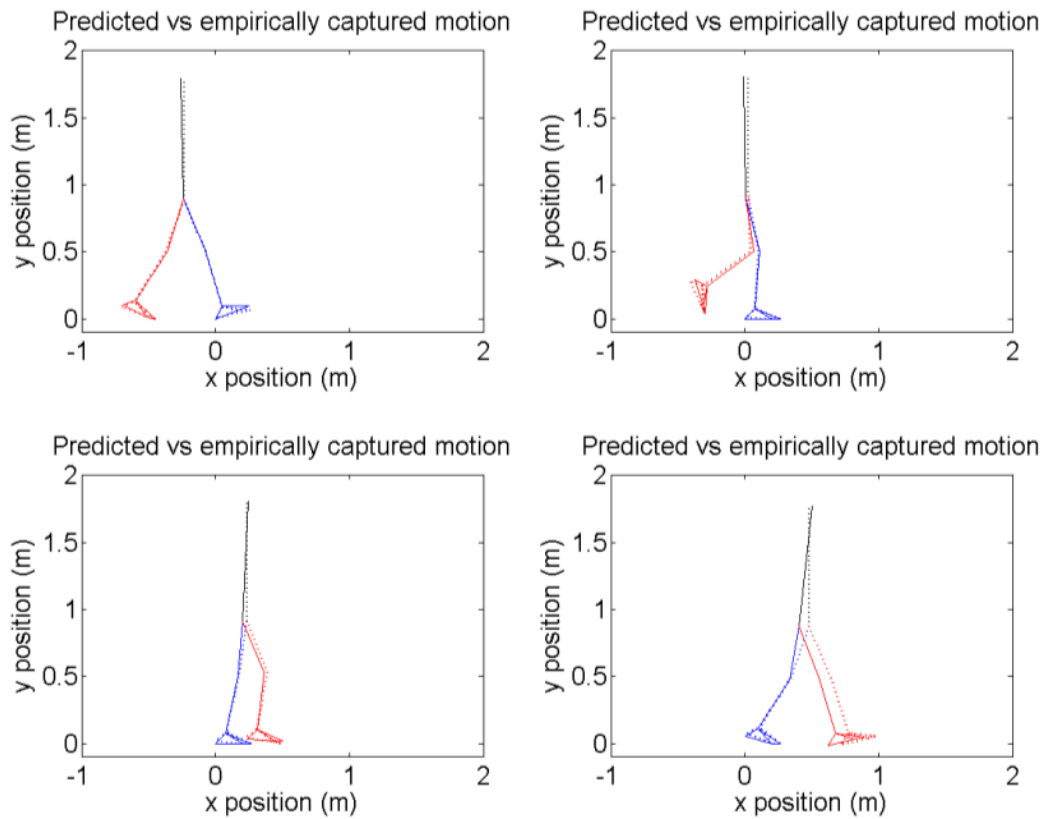


Figure A.2: The kinematic predictions (solid) vs the empirical means (dotted) for the Continuous model

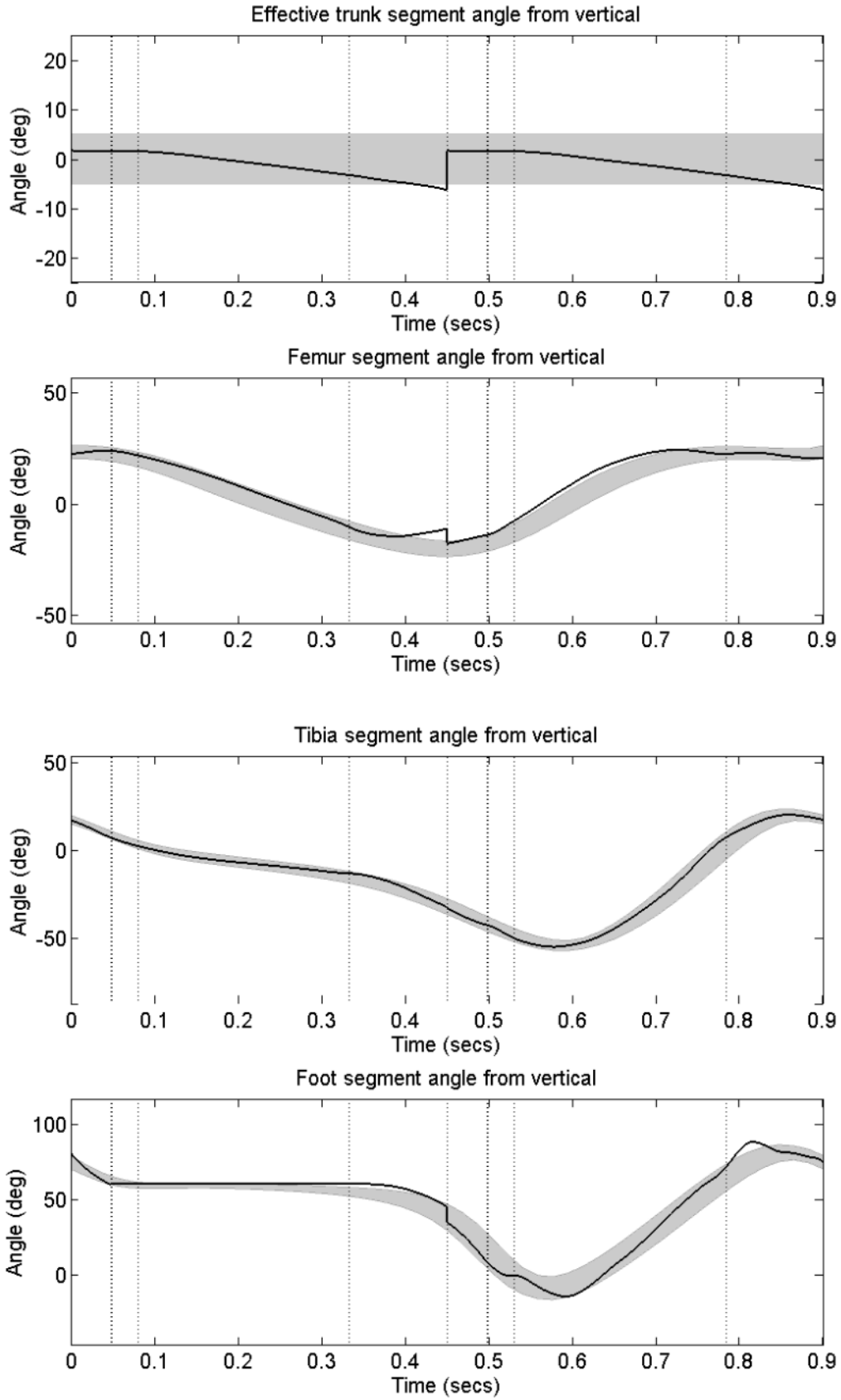


Figure A.3: The segment angle predictions for the Continuous model

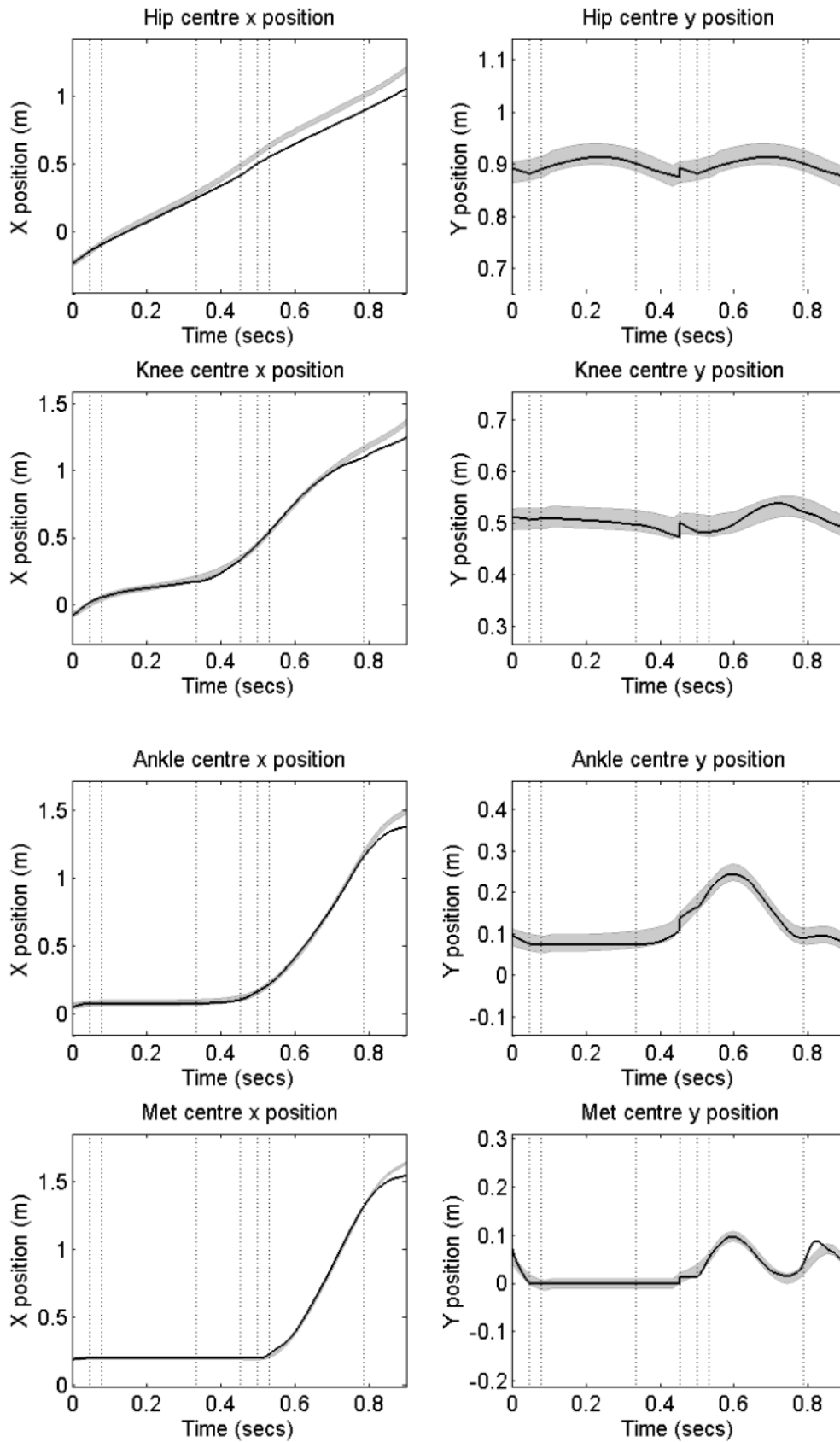


Figure A.4: The joint centre position predictions for the Continuous model

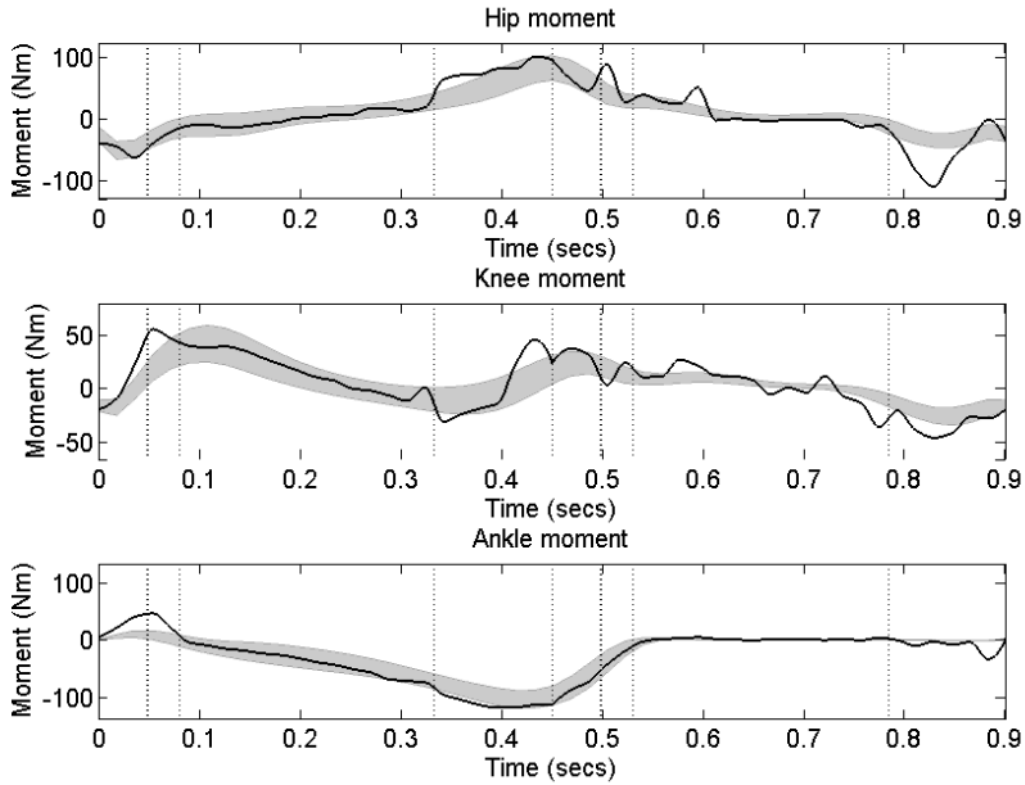


Figure A.5: The joint moment predictions for the Continuous model

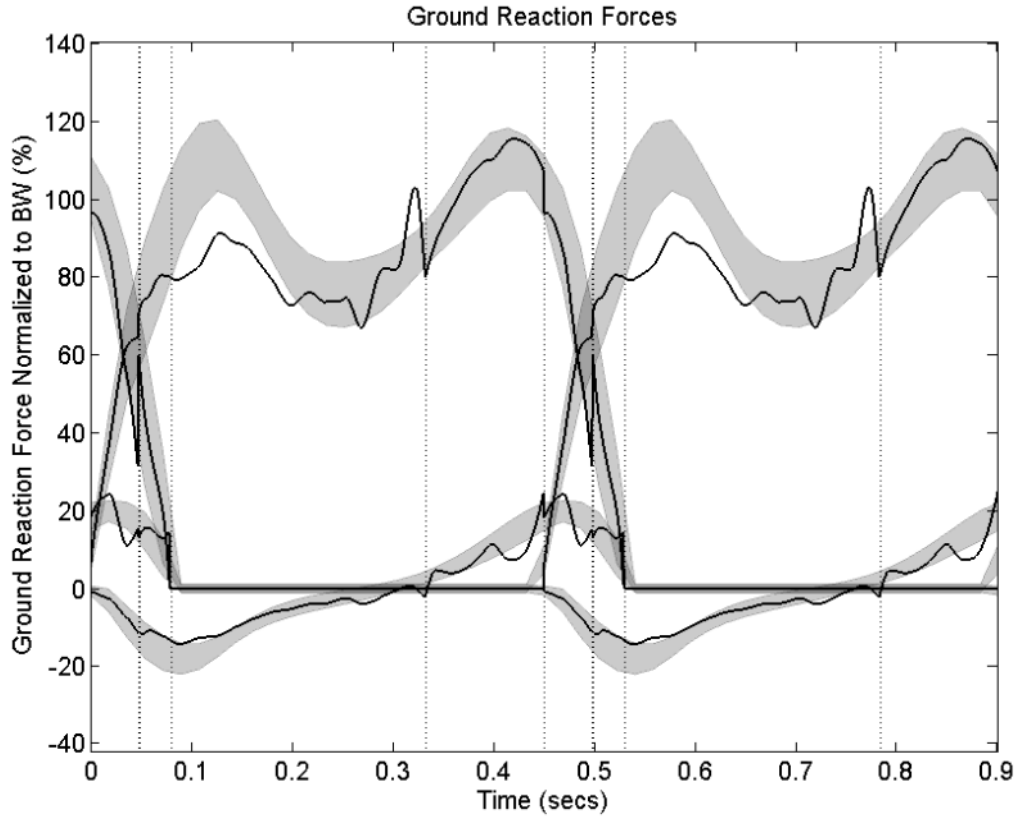


Figure A.6: The GRF moment predictions for the Continuous model

			Lead/stance	Trail/swing
Joint centre positions (mm)	Met	x	0.70	30.52
		y	3.14	10.12
	Ankle	x	6.30	33.74
		y	8.51	4.02
	Knee	x	14.33	36.49
		y	6.50	7.13
	Hip	x	31.99	31.99
		y	5.78	5.78
	HAT	x		19.67
		y		5.98
Segment angles (°)	Foot		4.10	5.53
	Tibia		1.28	2.11
	Femur		3.21	4.67
	HAT			2.80
	Ankle		14.32	7.22
Joint moments (Nm)	Knee		13.39	10.98
	Hip		12.92	22.83
		y	10.30	3.97
GRF (%BW)		x	2.67	1.81

Table A.23: The RMS error values for the Continuous model

In terms of kinematics, the model performed well. In Figure A.2 it appeared as if the predicted data performed too short a step but it was important to remember that this comparison was with the experimental means. A closer inspection of the segment angle plots (Figure A.3) showed that only the lead/stance femur and HAT were not within the standard deviation range at the end of the first half of the gait cycle. This was also visible when looking at the hip joint position in the x direction in Figure A.4.

The joint moment (Figure A.5) and GRF curves (Figure A.6) followed the correct patterns but were not smooth. There were numerous small spikes throughout. The maximum error in GRF came during single support, just before heel rise. Overall though, the mean GRF RMS error, despite being skewed by such spikes, was only 4.69% BW.

The problem of discontinuities between double and single support had been resolved by starting Phase 4 with the terminal conditions of Phase 3. However, the transition from step-to-step could only be constrained with a penalty function so there was still potential for error (except with the joint moments which had been made constant over the full gait cycle). Table A.24 shows the discontinuities that still occurred.

For the continuous full gait cycle model, the kinematic error is low before heel rise, but there are a number of obvious problems in late stance. The lead/stance femur finishes the simulation lagging behind the experimental data. One possible explanation for this could be that because the simulation is purely sagittal, factors such as pelvic rotation are neglected. This further justifies expanding to three dimensions.

The HAT segment leans too far forward at the end of the simulation. This may be due to the head, arms and trunk being modelled as a single segment. It is also possible that the optimiser has found a solution that uses this trunk lean as a compensatory measure for the hip joints being behind the experimental means. This could have been to progress the COP forward, allowing the heel of the stance foot to rise further or at a faster rate.

			TO 1	FC 1	TO 2	FC 2	Mean	
Joint centre positions (mm)	Met	x	0.00	0.00	2.26	0.00	0.56	
		y	0.00	14.11	1.28	33.15	12.14	
	Ankle	x	0.00	0.00	2.07	0.00	0.52	
		y	0.00	31.14	1.28	21.41	13.46	
	Knee	x	0.92	0.00	3.10	0.00	1.01	
		y	0.04	28.83	0.06	21.58	12.63	
	Hip	x	1.50	0.00	1.50	0.00	0.75	
		y	0.27	17.04	0.27	17.04	8.66	
	HAT	x	1.54	0.00	1.54	0.00	0.77	
		y	0.27	18.91	0.27	18.91	9.59	
	Segment angles (°)	Foot		0.00	10.10	0.23	1.74	3.02
		Tibia		0.12	0.56	0.21	0.08	0.24
Femur			0.09	6.76	0.07	6.37	3.32	
HAT			0.01	7.96	0.01	7.96	3.99	
Ankle			1.65	0.00	1.04	0.00	0.67	
Joint moments (Nm)	Knee		0.46	0.00	1.10	0.00	0.39	
	Hip		0.68	0.00	0.96	0.00	0.41	
		y	0.19	10.24	0.00	6.63	4.27	
GRF (%BW)		x	0.17	7.34	0.00	0.72	2.06	

Table A.24: Discontinuities for the Continuous model

Despite the efforts to produce a fully continuous simulation, there were still some discontinuities. They occurred at a different point in the gait cycle to those in the IP models, but they still occurred. This would be a key area for improvement for any future studies in this area. More complex constraint functions in the optimiser might be a solution.

It was noticed, upon closer inspection of the different kinematics of the Sum and Continuous models, that the greatest differences were the angular velocities of the trail/swing tibia and foot segments, particularly at the transition between double support and single support (Table A.25). It was likely that the reason for this was due to these being dependent segments during double support, giving more justification for studying the effects of changing the dependent segments.

Model	Lead foot	Lead tibia	Lead femur	HAT	Trail femur	Trail tibia	Trail foot
Sum	0.00	-161.57	-61.31	9.74	224.03	-81.93	-92.25
Continuous	0.00	-122.04	-87.09	-5.73	225.75	-215.43	91.67
Difference	0.00	-39.53	25.78	15.47	-1.72	133.50	-183.92

Table A.25: Comparison of the angular velocities, in °/s, at the transition from double to single support for the Sum and Continuous models. In bold are the largest differences.

A.9 Rationale behind sequential complexity increases

Chapters 3 and 4 in this thesis focussed on starting with the simplest model of human walking, the IP model, and sequentially adding extra complexities. This was done one by one, thus highlighting the effects each one had on the resulting kinematics and kinetics of gait. As stated in Section 7.7, the process performed by Saunders et al. (Saunders et al., 1953), which led to the proposal of the original Determinants of Gait, was a very similar one. They started with a compass gait, which just like the IP model, has straight, rigid legs, pivoting about a fixed point on the ground, and added their Determinants sequentially.

The order in which different mechanisms were added in this study was not the same as that of Saunders et al. The reason for this was that this study provided feedback at each step and so it was then inferred which extra complexities were likely to provide the desired effects.

The first change, from Model 1 to Model 2, was the addition of a HAT segment. This decision was based upon what was the greatest anatomical difference between Model 1 and reality. This also necessitated the addition of a hip joint moment which was able to provide extra insight. It was observed that the GRF component curves had not altered drastically and what were missing were the characteristic double peaks of the vertical GRF component. The next greatest anatomical change that was hypothesised to affect the GRF under the stance limb was knee flexion. Thus Model 3 incorporated a knee joint and the result was the first vertical GRF peak.

It was then decided that in order to achieve the second peak, a mechanism that has an effect in late single support would be required. This would be the incorporation of a foot. However, this change would require an ankle moment as well. In order to highlight the changes that could be attributed to each, Model 3.1 had the ankle moment only, with the foot remaining static, and Model 4 had both the ankle moment and a moving foot. It was shown that ankle moment improves the initial peak, contributes to the second peak and improves horizontal GRF prediction in late single support. However, heel rise was shown to have the greatest effect on the second vertical GRF peak and the horizontal GRF prediction in late single support.

The final change was to add a swing leg, creating Model 5. The reason this was added last was because the earlier changes were more likely to have a greater effect on the stance limb GRF curves, since they were changes made to the stance limb itself. The swing leg was shown to improve the prediction of the second peak in the vertical GRF, as well as improve the horizontal GRF prediction in late single support.

REFERENCES

- Adamczyk, P. G., & Kuo, A. D. (2009). Redirection of center-of-mass velocity during the step-to-step transition of human walking. *Journal of Experimental Biology*, 212(Pt 16), 2668-2678. doi: 212/16/2668 [pii]
10.1242/jeb.027581
- Alexander, M. (1976). Mechanics of bipedal locomotion. In P. Davis (Ed.), *Perspectives in experimental biology* (pp. 493-504). Oxford: Pergamon.
- Alkjaer, T., Simonsen, E. B., & Dyhre-Poulsen, P. (2001). Comparison of inverse dynamics calculated by two- and three-dimensional models during walking. *Gait & Posture*, 13(2), 73-77. doi: 10.1016/S0966-6362(00)00099-0
- Anderson, F. C., & Pandy, M. G. (2001a). Dynamic optimization of human walking. *American Society of Mechanical Engineers*, 123(5), 381-390.
- Anderson, F. C., & Pandy, M. G. (2001b). Static and dynamic optimization solutions for gait are practically equivalent. *Journal of Biomechanics*, 34(2), 153-161. doi: [http://dx.doi.org/10.1016/S0021-9290\(00\)00155-X](http://dx.doi.org/10.1016/S0021-9290(00)00155-X)
- Anderson, F. C., & Pandy, M. G. (2003). Individual muscle contributions to support in normal walking. *Gait & Posture*, 17(2), 159-169. doi: Pii S0966-6362(02)00073-5
- Ankarali, M. M., Cowan, N. J., & Saranli, U. (2012). *TD-SLIP: A Better Predictive Model for Human Running*. Paper presented at the Dynamic Walking Conference, Pensacola, FL, USA.
- Apkarian, J., Naumann, S., & Cairns, B. (1989). A three-dimensional kinematic and dynamic model of the lower limb. *Journal of Biomechanics*, 22(2), 143-155. doi: 10.1016/0021-9290(89)90037-7

- Arnold, E. M., Ward, S. R., Lieber, R. L., & Delp, S. L. (2010). A model of the lower limb for analysis of human movement. *Ann Biomed Eng*, 38(2), 269-279. doi: 10.1007/s10439-009-9852-5
- Baker, R., Kirkwood, C., & Pandy, M. (2004). *Minimising the vertical excursion of the center of mass is not the primary aim of walking*. Paper presented at the Eighth International Symposium on the 3D Analysis of Human Movement, Tampa, Florida.
- Benedetti, M. G., Manca, M., Ferraresi, G., Boschi, M., & Leardini, A. (2011). A new protocol for 3D assessment of foot during gait: Application on patients with equinovarus foot. *Clinical Biomechanics*, 26(10), 1033-1038. doi: <http://dx.doi.org/10.1016/j.clinbiomech.2011.06.002>
- Best, D. J., & Roberts, D. E. (1975). Algorithm AS 89: The upper tail probabilities of Spearman's rho. *Journal of the Royal Statistical Society. Series C (Applied Statistics)*, 24(3), 377-379. doi: citeulike-article-id:5381907
- Bonnefoy-Mazure, A., Turcot, K., Kaelin, A., De Coulon, G., & Armand, S. (2013). Full body gait analysis may improve diagnostic discrimination between hereditary spastic paraplegia and spastic diplegia: A preliminary study. *Research in Developmental Disabilities*, 34(1), 495-504. doi: <http://dx.doi.org/10.1016/j.ridd.2012.09.005>
- Breakwell, G. M., Smith, J. A., & Wright, D. B. (2012). *Research methods in Psychology* (4th Edition ed.). New York: SAGE Publications Ltd.
- Buczek, F. L., Cooney, K. M., Walker, M. R., Rainbow, M. J., Concha, M. C., & Sanders, J. O. (2006). Performance of an inverted pendulum model directly applied to normal human gait. *Clinical Biomechanics*, 21(3), 288-296. doi: 10.1016/j.clinbiomech.2005.10.007

- Bullimore, S. R., & Burn, J. F. (2007). Ability of the planar spring–mass model to predict mechanical parameters in running humans. *Journal of Theoretical Biology*, 248(4), 686-695. doi: <http://dx.doi.org/10.1016/j.itbi.2007.06.004>
- Cappozzo, A., Leo, T., & Pedotti, A. (1975). A general computing method for the analysis of human locomotion. *Journal of Biomechanics*, 8(5), 307-320. doi: 10.1016/0021-9290(75)90083-4
- Cavagna, G. A., Thys, H., & Zamboni, A. (1976). The sources of external work in level walking and running. *J Physiol*, 262(3), 639-657.
- Ceccato, J.-C., de Sèze, M., Azevedo, C., & Cazalets, J.-R. (2009). Comparison of Trunk Activity during Gait Initiation and Walking in Humans. *PLoS ONE*, 4(12), e8193. doi: 10.1371/journal.pone.0008193
- Channon, P. H., Hopkins, S. H., & Pham, D. T. (1992). Derivation of optimal walking motions for a bipedal walking robot. *Robotica*, 10(02), 165-172. doi: doi:10.1017/S026357470000758X
- Chen, G. (2006). Induced acceleration contributions to locomotion dynamics are not physically well defined. *Gait & Posture*, 23(1), 37-44. doi: <http://dx.doi.org/10.1016/j.gaitpost.2004.11.016>
- Crowninshield, R. D., & Brand, R. A. (1981). A physiologically based criterion of muscle force prediction in locomotion. *Journal of Biomechanics*, 14(11), 793-801. doi: [http://dx.doi.org/10.1016/0021-9290\(81\)90035-X](http://dx.doi.org/10.1016/0021-9290(81)90035-X)
- Crowninshield, R. D., Johnston, R. C., Andrews, J. G., & Brand, R. A. (1978). A biomechanical investigation of the human hip. *Journal of Biomechanics*, 11(1–2), 75-85. doi: [http://dx.doi.org/10.1016/0021-9290\(78\)90045-3](http://dx.doi.org/10.1016/0021-9290(78)90045-3)

- Davis III, R. B., Öunpuu, S., Tyburski, D., & Gage, J. R. (1991). A gait analysis data collection and reduction technique. *Human Movement Science, 10*(5), 575-587. doi: [http://dx.doi.org/10.1016/0167-9457\(91\)90046-Z](http://dx.doi.org/10.1016/0167-9457(91)90046-Z)
- Davy, D. T., & Audu, M. L. (1987). A dynamic optimization technique for predicting muscle forces in the swing phase of gait. *Journal of Biomechanics, 20*(2), 187-201. doi: [http://dx.doi.org/10.1016/0021-9290\(87\)90310-1](http://dx.doi.org/10.1016/0021-9290(87)90310-1)
- De Boor, C. (1978). *A practical guide to splines*. New York: Springer-Verlag.
- Delagi, E. F., & Perotto, A. (1980). *Anatomic guide for electromyographer* (Second ed.). Springfield, Illinois: Charles C Thomas Pub Ltd.
- Della Croce, U., Riley, P. O., Lelas, J. L., & Kerrigan, D. C. (2001). A refined view of the determinants of gait. *Gait & Posture, 14*(2), 79-84. doi: 10.1016/s0966-6362(01)00128-x
- Delp, S. L., Anderson, F. C., Arnold, A. S., Loan, P., Habib, A., John, C. T., . . . Thelen, D. G. (2007). OpenSim: open-source software to create and analyze dynamic simulations of movement. *IEEE Trans Biomed Eng, 54*(11), 1940-1950. doi: 10.1109/tbme.2007.901024
- Dempster, W. T. (1955). *Space requirements of the seated operator: geometrical, kinematic, and mechanical aspects of the body with special reference to the limbs*. Wright-Patterson Air Force Base, Ohio: Wright Air Development Center.
- Dempster, W. T., Gabel, W. C., & Felts, W. J. (1959). The anthropometry of the manual work space for the seated subject. *Am J Phys Anthropol, 17*, 289-317.
- Dobson, F., Morris, M. E., Baker, R., & Graham, H. K. (2011). Unilateral cerebral palsy: a population-based study of gait and motor function. *Dev Med Child Neurol, 53*(5), 429-435. doi: 10.1111/j.1469-8749.2010.03878.x

- Donelan, J. M., Kram, R., & Kuo, A. D. (2001). Mechanical and metabolic determinants of the preferred step width in human walking. *Proc Biol Sci*, 268(1480), 1985-1992. doi: 10.1098/rspb.2001.1761
- Donelan, J. M., Kram, R., & Kuo, A. D. (2002a). Mechanical work for step-to-step transitions is a major determinant of the metabolic cost of human walking. *Journal of Experimental Biology*, 205, 3717-3727.
- Donelan, J. M., Kram, R., & Kuo, A. D. (2002b). Simultaneous positive and negative external mechanical work in human walking. *Journal of Biomechanics*, 35(1), 117-124. doi: S0021929001001695 [pii]
- Drillis, R., & Contini, R. (1966). Body Segment Parameters (D. o. H. Office of Vocational Rehabilitation, Education and Welfare, Trans.). New York.
- Duan, X. H., Allen, R. H., & Sun, J. Q. (1997). A stiffness-varying model of human gait. *Medical Engineering & Physics*, 19(6), 518-524. doi: 10.1016/s1350-4533(97)00022-2
- Duysens, J., & Van de Crommert, H. W. A. A. (1998). Neural control of locomotion; Part 1: The central pattern generator from cats to humans. *Gait & Posture*, 7(2), 131-141. doi: [http://dx.doi.org/10.1016/S0966-6362\(97\)00042-8](http://dx.doi.org/10.1016/S0966-6362(97)00042-8)
- Elftman, H. (1966). Biomechanics of muscle with particular application to studies of gait. *Journal of bone and Joint Surgery - American*, 48(2), 363-377.
- Endo, K., & Herr, H. (2009). *Human walking model predicts joint mechanics, electromyography and mechanical economy*. Paper presented at the Proceedings of the 2009 IEEE/RSJ international conference on Intelligent robots and systems, St. Louis, MO, USA.

- Eng, J. J., & Winter, D. A. (1995). Kinetic analysis of the lower limbs during walking: What information can be gained from a three-dimensional model? *Journal of Biomechanics*, 28(6), 753-758. doi: 10.1016/0021-9290(94)00124-m
- Ephanov, A., & Hurmuzlu, Y. (2002). Generating pathological gait patterns via the use of robotic locomotion models. *Technol. Health Care*, 10(2), 135-146.
- Ferrari, A., Benedetti, M. G., Pavan, E., Frigo, C., Bettinelli, D., Rabuffetti, M., . . . Leardini, A. (2008). Quantitative comparison of five current protocols in gait analysis. *Gait & Posture*, 28(2), 207-216. doi: <http://dx.doi.org/10.1016/j.gaitpost.2007.11.009>
- Francis, C. A., Lenz, A. L., Lenhart, R. L., & Thelen, D. G. (2013). The modulation of forward propulsion, vertical support, and center of pressure by the plantarflexors during human walking. *Gait & Posture*(0). doi: <http://dx.doi.org/10.1016/j.gaitpost.2013.05.009>
- Garcia, M., Chatterjee, A., & Ruina, A. (1998, 16-20 May 1998). *Speed, efficiency, and stability of small-slope 2D passive dynamic bipedal walking*. Paper presented at the Robotics and Automation, 1998. Proceedings. 1998 IEEE International Conference on.
- Garcia, M., Chatterjee, A., Ruina, A., & Coleman, M. (1998). The Simplest Walking Model: Stability, Complexity, and Scaling. *Journal of Biomechanical Engineering*, 120(2), 281-288.
- Gard, S. A., & Childress, D. S. (1997). The effect of pelvic list on the vertical displacement of the trunk during normal walking. *Gait & Posture*, 5(3), 233-238. doi: 10.1016/s0966-6362(96)01089-2

- Gard, S. A., & Childress, D. S. (1999). The influence of stance-phase knee flexion on the vertical displacement of the trunk during normal walking. *Archives of Physical Medicine and Rehabilitation*, 80(1), 26-32. doi: 10.1016/s0003-9993(99)90303-9
- Gerus, P., Sartori, M., Besier, T. F., Fregly, B. J., Delp, S. L., Banks, S. A., . . . Lloyd, D. G. (2013). Subject-specific knee joint geometry improves predictions of medial tibiofemoral contact forces. *Journal of Biomechanics*, 46(16), 2778-2786. doi: <http://dx.doi.org/10.1016/j.jbiomech.2013.09.005>
- Gibbons, J. D. (1985). *Nonparametric Statistical Inference* (2nd ed.): M. Dekker.
- Glitsch, U., & Baumann, W. (1997). The three-dimensional determination of internal loads in the lower extremity. *Journal of Biomechanics*, 30(11-12), 1123-1131. doi: [http://dx.doi.org/10.1016/S0021-9290\(97\)00089-4](http://dx.doi.org/10.1016/S0021-9290(97)00089-4)
- Goswami, A. (1999). Postural Stability of Biped Robots and the Foot-Rotation Indicator (FRI) Point. *The International Journal of Robotics Research*, 18(6), 523-533. doi: 10.1177/02783649922066376
- Goswami, A., Espiau, B., & Keramane, A. (1997). Limit Cycles in a Passive Compass Gait Biped and Passivity-Mimicking Control Laws. *Autonomous Robots*, 4(3), 273-286. doi: 10.1023/a:1008844026298
- Goswami, A., Thuilot, B., & Espiau, B. (1998). A Study of the Passive Gait of a Compass-Like Biped Robot: Symmetry and Chaos. *The International Journal of Robotics Research*, 17(12), 1282-1301. doi: 10.1177/027836499801701202
- Gutierrez-Farewik, E. M., Bartonek, Å., & Saraste, H. (2006). Comparison and evaluation of two common methods to measure center of mass displacement in three dimensions during gait. *Human Movement Science*, 25(2), 238-256. doi: <http://dx.doi.org/10.1016/j.humov.2005.11.001>

- Hardt, D. E. (1978). Determining Muscle Forces in the Leg During Normal Human Walking--An Application and Evaluation of Optimization Methods. *Journal of Biomechanical Engineering*, 100(2), 72-78.
- Hardt, D. E., & Mann, R. W. (1980). A five body — Three dimensional dynamic analysis of walking. *Journal of Biomechanics*, 13(5), 455-457. doi: 10.1016/0021-9290(80)90040-8
- Harrington, M. E., Zavatsky, A. B., Lawson, S. E., Yuan, Z., & Theologis, T. N. (2007). Prediction of the hip joint centre in adults, children, and patients with cerebral palsy based on magnetic resonance imaging. *J Biomech*, 40(3), 595-602. doi: 10.1016/j.jbiomech.2006.02.003
- Hatze, H. (1981). A comprehensive model for human motion simulation and its application to the take-off phase of the long jump. *Journal of Biomechanics*, 14(3), 135-142. doi: [http://dx.doi.org/10.1016/0021-9290\(81\)90019-1](http://dx.doi.org/10.1016/0021-9290(81)90019-1)
- Hollander, M., & Wolfe, D. A. (1973). *Nonparametric Statistical Methods*: Wiley.
- Hong, H., Kim, S., Kim, C., Lee, S., & Park, S. (2013). Spring-like gait mechanics observed during walking in both young and older adults. *Journal of Biomechanics*, 46(1), 77-82. doi: <http://dx.doi.org/10.1016/j.jbiomech.2012.10.003>
- Horsak, B., & Baca, A. (2013). Effects of toning shoes on lower extremity gait biomechanics. *Clinical Biomechanics*, 28(3), 344-349. doi: <http://dx.doi.org/10.1016/j.clinbiomech.2013.01.009>
- Hurmuzlu, Y. (1993). Dynamics of Bipedal Gait: Part II---Stability Analysis of a Planar Five-Link Biped. *Journal of Applied Mechanics*, 60(2), 337-343.

- Jonkers, I., Stewart, C., & Spaepen, A. (2003). The study of muscle action during single support and swing phase of gait: clinical relevance of forward simulation techniques. *Gait & Posture*, *17*(2), 97-105. doi: 10.1016/s0966-6362(02)00057-7
- Juang, J. G. (2000). Fuzzy neural network approaches for robotic gait synthesis. *IEEE Transactions on Systems, Man, and Cybernetics, Part B: Cybernetics*, *30*(4), 594-601.
- Kadaba, M. P., Ramakrishnan, H. K., Wootten, M. E., Gaine, J., Gorton, G., & Cochran, G. V. (1989). Repeatability of kinematic, kinetic, and electromyographic data in normal adult gait. *J Orthop Res*, *7*(6), 849-860. doi: 10.1002/jor.1100070611
- Kendall, M. G. (1970). *Rank Correlation Methods*: Griffin.
- Kerrigan, D. C., Croce, U. D., Marciello, M., & Riley, P. O. (2000). A refined view of the determinants of gait: Significance of heel rise. *Archives of Physical Medicine and Rehabilitation*, *81*(8), 1077-1080. doi: 10.1053/apmr.2000.6306
- Kerrigan, D. C., Riley, P. O., Lelas, J. L., & Croce, U. D. (2001). Quantification of pelvic rotation as a determinant of gait. *Archives of Physical Medicine and Rehabilitation*, *82*(2), 217-220. doi: 10.1053/apmr.2001.18063
- Kim, S., & Park, S. (2011). Leg stiffness increases with speed to modulate gait frequency and propulsion energy. *Journal of Biomechanics*, *44*(7), 1253-1258. doi: <http://dx.doi.org/10.1016/j.jbiomech.2011.02.072>
- Kirtley, C. (2006). *Clinical Gait Analysis - Theory and Practice*. Edinburgh: Churchill-Livingstone.
- Koh, B.-I., Reinbolt, J. A., George, A. D., Haftka, R. T., & Fregly, B. J. (2009). Limitations of parallel global optimization for large-scale human movement problems. *Medical Engineering & Physics*, *31*(5), 515-521. doi: 10.1016/j.medengphy.2008.09.010

- Koolen, T., Boer, T. D., Rebula, J., Goswami, A., & Pratt, J. (2012). Capturability-based analysis and control of legged locomotion, Part 1: Theory and application to three simple gait models. *Int. J. Rob. Res.*, *31*(9), 1094-1113. doi: 10.1177/0278364912452673
- Koopman, B., Grootenboer, H. J., & de Jongh, H. J. (1995). An inverse dynamics model for the analysis, reconstruction and prediction of bipedal walking. *Journal of Biomechanics*, *28*(11), 1369-1376. doi: 10.1016/0021-9290(94)00185-7
- Krebs, D. E., Wong, D., Jevsevar, D., Riley, P. O., & Hodge, W. A. (1992). Trunk kinematics during locomotor activities. *Phys Ther*, *72*(7), 505-514.
- Kuo, A. D. (2007). The six determinants of gait and the inverted pendulum analogy: A dynamic walking perspective. *Human Movement Science*, *26*(4), 617-656. doi: 10.1016/j.humov.2007.04.003
- Kuo, A. D., Donelan, J. M., & Ruina, A. (2005). Energetic consequences of walking like an inverted pendulum: step-to-step transitions. *Exercise and Sport Sciences Reviews*, *33*(2), 88-97. doi: 00003677-200504000-00006 [pii]
- Lagarias, J. C., Reeds, J. A., Wright, M. H., & Wright, P. E. (1998). Convergence properties of the Nelder-Mead simplex method in low dimensions. *SIAM Journal of Optimization*, *9*, 112-147. doi: citeulike-article-id:1266919
- Liu, M. Q., Anderson, F. C., Pandy, M. G., & Delp, S. L. (2006). Muscles that support the body also modulate forward progression during walking. *Journal of Biomechanics*, *39*(14), 2623-2630. doi: 10.1016/j.jbiomech.2005.08.017
- Liu, M. Q., Anderson, F. C., Schwartz, M. H., & Delp, S. L. (2008). Muscle contributions to support and progression over a range of walking speeds. *Journal of Biomechanics*, *41*(15), 3243-3252. doi: <http://dx.doi.org/10.1016/j.jbiomech.2008.07.031>

- Marshall, R. N., Wood, G. A., & Jennings, L. S. (1989). Performance objectives in human movement: A review and application to the stance phase of normal walking. *Human Movement Science, 8*(6), 571-594. doi: [http://dx.doi.org/10.1016/0167-9457\(89\)90004-3](http://dx.doi.org/10.1016/0167-9457(89)90004-3)
- McGeer, T. (1990). Passive dynamic walking. *The international journal of robotics research, 9*(2).
- McGeer, T. (1993). Dynamics and control of bipedal locomotion. *Journal of Theoretical Biology, 163*(3), 277-314. doi: S0022-5193(83)71121-5 [pii]
10.1006/jtbi.1993.1121
- McMahon, T. A. (1984). *Muscles, Reflexes and Locomotion*. Princeton, New Jersey: Princeton University Press.
- Millard, M., Kubica, E., & McPhee, J. (2011). Forward dynamic human gait simulation using a SLIP target model. *Procedia IUTAM, 2*(0), 142-157. doi: 10.1016/j.piutam.2011.04.015
- Mochon, S., & McMahon, T. A. (1980). Ballistic walking. *Journal of Biomechanics, 13*(1), 49-57. doi: 10.1016/0021-9290(80)90007-x
- Morimoto, J., Zeglin, G., & Atkeson, C. G. (2003, 4-6 Aug. 2003). *Minimax differential dynamic programming: application to a biped walking robot*. Paper presented at the SICE 2003 Annual Conference.
- Nocedal, J., & Wright, S. J. (2006). *Numerical Optimization* (2nd ed.): Springer.
- O'Connor, S., & Kuo, A. (2007). *Walking, Skipping, and Running Produced From a Single Bipedal Model*. Paper presented at the Conference of the American Society of Biomechanics, Palo Alto, CA, USA.

- Ogihara, N., & Yamazaki, N. (2001). Generation of human bipedal locomotion by a bio-mimetic neuro-musculo-skeletal model. *Biological Cybernetics*, *84*(1), 1-11. doi: 10.1007/pl00007977
- Onyshko, S., & Winter, D. A. (1980). A mathematical model for the dynamics of human locomotion. *Journal of Biomechanics*, *13*(4), 361-368. doi: 10.1016/0021-9290(80)90016-0
- Opila-Correia, K. A. (1990). Kinematics of high-heeled gait. *Arch Phys Med Rehabil*, *71*(5), 304-309.
- Ortega, J., & Farley, C. (2005). Minimizing the center of mass vertical movement increases metabolic cost in walking. *Journal of Applied Physiology*, *99*, 2099-2107.
- Otten, E. (2003). Inverse and forward dynamics: models of multi-body systems. *Philos Trans R Soc Lond B Biol Sci*, *358*(1437), 1493-1500. doi: 10.1098/rstb.2003.1354
- Pandy, M. G. (2003). Simple and complex models for studying muscle function in walking. *Philosophical Transactions of the Royal Society of London. Series B: Biological Sciences*, *358*(1437), 1501-1509. doi: 10.1098/rstb.2003.1338
- Pandy, M. G., & Berme, N. (1988a). A numerical method for simulating the dynamics of human walking. *Journal of Biomechanics*, *21*(12), 1043-1051. doi: 10.1016/0021-9290(88)90250-3
- Pandy, M. G., & Berme, N. (1988b). Synthesis of human walking: A planar model for single support. *Journal of Biomechanics*, *21*(12), 1053-1060. doi: 10.1016/0021-9290(88)90251-5
- Patriarco, A. G., Mann, R. W., Simon, S. R., & Mansour, J. M. (1981). An evaluation of the approaches of optimization models in the prediction of muscle forces during

- human gait. *Journal of Biomechanics*, 14(8), 513-525. doi:
[http://dx.doi.org/10.1016/0021-9290\(81\)90001-4](http://dx.doi.org/10.1016/0021-9290(81)90001-4)
- Pedersen, D. R., Brand, R. A., & Davy, D. T. (1997). Pelvic muscle and acetabular contact forces during gait. *Journal of Biomechanics*, 30(9), 959-965. doi:
[http://dx.doi.org/10.1016/S0021-9290\(97\)00041-9](http://dx.doi.org/10.1016/S0021-9290(97)00041-9)
- Pedotti, A. (1977). A study of motor coordination and neuromuscular activities in human locomotion. *Biological Cybernetics*, 26(1), 53-62. doi: 10.1007/bf00363992
- Perry, J. (1992). *Gait Analysis*. Thorofare: SLACK.
- Perry, J., & Burnfield, J. (2010). *Gait Analysis: Normal and Pathological function* (Second ed.). Thorofare, NJ, USA: SLACK Incorporated.
- Poulakakis, I. (2010, 3-7 May 2010). *Spring Loaded Inverted Pendulum embedding: Extensions toward the control of compliant running robots*. Paper presented at the Robotics and Automation (ICRA), 2010 IEEE International Conference on.
- Poulakakis, I., & Grizzle, J. W. (2009). The Spring Loaded Inverted Pendulum as the Hybrid Zero Dynamics of an Asymmetric Hopper. *Automatic Control, IEEE Transactions on*, 54(8), 1779-1793. doi: 10.1109/tac.2009.2024565
- Raspovic, A. (2013). Gait characteristics of people with diabetes-related peripheral neuropathy, with and without a history of ulceration. *Gait & Posture*, 38(4), 723-728. doi: <http://dx.doi.org/10.1016/j.gaitpost.2013.03.009>
- Reinbolt, J. A., Seth, A., & Delp, S. L. (2011). Simulation of human movement: applications using OpenSim. *Procedia IUTAM*, 2(0), 186-198. doi:
<http://dx.doi.org/10.1016/j.piutam.2011.04.019>

- Ren, L., Howard, D., & Kenney, L. (2006). Computational Models to Synthesize Human Walking. *Journal of Bionic Engineering*, 3(3), 127-138. doi: 10.1016/s1672-6529(06)60016-4
- Ren, L., Jones, R. K., & Howard, D. (2007). Predictive modelling of human walking over a complete gait cycle. *Journal of Biomechanics*, 40(7), 1567-1574. doi: 10.1016/j.jbiomech.2006.07.017
- Riley, P. O., Paolini, G., Della Croce, U., Paylo, K. W., & Kerrigan, D. C. (2007). A kinematic and kinetic comparison of overground and treadmill walking in healthy subjects. *Gait & Posture*, 26(1), 17-24. doi: <http://dx.doi.org/10.1016/j.gaitpost.2006.07.003>
- Rodda, J. M., Graham, H. K., Carson, L., Galea, M. P., & Wolfe, R. (2004). Sagittal gait patterns in spastic diplegia. *J Bone Joint Surg Br*, 86(2), 251-258.
- Röhrle, H., Scholten, R., Sigolotto, C., Sollbach, W., & Kellner, H. (1984). Joint forces in the human pelvis-leg skeleton during walking. *Journal of Biomechanics*, 17(6), 409-424. doi: [http://dx.doi.org/10.1016/0021-9290\(84\)90033-2](http://dx.doi.org/10.1016/0021-9290(84)90033-2)
- Rose, J., & Gamble, J. G. (1994). *Human Walking* (2nd ed.). London: Williams & Wilkins.
- Rostami, M., & Bessonnet, G. (2001). Sagittal gait of a biped robot during the single support phase. Part 2: optimal motion. *Robotica*, 19(3), 241-253. doi: 10.1017/s0263574700003039
- Rueda, F. M., Diego, I. M. A., Sánchez, A. M., Tejada, M. C., Montero, F. M. R., & Page, J. C. M. (2013). Knee and hip internal moments and upper-body kinematics in the frontal plane in unilateral transtibial amputees. *Gait & Posture*, 37(3), 436-439. doi: <http://dx.doi.org/10.1016/j.gaitpost.2012.08.019>

- Saunders, J., Inman, V., & Eberhart, H. (1953). The major determinants in normal and pathological gait. *Journal of Bone and Joint Surgery* 35A, 543-558.
- Siegler, S., Seliktar, R., & Hyman, W. (1982). Simulation of human gait with the aid of a simple mechanical model. *Journal of Biomechanics*, 15(6), 415-425. doi: 10.1016/0021-9290(82)90078-1
- Soyguder, S., & Alli, H. (2012). Computer simulation and dynamic modeling of a quadrupedal pronking gait robot with SLIP model. *Computers & Electrical Engineering*, 38(1), 161-174. doi: <http://dx.doi.org/10.1016/j.compeleceng.2011.11.007>
- Srinivasan, M. (2010). Fifteen observations on the structure of energy-minimizing gaits in many simple biped models. *Journal of The Royal Society Interface*. doi: 10.1098/rsif.2009.0544
- Srinivasan, M., & Ruina, A. (2006). Computer optimization of a minimal biped model discovers walking and running. *Nature*, 439(7072), 72-75.
- Srinivasan, S., Westervelt, E. R., & Hansen, A. H. (2009). A low-dimensional sagittal-plane forward-dynamic model for asymmetric gait and its application to study the gait of transtibial prosthesis users. *J Biomech Eng*, 131(3), 031003. doi: 10.1115/1.3002757
- Steele, K. M., Seth, A., Hicks, J. L., Schwartz, M. H., & Delp, S. L. (2013). Muscle contributions to vertical and fore-aft accelerations are altered in subjects with crouch gait. *Gait & Posture*, 38(1), 86-91. doi: <http://dx.doi.org/10.1016/j.gaitpost.2012.10.019>
- Steele, K. M., Seth, A., Hicks, J. L., Schwartz, M. S., & Delp, S. L. (2010). Muscle contributions to support and progression during single-limb stance in crouch gait.

Journal of Biomechanics, 43(11), 2099-2105. doi:

<http://dx.doi.org/10.1016/j.jbiomech.2010.04.003>

Syczewska, M., Dembowska-Bagińska, B., Perek-Polnik, M., Kalinowska, M., & Perek, D.

(2010). Gait pathology assessed with Gillette Gait Index in patients after CNS

tumour treatment. *Gait & Posture*, 32(3), 358-362. doi:

<http://dx.doi.org/10.1016/j.gaitpost.2010.06.006>

Taga, G. (1995). A model of the neuro-musculo-skeletal system for human locomotion.

Biological Cybernetics, 73(2), 97-111. doi: 10.1007/bf00204048

Taga, G., Yamaguchi, Y., & Shimizu, H. (1991). Self-organized control of bipedal

locomotion by neural oscillators in unpredictable environment. *Biological*

Cybernetics, 65(3), 147-159. doi: citeulike-article-id:587332

Thelen, D. G., & Anderson, F. C. (2006). Using computed muscle control to generate

forward dynamic simulations of human walking from experimental data. *Journal*

of Biomechanics, 39(6), 1107-1115. doi: 10.1016/j.jbiomech.2005.02.010

Thelen, D. G., Anderson, F. C., & Delp, S. L. (2003). Generating dynamic simulations of

movement using computed muscle control. *J Biomech*, 36(3), 321-328. doi:

S0021929002004323 [pii]

Thorstensson, A., Carlson, H., Zomlefer, M. R., & Nilsson, J. (1982). Lumbar back muscle

activity in relation to trunk movements during locomotion in man. *Acta Physiol*

Scand, 116(1), 13-20. doi: 10.1111/j.1748-1716.1982.tb10593.x

Thummerer, Y., von Kries, R., Marton, M.-A., & Beyerlein, A. (2012). Is age or speed the

predominant factor in the development of trunk movement in normally

developing children? *Gait & Posture*, 35(1), 23-28. doi:

<http://dx.doi.org/10.1016/j.gaitpost.2011.07.018>

- Ugray, Z., Lasdon, L., Plummer, J., Glover, F., Kelly, J., Mart, R., & \#237. (2007). Scatter Search and Local NLP Solvers: A Multistart Framework for Global Optimization. *INFORMS J. on Computing*, 19(3), 328-340. doi: 10.1287/ijoc.1060.0175
- Ülker, H. (2010). *DYNAMIC ANALYSIS OF FLEXIBLE MECHANISMS BY FINITE ELEMENT METHOD*. (Master of Science), İzmir Institute of Technology.
- Van de Crommert, H. W. A. A., Mulder, T., & Duysens, J. (1998). Neural control of locomotion: sensory control of the central pattern generator and its relation to treadmill training. *Gait & Posture*, 7(3), 251-263. doi: [http://dx.doi.org/10.1016/S0966-6362\(98\)00010-1](http://dx.doi.org/10.1016/S0966-6362(98)00010-1)
- Van der Krogt, M., Seth, A., Steele, K., Bar-On, L., Desloovere, K., Harlaar, J., & Delp, S. (2013). A model of muscle spasticity in opensim. *Gait & Posture*, 38, Supplement 1(0), S16. doi: <http://dx.doi.org/10.1016/j.gaitpost.2013.07.039>
- Whittle, M. W. (2007). *Gait Analysis: An Introduction* (4th ed.). Oxford: Butterworth-Heinemann.
- Winter, D. A. (1979). *Biomechanics of Human Movement*: John Wiley & Sons, Inc.
- Winter, D. A. (1991). *The biomechanics and motor control of human gait: Normal, Elderly and Pathological* (2nd ed.). Waterloo: Waterloo Biomechanics.
- Yamaguchi, G. T., & Zajac, F. E. (1990). Restoring unassisted natural gait to paraplegics via functional neuromuscular stimulation: a computer simulation study. *Biomedical Engineering, IEEE Transactions on*, 37(9), 886-902.
- Yamazaki, N., Hase, K., Ogihara, N., & Hayamizu, N. (1996). Biomechanical analysis of the development of human bipedal walking by a neuro-musculo-skeletal model. *Folia Primatol (Basel)*, 66(1-4), 253-271.

Yen, V., & Nagurka, M. (1987). Suboptimal trajectory planning of a five-link human locomotion model. *Biomechanics of Normal and Prosthetic Gait*, 4, 17-22.

Zhe, T., Meng Joo, E., & Chien, C. J. (2008, 1-6 June 2008). *Analysis of human gait using an Inverted Pendulum Model*. Paper presented at the Fuzzy Systems, 2008. FUZZ-IEEE 2008. (IEEE World Congress on Computational Intelligence). IEEE International Conference on.